# Applications of Holography to Strongly Coupled Plasmas

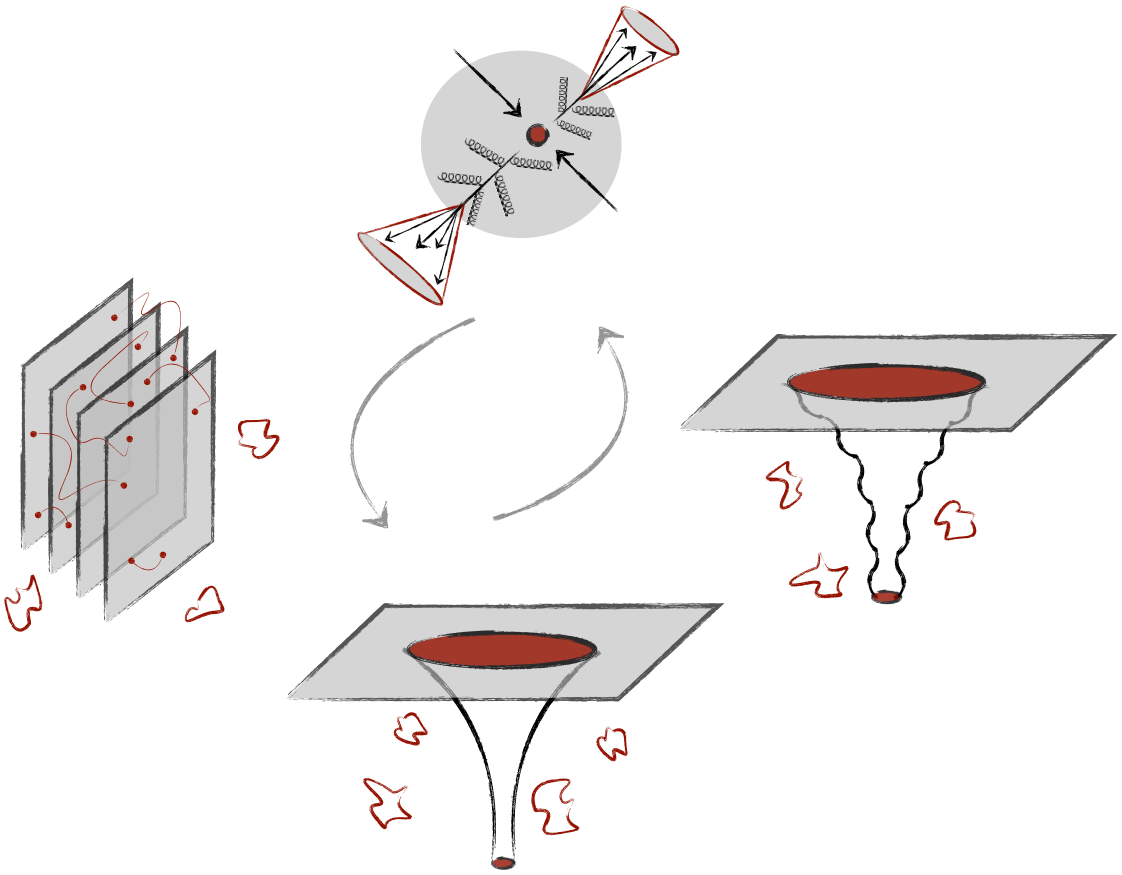

**Konrad Schade**

**Heidelberg, April 2, 2012**

# Dissertation

SUBMITTED TO THE

**Combined Faculties of the Natural Sciences and Mathematics of the Ruperto-Carola-University of Heidelberg, Germany**

FOR THE DEGREE OF

**Doctor of Natural Sciences**

PUT FORWARD BY

**Dipl.-Phys. Konrad Schade**

born in Jena, Germany

Oral examination: June 11, 2012

# Applications of Holography to Strongly Coupled Plasmas

**Referees:** **Prof. Dr. Carlo Ewerz**
**Prof. Dr. Thomas Gasenzer**

## Anwendungen des Holographischen Prinzips auf stark gekoppelte Plasmen

Die vorliegende Arbeit befasst sich mit der Untersuchung universeller Eigenschaften mehrerer physikalischer Größen in stark gekoppelten Plasmen, wie sie in relativistischen Schwerionenstreuprozessen – zum Beispiel am LHC – beobachtbar sind. Im Fokus stehen hierbei der Energieverlust eines sich gleichförmig bewegenden sowie eines rotierenden Quarks, die aus der freien Energie eines statischen Quark-Antiquark ($\mathrm{Q\bar{Q}}$)-Paares extrahierte laufende Kopplung sowie der maximale Bindungsabstand (Screening-Abstand) eines $\mathrm{Q\bar{Q}}$-Paares im Plasma. Diese Observablen wurden mit Hilfe der $AdS/\mathrm{CFT}$ Korrespondenz ausgewertet. Für die Untersuchung universeller Eigenschaften wurden neben der zur konformen $\mathcal{N} = 4$ supersymmetrischen Yang–Mills Theorie dualen Gravitationstheorie auf der $AdS_5$-Raumzeit auch drei weitere bezüglich $AdS_5$ deformierte, nicht-konforme Metriken analysiert. Zwei von diesen sind zudem Lösungen von supergravitativen Bewegungsgleichungen. Es wurde gezeigt, dass die Energieverluste in allen untersuchten Modellen bei gleichförmiger und rotierender Bewegung des Quarks robust gegenüber Deformationen sind. Bei der laufenden Kopplung zeigte sich bei Deformation des Modells ein universeller Anstieg mit größer werdendem Abstand des $\mathrm{Q\bar{Q}}$-Paares, der mit Ergebnissen aus der Gitter-QCD qualitativ übereinstimmt. Im Falle des maximalen Bindungsabstandes eines $\mathrm{Q\bar{Q}}$-Paares konnte die universelle Eigenschaft, dass die konforme $\mathcal{N} = 4$ supersymmetrische Yang–Mills Theorie bezüglich des Screening-Abstands eine untere Schranke darstellt, für kleine Deformationen analytisch gezeigt werden. Dies war zuvor aufgrund numerischer Untersuchungen für alle Deformationen in den oben genannten Modellen vermutet worden.

## Applications of Holography to Strongly Coupled Plasmas

This thesis is concerned with the analysis of universal properties of several physical observables in strongly coupled plasmas as they are studied in heavy-ion collisions – for example at the LHC. The focus lies on the energy loss of a uniformly moving and of a rotating quark, the running coupling as defined via the free energy of static quark-antiquark ($\mathrm{Q\bar{Q}}$)-pairs and the maximum distance (screening distance) of a $\mathrm{Q\bar{Q}}$-pair in the hot plasma. All of them have been computed using the $AdS/\mathrm{CFT}$ correspondence. In order to discover a universal behaviour in the observables, computations have been worked out in the free gravity theory in $AdS_5$ space-time which is dual to $\mathcal{N} = 4$ supersymmetric Yang–Mills theory as well as in three deformed, non-conformal metric models. Two of these are solutions to Einstein equations derived from a supergravity action. It has been shown that the energy loss of uniformly moving and of rotating quarks is very robust in all deformed models compared to the conformal results. In the case of the running coupling the introduction of deformations leads to a universal increase for larger $\mathrm{Q\bar{Q}}$-distances. This is qualitatively consistent with lattice QCD simulations. For the screening distance a proof has been presented for the conjecture that the conformal $\mathcal{N} = 4_T$ value for the screening distance is a lower bound for small perturbations around the conformal solution. Such a behaviour had been observed before in numerical studies in all of the above-mentioned deformed metric models.

# CONTENTS


Abstract i

Contents iii

1 Motivation 1

2 Introduction to Holography 9
- 2.1 The $AdS$/CFT Correspondence . . . 11
  - 2.1.1 Heuristic Derivation of $AdS_5$ Space-Time . . . 13
  - 2.1.2 String-Theoretic Derivation – D-branes . . . 16
- 2.2 Holographic Renormalisation . . . 22
  - 2.2.1 $AdS_5$-Schwarzschild Metric . . . 23
  - 2.2.2 Temperature in $AdS_5$-Schwarzschild Space-Time . . . 25
- 2.3 First Observations . . . 26

3 Non-Conformal Metric Models 29
- 3.1 The $\mathrm{SW}_T$-Model . . . 30
  - 3.1.1 Temperature . . . 31
  - 3.1.2 Thermodynamic Observables . . . 32
- 3.2 Consistently Deformed Metric Models . . . 34
  - 3.2.1 General Metric Ansatz . . . 35
  - 3.2.2 General Einstein Equations . . . 37
  - 3.2.3 1-Parameter Model . . . 38
  - 3.2.4 2-Parameter Model . . . 42

4 Physical Observables 49
- 4.1 Einstein- and String Frame . . . 50
- 4.2 Energy Loss of a Moving Quark . . . 52
- 4.3 Running Coupling $\alpha_{\mathrm{Q\bar{Q}}}$ . . . 63
  - 4.3.1 $Q\bar{Q}$-Distance $L$ . . . 64
  - 4.3.2 Free Energy $F$ . . . 68
  - 4.3.3 Running Coupling in $\mathcal{N} = 4_T$ . . . 69
  - 4.3.4 Running Coupling in Non-Conformal Models . . . 72
  - 4.3.5 Mimicking QCD? . . . 74
  - 4.3.6 Different Length Scales . . . 77

5 Screening-Distance Conjecture **81**
5.1 $Q\bar{Q}$-Distance for Small Deformations in the $SW_T$-Model . . . 82
5.2 Linearised Einstein-Equations Approach . . . 84
5.3 Solutions of the Linearised Einstein Equations . . . 88
5.3.1 Unperturbed Horizon Solution . . . 89
5.3.2 Solutions Including Horizon Perturbations . . . 90
5.4 Linearised $Q\bar{Q}$-Distance $L^{\mathrm{Lin}}$ . . . 93
5.4.1 Einstein-Frame Computation . . . 96
5.4.2 String-Frame Computation . . . 102

6 Rotating Quarks **109**
6.1 Conformal $AdS_5$ Metric . . . 111
6.2 Conformal $AdS_5$ Black-Hole Metric . . . 115
6.2.1 $\Pi$–$R_0$ Relation . . . 118
6.2.2 String Configuration in $\mathcal{N} = 4_T$ . . . 120
6.3 Non-Conformal Metric Models . . . 121
6.3.1 $SW_T$-Model . . . 121
6.3.2 1-Parameter Deformation . . . 125
6.3.3 2-Parameter Deformation . . . 130
6.4 Energy Loss at High and Low Velocities . . . 134
6.4.1 Linear Drag Limit . . . 137
6.4.2 Vacuum-Radiation Limit . . . 140
6.4.3 Crossover Regime . . . 144

7 Summary and Conclusions **147**

Appendix **152**

A Variation of Einstein–Hilbert action **153**
A.1 Derivation of $AdS_5$ Metric . . . 153
A.2 Variation of Extended Einstein–Hilbert Action . . . 154
A.3 Curvature Properties . . . 156

B Derivation of the Temperature Formula **159**

C Worldsheet Horizon **163**
C.1 Dragging Quark . . . 164
C.2 Rotating Quark . . . 164
C.3 Local Speed of Light in the Bulk . . . 165

D Primitive of Linearised $Q\bar{Q}$-Distance Integral **167**

References **169**

Danksagung **185**

Erklärung **187**

Chapter 1

# Motivation

We live in very exciting times and there are even more fascinating and groundbreaking days ahead of us. This might be a vague statement in general but it is in particular true for the current development of fundamental physics due to a handful of pioneering experiments. Among them the ATLAS, CMS, ALICE and LHCb experiments located at CERN close to Geneva are very likely to push our knowledge about physics to a new level within the upcoming years.

At the end of 2011 the ATLAS and CMS experiments presented the status of their searches for the Standard Model Higgs boson. The discovery of this particle would be a cornerstone of the theoretical framework, called the *Standard Model*, that explains the dynamics of subatomic particles. The results are based on the analysis of data taken over the last two years at the Large Hadron Collider (LHC) at CERN, which is the largest particle accelerator in the world, and are sufficient to make significant progress in the search for the Higgs boson. Although a conclusive statement on the existence or non-existence of the elusive Higgs is still missing, the two collaborations argued that the mass range is constrained to 122 – 129 GeV (ATLAS) [1–3] with an excess of events observed around $m_{\mathrm{H}} = 126\,\mathrm{GeV}$ and 115 – 127 GeV (CMS) [4–7] with an excess around $m_{\mathrm{H}} = 124\,\mathrm{GeV}$. In addition, the CDF and DZero collaborations at the Tevatron reported an excess with a significance of $2.2\,\sigma$ that might be interpreted as coming from a Higgs boson with a mass in the region of 115 – 135 Gev [8]. It is far too early to argue that ATLAS, CMS or the Tevatron collaborations have discovered the Higgs boson, but these results have generated a lot of interest in the particle physics community and a conclusive statement is expected to be given by the end of 2012.

The ALICE collaboration – also running an experiment at the LHC – studies, inter alia, collisions of lead ions at very high energies ($\sim 2.76\,A\mathrm{TeV}$ per nucleus) in order to probe a state of matter known as the *quark-gluon plasma* (QGP), which is believed to have existed shortly after the birth of our universe (Big Bang) [9–14]. Similar results can be found at ATLAS [15–17] and CMS [18, 19]. 12 years ago, similar experiments (STAR, BRAHMS, PHOBOS and PHENIX) have been initiated to recreate this primordial environment at the Relativistic Heavy Ion Collider (RHIC) at the Brookhaven National Laboratory (BNL) at lower energies ($\sim 200 - 500\,A\mathrm{GeV}$ per nucleus) and there is evidence that they successfully created the QGP [20–23] as well. Furthermore, several results indicate that even the SPS experiments at CERN have already produced the QGP in the mid 90s [24–27]. In Fig. 1.1 a typical non-central

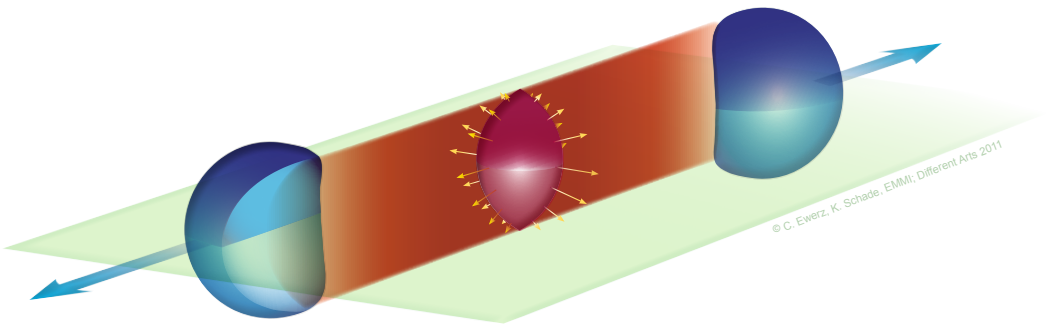


Figure 1.1: Sketch of the collision of two heavy ions. The almond-shaped region in the centre represents the expanding quark-gluon plasma.

heavy-ion collision that happens in the ALICE detector is sketched.

However, many steps in the creation and freeze out process of the QGP are still not fully understood by both experimental and theoretical physicists due to the surprising property of being strongly coupled. These strong interactions in the plasma led to the discovery of numerous interesting properties, e. g. collective behaviour like elliptic flow or charmonium suppression. However, several other aspects of this state of matter are still unclear.

To diminish the lack of knowledge this thesis tries to shed some light on the complicated problem of how to describe theoretically the QGP or non-abelian gauge theories at strong coupling in general. The most important question we want to address in this work is the following:

*What can string-theoretic approaches driven by holography tell us about strongly coupled plasmas like the QGP?*

This is a kind of guiding line through the thesis. Prior to answering this question, an understanding of the numerous challenges, experimental and theoretical physicists have to face when dealing with the QGP, is mandatory.

From a theoretical point of view, the physics happening in a heavy-ion collision is mainly governed by a particular gauge field theory called *quantum chromodynamics* (QCD). Within this framework one can understand the *strong force* which is one of the four fundamental forces in Nature describing the interaction between quarks and gluons. This force, for example, leads to the formation of protons and neutrons. The electromagnetic and weak forces are both written in terms of gauge field theories as well. Together with QCD they are the essential ingredients of the Standard Model that we have mentioned above in the context of the Higgs search. However, in the case of the gravitational force which can be described by Einstein's theory of general relativity, physicists are still searching for a quantum theory that fits into the framework of the Standard Model.

But this is not the only problem theoreticians have to cope with: although the fundamental equation (the Lagrangian) of QCD is known and presentable in one line it remains impossible to solve the associated equations for all values of the so-called *coupling parameter* $\alpha_s$. It controls the strength of interactions between the fundamental constituents of this theory which are the

quarks (fermions) and gluons (gauge bosons of SU(3) gauge group). An important property of QCD is the 'running' of the coupling that leads to the fact that interactions are not equally strong at all length scales. This is responsible for two fundamental phenomena, i. e. *asymptotic freedom* and *confinement*. The first causes interactions between particles to become arbitrarily weak at small length scales ($\sim 10^{-16}\,\mathrm{m}$), or, equivalently, at large energy scales ($\sim 2\,\mathrm{GeV}$), and corresponds to a small coupling parameter $\alpha_\mathrm{s}$ of the strong force. The latter denotes the physics phenomenon that colour charged particles (quarks and gluons) cannot be isolated. An individual observation is therefore impossible. This means that constituent quarks in a hadron (e. g. a proton) cannot be separated from their parent hadron since the coupling parameter $\alpha_\mathrm{s}$ becomes large. This happens at larger distances, or, equivalently at lower energies.

The computation of observables that probe the low-energy regime of QCD is a serious challenge due to the peculiar behaviour of the coupling constant $\alpha_\mathrm{s}$. While perturbative expansions in the coupling parameter $\alpha_\mathrm{s}$ are highly useful in the regime of small coupling, they are unreliable in the strong coupling regime, as each successive term in the series becomes larger than the previous one. This leads in the end to a break down of the approximation scheme. Another problem is the analysis of QCD at finite temperature which is necessary to study the QGP theoretically. An approach that tackles the non-perturbative sector at zero- and finite temperature goes under the name of lattice QCD [28–30]. It stands for the use of an extensive numerical machinery that allows for studying static problems at strong coupling and finite temperature, e. g. the computation of the energy density, pressure or entropy density; however, it falls short in the case of dynamical quantities, e. g. the energy loss of moving quarks (finite $T$) or scattering processes (zero $T$).

Another widely used approach is the construction of effective field theories, e. g. chiral perturbation theory [31, 32] or heavy quark effective theory [33, 34]. These are approximate theories including appropriate degrees of freedom to describe the physical phenomena occurring at a chosen length scale, while integrating out substructures and degrees of freedom at shorter distances. In addition to this, we should mention the applicability of functional renormalisation group methods [35–37] or the analysis of the Dyson-Schwinger equations that form a system of infinitely many coupled integral equations for the Green's functions of the theory.

From an experimental point of view, the general framework for studying properties of subatomic physical systems of order of $10^{-15}\,\mathrm{m}$ are scattering experiments. With the help of deep-inelastic scattering experiments where, inter alia, single protons and electrons are forced to collide, it has been possible to study the perturbative regime of QCD with great success. Whereas theorists have many problems studying finite temperature systems, this is an easy task in experiments with a lot of unforeseen results.

If normal matter is heated to sufficiently high temperatures, it is believed that a new state of matter is formed. The same happens if one compresses matter to sufficiently high densities. This new state consists of a 'soup' of quarks and gluons, instead of a sea of nucleons [38]. By soup we mean that the boundaries between nucleons are no longer well-defined. We have encountered this new state of matter – that Shuryak denoted by quark-gluon plasma [39] – in the context of the heavy-ion collisions in ALICE, ATLAS and CMS.

As we have already mentioned before, RHIC and LHC which have produced the QGP found evidence that the thermally equilibrated plasma exhibits some surprising properties. Among them, the large energy loss of high energy particles traversing the medium, known as jet quenching, Charmonium suppression and the strong collective behaviour (e. g. elliptic flow) indicate that interactions within the plasma are very strong [9–14, 20–23, 38]. This is why it is called strongly coupled plasma. Therefore, the first results of the LHC experiments are

already a perfect playground to study experimentally the non-perturbative sector of QCD. And definitely, ALICE, ATLAS, CMS are going to elicit the truth about all the essential processes occurring after the collision of heavy ions within the next five years.

Up to now – by following [38] – three different stages can be identified. Before the collision, the two colliding nuclei have the form of flat pancakes since they are Lorentz contracted ($\gamma > 100$). At this stage a concept called *colour glass condensate* [40] is an appropriate way to describe the two nuclei. After the collision ($\tau_{\text{coll}} \approx 0.1\,\text{fm}/c$), a part of the energy of the nuclei is transformed into a bunch of new particles, which rapidly thermalises at least locally. The amount of energy that is transformed depends on the centrality of the collision which is measured by the so-called *impact parameter b*. This quark-gluon plasma with a temperature of

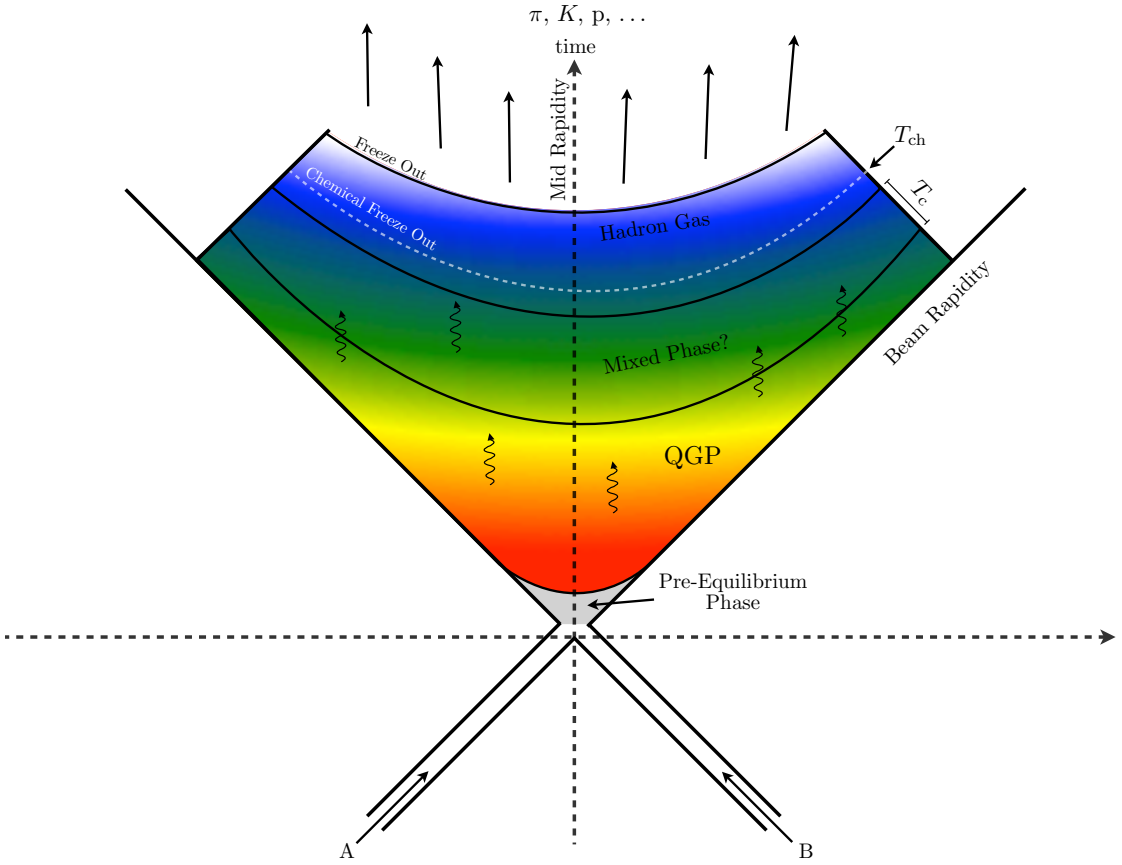


Figure 1.2: Sketch of the stages of the QGP during a heavy ion collision.

roughly $T_{\text{LHC}} \approx 1000\,\text{MeV}$ then expands and cools simultaneously and the matter hadronises into particles until the chemical freeze out at a temperature of $T_{\text{ch}} \approx 170\,\text{MeV}$ [41] is reached. Then, the final products can be observed in the detectors. This is visualised in Fig. 1.2. The problem is now that the time scale ($\tau \approx 1 - 20\,\text{fm}/c$) on which the QGP exists is very short and that a direct investigation of this state of matter is impossible. In addition to this, the initial (pre-equilibrium) and final (freeze out) stages of the heavy ion collision are theoretically difficult to treat. A full theoretical description of these phases is beyond the scope of this thesis, but for interested readers we recommend [42–44] for comprehensive reviews. Due to its strong coupling behaviour the QGP presents a problem for theoretical physicists because QCD

is hard to treat in this regime.

However, along with the success of the LHC experiments in studying the non-perturbative phase of QCD with the help of heavy-ion collisions a tremendous progress of how to theoretically treat the non-perturbative regime of QCD took place in the last eight years. This progress has been initiated by Maldacena and others in 1997, when the first practical realisation of the *principle of holography* [45, 46] was found. It is known as the *Maldacena conjecture* [47–49]. This conjecture consists of the duality between a certain gauge theory ($\mathcal{N} = 4$ supersymmetric Yang–Mills theory in four dimensions) and a string theory (type IIB string theory on an $AdS_5 \times S^5$ background). Since the gauge theory is a *conformal field theory*[1] (CFT) this conjecture is widely referred to as *AdS/CFT duality*. By the word duality we mean that both theories describe the same physics. Since those days many other dualities have been discovered between very different kinds of gauge and string theories. The $AdS$/CFT duality is highly useful due to an astonishing property. It is of the so-called *strong/weak type*. If one theory is strongly coupled, the dual one is weakly coupled and vice-versa. Thus, although describing the same physics, calculations may be easier in one theory than in the other.

This brings us back to the question posed above. One can immediately see the applications of strong/weak dualities to the study of the QGP or other non-abelian gauge theories at strong coupling [38]. By using the dual gravitational theory of QCD, computations can be done at weak coupling that lead to numerous new insights of how QCD behaves at strong coupling. Unfortunately, there is still a lot of work to be done before we can apply these techniques to QCD. Currently, the $AdS$/CFT correspondence or the more general class of *gauge/gravity* dualities is well developed for theories that include some important properties of QCD. However, up to now the exact string-theory dual of QCD has not been found. In addition to this, since it is still only a 'well-checked' conjecture, the whole theoretic framework needs to be mathematically proven. Nevertheless, in this thesis we make use of the $AdS$/CFT correspondence in order to investigate the non-perturbative regime of a large class of non-abelian gauge theories. However, due to the technical subtleties this approach has to cope with we have to rephrase the question above into a more accurate form:

*What are the possible applications of gauge/gravity dualities to strongly coupled plasmas?*

As we have already indicated above, the computation of properties of the quark-gluon plasma is one of the most interesting problems the $AdS$/CFT community has solve. Since the amount of tools available to tackle the strongly coupled, high temperature regime of QCD is very limited, gauge/gravity dualities are one of the best ways to proceed although this approach comes with its own problems. Of those, the lacking knowledge about the exact string theory dual to QCD is the most important. There are several ways how to resolve this issue [38]:

1. Many theorists are working on a proof of the gauge/gravity correspondence and try to find the string theory dual to QCD or change the basic string theory setup, e. g. by introducing 'flavor branes' in order to derive QCD-like dualities (top down approach) [50–57]. This is definitely the most elegant way, however, it is also the most complicated one.

[1] Conformal symmetry is the property of a physical system to be invariant under scale-, Poincaré- and special conformal transformations.

2. It is possible to use known gauge/gravity dualities and modify the string theory background in order to introduce some essential features of QCD (bottom up approach). This research field is often referred to as $AdS$/QCD [38, 58–69].

3. There is hope that many strongly coupled theories share some common features. By studying different kinds of strongly coupled systems one might discover a universal behaviour in some observables which is model independent [38]. Such a behaviour can then be used to conjecture that it would also be applicable to QCD at strong coupling (universality approach).

In this thesis, we mainly employ the third approach and only compare to QCD data (following the second approach) when it appears appropriate. The universality approach became very successful in the case of the ratio of shear viscosity to entropy density $\eta/s$, which combines transport coefficients necessary for the hydrodynamic description of the quark-gluon plasma [70, 71]. Kovtun, Son and Starinets showed in [72] that for a large class of theories with a gravity dual, $\eta/s$ takes on the universal value of $1/4\pi$ with $\hbar$ and $k_\mathrm{B}$ set to 1. It is very surprising that this result holds for both, conformal and non-conformal theories. This insight is the origin of the famous *KSS bound conjecture* [72] which states that all physical substances should satisfy

$$\eta/s \geq \frac{1}{4\pi}\,. \tag{1.1}$$

We are now able to discuss the tasks this thesis tries to tackle. Several QGP-relevant observables will be analysed in this work, e. g. thermodynamic quantities, the static quark-antiquark ($\mathrm{Q\bar{Q}}$) distance $L$, the free energy $F$ of a static $\mathrm{Q\bar{Q}}$-pair, the running of the coupling constant $\alpha_{\mathrm{Q\bar{Q}}}$ and the energy loss $\mathrm{d}E/\mathrm{d}t$ of uniformly moving and rotating quarks, in different dual gravity theories. In order to introduce notation and terminology, computations always start in the well-known and simple gravitational background of the five-dimensional anti-de Sitter ($AdS_5$) space-time which is – according to the Maldacena conjecture – dual to $\mathcal{N}=4$ supersymmetric Yang–Mills (SYM) theory in four dimensions. A complete derivation of the $AdS_5$ space-time will be given in Sec. 2.1.1 but until then we can think of this space-time as the ordinary four-dimensional Minkowski space-time plus an addition coordinate often denoted by $z$ or $r$ as well as an overall scaling factor proportional to $z^{-2}$. The real focus then lies on the analysis of the aforementioned observables in a large class of deformed $AdS_5$ space-times that correspond to non-conformal gauge theories. These metric models will be introduced in Chap. 3. In doing so we hope to find universal properties for the above-mentioned quantities in all theories under investigation. Furthermore, we will see that some of the results are even very close to real-world QCD which tempts us to pose the question whether our models are good enough to mimic QCD. This is not a completely unrealistic task since even the prototype realisation of the holographic principle, which is the Maldacena conjecture, can be applied to finite temperature QCD if temperatures are large enough.[2] This will be explained in greater detail in Sec. 2.3.

Now, the main structure of this work is as follows:

- In Chapter 2 we will give a brief introduction to the holographic principle and derive its prototype realisation, which is the $AdS_5/\mathrm{CFT}_4$ correspondence, in two ways. Firstly,

[2] Above $2T_\mathrm{c}$ with $T_\mathrm{c}$ being the critical temperature in QCD, $\mathcal{N}=4$ supersymmetric Yang–Mills theory and QCD are comparatively close to each other.

a *heuristic* derivation is presented (see Sec. 2.1.1); this represents a very descriptive way to obtain the five-dimensional metric of the $AdS_5$ space-time. It defines the weakly coupled gravitational theory dual to $\mathcal{N} = 4$ supersymmetric Yang–Mills theory in four dimensions at strong coupling. Secondly, for the reader interested in string theory the $AdS_5$ metric can be obtained by a string-theoretic derivation using well-known objects in string theory that are called D branes in Sec. 2.1.2. More relevant for the analysis of the QGP is a finite-temperature generalisation. This will be reviewed using very elementary methods in Sec. 2.2 leading to the $AdS_5$-Schwarzschild or $AdS_5$ black-hole metric which is the essential ingredient for the understanding of the subsequent chapters.

- In Chapter 3 we will introduce three different gravity theories, each of them being a deformation of the $AdS_5$ space-time. The first and simplest deformation is the so-called finite temperature soft-wall model (SW$_T$-model) which is not consistent but widely used in the literature [64, 73]. In addition, two consistent models (1-parameter and 2-parameter model) will be derived and analysed. In this context, consistency means that the metric solution of the deformed space is a solution to Einstein equations derived from a 5D Einstein–Hilbert-scalar action $S_{\text{EHs}}$. This is a five-dimensional Einstein–Hilbert action including a scalar that might be the dilaton in string theory. On the gauge-theory side, these deformations correspond to the breaking of conformality. Therefore, basic thermodynamic observables like the energy density $\varepsilon$, entropy density $s$, pressure $p$ and $\frac{\varepsilon-3p}{T^4}$ will be computed in order to estimate the amount of non-conformality that has been introduced.

- In Chapter 4 we will then study physical observables in order to analyse the potential existence of a universal behaviour. A full systematic discussion of the observables listed below has not been worked out for the above-mentioned class of models in the literature before. The energy loss of a moving parton (drag force $\mathrm{d}p/\mathrm{d}t$), the Q$\bar{\text{Q}}$-distance $L$, free energy $F$ and the running coupling $\alpha_{\text{Q}\bar{\text{Q}}}$ will be investigated. The latter quantity is only known for the original, conformal $AdS_5$ case [74] and has not been studied in the context of a larger class of non-conformal metric models yet. Unfortunately, we will conclude that apart from the quark-antiquark distance and the running coupling no other observable exhibits a systematic change in one direction, but all quantities are at least very robust when deforming the conformal system. The results of this analysis will be compared to QCD lattice computations in order to check the applicability of our models to real-world physics in Sec. 4.3.5.

- In Chapter 5 a particular property of the Q$\bar{\text{Q}}$-distance will be discussed. In our previous work [75, 76] we conjectured that the maximal value of the Q$\bar{\text{Q}}$-distance, which is called *screening distance* $L_{\text{S}}$, is bounded from below by the conformal $\mathcal{N} = 4$ SYM theory for a large class of theories. A numerical analysis for a large class of non-conformal models has confirmed this statement that can be cast into the following form

$$(L\pi T)_{\text{S}}^{\text{Def}} > (L\pi T)_{\text{S}}^{\mathcal{N}=4_T} , \tag{1.2}$$

  where we use the dimensionless combination $(L\pi T)_{\text{S}}$. However, an analytic proof is still to be found. Thus, small perturbations around the conformal solutions will be studied in the context of linearised Einstein equations. For the most general metric ansatz that satisfies the overall symmetries this conjecture will be proven in Sec. 5.4.

- In Chapter 6 the energy loss of a rotating quark will be analysed. This quantity allows for studying the energy loss of accelerated/decelerated particles in the presence of a strongly coupled, high temperature plasma that is very interesting for current LHC experiments. The exact string configurations will be worked out in all relevant non-conformal models. Furthermore, it is possible to distinguish three different regimes of energy loss: a drag regime (Sec. 6.4.1) where the rotating quark loses energy via elastic collisions, a radiation regime (Sec. 6.4.2) where the quark emits synchrotron radiation as if it would be in vacuum and a crossover regime (Sec. 6.4.3) where a destructive interference between collisional and radiation-induced energy loss can be observed. The computation will be reviewed in the $AdS_5$ case first, before we extend it to above-mentioned deformed models. Such a computation has not been done in the literature before. Again, the search for universal properties will be the guiding principle in this chapter.

- Finally, in Chapter 7, we draw our main conclusions about the study of universal properties in the physical observables that have been discussed. Among them only the screening distance and the running coupling show a systematic change in one direction for all theories under investigation. The other quantities are remarkably robust in a large regime that we find to be 'physically' meaningful. Finally, we mention open questions and prospects for future investigation. There, we focus on the additional possible content that can be introduced into the Einstein–Hilbert action, e. g. a gauge field $A^\mu$ leading to a non-vanishing chemical potential [77]. This is a straightforward and computationally tractable extension of our models.

Chapter 2

# Introduction to Holography

In this thesis we work with a particular realisation of the so-called holographic principle which is known as the $AdS/\mathrm{CFT}$ correspondence. The motivation and discussion of the latter is the essential part of this chapter. Due to its property of being very counterintuitive an ad hoc derivation of the $AdS/\mathrm{CFT}$ correspondence right from its string-theoretic foundation does not provide us with the amount of intuition which is necessary in order to deal with applications of this conjecture. Thus, it is very helpful to start with the general concept of holography to find a way through this intriguing theory. Here, we follow the introduction of Dobado in [78]. Afterwards the most important details of the $AdS/\mathrm{CFT}$ correspondence will be motivated. However, a complete derivation is far beyond the scope of this thesis. Good reviews on the subject are [79–86]. The focus here is on applications of this approach to strongly coupled plasmas; this is the main topic of the thesis and will be studied in detail in Chap. 4, 5 and 6.

The principle of holography was originally proposed to shed some light on the always obscure interplay between quantum mechanics and general relativity. A first intention was to find a way to solve the so-called *information paradox* [78, 87]. This is a paradox occurring when studying the thermodynamics of black holes. Stephen Hawking argued in the 70s that black holes emit black body radiation [88], which was a very surprising result that is still not confirmed experimentally. This radiation is thermal and can be related to a temperature $T = \frac{\kappa}{2\pi}$ with $\kappa$ denoting the surface gravity at the horizon of the black hole. This led to an explicit expression of the black hole entropy given by Bekenstein [89]

$$S_{\mathrm{BH}} = \frac{A}{4\,G_{\mathrm{N}}}\,\frac{c^3}{\hbar}\,, \tag{2.1}$$

with $A$ denoting the area of the black hole horizon and $G_{\mathrm{N}}$ being Newton's constant. From now on we will use Planck units defined by $c = G_{\mathrm{N}} = \hbar = k_{\mathrm{B}} = 1$ in most of our computations. An equation of entropy proportional to the area is incompatible with its usual understanding in the realm of non-gravitational physical systems where it scales like the volume since it is an extensive quantity. In addition to this, a problem arises when studying the evaporation of black holes. There is a loss of unitarity[1] arising in the analysis of the evolution of a gravitationally

[1] Unitarity originally denotes a restriction on the allowed evolution of quantum systems that ensures, inter alia, that the sum of probabilities of all possible outcomes of any event is always 1.

collapsed system. Since Hawking this problem is known as the (*information paradox*) [87]. It can be understood – according to Dobado [78] – by considering the case in which the initial state of the collapsed matter is a pure quantum state. After the black hole has evaporated, we are left with thermal radiation which has to be described by a density matrix. Thus, many prior quantum states can evolve into the same thermal state which cannot be a unitary process – described by a unitary operator – due to the loss of information. A possible solution to this problem[2] is the famous *holographic principle* that 't Hooft [45] suggested (followed by Susskind [46]). The basic idea can be cast into the following general form [78]:

> *The full physical description of some given region $\mathcal{R}$, in a d-dimensional universe (including gravity) with a $(d-1)$-dimensional boundary $\partial\mathcal{R}$, can be reflected in processes taking place in $\partial\mathcal{R}$.*

A fundamental consequence of this principle is an insight due to Susskind [46] stating that the maximum information a system can store scales with the area of its external surface and not with the volume as one might think:

$$S_{\mathrm{m}} \leq \frac{A}{4} \quad — \quad \text{'}\textit{Spherical Entropy Bound}\text{'}\,, \tag{2.2}$$

where $S_{\mathrm{m}}$ is the entropy of the matter and radiation content in this particular volume of space. This is closely related to the entropy of a black hole in (2.1). Therefore, information is not lost when 'falling' into a black hole but gets imprinted on the horizon leading to its conservation. Equation (2.2) then ensures that all of the information fits on the surface. This is in clear contradiction to our normal experience according to which the information capacity – analogous to the entropy – scales like the volume.

Of course, the formulation above is too vague to be of practical interest but still the holographic principle is regarded as a major clue since any fundamental theory should incorporate this counterintuitive result, e. g. Quantum Field Theories (QFT) including strong gravitational effects and string theory [96]. In the case of a QFT that includes gravity Dobado presented in [78] a nice example that is reviewed in the following. Consider this system to be defined in a finite volume $V$ in order to avoid infrared divergences. One might think that the number of degrees of freedom scales with the volume $V$ of the system and not with the external area even when ultraviolet divergences are regulated by introducing an energy cut-off. This is not the case since an enormous number of field configurations remains that are gravitationally unstable [97]. These states would collapse into a black hole. After removing all of them as well we are left with a finite number of states that scale with the external area of the system in agreement with the holographic principle.

Applied to the more concrete problems we are dealing with, the holographic principle can be recast into the following form which is visualised in Fig. 2.1:

> *The physics of a $(d+1)$-dimensional theory including gravity can be described by a non-gravitational d-dimensional boundary field theory.*

The most famous and first application of this principle is the $AdS$/CFT correspondence we have mentioned in Chap. 1. It basically relates the physics of a string theory – including gravity – on a five-dimensional anti-de Sitter ($AdS_5$) background to the physics of a four-dimensional maximally supersymmetric conformal field theory (CFT) defined on the boundary of the $AdS_5$

[2] For other approaches see [90–95].

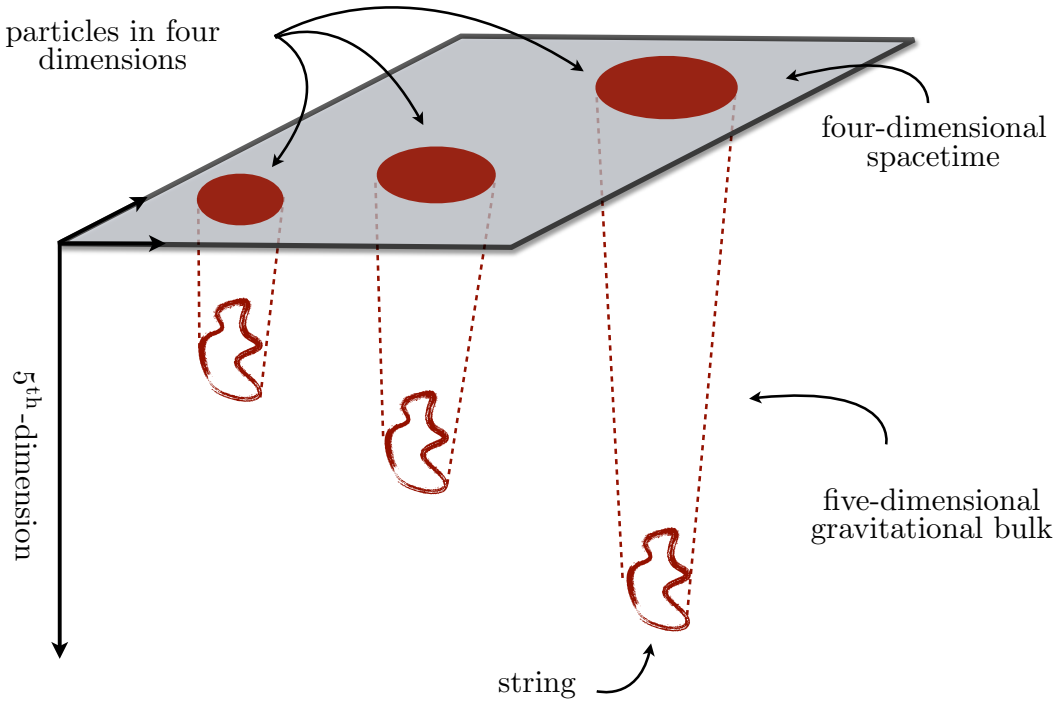


Figure 2.1: Visualisation of the holographic principle with a field theory living at the boundary and a string theory containing closed strings in the so-called *bulk*.

space-time [47, 48]. A detailed discussion of what this correspondence is all about and why we can use it to investigate strongly coupled systems in the realm of high-energy physics will be the subject of the following section.

## 2.1 The $AdS$/CFT Correspondence

The basic idea of relating a $(d+1)$-dimensional string theory to a quantum field theory with one dimension less was again conjectured by Susskind and 't Hooft by relating the Bekenstein–Hawking formula ($S \propto A$) to the property of any (local) QFT where entropy scales like volume $V$. The subsequent derivation follows [79–86].

In 1997, it was a seminal work by Maldacena [47] to find the first concrete realisation of the holographic principle[3] named $AdS_5/\mathrm{CFT}_4$ correspondence. By considering the low-energy limit of $N_\mathrm{c}$ parallel D3 branes he conjectured that type IIB String Theory on $AdS_5 \times S^5$ is dual to $\mathcal{N} = 4$ SU($N_\mathrm{c}$) supersymmetric Yang–Mills theory (without gravity) in four dimensions that lives on the boundary of $AdS_5$ space-time. Here, $\mathcal{N} = 4$ SYM is the maximally supersymmetric theory in four dimensions with $\mathcal{N} = 4$ supersymmetries. It contains a massless spin-1 gluon, 4 massless spin-$\frac{1}{2}$ gluinos (Weyl fermions) and 6 massless spin 0 scalars, all of them being in the adjoint representation [98–100]. This theory has a vanishing beta function to all orders in the

[3] Apart from $AdS$/CFT correspondence many other names are common for describing realisations of the holographic principle, e. g. gauge/gravity dualities, strong/weak correspondence, holographic dualities, ...

coupling constant [101–107]. Thus, $\mathcal{N}=4$ supersymmetric Yang–Mills theory[4] is a conformal theory. Conformal symmetry preserves, among other things, scale invariance and includes the Poincaré symmetry. In addition to this, $\mathcal{N}=4$ has no fundamental quarks. These two properties help us when applying it to real-world problems. The essentials of $\mathcal{N}=4$ at finite temperature ($\mathcal{N}=4_T$) will be outlined in Sec. 2.3.

From our naive understanding of gauge/gravity dualities we might think that this correspondence is unrelated to the holographic principle, since the gravity side (type IIB string theory) is living in a 10-dimensional space-time. However, we will focus on the limit in which the number of colours $N_\mathrm{c}$ and the effective coupling of the gauge theory in the large-$N_\mathrm{c}$ limit – that is called 't Hooft coupling ($\lambda = g_\mathrm{YM}\, N_\mathrm{c}^2$) – are assumed to be large. In this limit string theory in $AdS_5 \times S^5$ is described by its low-energy supergravity approximation, which in turn can be reduced to a gravity theory on pure $AdS_5$ space-time. Since the $S^5$ does not lead to any dynamical consequences, we will neglect the terms in the metric. This five-dimensional gravity theory is then dual to the four-dimensional large-$N_c$ supersymmetric Yang–Mills theory on the boundary and obeys the holographic principle.

Before we will present two explicit procedures how the $AdS_5$ space-time arises in the derivation of the $AdS_5/\mathrm{CFT}_4$ correspondence an obvious question appears:

*How can we ensure that a particular gauge theory and a gravitational theory describe the same physics?*

Although we might believe now in the existence of such a duality, it is still not clear what exactly is mapped from one side onto the other. The essential core of all dualities – according to [108] – is the assumption that there is a relation between partition functions (with Euclidean signature) of a $(d+1)$-dimensional string theory living in the so-called *bulk* and a $d$-dimensional QFT – living at the boundary of the bulk theory – which can be written as

$$Z_\mathrm{QFT}[\phi_0] \equiv \left\langle \exp\left(-\int \mathrm{d}^d x\, \phi_0 \mathcal{O}_\phi\right)\right\rangle_\mathrm{QFT} = Z_\mathrm{bulk}[\phi|_\mathrm{bdry} \sim \phi_0]\,. \tag{2.3}$$

$Z_\mathrm{QFT}$ and $Z_\mathrm{bulk}$ in (2.3) are functionals of a generating source $\phi_0$. On the right hand (bulk) side of (2.3), $\phi_0$ is the boundary (bdry) value of a scalar field $\phi$ living in the bulk, whereas in the QFT $\phi_0$ is the source to a dual operator $\mathcal{O}_\phi$. This relation was proposed in [49, 52]. In general, (2.3) is a statement for all values of the 't Hooft coupling $\lambda$ and the number of colours $N_c$, however, the right hand side simplifies in the limit when the bulk theory becomes classical. We will see in the next paragraphs that the string theory that lives in the bulk reduces to a classical, low-energy supergravity description in limit of large $N_c$ and large 't Hooft coupling $\lambda$. The classical supergravity theory is then equivalent to a saddle point approximation of the bulk partition function,

$$Z_\mathrm{bulk}[\phi_0] = \exp\left(-I_S(\phi)\right). \tag{2.4}$$

Here, $I_S(\phi)$ is the on-shell action of the gravity theory with boundary condition $\phi|_\mathrm{bdry} = \phi_0$.

Equation (2.3) is the basic tool to check whether a gauge theory is dual to a string theory and will be used in Chapter 4 to derive the dual expressions of known gauge theory quantities, like the distance and free energy of a heavy $\mathrm{Q\bar{Q}}$-pair and the energy loss of a moving quark, in the dual gravitational theory. In addition to the agreement of the partition functions in (2.3),

[4] $\mathcal{N}=4$ SYM theory will be abbreviated by $\mathcal{N}=4$ for short.

the amount of symmetries of each theory can be compared with each other and has to match exactly.

By virtue of (2.3) we know what to do when dealing with possible candidates for a gauge/gravity duality. However, to find those is by no means trivial. We will discuss in the subsequent Sec. 2.1.1 how a particular duality – the $AdS_5/\mathrm{CFT}_4$ correspondence – can be motivated heuristically without using any string theoretical terminology, followed by a more stringy description where the main facts and relations are stated. As already mentioned before, a complete and thorough derivation of this duality is not the focus of this thesis. Nevertheless, the content of Secs. 2.1.1 and 2.1.2 will fit for all subsequent problems this thesis deals with.

### 2.1.1 Heuristic Derivation of $AdS_5$ Space-Time

We want to motivate the $AdS$/CFT correspondence from a general gauge theory perspective, explaining why such a duality is possible. The following subsection is thus more heuristic without going into any details about string theory and D-branes, but may provide us with a more intuitive understanding why gauge/gravity dualities should exist. For more information about this way of motivating the $AdS_5/\mathrm{CFT}_4$ correspondence [86] is a good review to start with. The subsequent motivation follows the explanations given by Casalderry-Solana *& al.* in [86].

There, they focus on a quantum field theory in $d$-dimensional Minkowski space-time together with a short-distance cut-off $\varepsilon$. An important property of many physical systems is that degrees of freedom at widely separated scales are decoupled from each other. Thus, by organising the relevant physics in terms of energy, or equivalently, length scales allows us to find so-called *effective theories*. If we are interested for example in properties of the system at a certain length scale $z \gg \varepsilon$, we obtain an effective theory at $z$ by integrating out short-distance degrees of freedom. A systematic way of deriving effective theories at different length scales $z$ is the definition of a *renormalisation group (RG) flow*. Such an RG flow contains a continuous family of effective field theories in $d$-dimensional Minkowski space-time labelled by the scale $z$. Casalderry-Solana *& al.* argued that this family of $d$-dimensional theories along with an additional scale $z$, which has now the meaning of an additional spatial coordinate, can be interpreted as a single $(d+1)$-dimensional theory. An illustration of this process can be found in Fig. 2.2(a). Up to this point this construction owns inter alia two interesting properties:

1. The $(d+1)$-dimensional theory should have a reparameterisation invariance in the $z$-coordinate, since the physics of the original $d$-dimensional theory does not change under reparameterisations of the additional $z$ scale.

2. The amount of degrees of freedom in the $d$-dimensinal should be idential to the $(d+1)$-dimensional theory. This is clear since all physics happening at a length scale $z'$ which is larger than a particular scale $z$ (see Fig. 2.2(a)) should be describable by a $d$-dimensional effective theory defined at a length scale $z$.

Especially, the second statement fits nicely into the concept of holography that we mentioned earlier since the amount of degrees of freedom stays the same. However, it is physically not clear how to derive a coherent description of a $(d+1)$-dimensional system out of a continuous family of $d$-dimensional theories. A hint is given by the holographic principle indicating that we should favour a theory containing gravity. Again, we end up with saying that a $(d+1)$-dimensional string theory should be dual to a $d$-dimensional boundary field theory. In particular, one may

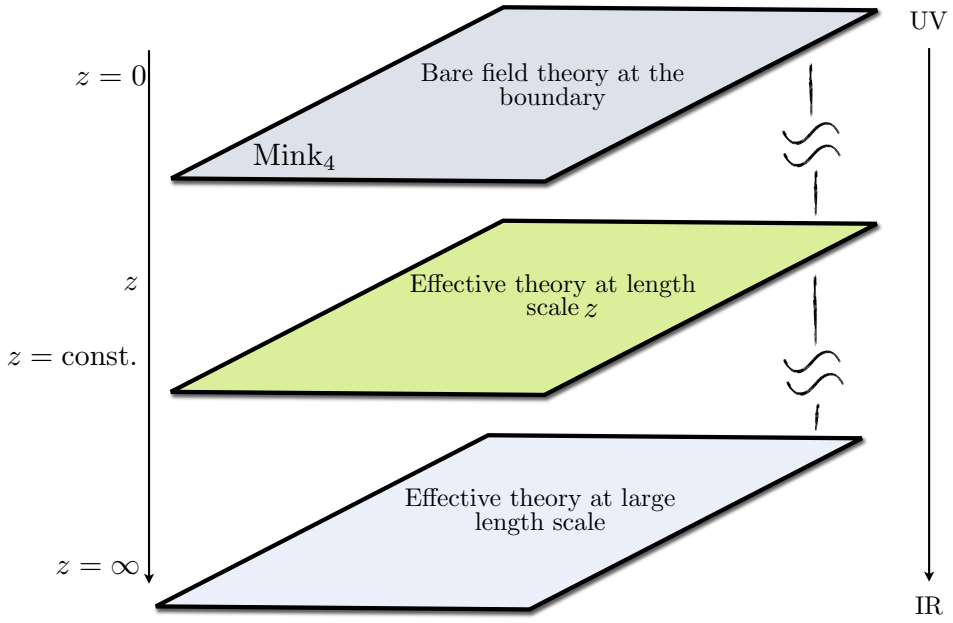


(a) Schematic picture of the RG-flow description of a four-dimensional field theory. $z$ represents the cut-off scale up to which smaller length scales are integrated out.

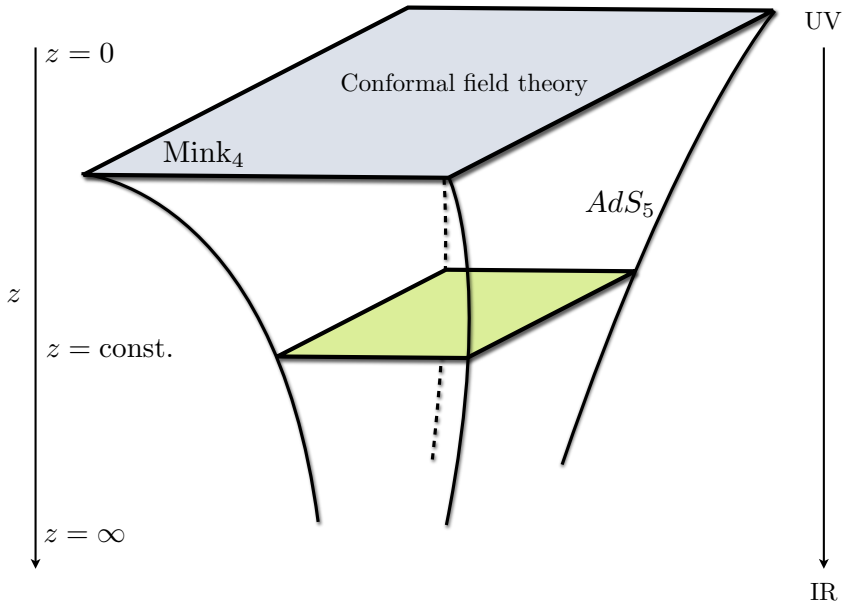


(b) Schematic picture of the geometrisation of the RG-flow with a conformal field theory at the boundary. The higher-dimensional volume represents an anti-de Sitter space-time $AdS_5$.

Figure 2.2: Heuristic derivation of the $AdS$/CFT correspondence starting with the geometerisation of the RG-flow and assuming a conformal field theory at the boundary.

think of the quantum field theory as living on the $z = 0$ slice which is the boundary of the entire space. Although some important properties of gauge/gravity dualities have emerged we are still far from being at the end of this heuristic discussion. We still do not have any clue which field theory should have a dual string theory; even less we know what kind of properties such a gravity system incorporates. A concrete hint was given by 't Hooft and his pathbreaking paper on large-$N_c$ limits [109] whose result has been already used in (2.4) when we simplified the bulk partition function $Z_{\text{bulk}}$. In the large $N_c$-limit the string theory can be approximated by its low-energy supergravity which is a non-interacting gravitational theory with some additional matter fields representing supersymmetry. Thus, by imposing some amount of symmetries on the gauge theory side we try to fix in the following the higher dimensional gravity description. The following brief derivation of the $AdS_5$ space-time has been worked out for example in [86]. The more symmetries our gauge theory contains the simpler it is to find a dual gravity theory.

According to the holographic principle we assume that a $d$-dimensional field theory can be described by a $(d+1)$-dimensional gravity theory and impose that the $(d+1)$-dimensional space-time should be consistent with $d$-dimensional Poincaré symmetry which can be made manifest in the general form of the metric

$$\mathrm{d}s^2 = \Omega^2(z)\,(-\mathrm{d}t^2 + \mathrm{d}\vec{x}^{\,2} + \mathrm{d}z^2)\,, \tag{2.5}$$

with $\Omega(z)$ being a global $z$-dependent function which has to be determined. In general not much can be said of the form of $\Omega(z)$ for a general field theory. As mentioned above, an increase of symmetries might help.

If we restrict ourselves to a conformal field theory (CFT), the additional amount of symmetry constraints determines the shape of $\Omega(z)$. One of the new symmetry conditions is scale invariance which means that the theory is invariant under the transformation

$$(t, \vec{x}) \longrightarrow (C\,t, C\,\vec{x})\,, \tag{2.6}$$

with constant $C$. The metric of the gravitational theory which is dual to the conformal field theory respects the scaling symmetry with the simultaneous scaling of the $z$ coordinate $z \to Cz$, since $z$ is an ordinary length scale defined in the boundary theory. This condition is fulfilled if $\Omega(z)$ scales as

$$\begin{aligned} \Omega(z) \longrightarrow C^{-1}\Omega(z) \quad \text{under} \quad z \longrightarrow Cz\,, \\ \Omega(Cz) = \frac{\Omega(z)}{C}\,. \end{aligned} \tag{2.7}$$

It can be solved for $\Omega(z)$ giving a unique solution that reads

$$\Omega(z) = \frac{L}{z}\,, \quad \text{with} \quad L = \text{const}\,, \tag{2.8}$$

where $L$ is called the $AdS$ length and reflects the radius of curvature of the $AdS_5$ space-time. Finally, we substitute (2.8) into (2.5) and obtain the metric $G_{\alpha\beta}$ of the anti-de Sitter space-time with curvature radius $L$ and constant negative curvature $\propto 1/L^2$:

$$\mathrm{d}s^2 = G_{\alpha\beta}\,\mathrm{d}X^\alpha \mathrm{d}X^\beta = \frac{L^2}{z^2}\,(-\mathrm{d}t^2 + \mathrm{d}\vec{x}^{\,2} + \mathrm{d}z^2)\,, \tag{2.9}$$

where $X^\alpha = (t, \vec{x}, z)$ denote the five-dimensional space-time coordinates. This is visualised in Fig. 2.2(b). The metric given in (2.9) is not only scale-invariant but has the additional property of being maximally symmetric (conformal) – meaning that it includes also special conformal transformations. In addition to this it is a solution to Einstein's equations derived from a five-dimensional Einstein–Hilbert action $S_{\text{EH}}$ with a negative cosmological constant $\Lambda$:

$$S_{\text{EH}} = \frac{1}{16\pi G_{\text{N}}^{(5)}} \int \mathrm{d}^5x\sqrt{-G}\left(\mathcal{R} - 2\Lambda\right), \quad \Lambda = -\frac{6}{L^2}\,. \tag{2.10}$$

with $G_{\text{N}}^{(5)}$ being Newton's constant in five dimensions, $G = \det(G_{\alpha\beta})$ being the determinant of the space-time metric, and $\mathcal{R}$ being the Ricci scalar. A derivation of the $AdS_5$ space-time by extremising (2.10) can be found in Appendix A. The relation to a five-dimensional Einstein–Hilbert action $S_{\text{EH}}$ is very important in the following. In order to study different gauge/gravity dualities we start with the Einstein–Hilbert action of the well-known $AdS_5$ space-time and introduce further fields leading to new metric solutions. It is believed that these solutions describe different dual field theories, all of them being non-conformal. That is an enormous step in the direction of describing non-abelian plasmas produced in heavy-ion collisions, which is one of our guiding tasks.

Altogether, this heuristic discussion in this subsection does not lead to $\mathcal{N} = 4$ as the dual gauge theory to $AdS_5$ although it would be a candidate since the symmetries match. Apart from scale invariance, a $d$-dimensional conformal field theory has $d$ special conformal transformations as additional symmetries forming the $d$-dimensional group $SO(2, d)$. Not by accident, the isometry group of the $AdS_d$ space-time is also $SO(2, d)$ due to its property of being maximally symmetric. This is a non-trivial hint that both theories describe the same physics. Another check would be the matching of gauge invariant operators on the field theory side with the fields living in $AdS$ space related via their partition functions (2.3). More precisely, the mass dimension of these fields have to be the same as the scaling dimensions of the gauge theory operators.

The current stage of our gauge/gravity duality so far is visualised in Fig. 2.2 and can be formulated in the following way:

*There should be a conformal field theory that has a string theory description in $AdS_5$ space-time.*

Further details and relations of both theories will be reviewed briefly in a string theory context in the subsequent section.

### 2.1.2 String-Theoretic Derivation – D-branes

The original motivation for a gauge/gravity duality is based on a remarkable discovery made by Polchinski in the mid 90s [110, 111]. He showed that string theory is not only a theory of strings but includes also extended membrane-like objects, called *branes*. D-branes – the D denotes 'Dirichlet' – are objects that serve as endpoints for open strings. Therefore, a typical string theory – we will specialise to a type called IIB string theory – consists of two types of excitations: Closed strings with no endpoints and open strings which have endpoints on a D-brane. Along with these modes the theory is characterised by the coupling constant $g_s$ and by the length of the strings $l_s$. In this paragraph we follow the detailed explanations in [38, 79–86].

In order to derive our desired duality we consider in the following a ten-dimensional type IIB string theory in the background of a stack of $N_c$ D3-branes which are located on top of each other. This is visualised in Fig. 2.3. Here, a D3-brane is a $(3+1)$-dimensional membrane with Dirichlet boundary conditions. $N_c$ is just a pure number telling us the number of single branes. The subscript '$c$' is in anticipation of the later duality since $N_c$ will be the number of colours in the dual gauge theory. The whole concept of the $AdS$/CFT correspondence is now based on considerations of the low-energy dynamics of this system from two different viewpoints.

In the first description we consider the D3-branes as endpoints of open strings in the limit of low energy. This low-energy assumption is necessary since a string theory is located at very high energies at order of the Planck-energy ($10^{19}\,\mathrm{GeV}$) or Planck-length ($10^{-33}\,\mathrm{cm}$). At lower energies strings behave like normal pointlike objects that can be adequately described by ordinary point particle theories, which is important to find a duality including gauge theories. Thus, the low-energy regime is equivalent to the limit of small string length $l_\mathrm{s}$:

$$l_\mathrm{s} = \sqrt{\alpha'} \to 0\,, \tag{2.11}$$

where $\alpha'$ is the so-called Regge slope which is related to the tension of the string via $T = (2\pi\alpha')^{-1}$.

An action describing the dynamics of such a physical system has three components resembling the string content:

1. $\boldsymbol{S_{\mathrm{brane}}}$ is the action governing the dynamics of the open strings living on the $N_\mathrm{c}$ D3-branes. This open string spectrum consists of a finite number of massless modes and an infinite tower of massive string modes with masses of order $m_\mathrm{s} \sim 1/l_\mathrm{s}$. We follow Casalderrey-Solana *& al.* [86] in this paragraph. Let us focus on the massless open string spectrum of $N_\mathrm{c}$ D3-branes separated by a distance $r'$. Open strings with both endpoints on the same brane give rise to massless gauge fields which can be denoted by $(A_\mu)^1{}_1$, $(A_\mu)^2{}_2$, …, $(A_\mu)^{N_\mathrm{c}}{}_{N_\mathrm{c}}$ with $\mu = 0,1,2,3$ for a D3 brane. The upper (lower) index labels the brane where the strings start (end). In addition there are six scalar fields $\phi^i(x)$, $i = 1,\dots,6$ as well as their superpartners which can be neglected in the present discussion. Along with the massless string modes there are strings connecting different branes which give rise to additional vector fields $(A_\mu)^i{}_j$, $i \neq j$; $i,j \in \{1,\dots,N_\mathrm{c}\}$ that have a mass proportional to the tension of the string times the distance of the branes, i. e. $m = r'/2\pi\alpha'$. In the case where branes lie on top of each other these modes become massless as well and altogether these massless vector fields correspond precisely to the gauge fields of a non-abelian $\mathrm{U}(N_\mathrm{c})$ gauge group [112]. In the low-energy limit the extremely massive modes can be integrated out and the dynamics is solely given by the massless gauge fields and scalars above, forming a non-abelian gauge theory which is $\mathcal{N} = 4$ supersymmetric Yang–Mills theory with gauge group $\mathrm{U}(N_\mathrm{c})$ in four dimensions [98–100]. The $\mathrm{U}(N_\mathrm{c})$ can be decomposed into

$$\mathrm{U}(N_\mathrm{c}) = \mathrm{SU}(N_\mathrm{c}) \times \mathrm{U}(1)\,. \tag{2.12}$$

The U(1) subgroup of (2.12) describes a motion of the branes' centre of mass which decouples from the inter-brane dynamics due to the overall translation invariance, leaving us with a $\mathcal{N} = 4$ SYM theory with gauge group $\mathrm{SU}(N_\mathrm{c})$.

2. $\boldsymbol{S_{\text{bulk}}}$ is the action governing the dynamics of the closed strings living far away from the stack of D3-branes. This is a supergravity theory coupled to massive modes of the string. Since the strength of interactions between the closed strings is controlled by Newton's constant $G_{\text{N}}^{(10)}$, which leads to a dimensionless coupling at energy $E$ scaling like $G_{\text{N}}^{(10)}\, E^8$, we have vanishing interactions at low energies. In summary, at low energies only free supergravity without any massive modes (see the discussion above) remains.

3. $\boldsymbol{S_{\text{int}}}$ is the action governing the interactions between $S_{\text{bulk}}$ and $S_{\text{brane}}$.

The final action has then the form

$$S = S_{\text{bulk}} + S_{\text{brane}} + S_{\text{int}}\,. \tag{2.13}$$

In the low-energy limit $\alpha' \to 0$, the massive strings can be integrated out and become infinitely heavy because the mass of the strings scales like $1/l_{\text{s}}$. In deriving $\mathcal{N} = 4$ as the correct low-energy theory an important relation between the gauge theory coupling $g_{\text{YM}}$ and the string coupling $g_{\text{s}}$ can be found:

$$g_{\text{YM}}^2 = 4\pi g_{\text{s}}\,. \tag{2.14}$$

That this relation is indeed true can be seen in the following way. In the low-energy limit $g_{\text{YM}}$ is the coupling of the above-mentioned massless gauge fields $(A_\mu)^i{}_j$. However, out of two open strings governed by the $g_{\text{YM}}$ open string coupling, we can build up a closed string governed by the $g_{\text{s}}$ coupling which gives rise to the quadratic dependence of the two couplings.

Analogous to the interactions between closed strings the interactions between the closed and open string sector can be neglected leading to:

$$S_{\text{int}} \propto \sqrt{G_{\text{N}}^{(10)}} \sim g_{\text{s}}\, \alpha'^2 \xrightarrow{\alpha' \to 0} 0\,. \tag{2.15}$$

Thus, we arrive at a free (non-interacting) supergravity bulk theory which is decoupled from the open string sector. In summary, the low-energy limit of this system consists of two fully decoupled regions (see Fig. 2.3): a $\mathcal{N} = 4$ SYM theory living on the branes and free supergravity in the bulk.

The second description starts by realising that $N_c$ D3-branes on top of each other carry considerable amount of energy leading to a curvature of the space-time. Horowitz and Strominger found in [113] that the resulting supergravity equations of motion allow black-hole type solutions for the metric given by

$$\mathrm{d}s^2 = \frac{1}{\sqrt{1 + L^4/r^4}} \left( -\mathrm{d}t^2 + \mathrm{d}\vec{x}^{\,2} \right) + \sqrt{1 + \frac{L^4}{r^4}} \left( \mathrm{d}r^2 + r^2 \mathrm{d}\Omega_5^2 \right), \tag{2.16}$$

which is called an *extremal solution* in the supergravity context [114, 115]. With $\vec{x}$ we denote the three-dimensional space, $r$ is a radial coordinate of the remaining six-dimensional space orthogonal to the 3D-space and $\Omega_5$ is the corresponding five dimensional angular element. Here, $L$ denotes the characteristic length scale in this system which is the *curvature radius* of the space-time and is related to the other quantities via

$$L^4 = 4\pi\, g_{\text{s}}\, N_{\text{c}}\, l_{\text{s}}^4 \quad \Longleftrightarrow \quad L^8 = 2\pi^{-4}\, G_{\text{N}}^{(10)}\, N_{\text{c}}^2, \tag{2.17}$$

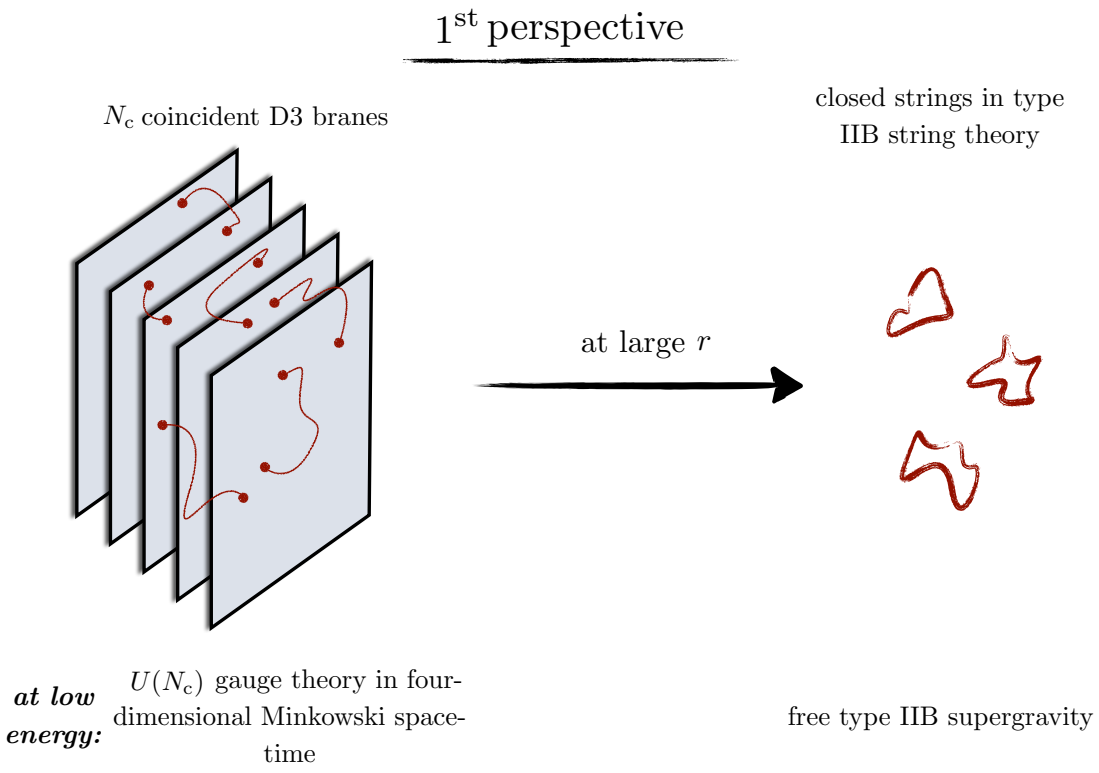


Figure 2.3: Visualisation of the first perspective of a stack of $N_c$ D3-branes in a flat 10-dimensional Minkowski space-time. The low-energy description consists of a $U(N_c)$ gauge theory theory in $(3+1)$ dimensions.

with $G_N^{(10)} = 8\pi^6 g_s^2 \alpha'^4$. It can also be understood as the length scale characteristic of the range of the gravitational effects of $N_c$ D3-branes. At $r = 0$ we have a singularity in this metric. Along with this metric there are further massless excitations (scalar dilaton and five-form) which can be neglected for the moment in the derivation of the $AdS$/CFT correspondence. As indicated in Fig. 2.4 the second description consists of the ten-dimensional Minkowski space-time far away from the branes and a 'throat' geometry of the form $AdS_5 \times S^5$ close to the branes which is given by

$$ds^2 = \frac{r^2}{L^2}\left(-dt^2 + d\vec{x}^2\right) + \frac{L^2}{r^2}dr^2 + L^2 d\Omega_5 \,. \tag{2.18}$$

That this is indeed the $AdS_5$ space-time mentioned in sec. 2.1.1 can be seen by applying a coordinate transformation of the form $z = \frac{L^2}{r}$ which directly yields (2.9).

First, we have to note that in this description only closed strings propagate since there are no open strings. The low-energy limit now consists of focusing on excitations that have arbitrarily low energy with respect to an observer in the asymptotically flat Minkowski space-time. Again, we find two distinct sets of low energy excitations which are decoupled. One set is located in the flat Minkowski region whereas the other lives in the throat space-time. In analogy to the first description the massive closed string modes in the bulk can be integrated out and the interactions can be neglected in the low-energy limit leaving free, massless supergravity. In the throat region, however, the whole tower of massive string excitations survives after taking

$\alpha' \to 0$. This can be understood – according to Nastase in [85] – by computing the relation between the energy $E_\mathrm{p}$ of any kind of object at a point $r$ and the corresponding energy $E$ measured at infinity which is given by

$$E_\mathrm{p} \sim \frac{\mathrm{d}}{\mathrm{d}\tau} = \frac{1}{\sqrt{G_{00}}}\frac{\mathrm{d}}{\mathrm{d}t} \sim \frac{1}{\sqrt{G_{00}}}E \quad \Longrightarrow \quad E = \left(1 + L^4/r^4\right)^{-1/4} E_\mathrm{p} \sim r\, E_\mathrm{p}\,. \tag{2.19}$$

This means that for fixed $E_\mathrm{p}$, as $r \to 0$, the energy observed at infinity ($E$) goes to 0 due to the gravitational redshift. Consequently, a closed string of high energy close to the throat singularity at $r = 0$ may have an arbitrarily low energy as seen by an observer at infinity, provided the string is located sufficiently deep down the throat. As we focus on lower and lower energies the massive string modes fall deeper in the throat and decouple from the closed string modes in the flat Minkowski space-time. We can conclude that in this description, the interacting sector of the system reduces to a string theory of type IIB in $AdS_5 \times S^5$ at low energies along with a decoupled free supergravity theory in the bulk. This is visualised in Fig. 2.4. These two descriptions can now be compared: we have found two decoupled pieces in

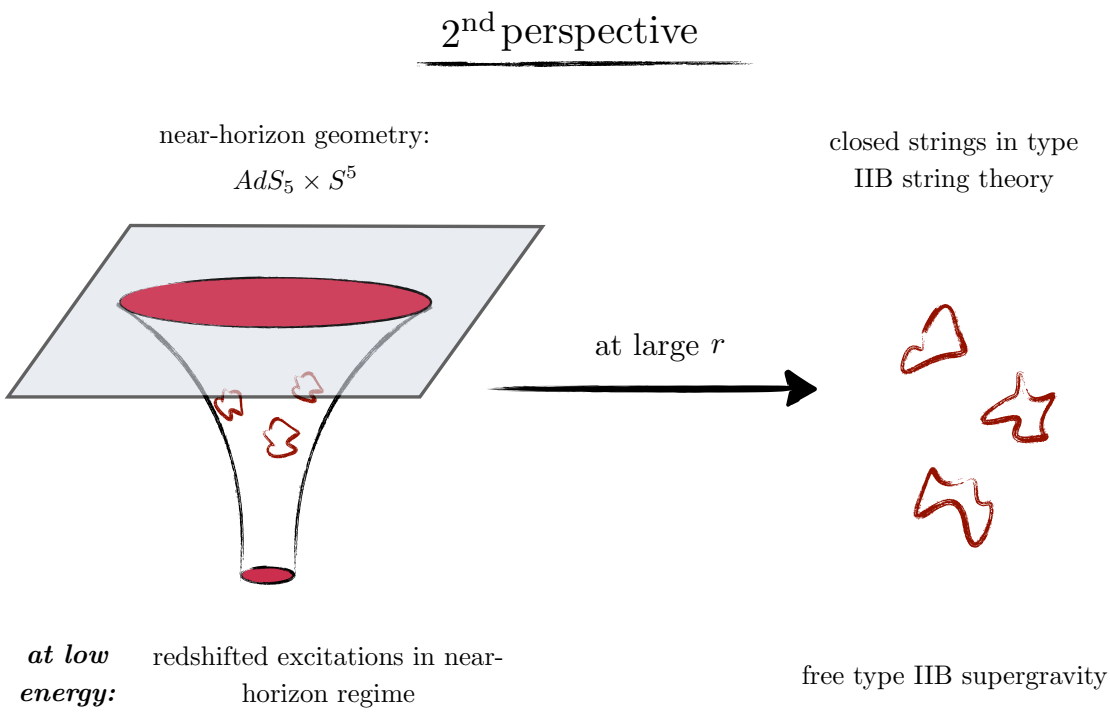


Figure 2.4: Visualisation of the second perspective of a stack of $N_\mathrm{c}$ D3-branes in a flat ten-dimensional Minkowski space-time. If the stack of D3-branes is large, the curved space-time can be described by a classical metric.

each description. The first system consists of $\mathcal{N} = 4$ SYM gauge theory and low-energy closed string modes. The second system consists of string excitations in the near-horizon regime of the singularity and low-energy closed string modes deep in the bulk. The conjecture by Maldacena states now that both systems describe the same physics [47]. After subtracting the closed string modes far away from the singularity we should equate the remaining elements giving us Maldacena's conjecture

*$\mathcal{N} = 4$ SYM theory in four dimensions is dual to type IIB string theory on $AdS_5 \times S^5$ at all scales.*

After reaching this step we have to ask two important questions, since we want to obtain a description of the QGP at the end:

- What is the advantage of describing a gauge theory, that can be tackled perturbatively, by a quantum string theory which is much harder to solve?
- What is the relation between $\mathcal{N} = 4$ SYM and QCD, since the quark-gluon plasma is a realisation of the latter theory?

The first question will be answered in the following, whereas the answer to the second question will be postponed until Sec. 2.3.

The main advantage of all types of these dualities is that they reduce to *strong/weak dualities* in certain limits meaning that whenever one part of the duality is strongly coupled the other part has to be weakly coupled, and vice versa. To show this, we recall the relations we have learned so far between parameters of the gauge and the string theory in (2.14) and (2.17):

$$g_{\mathrm{YM}}^2 = 2\pi g_{\mathrm{s}}\,, \quad L^4 = 4\pi g_{\mathrm{s}} N_{\mathrm{c}} l_{\mathrm{s}}^4\,, \quad \lambda \equiv g_{\mathrm{YM}}^2 N_{\mathrm{c}}\,. \tag{2.20}$$

In (2.20) we have defined the 't Hooft coupling $\lambda$. It describes the effective coupling of the gauge theory in the large-$N_{\mathrm{c}}$ limit. This has been shown by 't Hooft in his seminal work [109]. By taking the large-$N_{\mathrm{c}}$ limit and holding the 't Hooft coupling $\lambda$ fixed we find

$$\lambda \text{ fixed}\,, \quad N_{\mathrm{c}} \longrightarrow \infty : \quad g_{\mathrm{s}} \sim \lambda/N_{\mathrm{c}}\,, \quad l_{\mathrm{pl}}\, N_{\mathrm{c}} \sim L\,. \tag{2.21}$$

The first relation in (2.21) suggests that the coupling $g_{\mathrm{s}}$ of the string theory becomes weak, whereas the second relation tells us that the characteristic gravitational length $L$ of the $AdS_5$ system is much larger than the Plank length $l_{\mathrm{pl}}$ meaning that all quantum fluctuations of the string can be neglected and we just have to deal with a classical string theory. On the gauge theory side we are now in the limit of large number of colours. In addition, we take the limit of large 't Hooft coupling which gives us

$$\lambda \longrightarrow \infty : \quad L^4 \sim \lambda\, l_{\mathrm{s}}^4\,. \tag{2.22}$$

The gauge theory is thus strongly coupled and the classical type IIB string theory reduces to classical supergravity which is just Einstein gravity including further matter fields representing supersymmetry. That this is indeed the case can be seen by focusing on the behaviour of massive string modes in this limit. The typical mass of a string excitation in classical string theory scales like $1/l_{\mathrm{s}}$. Thus, all the massive states become very heavy in the large-$\lambda$ limit and decouple, leaving a massless state, i. e. the graviton. Hence, classical string theory reduces to a free, weakly coupled gravitational theory. From now on we will focus exclusively on the following version of the $AdS$/CFT correspondence:

*The large-$N_{\mathrm{c}}$ limit of $\mathcal{N} = 4$ SYM theory in four dimensions at strong coupling is dual to weakly coupled type IIB supergravity on an $AdS_5 \times S^5$ background.*

This is an immense progress in the usefulness of the Maldacena conjecture since we are able to solve strongly coupled problems in the gauge theory by doing classical computations in a weakly coupled gravity theory. This has many obvious applications. We hope to gain new insights by applying this duality to the case of strongly coupled, non-conformal systems, e. g. the quark-gluon plasma. But – as we asked already earlier in this section – do $\mathcal{N} = 4$ and QCD share some fundamental properties? We will focus on this question in the subsequent sections before proceeding with a general discussion of why we include additional deformations in the $AdS_5$ metric models for our computations.

## 2.2 Holographic Renormalisation

Our main task remains the study of strongly coupled systems at finite temperature (e. g. the QGP) and we arrived at a description of a strongly coupled gauge theory – which is not QCD – in terms of a free, gravitational theory in an $AdS_5$ background. Before trying to get closer to QCD and to study general properties of non-conformal, strongly coupled theories by breaking the conformal invariance (including deformations) on the $AdS$ side of the duality, we have to find a way to include finite temperature since the duality so far describes both theories at zero temperature. Again, two ways seem to be appropriate to achieve this goal.

The first way is to excite the degrees of freedom on the D3-branes to finite temperature $T$. By following the same string theoretical computation as in Sec. 2.1.2 it has been shown in [52, 116] that we end up with the so-called *non-extremal solution* on the supergravity side [113]. It turns out that the net effect of this is solely a modification of the $AdS_5$ part of the metric given by (2.18).

$$\mathrm{d}s^2 = G_{\alpha\beta}\,\mathrm{d}X^\alpha \mathrm{d}X^\beta = \frac{L^2}{z^2}\left(-h(z,z_\mathrm{h})\,\mathrm{d}t^2 + \mathrm{d}\vec{x}^{\,2} + \frac{\mathrm{d}z^2}{h(z,z_\mathrm{h})}\right),$$
$$\text{with} \quad h(z,z_\mathrm{h}) = 1 - \frac{z^4}{z_\mathrm{h}^4}\,. \tag{2.23}$$

The $S^5$-sphere remains unchanged and has already been neglected in this discussion. Equation (2.23) is called *$AdS_5$-Schwarzschild metric* where a black hole of the Schwarzschild type[5] is included in the space filling out the three dimensional space as well as the $S^5$ and being located at a certain depth $z = z_\mathrm{h}$ in the $5^{\text{th}}$-dimensional coordinate. Unfortunately, the string theoretical derivation is again not very intuitive. That is why we proceed with a more pedagogical way [117–119] of deriving (2.23) by starting with ordinary $AdS_5$.

According to the basic relation of the $AdS$/CFT correspondence (2.3) vacuum expectation values of a class of local operators in the gauge theory can be reconstructed from the asymptotics of the dual supergravity fields near the boundary [120]. In the case of the energy-momentum tensor $T_{\mu\nu}$, the dual field in the bulk is just the metric $G_{\alpha\beta}$. Thus, it is possible to reconstruct the vacuum expectation value (VEV) $\langle T_{\mu\nu}\rangle$ from the near-boundary asymptotics of the gravity solution which has been studied in detail in [121–123]. The pure $AdS_5 \times S^5$ metric corresponds to a vanishing VEV of the energy-momentum tensor in the boundary $\mathcal{N} = 4$ SYM gauge theory. If we now excite some gravitons in $AdS_5 \times S^5$ this corresponds to some states in the gauge theory with $\langle T_{\mu\nu}\rangle \neq 0$ and is identical to the procedure of exciting degrees of freedom on the D3-branes. When many gravitons are excited it is better to interpret this as a change

[5] The original Schwarzschild horizon function is given by $h = 1 - \frac{r_\mathrm{h}}{r}$.

in the background metric $G_{\alpha\beta}$. In deriving the exact relation between the metric and the energy-momentum tensor we will follow in this paragraph the argument of [119, 123]. So let us go back to what we already have. We found in the zero-temperature case the basic $AdS$ metric (2.9). In order to allow the boundary theory to have a non-trivial energy-momentum tensor we generalise the Minkowski space-time metric $\eta_{\mu\nu}$ to a general four-dimensional space-time metric $g_{\mu\nu}(x^\rho, z)$ including an additional $z$-dependence. The fact that this is not a contradiction to the necessary condition of having Minkowski space-time at the boundary – where the gauge theory is located – will become clear in the following. The generalised $AdS_5$ metric can now be written in the form

$$\mathrm{d}s^2 = \frac{L^2}{z^2}\left(g_{\mu\nu}(x^\rho, z)\,\mathrm{d}x^\mu \mathrm{d}x^\nu + \mathrm{d}z^2\right), \quad \text{with} \quad \mu,\nu,\rho \in \{t,\vec{x}\}\,. \tag{2.24}$$

At this level of generality we have no remaining diffeomorphism (coordinate) freedom. Equation (2.24) as well as its near-boundary expansion at $z = 0$ shall, nevertheless, be a solution to vacuum Einstein equations, with a negative cosmological constant $\Lambda = -6/L^2$, and is given by

$$g_{\mu\nu} = g^{(0)}_{\mu\nu} + z^2\, g^{(2)}_{\mu\nu} + z^4\, g^{(4)}_{\mu\nu} + z^6\, g^{(6)}_{\mu\nu} + \dots\,. \tag{2.25}$$

Note that we are still solving *vacuum* Einstein equations since there is no energy-momentum tensor in the dual gravity theory construction. Since we impose Minkowski space-time at the boundary we set $g^{(0)}_{\mu\nu}$ to the flat Minkowski metric $g^{(0)}_{\mu\nu} = \eta_{\mu\nu}$. By proceeding to solve Einstein equations it can be found in [123] that $g^{(2)}_{\mu\nu}$ is zero, while $g^{(4)}_{\mu\nu}$ is proportional to the VEV of the boundary energy-momentum tensor:

$$\langle T_{\mu\nu}(x^\rho)\rangle = \frac{N_c^2}{2\pi^2}\, g^{(4)}_{\mu\nu}(x^\rho)\,. \tag{2.26}$$

Hence, this method – called *holographic renormalisation* – allows us to read off the VEV of the gauge theory energy-momentum tensor $\langle T_{\mu\nu}\rangle$ directly from the metric in the bulk. This is a powerful statement in general. The inverse problem of solving for the metric when $\langle T_{\mu\nu}\rangle$ is known can be posed as well which helps us determining the shape of the full bulk metric in a situation where the energy-momentum tensor at the boundary is given.

### 2.2.1 $AdS_5$-Schwarzschild Metric

In order to derive the bulk metric dual to $\mathcal{N} = 4$ SYM at finite temperature we consider a static, isotropic energy-momentum tensor with $\varepsilon = 3P \equiv$ const. with $\varepsilon$ being the energy density and $P$ the pressure. The following analysis has been worked out the first time in [119, 123]. After imposing translation invariance in the three spatial directions $(x^1, x^2, x^3)$ and relabelling the $z$ coordinate to $\tilde{z}$ our metric ansatz is given by

$$ds^2 = \frac{L^2}{\tilde{z}^2}\left(-\mathrm{e}^{a(\tilde{z})}\mathrm{d}t^2 + \mathrm{e}^{b(\tilde{z})}\mathrm{d}\vec{x}^2 + \mathrm{d}\tilde{z}^2\right), \tag{2.27}$$

with $a(\tilde{z})$, $b(\tilde{z})$ being arbitrary real functions. The relabelling is needed since we have to impose a coordinate transformation at the end of the computation where we resubstitute the convenient $z$ notation. Equation (2.27) can now be substituted into the Einstein equations derived from the Einstein–Hilbert action in (2.10) given by

$$\mathcal{R}_{\alpha\beta} - \frac{1}{2}\,\mathcal{R}\,\tilde{G}_{\alpha\beta} - \frac{6}{L^2}\,\tilde{G}_{\alpha\beta} = 0\,, \quad \text{with} \quad \alpha,\beta \in \{t,\vec{x},\tilde{z}\}\,. \tag{2.28}$$

Out of the five second order non-linear differential equations for $a(\tilde{z})$ and $b(\tilde{z})$ three are algebraically independent. This is a common effect in General Relativity and will reappear in Chapter 3 when possible solutions to the Einstein equations are under investigation in a broader context. The remaining equations have the following form

$$-3b' + \tilde{z}b'^2 + \tilde{z}b'' = 0\,, \tag{2.29}$$

$$\tilde{z}a'^2 - 12\,b' + 3\tilde{z}b'^2 + 2a'\left[\tilde{z}b' - 3\right] + 2\tilde{z}\left[a'' + 2b''\right] = 0\,, \tag{2.30}$$

$$b'\left[\tilde{z}b' - 6\right] + a'\left[\tilde{z}b' - 2\right] = 0\,. \tag{2.31}$$

Together with the boundary conditions $a(0) = b(0) = a'(0) = b'(0) = 0$ preserving the Minkowski metric at the boundary and the tracelessness of the energy-momentum tensor we can derive the following metric

$$\mathrm{d}s^2 = \tilde{G}_{\alpha\beta}\,\mathrm{d}\tilde{X}^\alpha \mathrm{d}\tilde{X}^\beta = \frac{L^2}{\tilde{z}^2}\left(-\frac{\left(\tilde{z}^4 - \tilde{z}_\mathrm{h}^4\right)^2}{\tilde{z}_\mathrm{h}\left(\tilde{z}^4 + \tilde{z}_\mathrm{h}^4\right)}\mathrm{d}t^2 + \left(1 + \frac{\tilde{z}^4}{\tilde{z}_\mathrm{h}^4}\right)\mathrm{d}\vec{x}^2 + \mathrm{d}\tilde{z}^2\right), \tag{2.32}$$

that can be recast by a coordinate transformation $z = \tilde{z}/\sqrt{1 + \tilde{z}^4/\tilde{z}_\mathrm{h}^4}$ into the standard form of the gravity dual metric of $\mathcal{N} = 4_\mathrm{T}$:

$$\mathrm{d}s^2 = G_{\alpha\beta}\,\mathrm{d}X^\alpha \mathrm{d}X^\beta = \frac{L^2}{z^2}\left(-h(z, z_\mathrm{h})\,\mathrm{d}t^2 + \mathrm{d}\vec{x}^2 + \frac{\mathrm{d}z^2}{h(z, z_\mathrm{h})}\right),$$
$$\text{with} \quad h(z, z_\mathrm{h}) = 1 - \frac{z^4}{z_\mathrm{h}^4}\,. \tag{2.33}$$

Equation (2.33) includes a black hole of the Schwarzschild-type with horizon at $z = z_\mathrm{h}$ for which reason (2.33) is often called *$AdS_5$-Schwarzschild metric* or *$AdS_5$-BH metric* for short. Thus, the temperature of the $AdS_5$-BH space (which is identical to that of the gauge theory) is related to the length scale $z_\mathrm{h}$ and by dimensional analysis we can state

$$T_{\mathcal{N}=4_T} \equiv T_{AdS-\mathrm{BH}} \propto \frac{1}{z_\mathrm{h}}\,. \tag{2.34}$$

This relation is easy to understand because $z_\mathrm{h}$ is the only length scale that has been introduced when temperature is concerned. Furthermore temperature has dimensions of energy, or equivalently, inverse length. It is interesting to note that $\mathcal{N} = 4$ at finite temperature ($\mathcal{N} = 4_T$) is not conformal anymore because the horizon $z_\mathrm{h}$ defines a length scale in the system. Due to our construction there is no trace anomaly but we will compute the coupling $\alpha_{\mathrm{Q}\bar{\mathrm{Q}}}$ by differentiating the free energy of a quark-antiquark pair in Sec. 4.3.2 and see that it changes at length scale $z_\mathrm{h}$. Determining the proportionality constant in (2.34) can now be achieved in two ways by using two fundamental relations of black hole thermodynamics derived by Hawking and Bekenstein [88, 89]:

$$1^\mathrm{st}\ \text{method}: \quad S = \frac{A}{4G_\mathrm{N}^{(10)}}\,, \tag{2.35}$$

$$2^\mathrm{nd}\ \text{method}: \quad T = \frac{\kappa}{2\pi}\,. \tag{2.36}$$

Here, $S$ is the entropy of the black hole, $A$ the area of the eight-dimensional horizon $(\vec{x}, S^5)$, $G_{\mathrm{N}}^{(10)}$ Newton's constant in ten dimensions and $\kappa$ the surface gravity[6] at the horizon. In chapter 4 we study general thermodynamical quantities in the (deformed)-$AdS$ space where we make use of (2.36) extensively in order to compute the temperature. A derivation of $T$ with the help of (2.36) can be found in Appendix B. In the following we use (2.35) since it leads to a very intuitive picture of how temperature arises in the graviton excited $AdS_5$ space.

### 2.2.2 Temperature in $AdS_5$-Schwarzschild Space-Time

In deriving the temperature in $AdS_5$-BH the expression for the energy density $\varepsilon \equiv \langle T_{00} \rangle$ has to be extracted from (2.32):

$$\tilde{G}_{00} = -\frac{\left(\tilde{z}^4 - \tilde{z}_{\mathrm{h}}^4\right)^2}{\tilde{z}_{\mathrm{h}}\left(\tilde{z}^4 + \tilde{z}_{\mathrm{h}}^4\right)} \quad \Longrightarrow \quad \tilde{G}_{00}^{(4)} = \frac{3}{\tilde{z}_{\mathrm{h}}^4}\,,$$
$$\varepsilon \equiv \langle T_{00} \rangle = \frac{N_{\mathrm{c}}^2}{2\pi^2}\,\frac{3}{\tilde{z}_{\mathrm{h}}^4}\,. \tag{2.37}$$

Since the standard coordinate $z$ is more convenient in the literature we note that $z_{\mathrm{h}} = \tilde{z}_{\mathrm{h}}/\sqrt{2}$ and end up with the following form of the energy density in terms of $z_{\mathrm{h}}$:

$$\varepsilon = \frac{3}{8\pi^2}\,N_{\mathrm{c}}^2\,\frac{1}{z_{\mathrm{h}}^4}\,. \tag{2.38}$$

This is already a remarkable result because it is an expression of the energy density in strongly coupled $\mathcal{N} = 4$ SYM at finite temperature. The factor of $N_{\mathrm{c}}^2$ represents the degrees of freedom on the gauge theory side. The gauge theory content scales like $N_{\mathrm{c}}^2 - 1$ – due to the $\mathrm{SU}(N_{\mathrm{c}})$ gauge group – that reduces to $N_{\mathrm{c}}^2$ in the large-$N_{\mathrm{c}}$ limit.

The derivation now goes as follows: (2.35) provides us with an expression for the entropy density $s$ which can be related to the energy density $\varepsilon$ via the fundamental thermodynamical relation $\mathrm{d}\varepsilon = T\,\mathrm{d}s$. In order to compute the entropy $S$ we need to evaluate the area $A$ of the eight dimensional horizon $(\vec{x}, S^5)$. The expression for $A$ can be written in the form

$$\begin{aligned} A &= \int \mathrm{d}x_1 \mathrm{d}x_2 \mathrm{d}x_3 \sqrt{G_{11}\,G_{22}\,G_{33}} \cdot V_{S^5} \\ &= V_3 \frac{L^3}{z_{\mathrm{h}}^3} \underbrace{\frac{2\pi^{6/2} L^{6-1}}{\Gamma(6/2)}}_{=V_{S^5}} \\ &= \frac{\pi^3\,L^8\,V_3}{z_{\mathrm{h}}^3}\,, \end{aligned} \tag{2.39}$$

where $V_3$ is the infinite three dimensional volume, $V_{S^5}$ is the area of the five-sphere and $G_{ii}$ for $i = x_1,\, x_2,\, x_3$ is defined in (2.33). After dividing by $V_3$ and using (2.17) and (2.35) we obtain the following expression for the entropy density

$$s = \frac{S}{V_3} = \frac{N_{\mathrm{c}}^2}{2\pi z_{\mathrm{h}}^3}\,. \tag{2.40}$$

[6] The surface gravity $\kappa$ denotes the gravitational acceleration an object experience at a certain surface. At the horizon of an ordinary three-dimensional, non-rotating, electrically neutral black-hole $\kappa$ takes on a value of $\kappa = M/r_{\mathrm{h}}^2$.

The degrees of freedom as well as the dimensions ($z_\mathrm{h}^{-3} \sim E^3$) match perfectly with the expectation of an entropy density in the gauge theory. The rest of the derivation is simple. By using the first law of thermodynamics[7] $\mathrm{d}\varepsilon = T\,\mathrm{d}s$ we derive the temperature which is given by

$$T = \frac{\mathrm{d}\varepsilon/\mathrm{d}z_\mathrm{h}}{\mathrm{d}s/\mathrm{d}z_\mathrm{h}} = \frac{1}{\pi z_\mathrm{h}}\,. \tag{2.41}$$

At this step of the computation we have obtained a formulation of strongly coupled $\mathcal{N}=4$ SYM at finite temperature in terms of weakly coupled pure gravity description in an $AdS$-BH background. Furthermore, we note that the trace of the energy momentum tensor $\varepsilon - 3p$ vanishes by construction of the finite-temperature plasma.

With this powerful description in our hand we are able to tackle an important question in the subsequent section which is a direct consequence of our considerations in Chap. 1:

*Can we use the weakly coupled gravity dual to $\mathcal{N}=4_T$ in order to study strongly coupled, non-conformal plasmas like the QGP?*

## 2.3 First Observations

With the help of the $AdS$/CFT correspondence we were able to find a weak coupling gravity description of strongly coupled $\mathcal{N}=4$ at finite temperature. But this theory is not QCD. Let us briefly list the differences:

1. $\mathcal{N}=4$ is a maximally supersymmetric theory whereas QCD does not contain supersymmetry.

2. $\mathcal{N}=4$ is a conformal theory. The coupling is constant and the $\beta$-function vanishes to all orders.

3. $\mathcal{N}=4$ has no confinement and no chiral symmetry breaking.

4. $\mathcal{N}=4$ is investigated in the large-$N_\mathrm{c}$ limit within the gauge/gravity duality approach and in QCD $N_\mathrm{c}=3$. However, one expects corrections to be of order $1/N_\mathrm{c}^2$ for many observables.

Thus, at first sight there is no evidence that analysing $\mathcal{N}=4$ helps in understanding the properties and dynamics of the quark-gluon plasma. Fortunately, this is indeed not the full truth. The properties of QCD and $\mathcal{N}=4$ change dramatically in the high-$T$ regime as pointed out for example by Liu *& al.* in [124]:

1. Above about twice the critical temperature $T_\mathrm{c}$ of the QCD phase transition between the confined and deconfined phase, QCD becomes more and more conformal. An example for this can be given by comparing the ratio of the pressure $P$ in 2- or 3-flavour QCD to that of a non-interacting gas which is about 0.8. This behaviour is also true in $\mathcal{N}=4_T$ and can be observed in the energy density $\varepsilon$ as well [116, 125]. However, non-conformal properties of QCD become important at temperatures of $T < 2T_\mathrm{c}$. Thus, below this temperatures the use of a conformal theory in order to describe QCD is unreliable.

[7] Due to constant volume $V$ and zero chemical potential the terms $p\,\mathrm{d}V$ as well as $\mu\,\mathrm{d}N$ drop out.

2. At twice the critical temperature $T_c$ QCD is not confining anymore.

3. Finite $T$ breaks supersymmetry in $\mathcal{N} = 4$.

Therefore, the differences between these two theories are getting smaller and a valid description of the QGP in terms of $\mathcal{N} = 4$ at large $T$ seems possible. However, even at finite $T$, $\mathcal{N} = 4$ has some features that do not match with QCD making a quantitative analysis unreliable. Nevertheless, many systems at strong coupling that seem to be totally unrelated with each other share some common physics due to the appearance of a collective behaviour in the strong coupling phase. A famous example is the study of the expansion of an ultracold fermionic gas of atoms that leads to a very small number of the shear viscosity to entropy density ratio $\eta/s$ [126]. A hydrodynamic description is also possible in the realm of a hot, dense quark-gluon plasma an it turns out that $\eta/s$ is again very small [127, 128] and can be related to that for the ultracold fermionic gas. And there are other observables (e. g. the bulk viscosity $\zeta$) that are comparable in both systems, although these physical systems are located at different extremal conditions.

One of the main tasks of this thesis is the study of general properties (qualitative or quantitative) of strongly coupled systems at finite temperature. The comparison to the QGP as one particular realisation of a strongly coupled system will be a non-trivial check for the validity of our models under investigation. Fortunately, $\mathcal{N} = 4$ at finite temperature is not the only way to study strongly coupled systems with the help of holography. The next chapter deals with the question how to extend the known $AdS_5/\mathrm{CFT}_4$ correspondence to a larger class of theories. Here, we introduce deformations in the metric on the gravity side of the duality in order to break conformality explicitly leading to a large class of possible models. This has the great advantage that the calculations of the physical observables (see Chapter 4) do not differ dramatically from the easy $\mathcal{N} = 4_T$ computations but let us gain new insight. Furthermore, there is some chance that QCD shares properties with the class of strongly coupled, non-conformal metric models that we will study. Unfortunately, this approach has a strong caveat: by just deforming the well-known $AdS_5$-BH space we lose control over the dual field theory. That means that we cannot even state what the particle spectrum looks like, although we can compute plenty of observables.

Finding the gravity dual of QCD is definitely too much to hope for within this approach. There are a lot of different realisations of the holographic principle beyond the prototype $AdS/\mathrm{CFT}$ approach that resembles many properties of QCD, e. g. the so-called Sakai-Sugimoto model [57]. The simple approach we are dealing with can be further improved by not only breaking conformal invariance but e. g. by introducing a chemical potential $\mu$ or fundamental matter [68, 129–132]. The goal of this thesis is not primarily the investigation of a possible QCD dual but the study of a large class of strongly coupled non-conformal plasmas and their common properties.

So, let us start in the subsequent chapter by introducing our deformed metric models and discuss their properties in detail. Thereafter, we proceed with the main part of this thesis, namely the qualitative and quantitative analysis of physical observables in strongly coupled systems.

Chapter 3

# Non-Conformal Metric Models

In the last chapter we have introduced the essential ingredients of a concrete gauge/gravity duality ($AdS_5/\mathrm{CFT}_4$) which we would like to apply to hot plasmas in this thesis. We pose now the following question which will be a guiding line through this chapter:

*Is it possible to extend the analysis of physical observables beyond $\mathcal{N} = 4$ at finite $T$ to a larger class of non-conformal theories?*

Due to the restrictions of purely conformal models, it is natural to enlarge our discussion to metric models that incorporate more and more QCD-like properties. However, it is important to emphasise that we are not trying to derive the string theory dual of QCD but investigate a large class of different theories that allows us to compare with QCD observables. The QCD results can be obtained for example with the help of lattice simulations or from experiments.

The simplest way of enlarging our theory is by breaking conformal invariance explicitly in the metric. One way to achieve this is by including additional deformations into the metric. This method has some interesting properties:

1. The changes in the metric are small, and thus the computations – on which we will focus in Chapter 4 – are similar to the well-known conformal case.

2. We have full control of the number of included additional parameters and their strength.

3. It is simple to include additional fields, e. g. the scalar dilaton $\Phi$ into the general Einstein–Hilbert action.

However, in doing so we lose control over the corresponding dual field theory. By breaking conformal invariance in the gravitational theory, we do not know the particular properties of the dual field theory, e. g. the amount of symmetries, or the particle content. Fortunately, we will see in the next chapters that these deformed metric models reproduce many properties that non-conformal field theories at finite temperature and strong coupling have in common. That the finding of such universal properties is not an unrealistic task has been shown in [72] for the case of the shear viscosity of entropy density ratio ($\eta/s$) which turns out to be very small in a very large class of non-conformal gravity duals. In addition, this quantity obeys the

bound conjectured by Kovtun, Starinets and Son (*KSS* bound),

$$\frac{\eta}{s} \geq \frac{1}{4\pi}\,, \tag{3.1}$$

which we have reviewed in Chap. 1. Another interesting example is the ratio of bulk viscosity $\zeta$ and shear viscosity $\eta$ where Buchel [133] conjectured that this ratio has to obey the so-called viscosity ratio bound

$$\frac{\zeta}{\eta} \geq 2\left(\frac{1}{3} - c_{\mathrm{s}}^2\right), \tag{3.2}$$

with $c_{\mathrm{s}}^2$ being the speed of sound squared. This bound has been verified in [134–136] for a large class of $(3+1)$-dimensional finite-temperature field theories. However, also some theories are known that violate (3.2) [137].

In order to warm up, we study thermodynamic properties of deformed metric models which will be introduced in the following. More advanced observables like the running coupling defined via the free energy $F$ of static quark-antiquark pairs, which resembles many properties of QCD, will be postponed until Chapter 4. The focus is now set on three different ways of introducing deformations in the basic $AdS_5$-BH background: The SW$_T$-model, the 1-parameter model and the 2-parameter model. The main difference in these approaches is the property of being a solution or not to equations of motion derived from a 5D-Einstein–Hilbert action including an additional real scalar $\Phi$.

## 3.1 The SW$_T$-Model

The simplest way of deforming the metric which corresponds to a breaking of the conformal invariance is the insertion of an exponential factor of the form $\mathrm{e}^{-cz^2}$ without changing anything else. The deformed $AdS_5$-BH metric extension of (2.33) is then given by

$$\begin{aligned} \mathrm{d}s^2 = \frac{L^2}{z^2}\,\mathrm{e}^{-c\,z^2}\left(-h(z,z_{\mathrm{h}})\,\mathrm{d}t^2 + \mathrm{d}\vec{x}^{\,2} + \frac{\mathrm{d}z^2}{h(z,z_{\mathrm{h}})}\right), \\ \text{with} \quad h(z,z_{\mathrm{h}}) = 1 - \frac{z^4}{z_{\mathrm{h}}^4}\,. \end{aligned} \tag{3.3}$$

The free parameter $c$ can take any real number ($c \in \mathbb{R}$) without leading into any singularities. This model was proposed by Andreev in [138] and Kajantie, Tahkokallio and Yee (KTY) in [64]. The latter authors claimed that this metric extremises a five dimensional Einstein–Hilbert action – similar to the $AdS_5$-BH case (see (2.10)) – including an additional scalar field $\Phi(z)$ called the *dilaton* and an undetermined matter part. The dilaton is a scalar well-known in string theory and has some interesting properties.[1] For the current task we just need to know how a scalar is implemented in an overall Einstein–Hilbert action which is shown in (3.4) and (4.5). For the more interested reader we recommend [139] as a review. Furthermore, a brief discussion on how to motivate the Einstein–Hilbert-scalar action as the low-energy limit of a

[1] A naive implementation of a scalar into string theory would lead to a violation of Weyl invariance. In order to overcome this problem, the beta function $\beta(\Phi)$ for the dilaton has to vanish. In addition to this, the constant mode of the dilaton $\Phi_0$ is related to the string coupling via $g_s = \mathrm{e}^{\Phi_0}$.

full type IIB string theory can be found in Sec. 4.1. In the case of the KTY approach the full action is written in the form

$$S_{\mathrm{SW}_T} = \frac{1}{16\pi G_{\mathrm{N}}^{(5)}} \int \mathrm{d}^5x \sqrt{-G} \left( \mathcal{R} - \frac{1}{2}(\partial\Phi)^2 - V(\Phi) \right) + \int \mathrm{d}^5x \sqrt{-G}\, \mathrm{e}^{a\Phi}\, \mathcal{L}_{\mathrm{m}}\,, \tag{3.4}$$

where $\Phi(z) = \phi\, z^2$ and the negative cosmological constant $\Lambda$ has been absorbed in the scalar potential $V(\Phi)$. The scalar $a$ is constant and $G_{\mathrm{N}}^{(5)}$ is again the Newton's constant in five dimensions and $G = \det G_{\alpha\beta}$ the determinant of the space-time metric.

KTY added a matter part $\mathcal{L}_{\mathrm{m}}$ since the pure 5D Einstein–Hilbert-scalar action with a scalar profile proportional to $z^2$ does not allow for the metric in (3.3) which we will call soft-wall metric or SW$_T$-metric from now on. However, they could not specify the necessary matter parts. Thus, it is not a solution to Einstein equations derived from a pure 5D-Einstein–Hilbert-scalar action and therefore inconsistent in our understanding of consistency. That this model has nevertheless quite some success is a consequence of the good agreement with QCD thermodynamic observables (energy density, pressure, trace anomaly) [64, 73]. It is important to note that the choice of the dilaton profile is not arbitrary. Karch *& al.* showed in [60, 140] that a dilaton quadratic in the 5$^{\mathrm{th}}$-dimension coordinate reproduces linear Regge trajectories of the low-lying mesons in agreement with experiments and QCD lattice simulations. In this context the notion *soft-wall model* was invented denoting models with a quadratic dilaton in contrast to earlier approaches called *hard-wall models* that use a constant dilaton which jumps to infinity at a certain point. This leads to a sharp cut-off of the *AdS* space-time and has been studied extensively in [58, 141–143].

We will use metrics of the soft-wall type in the following chapters in order to study deformations in general and how observables change with respect to them. This is interesting because many observables are very robust with respect to deformations or change systematically in one direction. Nevertheless, some irregularities occur that can be fixed by using more sophisticated metric models that are of the soft-wall type as well. They also include a breaking of conformal invariance, but being solutions to the above-mentioned Einstein equations. We will focus on these models in Sec. 3.2.

The remaining part of this section will be used to discuss this general approach of introducing deformation in the $AdS_5$ background by studying basic thermodynamic properties of the SW$_T$-model. In doing so we will gain some insights why this model has been quite successful in the last years.

### 3.1.1 Temperature

We have studied the derivation of a finite temperature gravitational background by including a Schwarzschild type black hole in Sec. 2.2.1. Deriving the temperature with the help of (2.35) has been shown in sec. 2.2.2. The second approach (2.36) is less intuitive but simplifies calculations. In the following we use the final result of the temperature derivation that can be found in Appendix B for a general metric of the form

$$\mathrm{d}s^2 = \mathrm{e}^{2A(z)} \left( -h(z)\, \mathrm{d}t^2 + \mathrm{d}\vec{x}^{\,2} \right) + \frac{\mathrm{e}^{2B(z)}}{h(z)}\, \mathrm{d}z^2\,. \tag{3.5}$$

This metric will be very important in the following chapters and will be derived in the next section. The temperature is then given by

$$T = \mathrm{e}^{A(z_\mathrm{h})-B(z_\mathrm{h})}\,\frac{|h'(z_\mathrm{h})|}{4\pi}\,. \tag{3.6}$$

which is identical to (B.17). Using the $\mathrm{SW}_T$-model defined in (3.6) yields

$$T = \frac{1}{\pi\, z_\mathrm{h}}\,. \tag{3.7}$$

This is a remarkable result because the temperature stays the same although we have entered a non-conformal regime with strong deformations. This is a nice side effect simplifying the model even further. That it is still powerful can be seen by computing the entropy density $s$, energy density $\varepsilon$, pressure $P$ and $\varepsilon - 3P$. These observables lead to first insights into how sensitive this model is with respect to large deformations. The same computations will be repeated in less detail for more sophisticated models before we focus on dynamical quantities like the energy loss of moving quarks, the running coupling and the screening distance of quark-antiquark pairs.

### 3.1.2 Thermodynamic Observables

The entropy density $s$ is computed with the help of (2.39) in a background given by (3.3). A similar computation has been worked out in [64]. Since the computation is straightforward and analogous to the $AdS_5$-BH case we just quote the result:

$$s(T,\,c) = \frac{\pi^2}{2}\,N_\mathrm{c}^2\,T^3\,\mathrm{e}^{-\frac{3c}{2\pi^2T^2}}\,. \tag{3.8}$$

Now, we follow the reverse direction of Sec. 2.2.2. With the help of the temperature given by (3.7) and the fundamental relation $\mathrm{d}\varepsilon = T\,\mathrm{d}s$ we solve for the energy density and obtain the following expression

$$\begin{aligned}\varepsilon &= \int_0^T \mathrm{d}T'\,T'\,\frac{\mathrm{d}s(T',\,c)}{\mathrm{d}T'}\\ &= \frac{3}{2}\,N_\mathrm{c}^2\left[\frac{1}{8}\,\mathrm{e}^{-\frac{3c}{2\pi^2T^2}}\,T^2\left(c+2\pi^2T^2\right)+\frac{c^2}{16\,\pi^2}\,\mathrm{Ei}\Big(-\frac{3c}{2\pi^2T^2}\Big)\right],\end{aligned} \tag{3.9}$$

with $\mathrm{Ei}(z)$ being the exponential integral function $\mathrm{Ei}(z) \equiv \int_z^\infty \mathrm{e}^{-t}/t\,\mathrm{d}t$. The pressure $P$ can be obtained by using another relation known from standard thermodynamics

$$\begin{aligned}P(T,\,c) &\equiv T\,s(T,\,c) - \varepsilon(T,\,c)\\ &= \frac{N_\mathrm{c}^2}{32}\left[\mathrm{e}^{-\frac{3c}{2\pi^2T^2}}\left(4\pi^2T^4-6c\,T^2\right)-\frac{9c^2}{\pi^2}\,\mathrm{Ei}\Big(-\frac{3\,c}{2\pi^2T^2}\Big)\right].\end{aligned} \tag{3.10}$$

With the help of (3.9) and (3.10) we can compute the quantity $\varepsilon - 3p$ which we will call *trace anomaly* for convenience, although there is no anomaly of an underlying symmetry since non-conformality is introduced by an ad hoc change in the metric.

$$\frac{\varepsilon-3P}{T^4} = \frac{3c}{8T^4}\,N_\mathrm{c}^2\left[2\,\mathrm{e}^{-\frac{3c}{2\pi^2T^2}}\,T^2+\frac{3c}{\pi^2}\,\mathrm{Ei}\Big(-\frac{3c}{2\pi^2T^2}\Big)\right]. \tag{3.11}$$

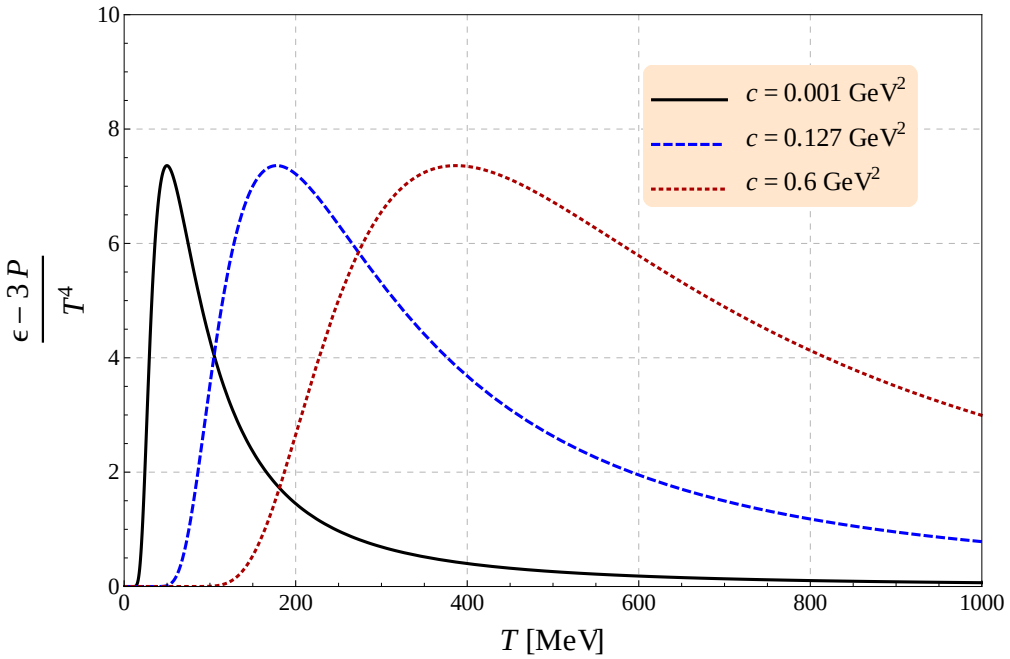


(a) Visualisation of the trace anomaly $(\varepsilon - 3P)/T^4$ in the SW$_T$-model for three values of the deformation parameter $c$, $c = 0.01\,\mathrm{GeV}^2$, $0.127\,\mathrm{GeV}^2$ and $0.6\,\mathrm{GeV}^2$ and $N_c = 3$.

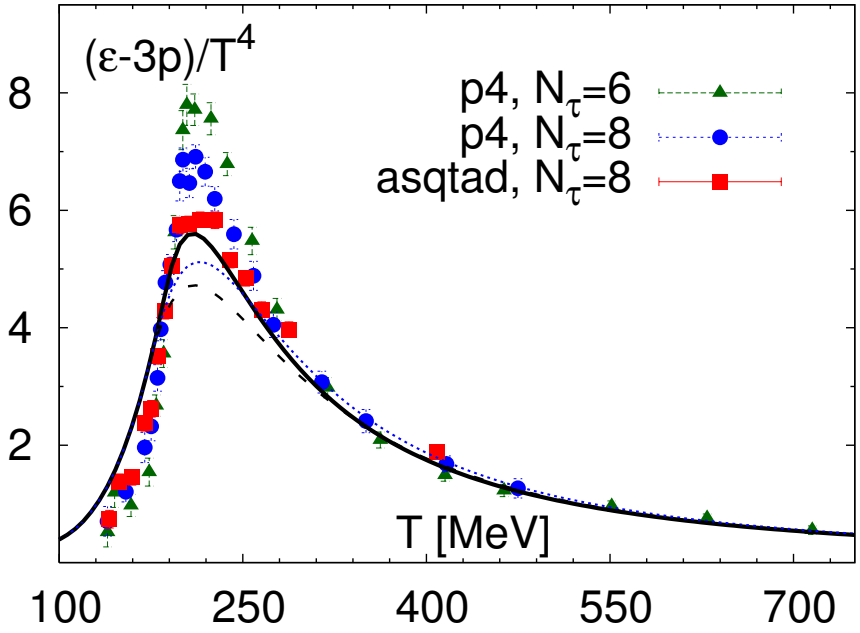


(b) Trace anomaly $(\varepsilon - 3P)/T^4$ in lattice QCD computations with $N_c = 3$ and with p4 and asqtad actions on $N_\tau = 6$ and 8 lattices. The solid, dashed and dotted lines represent several computations with the help of a hadron resonance gas (HRG) model. Figure from Huovinen and Petreczky [144].

Figure 3.1: Comparison of the trace anomaly computed in the SW$_T$-model and a lattice QCD calculation of [144]. The computation with $c = 0.127\,\mathrm{GeV}^2$ has a significant overlap with QCD. In the gauge/gravity computation we set $N_c$ equal to 3.

If we choose $N_c \equiv 3$ we can adjust the deformation $c$ in a way that the sharp increase of the trace anomaly occurs at a temperature $T = T_c$ with $T_c \equiv 176\,\mathrm{MeV}$. $T_c$ has been chosen from recent computation using particle ratios at RHIC in [145]. The corresponding optimal deformation $c_{\mathrm{opt}}$ is $c_{\mathrm{opt}} = 0.127\,\mathrm{GeV}^2$ leading to a trace anomaly that can be compared to QCD lattice data [144, 146–149]. This is plotted in Fig. 3.1 together with recent lattice results by Huovinen and Petreczky [144]. The optimal value $c_{\mathrm{opt}} = 0.127\,\mathrm{GeV}^2$ for the deformation has been worked out for this model in [64] for the first time.

The finding of such a strong agreement with QCD lattice data by the use of such a simple computation is a very interesting result. However, we should recall that the $\mathrm{SW}_T$ model is very crude and inconsistent. Thus, the computation of thermodynamical observables in a consistently deformed model will be the main task in the next section. Such an analysis has not been done in the literature for our class of metric models[2]. The main focus is on the general behaviour of thermodynamic observables when leaving the conformal background. The determination of a concrete value for the deformation parameter in order to resemble QCD at strong coupling and finite temperature is only a side note because other gauge/gravity duals have been developed that contain more QCD properties right from the string theoretical beginning [129, 151, 152].

## 3.2 Consistently Deformed Metric Models

We now focus on a consistent deformation of the $AdS_5$-BH model. Consistency means in this context that the metric should be a solution to the Einstein equations derived from a 5D Einstein–Hilbert-scalar action which is given in standard notation by

$$S_{\mathrm{EHs}} = \frac{1}{16\pi G_{\mathrm{N}}^{(5)}} \int \mathrm{d}^5x \sqrt{-G} \left( \mathcal{R} - \frac{1}{2}(\partial\Phi)^2 - V(\Phi) \right). \tag{3.12}$$

Here $16\pi G_{\mathrm{N}}^{(5)} = 2\kappa^2$ is the five dimensional Newton's constant, $G$ is the determinant of the space-time metric $G_{\alpha\beta}$, $\mathcal{R}$ is the Ricci scalar, $\Phi$ is the scalar (or dilaton) and $V(\Phi)$ the scalar potential. There is one condition the scalar potential $V(\Phi)$ has to satisfy which is the reduction to the conformal $AdS_5$ case $-V(\Phi) \longrightarrow -2\Lambda$ in the limit of a vanishing scalar (dilaton). Whether the scalar is treated as the dilaton or not will be discussed in Sec. 4.1. Fortunately, no differences occur when studying thermodynamic quantities in an empty space. However, if we insert macroscopic objects, e. g. macroscopic strings into the space-time background we have to take a non-trivial contribution of the dilaton into account. This will be done in the next chapter. There are many other fundamental actions to start with, e. g. Gauss-Bonnet type actions [153, 154] or actions including gauge potentials [155]. Metric solutions to this actions have been studied for example in [61, 62, 156] but a general study for a large class of deformations is still missing. In nearly all cases that can be found in the literature a specific scalar potential has been chosen in order to resemble some properties of QCD-like systems. The results are quite remarkable but there is still a lack of knowledge of how these deformed models behave for large classes of deformations.

The derivation of the Einstein equations from the action given in (3.12) is presented in

[2] Similar approaches are [67–69, 150].

Appendix A and we just quote the final expressions:

$$\mathcal{R}_{\alpha\beta} - \frac{1}{2}\mathcal{R}\,G_{\alpha\beta} = \mathcal{T}_{\alpha\beta}\,,$$
$$\text{with}\quad \mathcal{T}_{\alpha\beta} = \frac{1}{2}\,\partial_\alpha\Phi\,\partial_\beta\Phi - \frac{1}{4}G_{\alpha\beta}(\partial\Phi)^2 - \frac{1}{2}G_{\alpha\beta}V(\Phi)\,, \tag{3.13}$$

and

$$\Box_{LB}\,\Phi = V'(\Phi)\,. \tag{3.14}$$

Here, $\alpha, \beta \in \{t, \vec{x}, z\}$. Furthermore, we have to remember that on general pseudo-Riemannian manifolds the d'Alembert operator $\Box$ generalises to the Laplace-Beltrami operator that has the following form when applied to a scalar $\Phi$ in local coordinates:

$$\Box_{LB}\Phi = \nabla_\alpha\nabla^\alpha\Phi = \frac{1}{\sqrt{-G}}\partial_\alpha\Big(\sqrt{-G}\,G^{\alpha\beta}\partial_\beta\Phi\Big)\,, \tag{3.15}$$

where a summation is implied over indices occurring twice. Altogether we have six coupled, second order differential equations depending on the radial coordinate $z$. For convenience, we will abbreviate the Einstein equations by defining

$$\mathcal{E}_{\alpha\beta} \equiv \mathcal{R}_{\alpha\beta} - \frac{1}{2}\mathcal{R}\,G_{\alpha\beta} - \mathcal{T}_{\alpha\beta} = 0\,. \tag{3.16}$$

In (3.13) and (3.16) $\mathcal{T}_{\alpha\beta}$ denotes the energy-momentum tensor.

In order to be able to solve the system of coupled, non-linear differential equations given in (3.13) we have to pose the question how the general metric ansatz has to look like. In Sec. 2.1.1 we have imposed scale invariance which has led us to the $AdS_5$ metric given by (2.9). Since the focus is now on theories which are non-conformal we cannot use such a strong condition on the metric anymore. In the following subsection we start with a general metric ansatz and impose the basic symmetries that should be conserved on the gauge theory side. The final result for the metric can also be found in [62, 136].

### 3.2.1 General Metric Ansatz

The dual field theory – living on the boundary of the gauge theory – shall describe a four dimensional Lorentz-invariant gauge theory. Thus, we demand the metric to satisfy the following conditions:

1. Translation invariance in the $\mathbb{R}^{3,1}$ directions parameterised by $(t, \vec{x})$.
2. SO(3) symmetry in the $\vec{x}$-directions but not SO(1,3) boost invariance because boost invariance is broken by finite temperature.
3. All functions appearing in the metric depend on the radial $5^{\text{th}}$-dimensional coordinate $z$ only.

With the help of these symmetries we can write down a general metric ansatz agreeing with the aforementioned conditions,

$$\begin{aligned}\mathrm{d}s^2 = A(z)\left(\mathrm{d}\vec{x}^{\,2} - \mathrm{d}t^2\right) + \sum_{i=1}^{3} C_i(z)\big(\mathrm{d}x_i\,\mathrm{d}z + \mathrm{d}z\,\mathrm{d}x_i\big) \\ + D(z)\big(\mathrm{d}t\,\mathrm{d}z + \mathrm{d}z\,\mathrm{d}t\big) + E(z)\mathrm{d}z^2\,.\end{aligned} \tag{3.17}$$

In addition, we have three more parameterisation invariances. First we are free to reset our clocks by defining a new time coordinate

$$t' \equiv t + \varphi(z)\,, \tag{3.18}$$

with $\varphi$ being an arbitrary function of $z$. This allows us to eliminate one of the off-diagonal metric elements by setting

$$\frac{\mathrm{d}\varphi}{\mathrm{d}z} \equiv -\frac{D(z)}{A(z)}\,. \tag{3.19}$$

The total derivative of the new time coordinate $t'$ is then given by

$$\mathrm{d}t' = \mathrm{d}t + \frac{\partial\varphi}{\partial z}\,\mathrm{d}z \quad\Longrightarrow\quad \mathrm{d}t^2 = \mathrm{d}t'^2 - \frac{\partial\varphi}{\partial z}\left(\mathrm{d}t\mathrm{d}z + \mathrm{d}z\mathrm{d}t\right) - \left(\frac{\partial\varphi}{\partial z}\right)^2\mathrm{d}z^2\,, \tag{3.20}$$

and the line element (3.17) can now be transformed into a more elegant form

$$\begin{aligned}\mathrm{d}s^2 &= A(z)\left(\mathrm{d}\vec{x}^{\,2} - \mathrm{d}t^2\right) + \sum_{i=1}^{3} C_i(z)\big(\mathrm{d}x_i\mathrm{d}z + \mathrm{d}z\mathrm{d}x_i\big) + H(z)\mathrm{d}z^2\,,\\ &\text{with}\quad H(z) \equiv E(z) + \frac{D(z)^2}{A(z)}\,.\end{aligned} \tag{3.21}$$

Furthermore, we are free to redefine the spatial coordinates $x_i$

$$x_i' = x_i + \gamma_i(z)\,,\quad \text{with}\quad \frac{\mathrm{d}\gamma_i(z)}{\mathrm{d}z} \equiv \frac{C_i}{A}\,,\quad \text{for}\quad i = x_1,\, x_2,\, x_3\,. \tag{3.22}$$

The total derivative for each of the three spatial coordinates then reads

$$\mathrm{d}x_i' = \mathrm{d}x_i + \frac{\partial\gamma_i(z)}{\partial z}\,\mathrm{d}z \quad\Longrightarrow\quad \mathrm{d}x_i^2 = \mathrm{d}x_i'^2 - \frac{C_i}{A}\left(\mathrm{d}x_i\mathrm{d}z + \mathrm{d}z\mathrm{d}x_i\right) - \frac{C_i^2}{A^2}\mathrm{d}z^2\,. \tag{3.23}$$

The line element can now be written as

$$\begin{aligned}\mathrm{d}s^2 &= A(z)\big(\mathrm{d}\vec{x}^{\,2} - \mathrm{d}t^2\big) + \underbrace{\left(-\sum_{i=1}^{3}\frac{C(z)_i^2}{A(z)} + H(z)\right)}_{J(z)}\mathrm{d}z^2\\ &= A(z)\big(\mathrm{d}\vec{x}^{\,2} - \mathrm{d}t^2\big) + J(z)\mathrm{d}z^2\,.\end{aligned} \tag{3.24}$$

In the literature a slightly different notation is used where one identifies $A(z) \equiv \mathrm{e}^{2A'(z)}$ and $J(z) \equiv \mathrm{e}^{2B(z)}$ and drops the prime $'$ of the $A'$-function. The final expression of the line element – which we will use in all the subsequent chapters – has the form

$$\mathrm{d}s^2 = \mathrm{e}^{2A(z)}\left(-h(z)\mathrm{d}t^2 + \mathrm{d}\vec{x}^{\,2}\right) + \mathrm{e}^{2B(z)}\,\frac{\mathrm{d}z^2}{h(z)}\,, \tag{3.25}$$

where we have already included the Schwarzschild type horizon $h(z)$ that provides us with temperature. As we have mentioned above there is a third reparameterisation invariance we have not used yet. This is the reparameterisation invariance of the $z$-coordinate. By applying this to our model we can absorb $B(z)$ or $A(z)$ into a new coordinate $z'$. But there are other methods how to make use of this reparameterisation invariance which will be explained in the next paragraph.

With this general metric ansatz in our hands we return to the Einstein equations (3.13) and try to derive the differential equations for the metric functions $A(z)$, $B(z)$, $h(z)$, $\Phi(z)$ and the scalar potential $V(\Phi(z))$.

### 3.2.2 General Einstein Equations

After computing the necessary curvature tensors[3] $(\mathcal{R}, \mathcal{R}_{\alpha\beta})$ by making use of the general metric in (3.25) we can substitute the final expressions into (3.13) and end up after some massage with the following system of non-linear, second order differential equations:

**Without specifying a gauge:**

$$(\mathcal{E}_{00} - \mathcal{E}_{11}): \qquad h'\left(4\,A' - B'\right) + h'' = 0 \tag{3.26}$$

$$(\mathcal{E}_{00} - \mathcal{E}_{55}): \qquad 6A'' - 6A'B' + (\Phi')^2 = 0 \tag{3.27}$$

$$\mathcal{E}_{55}: \qquad 6\,A'h' + h\Big(24\,A'^2 - (\Phi')^2\Big) + 2\,V\,e^{2B} = 0 \tag{3.28}$$

$$\text{Scalar equation}: \qquad h\big(4\,A'\Phi' - B'\Phi' + \Phi''\big) + h'\Phi' - \frac{\partial V}{\partial \Phi}\,e^{2B} = 0\,. \tag{3.29}$$

Remember that $\mathcal{E}_{\alpha\beta}$ is given by

$$\mathcal{E}_{\alpha\beta} \equiv \mathcal{R}_{\alpha\beta} - \frac{1}{2}\,\mathcal{R}\,G_{\alpha\beta} - \mathcal{T}_{\alpha\beta}\,. \tag{3.30}$$

Two things have to be stated here. Firstly, only three of the four equations are algebraically independent. By adding, subtracting and differentiating eqs. (3.26), (3.27) and (3.28) we are able to derive (3.29). On the other hand we have five unknown functions that we have to determine.

By using the remaining reparameterisation invariance of $z$ we can identify the $z$-coordinate with the scalar function $\Phi$. This method was proposed by Gubser in [62]. The metric then reads

$$\mathrm{d}s^2 = \mathrm{e}^{2A(\Phi)}\left(-h(\Phi)\mathrm{d}t^2 + \mathrm{d}\vec{x}^{\,2}\right) + \mathrm{e}^{2B(\Phi)}\,\frac{\mathrm{d}\Phi^2}{h(\Phi)}\,, \tag{3.31}$$

and the system of differential equations derived from the Einstein equations in (3.13) can be written in the form

**With gauge $\Phi = z' \propto z^2$**

$$(\mathcal{E}_{00} - \mathcal{E}_{11}): \qquad h'\left(4\,A' - B'\right) + h'' = 0 \tag{3.32}$$

$$(\mathcal{E}_{00} - \mathcal{E}_{55}): \qquad A'' - A'B' + \frac{1}{6} = 0 \tag{3.33}$$

$$\mathcal{E}_{55}: \qquad 6\,A'h' + h\Big(24\,A'^{\,2} - 1\Big) + 2\,V\,e^{2B} = 0 \tag{3.34}$$

$$\text{Scalar equation}: \qquad 4\,A' - B' + \frac{h'}{h} - \frac{V'}{h}\,e^{2B} = 0\,. \tag{3.35}$$

Now we start with the derivation of the two consistent metric models, i. e. the 1- and 2-parameter model.

[3] See Appendix A.3 for a complete list of the curvature related tensors.

### 3.2.3 1-Parameter Model

In order to obtain a one-parameter model – with parameter $\phi$ – we use the ungauged Einstein equations (3.26) - (3.29) along with a specific choice of the scalar profile $\Phi(z)$ and the horizon function $A(z)$. This model is intended to be a minimal, non-trivial, consistent generalisation of $AdS_5$ including deformations via a scalar. We reach the conformal limit smoothly for vanishing parameter $\phi$.

As mentioned before, Karch *& al.* suggested a quadratic scalar profile in [60]. In order to obtain a minimal generalisation of $AdS_5$ the horizon function $A(z)$ has to be identical to the conformal case. This choice has the main advantage that we analyse a non-conformal model solving equations of motion whose non-conformality is based only on a non-trivial scalar function $\Phi(z)$. In the 2-parameter model we will include an extra deformation of the $\mathrm{SW}_T$-model type in the metric with parameters $\phi$ and $c$. With these two models in our hand we are able to discuss the different strengths of metric and scalar deformations, respectively. A quantitative analysis for several observables is the topic of Chapter 4.

After defining $\Phi(z)$ and $A(z)$ as described above by

$$\Phi(z) \equiv \sqrt{\frac{3}{2}}\,\phi z^2\,, \quad \text{and} \quad A(z) \equiv \frac{1}{2}\,\log\frac{L^2}{z^2}\,, \tag{3.36}$$

(3.27) can be used to solve for $B(z)$,

$$B(z) = -\frac{1}{4}\big(z^4\phi^2 + 4\,\log z\big) + \mathcal{C}\,. \tag{3.37}$$

The appearance of the numerical factor $\sqrt{3/2}$ in (3.36) will be explained in Sec. 4.1 when the string theoretic background is described in more detail. In principle, this factor can be absorbed in the parameter $\phi$ but the final equations turn out to be more elegant when the factor is included explicitly. The integration constant $\mathcal{C}$ can be determined by imposing the condition that our model has to behave like conformal $AdS_5$ for $z \longrightarrow 0$. This is a reasonable condition because small $z$ correspond to high temperature as we know from dimensional analysis ($T \propto 1/z_\mathrm{h}$) and in the very high temperature regime all the non-conformal models under investigation shall become conformal. This is approximately the same in QCD. Thus, we can impose:

$$B(z) \xrightarrow{z\to 0} A(z) \quad \Longrightarrow \quad \mathcal{C} = \log L\,. \tag{3.38}$$

After substituting eqs. (3.36) and (3.37) into (3.26) the horizon function $h(z)$ can be written as

$$h(z) = h_0 - \frac{h_1}{\phi^2}\left(1 - \mathrm{e}^{-\frac{1}{4}z^4\phi^2}\right). \tag{3.39}$$

Again, integration constants – in this case two $(h_0, h_1)$ – appear and we have to think about boundary conditions that we still have to impose. By recalling the derivation of the temperature function in the conformal case (Sec. 2.2.1) we find that the metric has to be flat four dimensional Minkowski space-time at the boundary in order to allow for a boundary gauge theory that describes real-world physics. Thus, $h(z)$ has to become unity at $z = 0$ which is our first condition. Secondly, the horizon function defines a black hole horizon $z_\mathrm{h}$ at the first zero.

Hence, we impose the following conditions:

$$\begin{aligned} h(0) \equiv 1 \quad &\Longrightarrow \quad h_0 = 1\,, \\ h(z_\mathrm{h}) \equiv 0 \quad &\Longrightarrow \quad h_1 = \frac{\mathrm{e}^{\left(\frac{1}{4} z_\mathrm{h}^4 \phi^2\right)} \phi^2}{\mathrm{e}^{\left(\frac{1}{4} z_\mathrm{h}^4 \phi^2\right)} - 1}\,. \end{aligned} \tag{3.40}$$

Before deriving the scalar potential $V(\Phi(z))$ we have to mention that in the limit $\phi \longrightarrow 0$ the conformal $AdS_5$ space-time can be recovered. Up to now $\phi$ takes on any value in $\mathbb{R}$.

In a last step we can derive the scalar potential $V(\Phi(z))$. This is not of practical interest for the following computations since only the metric functions contribute. However, this potential has some general importance. With the help of (3.28) the dilaton potential $V(\Phi)$ is fixed and has the following form

$$\begin{aligned} V(\Phi) &= \frac{2\,\mathrm{e}^{\Phi^2/3}}{1 - \mathrm{e}^{\Phi_\mathrm{h}^2/6}} \left( \Phi^2 + 6\,\mathrm{e}^{\frac{1}{6}\left(\Phi_\mathrm{h}^2 - \Phi^2\right)} - 6 \right), \\ \Longrightarrow \quad V(\Phi) &\approx -\frac{12}{L^2} - 2\frac{\Phi^2}{L^2} + \mathcal{O}\left(\Phi^3\right). \end{aligned} \tag{3.41}$$

Here, $\Phi_\mathrm{h}$ is the scalar $\Phi(z)$ evaluated at $z = z_\mathrm{h}$. We can state immediately that the condition of reproducing the cosmological constant $2\Lambda = -12/L^2$ in the limit of a vanishing dilaton is satisfied perfectly. Furthermore, the $\Phi^2$-coefficient in the series expansion can be interpreted as half the scalar mass squared $\frac{1}{2} M_\Phi^2$. This is a very interesting quantity in string theory. In our models we obtain a negative mass squared which can be interpreted in general as a tachyonic behaviour. As a result we would obtain unstable physical solutions. Fortunately, Breitenlohner and Freedman derived a lower bound [157, 158] for the mass squared of the scalar $M_\Phi^2$ where the physical solutions are not unstable. The bound can be written as

$$M_\Phi^2 \geq -\frac{4}{L^2}\,, \tag{3.42}$$

for the case of one extra dimension. The Taylor expansion of (3.41) leads to the following result for the scalar mass squared

$$M_\Phi^2 = -\frac{4}{L^2}\,, \tag{3.43}$$

which obviously satisfies the Breitenlohner–Freedman bound. Although the mass squared is negative we should not worry since no instabilities occur in the solutions. Although the dilaton potential is not of computational interest since it does not appear in the metric functions which are the only ingredients in the calculation of our observables, it is important when theories with different temperatures and deformations are compared. By choosing different deformations, it is obvious that the dilaton potential $V$ is changed and we obtain a different theory. However, the dilaton potential is very robust with respect to the deformation as we can see in (3.41). A deviation in the $V$ arises at second order in the deformation.

In contrast to this, we hope that changing the temperature for a fixed deformation does not change the theory. This is in general not the case due to a dependence of the dilaton potential on the horizon $\Phi_\mathrm{h}$, or equivalently, $z_\mathrm{h}$. A change in the temperature leads a priori to a different theory. Thus, we can only compare theories with different temperatures for a fixed deformation if the deviation in the dilaton potential is not too large. A quantitative discussion

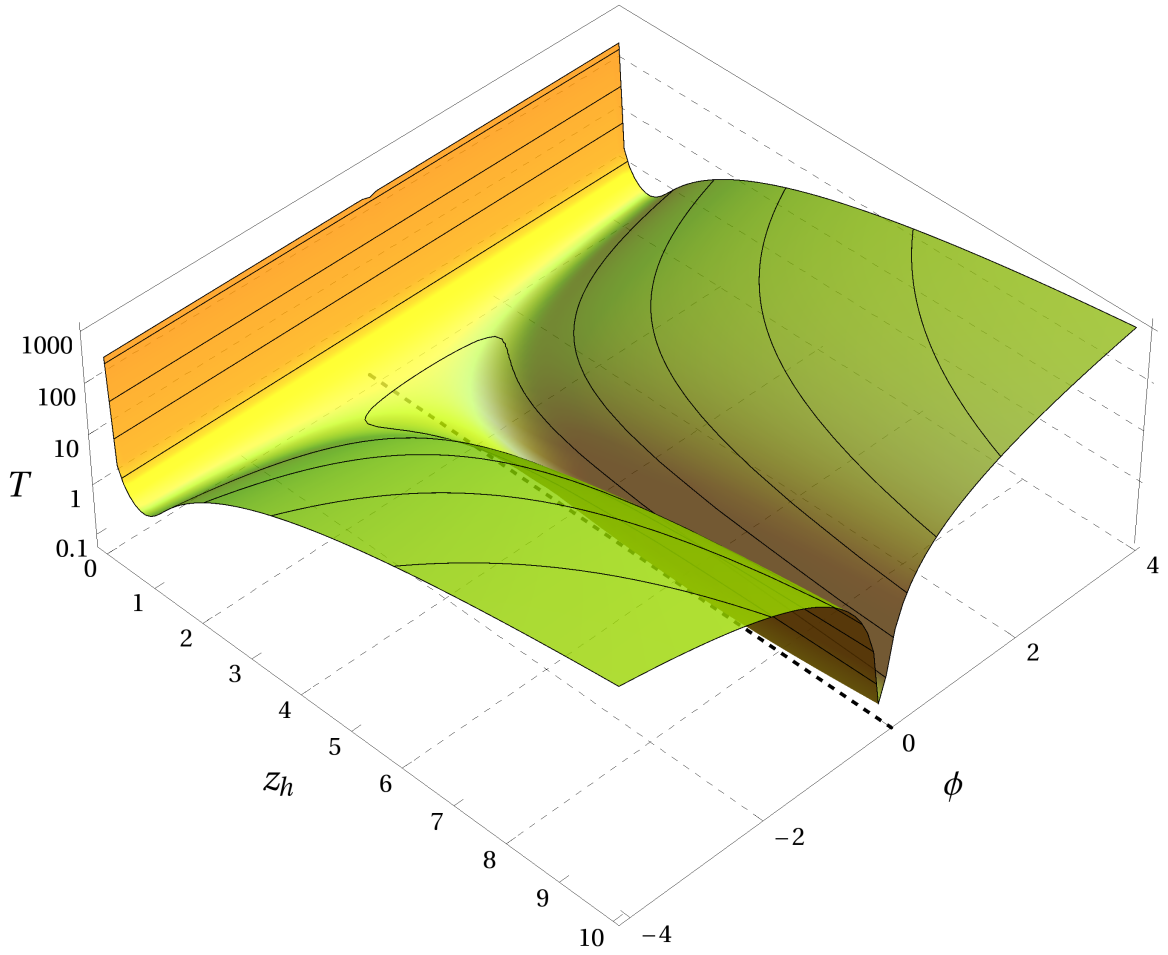


Figure 3.2: Visualisation of temperature $T$ in the 1-parameter model. It reproduces the conformal temperature $T = (\pi z_\mathrm{h})^{-1}$ for $\phi = 0$ and is symmetric under $\phi \longrightarrow -\phi$.

of this problem will be worked out in the next paragraph after introducing the formula for the temperature. For a 2-parameter model being a solution to Einstein equations this problem has been argued in detail by Dewolfe and Rosen in [156]. Before we start with the applications of this model let us note that it nicely reproduces conformal $\mathcal{N} = 4$ at finite $T$ in the limit of $\phi$ going to zero. Thus, we can study a smooth, consistent deviation from the conformal $AdS_5$ model. With the full metric in our hand we can now start computing thermodynamical quantities that have not been studied in the 1- and 2-parameter model before in the literature. A simpler model has been studied by Gubser and Nellore in [62].

By using the temperature formula in (3.6) we obtain

$$T_{1\mathrm{p}} = \mathrm{e}^{A(z)-B(z)}\,\frac{h'(z_\mathrm{h})}{4\pi} = \frac{z_\mathrm{h}^3\phi^2}{4\pi}\left(1-\mathrm{e}^{-\frac{1}{4}\,z_\mathrm{h}^4\phi^2}\right). \tag{3.44}$$

This function is visualised in Fig. 3.2 for a large range of deformations $\phi$ and $z_\mathrm{h}$. Three properties are remarkable concerning the temperature. Firstly, in the zero-deformation limit we obtain the conformal temperature $T = (\pi z_\mathrm{h})^{-1}$. Secondly, the temperature is quadratic in $\phi$. This means that there is no difference between negative and positive deformations and we

can restrict ourselves to positive deformations only. The third and most important fact is that the temperature has a minimum value $T_{\text{min}}$ for each $\phi$ different from zero. This restricts our model to a specific temperature regime but since we are interested in the high-$T$ behaviour of strongly coupled systems (e. g. QGP) this is not a severe restriction.

Furthermore, we can now resolve the issue of the differences in the dilaton potential (3.41) when the temperature is changed. We plot in Fig. 3.3 the dilaton potential $V(z)\,L^2$ in the 1-parameter model against $z$ for a fixed deformation $\phi = 0.3$ and several values of the temperature $T$, $T = T_{\text{min}}$, 1, 2, 3. The coloured dots represent the position of the black-hole

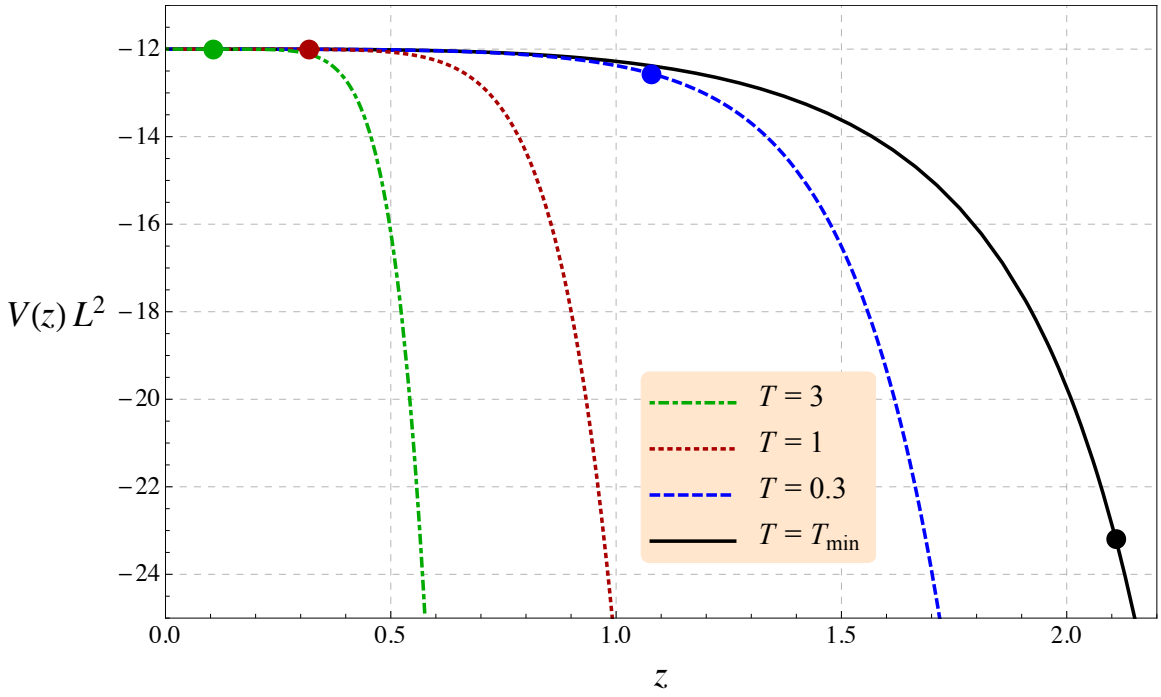


Figure 3.3: Dilaton potential $V(z)\,L^2$ in the 1-parameter model against $z$ for fixed deformation $\phi = 0.3$ and several values of the temperature $T$, $T = T_{\text{min}}$, 1, 2, 3. The coloured dots represent the position of the horizon $z_{\text{h}}$.

horizon $z_{\text{h}}$. Although all dilaton potentials in Fig. 3.3 differ from each other, thus, describing different theories we can argue that the deviation is not relevant for most of our computations. The reason for this is the following. By comparing two different temperatures we have to make sure that the dilaton potentials are similar up to the first horizon[4] $z_{\text{h}}$ occuring along the $z$-coordinate. This means – according to Fig. 3.3 – that for example a comparison with $T = 3$ is always possible since each dilaton potential is identical up to the green dot which indicates the horizon for $T = 3$. We can state that similar theories are going to compared if large temperatures are concerned. We have to be careful if we compare small temperatures of order of $T_{\text{min}}$ because the dilaton potential varies significantly in this regime. This is visualised for example for $T = T_{\text{min}}$ and $T = 0.3$ in Fig. 3.3. At the blue point which indicates the horizon of $T = 0.3$ the scalar potential has already changed significantly compared to the black curve. The same behaviour can be found in the 2-parameter model as well.

[4]The first horizon is the one that corresponds to the higher temperature.

Before introducing the 2-parameter model let us shortly discuss the thermodynamic properties of this consistent model where a non-conformality is introduced solely in the profile of the scalar. No further explicit metric deformations are used because the warp factor in front of the Minkowskian part remains conformal ($L^2/z^2$). This enables us to study the different behaviour of an explicit metric deformation (e. g. the $\mathrm{SW}_T$, 2-parameter model) in contrast to the contribution of a purely dilatonic function (e. g. 1-parameter model) since the 2-parameter model will include both possibilities of breaking conformality.

Similar to the $\mathrm{SW}_T$ case (Sec. 3.1.2) we use the following fundamental thermodynamic equations to compute the energy density $\varepsilon_{1\mathrm{p}}$ and pressure $P_{1\mathrm{p}}$ in the 1-parameter model:

$$\mathrm{d}\varepsilon_{1\mathrm{p}} = T\,\mathrm{d}s_{1\mathrm{p}} \quad \Longrightarrow \quad \varepsilon_{1\mathrm{p}}(T) = \int_{T_{\min}}^{T} T' \frac{\partial s}{\partial T'}\,\mathrm{d}T' = -\int_{z_{\mathrm{h}}}^{z_{\mathrm{h}}^{\max}} T(z'_{\mathrm{h}}) \frac{\partial s}{\partial z'_{\mathrm{h}}}\,\mathrm{d}z'_{\mathrm{h}}\,, \tag{3.45}$$

$$\mathrm{d}P_{1\mathrm{p}} = s_{1\mathrm{p}}\,\mathrm{d}T \quad \Longrightarrow \quad P_{1\mathrm{p}}(T) = \int_{T_{\min}}^{T} s(T')\,\mathrm{d}T' = -\int_{z_{\mathrm{h}}}^{z_{\mathrm{h}}^{\max}} s(z'_{\mathrm{h}}) \frac{\partial T}{\partial z'_{\mathrm{h}}}\,\mathrm{d}z'_{\mathrm{h}}\,, \tag{3.46}$$

where the remaining integration constants are set to zero. The minus sign in (3.45) arises due to the monotonously falling relation between $T$ and $z_{\mathrm{h}}$. The upper integration limit $z_{\mathrm{h}}^{\max}$ is the corresponding $z_{\mathrm{h}}$ value of the minimal temperature for a given deformation $\phi$. With the help of (3.45) and (3.46) we can easily compute the trace anomaly that is shown in Fig. 3.4(a).

We compare our calculations to lattice results by Panaro [159, 160] and Gursoy *& al.* [161, 162] which are shown in Fig. 3.4(b). The figure is taken from [159] and includes a holographic computation by Gursoy *& al.* [65, 66] who used a similar approach of a 5D-Einstein–Hilbert-scalar action in order to mimic QCD. As we can see in Fig. 3.4(a) the shape of our results is very robust for all values of the deformation. Thus, it is not very surprising that Kiritsis found a concrete realisation that resembles this QCD data very nicely since these models based on the introduction of further scalars in the Einstein–Hilbert action are very robust in general with respect to changes in the deformations. Many different choices of a particular metric would lead to similar results. However, it is remarkable that the amount of non-conformality is almost equal to large-$N_{\mathrm{c}}$ computations on the lattice. By choosing different values of the deformation $\phi$ we can only shift the critical temperature $T_{\mathrm{c}}$. Although it is a small leap ahead we would like to state here that even in the 2-parameter case we find a very robust behaviour. One task in the next chapter will be the investigation whether this robustness hold also for different observables.

### 3.2.4 2-Parameter Model

In the last part of this chapter we would like to introduce a recent model proposed by DeWolfe *& al.* in [156] that includes the deformation of the $\mathrm{SW}_T$-model but in a consistent way by solving Einstein equations (3.32) – (3.35). The authors of [156] used this model to study jet quenching in hot plasmas. We will enlarge the analysis of this model to all available parameters and many other observables in order to gain new insights into how non-conformal theories at strong coupling and finite temperature behave.

Firstly, let us switch to the specific gauge where we identify the $z$-coordinate by the dilaton $\Phi$. This has the advantage that all the final expressions become much shorter. The metric has the general form of (3.31) and we have to solve equations of motion given by (3.32) – (3.35).

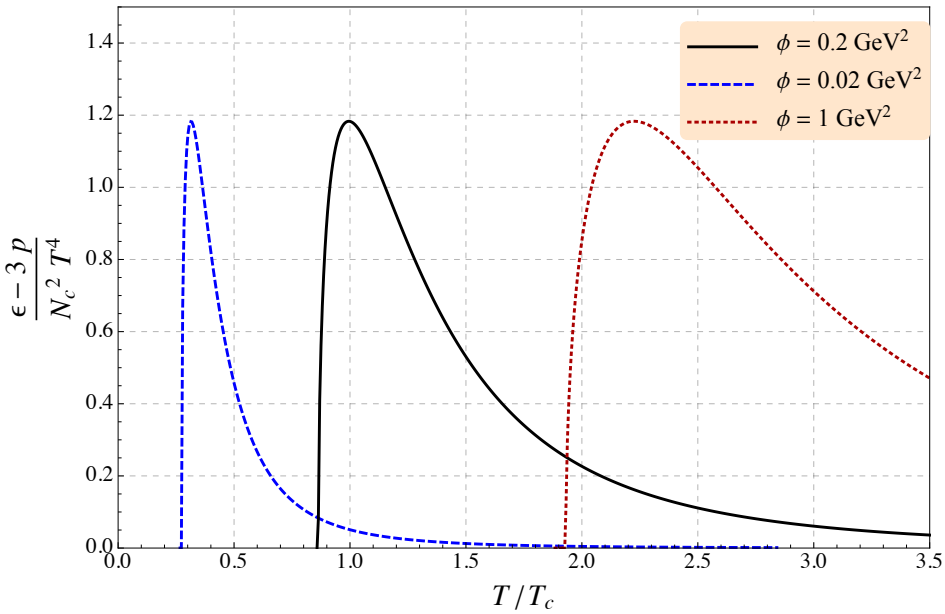


(a) Trace anomaly $(\varepsilon - 3P)/T$ in the 1-parameter model for three different deformations $\phi$, $\phi = 0.02\,\mathrm{GeV}^2, 0.2\,\mathrm{GeV}^2$ and $1\,\mathrm{GeV}^2$.

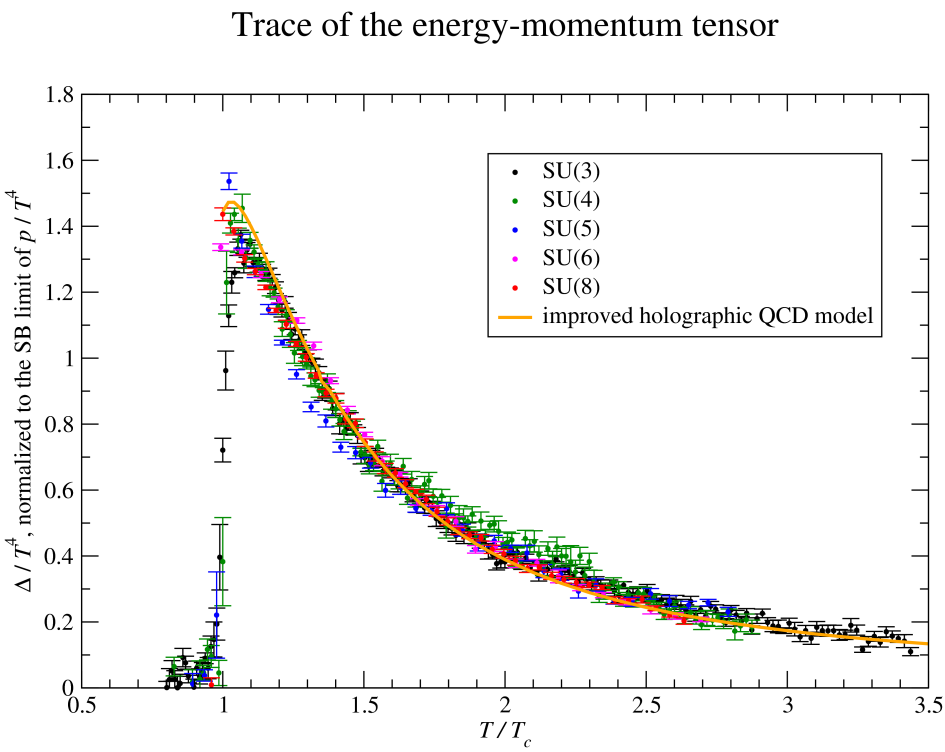


(b) Trace anomaly $\triangle = (\varepsilon - 3P)/N_c^2$ in a lattice simulation for gauge field theories with large-$N_c$ gauge groups of the form SU($N_c$) together with an improved holographic model proposed by Kiritsis [65, 66, 161, 162]. This figure is taken from Panero [159].

Figure 3.4: Comparison of the trace anomaly computed in the 1-parameter model and a lattice QCD computation made by [159, 160]. The computation with $\phi = 0.2\,\mathrm{GeV}^2$ is in good agreement with large-$N_c$ gauge theories with gauge group SU($N_c$).

We use the three independent equations to solve for $B(\Phi), h(\Phi)$ and $V(\Phi)$ by assuming a $\mathrm{SW}_T$-like function for $A(\Phi)$ that can be rewritten in $\Phi$-form as

$$\begin{aligned} A(\Phi) &\equiv \frac{1}{2}\,\log\left(\frac{L^2}{z^2}\right) - \frac{1}{2}cz^2 \\ &= \frac{1}{2}\log\left(\frac{\sqrt{\frac{3}{2}}\phi L^2}{\sqrt{\frac{3}{2}}\phi\, z^2}\right) - \frac{c}{\phi\sqrt{6}}\sqrt{\frac{3}{2}}\,\phi\, z^2 \\ &= \frac{1}{2}\log\left(\sqrt{\frac{3}{2}}c\frac{L^2}{\alpha}\right) - \frac{1}{2}\,\log\Phi - \frac{\alpha}{\sqrt{6}}\,\Phi\,. \end{aligned} \tag{3.47}$$

Here, the following definitions of the running scalar $\Phi$ and $\alpha$ are used:

$$\Phi = \sqrt{\frac{3}{2}}\phi z^2\,, \quad \text{and} \quad \alpha \equiv \frac{c}{\phi}\,. \tag{3.48}$$

Thus, we have used implicitly the exact relation between $\Phi$ and $z$ within the definition of $A(\Phi)$. In addition to this, the horizon $\Phi_{\mathrm{h}}$ is defined as the first zero of the horizon function $h(\Phi)$. With the help of (3.47) and eqs. (3.32) – (3.35) we can now determine $B(\Phi)$, $h(\Phi)$ and $V(\Phi)$ which are given by

$$\begin{aligned} B(\Phi) &= \log\left(\frac{L}{2}\right) + \frac{1+2\alpha^2}{2\alpha^2}\,\log\left(1+\alpha\sqrt{\frac{2}{3}}\,\Phi\right) - \log\Phi - \frac{1}{\alpha\sqrt{6}}\,\Phi\,, \\ h(\Phi) &= 1 - \frac{\mathcal{K}(\Phi,\alpha)}{\mathcal{K}(\Phi_{\mathrm{h}},\alpha)}\,, \\ V(\Phi,\,\alpha,\,\Phi_{\mathrm{h}}) &= -\frac{1}{2}\,\mathrm{e}^{-2B(\Phi,\alpha)}\left(-h(\Phi) + 24\,h(\Phi)\,A'(\Phi)^2 + 6A'(\Phi)\,h'(\Phi)\right), \end{aligned} \tag{3.49}$$

with

$$\begin{aligned} \mathcal{K}(\Phi,\alpha) \equiv{}& \left(4\alpha^2-1\right)\Gamma\left[2+\frac{1}{2\alpha^2}, \frac{1}{2\alpha^2}-2\right] \\ &+ \left(1-4\alpha^2\right)\Gamma\left[2+\frac{1}{2\alpha^2}, -\frac{1}{6\alpha^2}\left(4\alpha^2-1\right)\left(3+\sqrt{6}\alpha\Phi\right)\right] \\ &+ 2\alpha^2\,\Gamma\left[3+\frac{1}{2\alpha^2}, \frac{1}{2\alpha^2}-2\right] \\ &- \Gamma\left[3+\frac{1}{2\alpha^2}, -\frac{1}{6\alpha^2}\left(4\alpha^2-1\right)\left(3+\sqrt{6}\alpha\Phi\right)\right]. \end{aligned} \tag{3.50}$$

Here, $\Gamma[\ldots,\ldots]$ denotes the incomplete Gamma function $\Gamma[a,x] \equiv \int_x^\infty t^{a-1}\,\mathrm{e}^{-t}\,\mathrm{d}t$. In this derivation we have fixed the appearing integrations constants in a way that $B$ reduces to $AdS_5$ space-time with matching length scale $L$ in the $\Phi \to 0$ limit. The horizon function $h(\Phi)$ has to fulfil the same boundary conditions that we have introduced in (3.40).

Before we proceed with the computation of the scalar function function, we have to specify the range of validity for the parameters $c$ and $\alpha$. Firstly, we have to show that the conformal

$AdS_5$-BH scenario can be obtained in a certain limit. This can be achieved by taking the limit $c \longrightarrow 0$ by keeping $\phi$ fixed. This is trivial for $A(z)$ and can be shown for $B(z)$ if we transform it back into the $z$-coordinates. $B(\Phi)\,\mathrm{d}\Phi^2$ which appears in the metric (see (3.25)) reduces then to

$$\mathrm{e}^{2B(\Phi)}\,\mathrm{d}\Phi^2 = \mathrm{e}^{-\frac{z^2\,\phi^2}{c}}\,\frac{L^2}{z^2}\,(1+c\,z)^{2+\frac{\phi^2}{c^2}} \quad \xrightarrow{c\to 0} \quad \mathrm{e}^{-\frac{1}{2}\,z^4\,\phi^2}\,\frac{L^2}{z^2} = \mathrm{e}^{2B(z)}\,\mathrm{d}z^2\,. \tag{3.51}$$

Now, the limit $\phi \longrightarrow 0$ can be taken in order to obtain the pure $AdS_5$-BH metric as it was shown in Sec. 3.2.3. In total, we expect the conformal limit by taking the limits $c \longrightarrow 0$ and $\alpha \longrightarrow \infty$. This limit is sometimes difficult to visualise since all figures are plotted versus $\Phi$ or $\Phi_\mathrm{h}$ where $c$ and $\alpha$ are intrinsically included. Thus, taking one of these limits always changes the scaling of the curves. Secondly, we have to fix the overall range of values that these parameter can take on. The integral for $h(\Phi)$ in (3.49) can be solved for all positive values of $\alpha$. This has been shown by Helmboldt in [163]. In principle, all real numbers can be chosen for $c$. However the computation of the temperature (3.54) reveals a $T \propto \sqrt{c}$ dependence that restricts $c$ to positive values only. In summary, $c$ and $\alpha$ can take on the following values:

$$c \in [0,\infty]\,, \quad \text{and} \quad \alpha \in [0,\infty]\,. \tag{3.52}$$

The scalar potential in (3.49) can be expanded for small values of $\Phi$ leading to

$$V(\Phi,\,\alpha,\,\Phi_\mathrm{h}) \approx -\frac{12}{L^2} - \frac{2}{L^2}\,\Phi^2 + \mathcal{O}(\Phi^3)\,. \tag{3.53}$$

This expansion shows that the potential obeys the Breitenlohner–Freedman bound again, which is a general property of the metric models under investigation. The most important quantity is the temperature $T$ which is calculated via the same formula as in the 1-parameter case given by (3.6) and is cast into a form given by

$$\begin{aligned} T_\mathrm{2p}(\Phi_\mathrm{h},\alpha,c) = \frac{-1}{\pi\mathcal{K}(\Phi_\mathrm{h},\alpha)} \Bigg( & 2^{-\frac{9}{4}-\frac{1}{2\alpha^2}}\,3^{-\frac{3}{4}-\frac{1}{2\alpha^2}}\,\mathrm{e}^{2-\frac{1}{2\alpha^2}+\sqrt{\frac{2}{3}}\,\alpha\,\Phi_\mathrm{h}}\,\sqrt{\frac{c}{\alpha}}\,\left(4\alpha^2-1\right)^3 \\ & \cdot \Phi_\mathrm{h}^{3/2}\left(1+\sqrt{\frac{2}{3}}\,\alpha\,\Phi_\mathrm{h}\right)^{-\frac{1}{2\alpha^2}}\left(\frac{-1}{\alpha^2}\left(4\alpha^2-1\right)\left(3+\sqrt{6}\,\alpha\Phi_\mathrm{h}\right)\right)^{\frac{1}{2\alpha^2}}\Bigg)\,. \end{aligned} \tag{3.54}$$

The temperature in the 2-parameter case is shown in Fig. 3.5 for a large range of $\alpha$-values and four different deformations $c$, $c = 0.1$ (lowest surface), 0.4, 0.7 and 1.1 (highest surface) in units where the $AdS$ length $L$ is set to 1. The most important fact we would like to note is the existence of a minimal temperature $T_\mathrm{min}$ for each value of the two parameters $(\alpha, c)$ analogous to the 1-parameter model. In other words, for a given temperature we find a maximal deformation since the minimal temperature is rising for stronger deviations from the conformal case. In order to specify a preferred regime of parameters we also compute the trace anomaly for the 2-parameter model. Although the general focus lies on the general behaviour for all parameters, it is nevertheless useful to have a particular regime in mind where our model is similar to real-world physics. Since the fundamental thermodynamic expressions are in principle similar to (3.45) and (3.46), we skip the details of the computation and focus on the results of the trace anomaly which are shown for a large class of $\alpha$- and $c$-deformations in Fig. 3.6 with the critical temperature $T_\mathrm{c}$ set to 176 MeV. For the combination $\alpha = 0.31$ and $c = 0.1\,\mathrm{GeV}^2$ we are closest to a QCD-like behaviour since the increase occurs at the critical

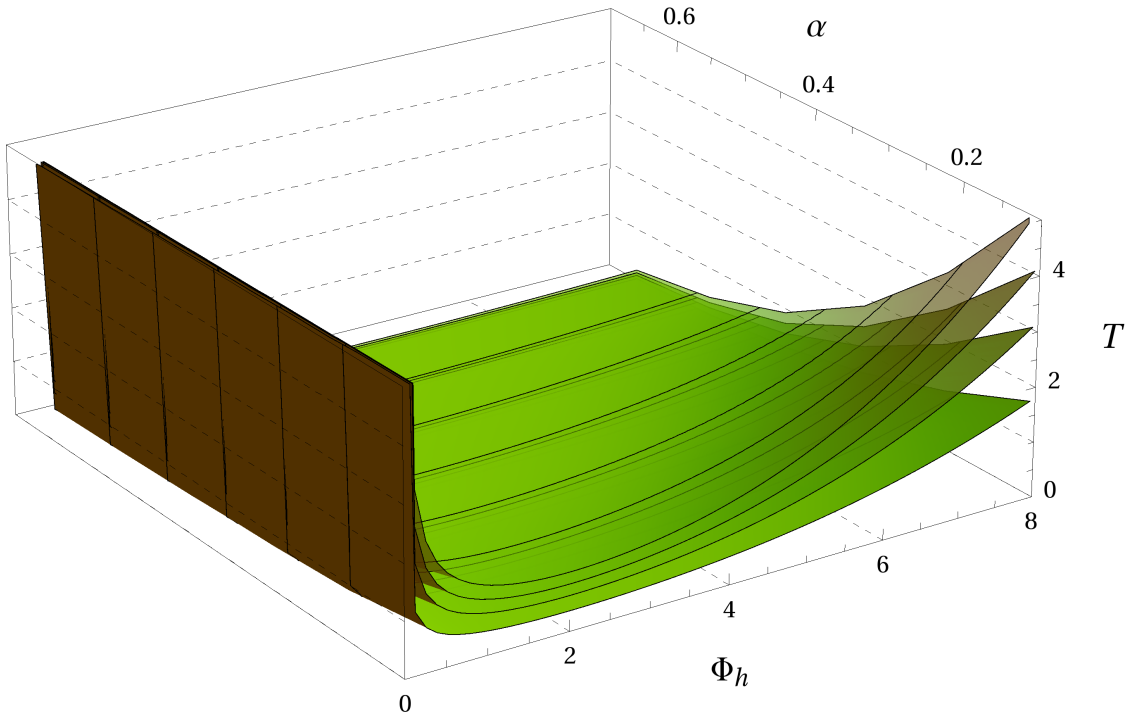


Figure 3.5: Temperature $T$ in the 2-parameter model against the parameter $\alpha$ and the horizon $\Phi_{\rm h}$ for four different deformations $c$, $c = 0.1$ (lowest surface), 0.4, 0.7 and 1.1 (highest surface) in units where the $AdS$ length $L$ is set to 1. It reproduces the conformal temperature in the $c \longrightarrow 0$ and large-$\alpha$ limit.

temperature. Thus, we will keep this values in mind for later use. It is important to note that the amplitude of the trace anomaly is almost constant for a large range of $\alpha$ values and in good agreement with the lattice computations by Panero in Fig. 3.4(b). Larger values of the parameter $c$ shift the whole curve along the temperature axis towards higher temperatures but the shape stays almost the same.

In summary, we have extended in this chapter the prototype $AdS$/CFT correspondence to non-conformal metric models that allow for a more complete study of strongly coupled, non-conformal systems. After introducing an inconsistent deformation ($\mathrm{SW}_T$-model), two more sophisticated metrics were presented which will be used in the next chapters to study other physical observables. A complete analysis of the systems we have introduced in this chapter has not been worked out yet in the literature.

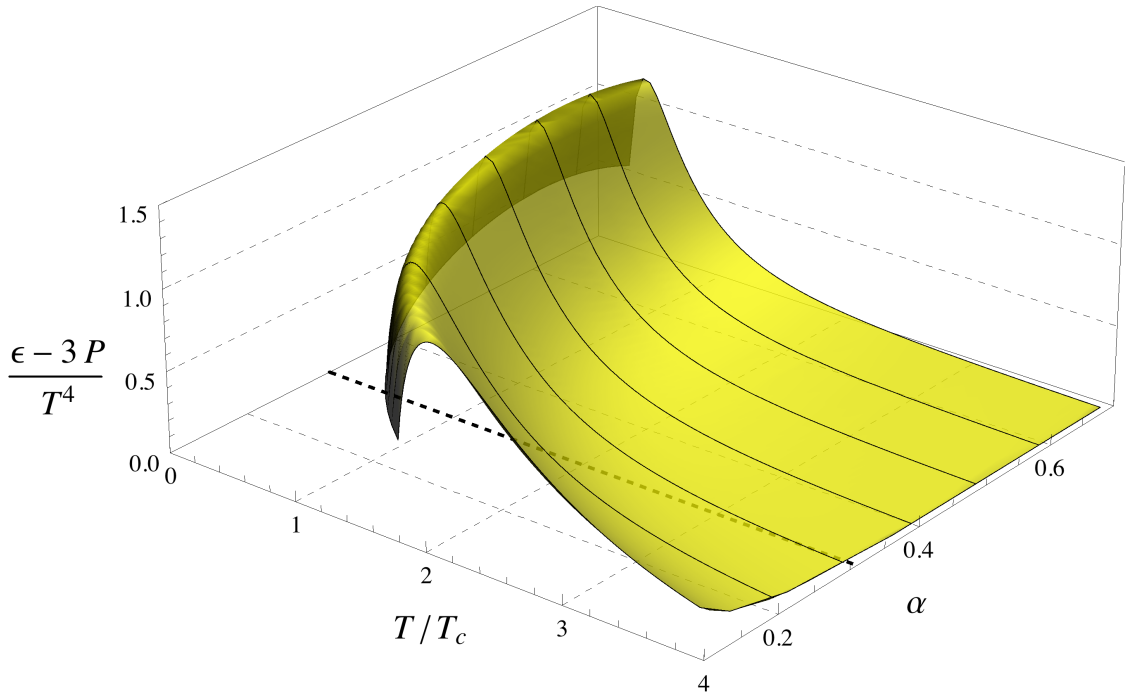


Figure 3.6: Trace anomaly in the 2-parameter model against the temperature in units of $T_c$ and the deformation $\alpha$ for $c = 0.1\,\mathrm{GeV}^2$. Higher values of $c$ result in a moderate shift of the whole curve along the $T$-direction analogously to the 1-parameter computation in Fig. 3.4(a). The curve with $\alpha = 0.31$ and $c = 0.1\,\mathrm{GeV}^2$ is closest to QCD which is indicated by the black, dashed line. The critical temperature $T_c$ fixed at 176 MeV since the steepest increase in the trace anomaly occurs at the critical temperature.

Chapter 4

# Physical Observables

With the help of the three deformed metric models that describe non-conformal physics at strong coupling and high temperature we are now able to study many physical quantities which are related to the quark-gluon plasma. The main focus of this and the next chapter is on the following observables:

1. Energy loss of a trailing string in the 1- and 2-parameter model which has not been worked out in full detail in the literature.
2. Review of the $Q\bar{Q}$-distance computation (see [75] for further reference) as well as definition and analysis of a running coupling $\alpha_{\mathrm{Q\bar{Q}}}$.
3. Analytic derivation of the screening distance for small perturbations.

By studying the aforementioned observables we will focus on two possible effects: firstly, there might be evidence for a *robust* behaviour. This means that switching on non-conformality results in very small changes for a large range of deformations or even no deviation from the conformal $\mathcal{N} = 4_T$ result. We have encountered this in the last chapter when discussing the trace anomaly in the 2-parameter model. There, the deformations in $\alpha$ and $c$ have not changed the amplitude of the trace anomaly at all and the curves were only shifted to different temperature regimes.

Secondly, there might be a systematic change detectable in one particular direction. In the case of the shear viscosity over entropy density ratio $\eta/s$, Kovtun, Starinets and Son observed in [72, 164] that the conformal value in $\mathcal{N} = 4_T$,

$$\frac{\eta}{s} = \frac{1}{4\pi}\,, \tag{4.1}$$

is a universal lower bound for a large class of gauge theories with a dual gravitational theory. To be more precise, $\eta/s$ is exactly $1/(4\pi)$ in all theories we study in this thesis and increases if higher corrections are included. Evidence for a similar bound has been found in a previous paper [75] where we studied the maximal distance $L_{\mathrm{max}}$ of a $\mathrm{Q\bar{Q}}$-pair. Unfortunately, this computation could only be done numerically. We conjectured that this maximum distance $L_{\mathrm{max}}$ – also called screening distance – is bounded from below by the value in $\mathcal{N} = 4_T$

$$(L\pi T)_{\mathrm{max}}^{\mathcal{N}=4_T} \approx 0.86912\,, \tag{4.2}$$

for a large class of gauge theories with a dual gravitational description. Here, $(L\pi T)^{\mathcal{N}=4_T}_{\max}$ is just the corresponding dimensionless quantity to $L^{\mathcal{N}=4_T}_{\max}$ which plays the rôle of a universal number. That this conjecture can be verified analytically at least for small perturbations around the conformal solution will be derived in Chap. 5.

Before we start with the derivation of the energy loss of uniformly moving quark – which is often written in terms of a drag force – it is necessary to review a particular property of the consistent metric models. The scalar $\Phi$ can be interpreted in two different ways. If it is just an additional scalar of the theory without any special properties, the particular model is said to be in the *Einstein frame*. If the scalar $\Phi$ is the dilaton which has some neat features important in string theory, the metric has to be transformed into the *string frame* in order to study non-thermodynamic observables appropriately. The differences between these two different theories and their relation will be worked out in the next section.

## 4.1 Einstein- and String Frame

In Sec. 3.2 we have started with a derivation of a consistent metric by using the 5D-Einstein–Hilbert-scalar action,

$$S_{\mathrm{EHs}} = \frac{1}{16\pi G^{(5)}_{\mathrm{N}}} \int \mathrm{d}^5x \, \sqrt{\text{-}G} \left( \mathcal{R} - \frac{1}{2}\big(\partial\Phi\big)^2 - V(\Phi) \right). \tag{4.3}$$

without any explanations. We have used the basic Einstein–Hilbert action that was solved by the $AdS_5$ metric in Sec. 2.1.1 and implemented a further scalar $\Phi$ along with a potential $V(\Phi)$. However, in string theory, implementing a particular background scalar field usually called *dilaton field* is something well-known. It has some interesting properties, e. g. the constant mode of the dilaton $\Phi_0$ determines the string coupling constant $g_{\mathrm{s}}$ by

$$g_{\mathrm{s}} = \mathrm{e}^{\Phi_0}\,, \tag{4.4}$$

and it violates Weyl invariance classically. In the low-energy limit of our five-dimensional theory – where we are always located – an effective action can be derived which is given by

$$S^{\mathrm{s}} = \frac{1}{16\pi G^{(5)}_{\mathrm{N}}} \int \mathrm{d}^5x \, \sqrt{\text{-}G^{\mathrm{s}}}\, \mathrm{e}^{-2\Phi_5} \left( \mathcal{R}^{\mathrm{s}} + 4\big(\partial\Phi_5\big)^2 - V^{\mathrm{s}}(\Phi_5) \right), \tag{4.5}$$

where $G^{\mathrm{s}}$ is the determinant of the space-time metric $G^{\mathrm{s}}_{\alpha\beta}$, $\Phi_5$ is the five-dimensional dilaton field, $\mathcal{R}^{\mathrm{s}}$ the Ricci scalar derived from $G^{\mathrm{s}}_{\alpha\beta}$, and $V^{\mathrm{s}}(\Phi_5)$ the dilaton potential. The term $\mathrm{e}^{-2\Phi_5}$ in front of the brackets in (4.5) is crucial and represents the coupling of the dilaton to the metric and other fields. The formulation in (4.5) is called *string frame* action and is reflected by the superscript 's' in (4.5).

Equation (4.5) can also be used to derive the metric $G^{\mathrm{s}}_{\alpha\beta}$ in the background of a scalar dilaton field by making use of the variational principle. However, the dilaton coupling term $\mathrm{e}^{-2\Phi_5}$ complicates the derivation of the metric. Therefore, we use a conformal scaling transformation of the metric in order to simplify the action. By using

$$G^{\mathrm{s}}_{\alpha\beta} = \mathrm{e}^{-2\Omega}\, G^{\mathrm{E}}_{\alpha\beta}\,, \tag{4.6}$$

where $G^{\mathrm{E}}_{\alpha\beta}$ denotes the space-time metric in the transformed frame, we can relate the scalar curvatures in the two frames by

$$\mathrm{e}^{-2\Omega}\,\mathcal{R}^{\mathrm{s}} = \mathcal{R}^{\mathrm{E}} - (D-1)(D-2)\,\partial_\alpha\Omega\,\partial^\alpha\Omega - 2(D-1)\,\nabla^2\Omega\,. \tag{4.7}$$

Here, $D = 5$ is the dimension and $\nabla^2$ is defined by $\frac{1}{\sqrt{-G^{\mathrm{E}}}}\,\partial_\alpha\sqrt{-G^{\mathrm{E}}}\,\partial^\alpha$. Thus, the first part of (4.5) transforms as

$$\begin{aligned}\int \mathrm{d}^5x\,\sqrt{-G^{\mathrm{s}}}\,\mathrm{e}^{-2\Phi_5}\,\mathcal{R}^{\mathrm{s}} &= \int \mathrm{d}^5x\,\sqrt{-G^{\mathrm{E}}}\,\mathrm{e}^{-3\Omega-2\Phi_5}\,\mathrm{e}^{-2\Omega}\mathcal{R}^{\mathrm{s}} \\ &= \int \mathrm{d}^5x\,\sqrt{-G^{\mathrm{E}}}\left[\mathcal{R}^{\mathrm{E}} - 12(\partial_\alpha\Omega)^2\right], \quad \text{with} \quad \Omega = -\frac{2}{3}\,\Phi_5\,.\end{aligned} \tag{4.8}$$

By choosing $\Omega = -\frac{2}{3}\,\Phi_5$ the $\nabla^2\Omega$ contribution of the rescaled Ricci scalar drops out. Thus the string frame action (4.5) reduces to the action $S^{\mathrm{E}}$ in the so-called *Einstein frame* which can be written as:

$$\begin{aligned}S^{\mathrm{s}}[G^{\mathrm{s}}_{\alpha\beta},\,\mathcal{R}^{\mathrm{s}},\,V^{\mathrm{s}}] &= \frac{1}{16\pi G^{(5)}_{\mathrm{N}}}\int \mathrm{d}^5x\,\sqrt{-G^{\mathrm{s}}}\,\mathrm{e}^{-2\Phi_5}\left(\mathcal{R}^{\mathrm{s}} + 4\big(\partial\Phi_5\big)^2 - V^{\mathrm{s}}(\Phi_5)\right) \\ &= \frac{1}{16\pi G^{(5)}_{\mathrm{N}}}\int \mathrm{d}^5x\,\sqrt{-G^{\mathrm{E}}}\left(\mathcal{R}^{\mathrm{E}} - \frac{4}{3}\,(\partial\Phi_5)^2 - V^{\mathrm{E}}(\Phi_5)\right) = S^{\mathrm{E}}[G^{\mathrm{E}}_{\alpha\beta},\,\mathcal{R}^{\mathrm{E}},\,V^{\mathrm{E}}]\,.\end{aligned} \tag{4.9}$$

The corresponding metric $G^{\mathrm{E}}_{\alpha\beta} = \mathrm{e}^{-\frac{4}{3}\Phi_5}\,G^{\mathrm{s}}_{\alpha\beta}$ is then called Einstein-frame metric and the potentials are related by

$$V^{\mathrm{s}} = V^{\mathrm{E}}\,\mathrm{e}^{-\frac{4}{3}\Phi_5}\,. \tag{4.10}$$

The Einstein frame action in (4.9) is already very similar to (4.3) which we used in the last chapter. In a last step we make use of a renormalisation of the scalar dilaton $\Phi_5$ of the form

$$\Phi_5 \equiv \sqrt{\frac{3}{8}}\,\Phi\,, \tag{4.11}$$

and absorb the cosmological constant $-2\Lambda$ into the dilaton potential in order to derive the explicit expression in (4.3).

But, why do we discuss both frames in great detail if they are equivalent nonetheless? A problem arises when we go beyond the analysis of thermodynamic observables. In the following sections we do not study the empty deformed $AdS_5$ space-time but implement a macroscopic string that is connected to the boundary at $z = 0$ and is hanging into the $5^{\mathrm{th}}$-dimension. A sketch of this configuration is shown in Fig. 4.2. This allows for studying the energy loss of a moving heavy parton at the boundary and a similar configuration is needed to analyse the screening distance of a quark-antiquark pair. In both cases this macroscopic string is governed by a Nambu–Goto action $S_{\mathrm{NG}}$

$$\begin{aligned}S_{\mathrm{NG}} &= \frac{1}{2\pi\alpha'}\int \mathrm{d}\sigma\mathrm{d}\tau\,\sqrt{-\det g^{\mathrm{s}}_{ab}}\,, \quad \text{with} \quad g^{\mathrm{s}}_{ab} = G^{\mathrm{s}}_{\alpha\beta}\,\partial_a X^\alpha\,\partial_b X^\beta\,, \\ &= \frac{1}{2\pi\alpha'}\int \mathrm{d}\sigma\mathrm{d}\tau\,\mathrm{e}^{\frac{4}{3}\Phi_5}\,\sqrt{-\det g^{\mathrm{E}}_{ab}}\,, \quad \text{with} \quad g^{\mathrm{E}}_{ab} = G^{\mathrm{E}}_{\alpha\beta}\,\partial_a X^\alpha\,\partial_b X^\beta\,,\end{aligned} \tag{4.12}$$

that can be written in Einstein- and string frame as well. It is a two-dimensional generalisation of the action governing the motion of the relativistic point particle. Thus, extremising (4.12) is easier using the string frame metric. Altogether, the procedure of computing non-thermodynamic observables in a dilatonic theory is the following: derivation of the space-time metric $G^{\mathrm{E}}_{\alpha\beta}$ in Einstein frame, transformation into string frame and computation of the extremised Nambu–Goto action.

In principle, it is possible to add a scalar field in the Einstein–Hilbert action without identifying it with the dilaton. It is then just an additional scalar in the theory. This led to some confusion in the literature since theories including a scalar which is not the dilaton are often called Einstein frame models whereas models with a dilaton are denoted by string frame models, although they are not equivalent but represent a totally different theory. In these Einstein frame models the dilaton is trivial.

In the following we will study both theories. In the model with a non-dilatonic scalar the Einstein and string frame metric are identical. Thus, we use the Einstein frame action in order to derive the (Einstein-frame) space-time metric that obeys the equation

$$G^{\mathrm{E}}_{\alpha\beta} = G^{\mathrm{s}}_{\alpha\beta}\,, \tag{4.13}$$

since the dilaton is trivial. This result can be used to extremise the Nambu–Goto action in the string frame. If we are interested in a dilatonic model we compute the Einstein metric as well which is identical to the metric in the other approach but then transform this metric into the string frame via $G^{\mathrm{s}}_{\alpha\beta} = \mathrm{e}^{\sqrt{\frac{2}{3}}\Phi}\, G^{\mathrm{E}}_{\alpha\beta}$ which can then be used to extremise the Nambu–Goto action in the string frame. In order to conform with the conventions in the literature we will refer to the scalar model as an Einstein-frame setup and to the dilaton approach as a string-frame setup, respectively. Keeping these formal remarks in mind we proceed now with the computation of several physical quantities in all our models, i. e. $\mathrm{SW}_T$-, 1-parameter (string and Einstein frame) and 2-parameter model (string and Einstein frame).

## 4.2 Energy Loss of a Moving Quark

In this section we study the energy loss of a uniformly moving quark with velocity $v$ or rapidity $\eta$ in a non-conformal background at strong coupling and finite temperature. The analysis in a conformal background at finite temperature and in the $\mathrm{SW}_T$-model is well-known and can be found in [165–168] and [73], respectively. The investigation in a general, large class of non-conformal models has not been worked out yet and is the main task of this section. It will be very interesting to see if one of the above-mentioned behaviours (robustness or universal change) arise in the computation of the energy loss. In addition to this, studying energy loss of moving particles in strongly coupled plasmas is also very interesting from a practical point of view.

RHIC and LHC data exhibit strong quenching of single-hadron spectra connected with large energy loss in dense, strongly coupled plasmas [169]. However, a full theoretical description of the essential interactions occurring when a heavy, fast parton traverses the plasma is missing. The whole process is sketched in Fig. 4.1. Theorists have a good understanding of how the fast partons get produced due to the large momentum transfer that allows for a precise perturbative description (see (1) in Fig. 4.1). In the case of the fragmentation process that leads to the large amount of hadrons observed in the jets at the end, one has several well-developed approaches although the interactions are non-perturbative (see (3) in Fig. 4.1). Unfortunately,

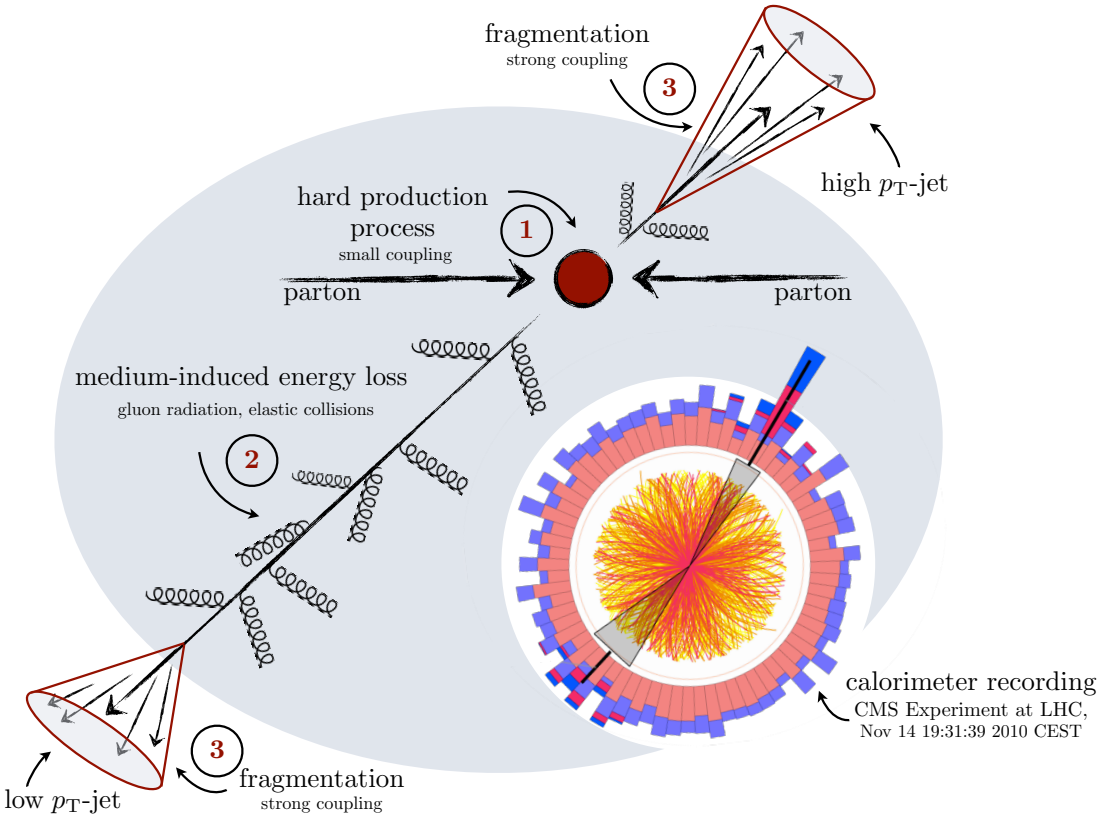


Figure 4.1: Schematic picture of the different stages two high energy partons experience on their way through the plasma including in-medium energy loss effects causing jet quenching in the end.

for the in-medium energy loss one has relevant contributions from interactions at different coupling scales [170–173] (see (2) in Fig. 4.1). In principle, one can distinguish between elastic, collisional energy loss $\Delta E_{\text{coll}}$ [174–176] and radiative energy loss $\Delta E_{\text{rad}}$ [177–180] which is an inelastic process due to gluon bremsstrahlung. Furthermore, a distinction between light and heavy partons [181–183] is important. In the first case, radiative energy loss is the most important process at high energy[1]. In the latter case, collisional energy loss is dominant [174, 175, 184–188]. In addition, there is a suppression of the radiative energy loss due to the so-called *Dead Cone Effect* [182, 189] telling us that the radiative energy loss gets suppressed for angles $\theta < m/E$. Here, $\theta$ measures the angle between the parton direction and the emitted gluon.

In the context of gauge/gravity dualities – according to Fadafan *& al.* [190] – two strategies are available to tackle this in-medium energy loss. The first approach – we pursue in the following – assumes that the initial production of hard probes that traverse the plasma is perturbative. The interactions responsible for the energy loss are then treated to be non-perturbatively strong at all scales [190]. This is a reasonable ansatz since at low and high

[1]The Coulomb contribution for the collisional energy loss is weak. For heavy quarks Compton scattering is getting more and more important which leads to a shift in the dominant energy loss process towards the collisional contribution

energies interactions with the plasma occur that involve small momentum transfers which have to be described non-perturbatively. Furthermore, this system that includes only non-perturbatively strong interactions at all scales can be perfectly described by the $AdS$/CFT correspondence. Within this framework we can compute for example the energy loss $\mathrm{d}E/\mathrm{d}t$ of a heavy parton at constant velocity traversing the plasma which is equivalent to the computation of the external force required to pull the parton through the plasma at a constant velocity $v$ [74, 165, 167]. This can be worked out in the gravity dual by focusing on a macroscopic string (bulk analog of the quark in the field theory) that trails behind the quark. This is sketched in Fig. 4.2. It is important to note that in the conformal computation it was argued that the force which is needed to keep the quark moving is proportional to the quark momentum [165], meaning that energy loss occurs via drag. This discussion will be extended in chapter 6 to non-uniformly moving particles when the energy loss of a rotating quark will be analysed which is very interesting since acceleration/deceleration opens the possibility of additional mechanisms of parton energy loss. In the regime of a very fast rotating quark for example we think of the energy loss to be as if the quark radiates in vacuum.

In the other approach that have been mentioned by Fadafan *& al.* [190] one uses light-like Wilson loops [191] that incorporate the non-perturbative properties of the strongly coupled medium. These quantities can then be evaluated via gauge/gravity dualities [124, 192] in order to obtain for example the jet quenching parameter $\widehat{q}$. This computation is, however, valid in the regime of very energetic partons only, where the dominant energy loss mechanism is radiative.

We will focus in the following on the first approach without exception. In the current setup we will start by reviewing the computational steps that lead to an expression for the energy loss $\mathrm{d}E/\mathrm{d}t$ in $\mathcal{N}=4$ at finite temperature [165] and proceed with a computation of $\mathrm{d}E/\mathrm{d}t$ in a large class of metric models with a string configuration given by (3.5) that has not been worked out before in the literature. The well-defined gravity dual of a heavy, moving quark in the boundary theory – as we have indicated above – is given by an open macroscopic string hanging into the bulk that is connected to the boundary, extremising a classical action of the two-dimensional worldsheet. With worldsheet we denote the two-dimensional surface spanned by a direction along the string and the time coordinate [165, 168]. The basic setup is illustrated in Fig. 4.2. The action governing the motion of the string is the above-mentioned Nambu–Goto action $S_{\mathrm{NG}}$ that is given by

$$S_{\mathrm{NG}} = \frac{1}{2\pi\alpha'} \int \mathrm{d}\sigma \mathrm{d}\tau \, \sqrt{-\det g_{ab}}\,, \quad \text{with} \quad g_{ab} = G_{\alpha\beta}\, \partial_a X^\alpha \, \partial_b X^\beta\,, \tag{4.14}$$

where $g_{ab}$ is the *induced* or *worldsheet* metric, $X^\alpha$ are the space-time coordinates and $\alpha'$ is the Regge slope which is a string theory parameter related to the string tension $T_{\mathrm{s}} = (2\pi\alpha')^{-1}$ and to the string length $l_{\mathrm{s}} = \sqrt{\alpha'}$. The coordinates $\tau$ and $\sigma$ parameterise the worldsheet described by the string.

It is noteworthy that a macroscopic string should in principle influence the background metric $G_{\alpha\beta}$ which we have derived with the help of the Einstein–Hilbert-(scalar) action without considering any macroscopic string. Per se, one has to add the Nambu–Goto action of (4.14) to the full Einstein–Hilbert-(scalar) action in (4.9) and solve the full system for the space-time metric. This is a very tough task, however. The influence of the Nambu–Goto action – which is called *back-reaction* – is a first order effect and can be neglected in our approach. Besides, a similar argumentation leads to the suppression of flavour. The $N_{\mathrm{f}}$ flavour degrees of freedom which can be represented in the dual gravity theory by flavour branes are strongly

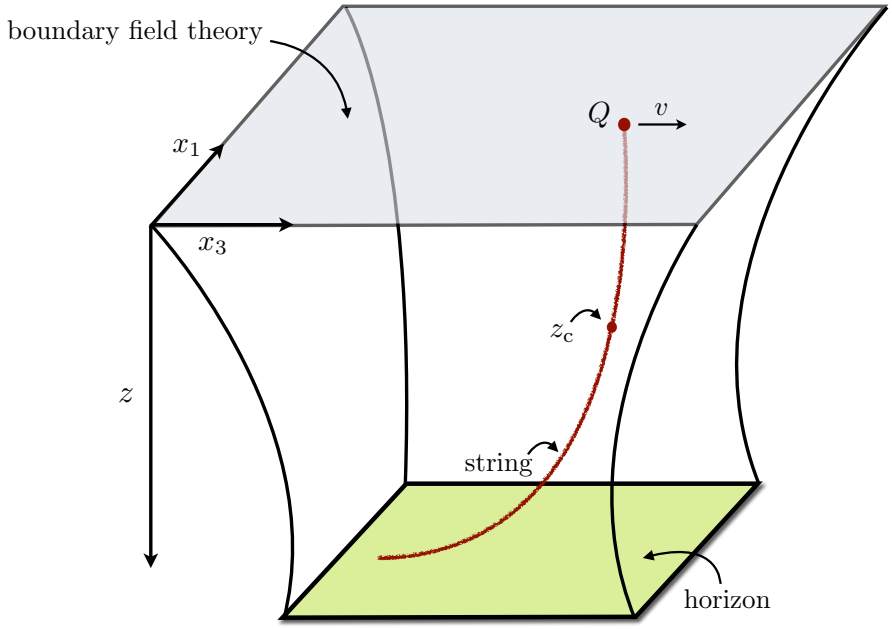


Figure 4.2: Schematic picture of a quark moving at constant velocity through a hot plasma including the dual gravity scenario of a trailing string dragging behind the quark. $z_c$ in the bulk denotes the point where the string velocity exceeds the local speed of light.

suppressed in the large-$N_c$ limit. In particular, this means that we take the so-called *probe limit*, $N_f \ll N_c$ [51, 193]. This is an effect of the large-$N_c$ limit and going beyond cannot be achieved without increasing difficulty dramatically. Up to now, some frameworks are available where the supergravity solution is known beyond the probe limit [57, 129, 194]. This limit is also well-known in the lattice literature where it is called *quenched approximation*. The full dynamics of the glue and its effect on the fermions is included, but the back-reaction of the fermions on the glue is dropped. In the probe limit this approximation becomes exact.

The last assumption we include in the following analysis of the energy loss is the property of having infinitely massive partons. They are therefore located on a D3 brane at the $z = 0$ boundary. Putting the partons into the bulk at a certain position $z_m$ is equivalent to shifting the D3 brane into the bulk to a new position $z_m$. This corresponds to a finite quark mass $M$ of

$$M = \frac{\sqrt{\lambda}}{2\pi\, z_m}\,. \tag{4.15}$$

$M$ can be computed with the help of the free energy which we will derive in Sec. 4.3.2. Including finite mass is in principle possible, but there are more sophisticated models where higher-dimensional branes are included in order to describe flavour and mass. In addition to this, infinite and finite mass differ only slightly in the observables analysed in the next sections.

After the remarks on the physical background of this computation let us come back to the evaluation of the Nambu–Goto action in the limit of infinitely heavy quarks and suppression of flavour. Since the argument in the Nambu–Goto action (4.14) is the Lagrange density $\mathcal{L} \equiv \sqrt{-g}$ we can use classical Euler–Lagrange mechanics to solve for the equations of motion. The derivation of the energy loss of a trailing string can thus be divided into four parts:

1. Choose an appropriate parameterisation of the string worldsheet. This means that the embedding $X^\mu(\tau, \sigma)$ has to be defined.
2. Derive the Euler–Lagrange equation of the Nambu–Goto action.
3. Use appropriate boundary conditions to derive the string configuration.
4. The energy loss or drag force of a trailing string is then given by the momentum flux on the worldsheet of the trailing string along the $5^{\text{th}}$-dimensional direction,

$$\frac{\mathrm{d}p^{(3)}}{\mathrm{d}t} = -\frac{\delta S_{\text{NG}}}{\delta \partial_\sigma x^3}\bigg|_{\text{trailing string}} . \tag{4.16}$$

As we will see below, the right-hand side of (4.16) is a conserved quantity on the worldsheet.

According to Fig. 4.2 we think of the quark to be moving along the $x_3$-direction with velocity $v$. The parameterisation of the worldsheet in the convenient *static gauge* is given by

$$X^\alpha \equiv \big(t = \tau,\, 0,\, 0,\, x_3(\tau, \sigma),\, z = \sigma\big)\,, \quad \text{with} \quad x_3(\tau, \sigma) = v\tau + \xi(\sigma)\,. \tag{4.17}$$

We present this computation for the general metric ansatz given in Sec. 3.2.1 that is quoted here for simplicity

$$\mathrm{d}s^2 = \mathrm{e}^{2A(z)}\left(-h(z)\mathrm{d}t^2 + \mathrm{d}\vec{x}^{\,2}\right) + \mathrm{e}^{2B(z)}\,\frac{\mathrm{d}z^2}{h(z)}\,. \tag{4.18}$$

By substituting (4.17) and (4.18) into (4.14) and taking the square root of the negative determinant we obtain the Lagrange density $\mathcal{L}$:

$$\mathcal{L} \equiv \left[\mathrm{e}^{4A(z)}\,h(z)\,\xi'^{\,2}(z) - \frac{\mathrm{e}^{2A(z)+2B(z)}}{h(z)}\left(v^2 - h(z)^2\right)\right]^{1/2}, \tag{4.19}$$

where $'$ denotes a derivation $\frac{\partial}{\partial z}$. Due to the $\xi$-independence of (4.19) the Euler–Lagrange equation reduces to

$$\frac{\partial \mathcal{L}}{\partial \xi'} = \text{const.} \quad \Longleftrightarrow \quad \mathrm{e}^{4A(z)}\,\frac{h\,\xi'}{\mathcal{L}} = \text{const.} \equiv q\,. \tag{4.20}$$

Furthermore, we find a relation between the constant $q$ and the definition of the drag in (4.16):

$$\frac{\mathrm{d}p^{(3)}}{\mathrm{d}t} = -\frac{\delta S_{\text{NG}}}{\delta \partial_\sigma x^3}\bigg|_{\text{trailing string}} = -\frac{1}{2\pi\alpha'}\,\frac{\partial \mathcal{L}}{\partial \xi'} = -\frac{1}{2\pi\alpha'}\,q\,, \tag{4.21}$$

where we used $\partial_\sigma x^3 = \xi'$ according to our parameterisation. Thus, we just have to fix the conserved canonical momentum $q$ in order to get the energy loss of a moving quark. Unfortunately, the only given boundary condition is the vanishing of $\xi(z)$ at the boundary

($z = 0$) which is not useful at this stage of the computation. However, by solving (4.20) for $\xi'$ we can extract a reality condition:

$$\xi' = -\frac{q}{h(z)} \left[ \mathrm{e}^{2B(z)-2A(z)} \frac{v^2 - h(z)}{q^2 - \mathrm{e}^{4A(z)}\, h(z)} \right]^{1/2} . \tag{4.22}$$

The negative root has to be chosen in order to have a string trailing behind the quark. Since $\xi'$ has to be real for all values of $z$ in order to give a physically meaningful interpretation of a string hanging into the bulk, the numerator and the denominator have to change signs simultaneously. This leads to the existence of a point in $z$-direction which we denote by $z_\mathrm{c}$ and which has to fulfil the following conditions

$$v^2 = h(z_\mathrm{c})\,, \quad \text{and} \quad q = \mathrm{e}^{2A(z_\mathrm{c})} \sqrt{h(z_\mathrm{c})} = \mathrm{e}^{2A(z_\mathrm{c})}\, v\,. \tag{4.23}$$

$z_\mathrm{c}$ has a very remarkable property. It defines a so-called *worldsheet horizon* since the $\tau\tau$-component of the induced metric vanishes at this point. In addition to this, the velocity of the string at this point reaches the local speed of light in the bulk. A derivation of these important facts is given in Appendix C. This means that there is a causal disconnection between the string above and below this point. We will discuss the physical effects of this value in the later part of this section and in Chapter 6, where a similar point arises in the discussion of rotating quarks. By integrating (4.22) and implementing the condition $\xi(0) = 0$ as well as (4.23) that relates $q$ and $v$ we can numerically solve for the explicit string configuration. Results of this computation are shown in Fig. 4.3, where we plot the string configuration of a trailing

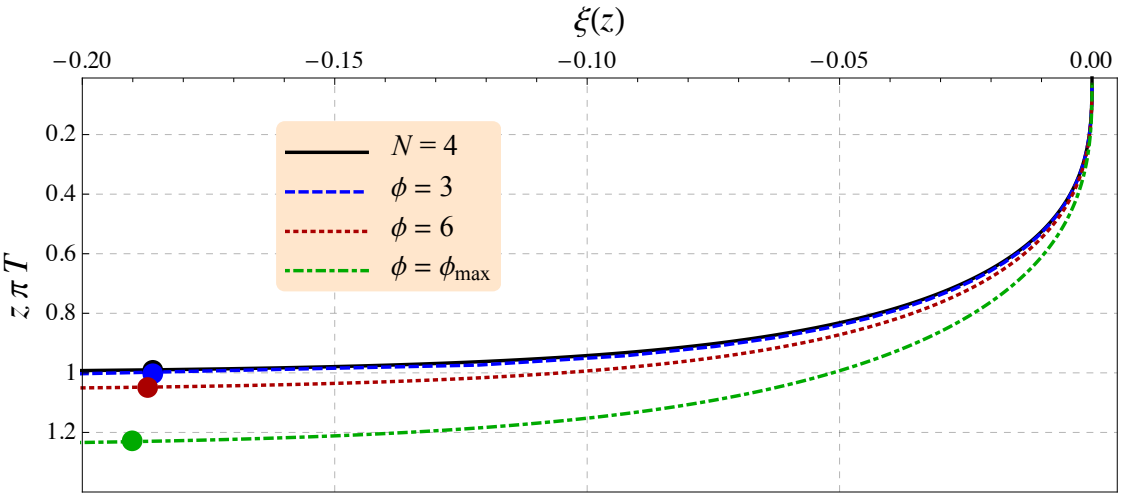


Figure 4.3: String configuration of a trailing string for the conformal $\mathcal{N} = 4$ case and in the 1-parameter (Einstein frame) model for fixed velocity $v = 0.2$ and fixed temperature $T = 1$. The coloured dots represent the critical point $z = z_\mathrm{c}$. For sake of clarity the results of the other models are neglected since the results are very similar.

string in $\mathcal{N} = 4$ and in the 1-parameter (Einstein frame) model for fixed velocity $v = 0.2$ and fixed temperature $T = 1$. Analogous to the computation of thermodynamic quantities we compute all the observables in arbitrary units. If one observable assumes certain dimensions all other related quantities are fixed as well. $\xi(z)$ is identical to the $x_3$ coordinate for time $\tau = 0$ (see (4.17)). All curves reach their corresponding horizon asymptotically. Although

the temperature is the same for all curves the horizon is different due to the $\phi$-dependence in the temperature function in (3.44). A nice fact to note is the robustness of this model. For the given temperature $T = 1$ in Fig. 4.3 the maximal deformation ($\phi_{\max} = 8.6$) deviates only about 20% from the conformal result. The existence of a maximal deformation is a particular property of the consistent models. As we have seen in Figs. 3.2 and 3.5 both models have a minimal temperature $T_{\min}$ for every value of the deformation, or conversely, each temperature can be related to a maximal deformation $\phi_{\max}$. The coloured dots represent the point where the upper and lower part of the string are causally disconnected because the velocity of the string exceeds the local speed of light. This point exists in all our models. We do not show results for the other models because the shape of the string configuration is almost identical.

In the simple $\mathcal{N} = 4$ case at finite temperature Gubser *& al.* found in [195] an analytic expression of the string configuration that reads

$$x^3(t,\, z) = vt + \xi(z,\, z_{\rm h},\, v)\,,$$
$$\text{with}\quad \xi(z, z_{\rm h},\, v) = \frac{{\rm i}\, v\, z_{\rm h}}{4}\left(\log\left[-\frac{z + {\rm i} z_{\rm h}}{z - {\rm i} z_{\rm h}}\right] + {\rm i}\log\left[-\frac{z + z_{\rm h}}{z - z_{\rm h}}\right]\right). \tag{4.24}$$

In the other more advanced models we have to use a numerical integration method in order to solve (4.22) for $\xi(z)$.

By using (4.21) and (4.23) we obtain the following expression for the energy loss of a moving quark at constant velocity

$$\frac{{\rm d}p^{(3)}}{{\rm d}t} = -\frac{1}{2\pi\alpha'}\, q = -\frac{\sqrt{\lambda}}{2\pi L^2}\, {\rm e}^{2A(z_{\rm c})}\, v\,. \tag{4.25}$$

Here, the general relation $L^4 = \lambda\, \alpha'^2$ has been used.[2] $z_{\rm c}$ in (4.25) can be replaced by $v$ with the help of a numerical routine using (4.23).

In the context of conformal $AdS_5$ at finite temperature the drag force can be written as

$$\frac{{\rm d}p^{(3)}}{{\rm d}t} = -\frac{\pi\sqrt{\lambda}}{2}\, T^2\, \frac{v}{\sqrt{1 - v^2}} = -\frac{\pi\sqrt{\lambda}}{2}\, T^2\, \frac{p^{(3)}}{m}\,, \tag{4.26}$$

where the proportionality with respect to the momentum is obvious. The results for the 1- and 2-parameter models are shown in Figs. 4.5 and 4.7, Figs. 4.4 and 4.6, respectively. Fig. 4.4 shows the ratio of the drag force in the 2-parameter model in the Einstein frame and the corresponding conformal result for two fixed temperatures $T$, $T = 0.3$ (lower surface) and 1 (upper surface). Four important facts can be extracted from this plot:

1. The higher the temperature $T$ the more robust is the drag force when a deformation is switched on. This is clear because high $T$ is closer to the undeformed case due to the suppression of other effects.

2. In the limit of vanishing deformation ($\alpha \to \infty$ and $c \to 0$) we reach the $\mathcal{N} = 4$ limit.

3. The excluded parameter regime (close to $\alpha = 0$) for a given fixed temperature is larger for lower temperatures since for a given choice of parameters only temperatures $T$ with

[2] These relations have been derived for the particular gauge/gravity correspondence of $\mathcal{N} = 4$ and $AdS_5$. It is not fully understood whether these fundamental relations change if the $AdS_5$ space-time gets deformed.

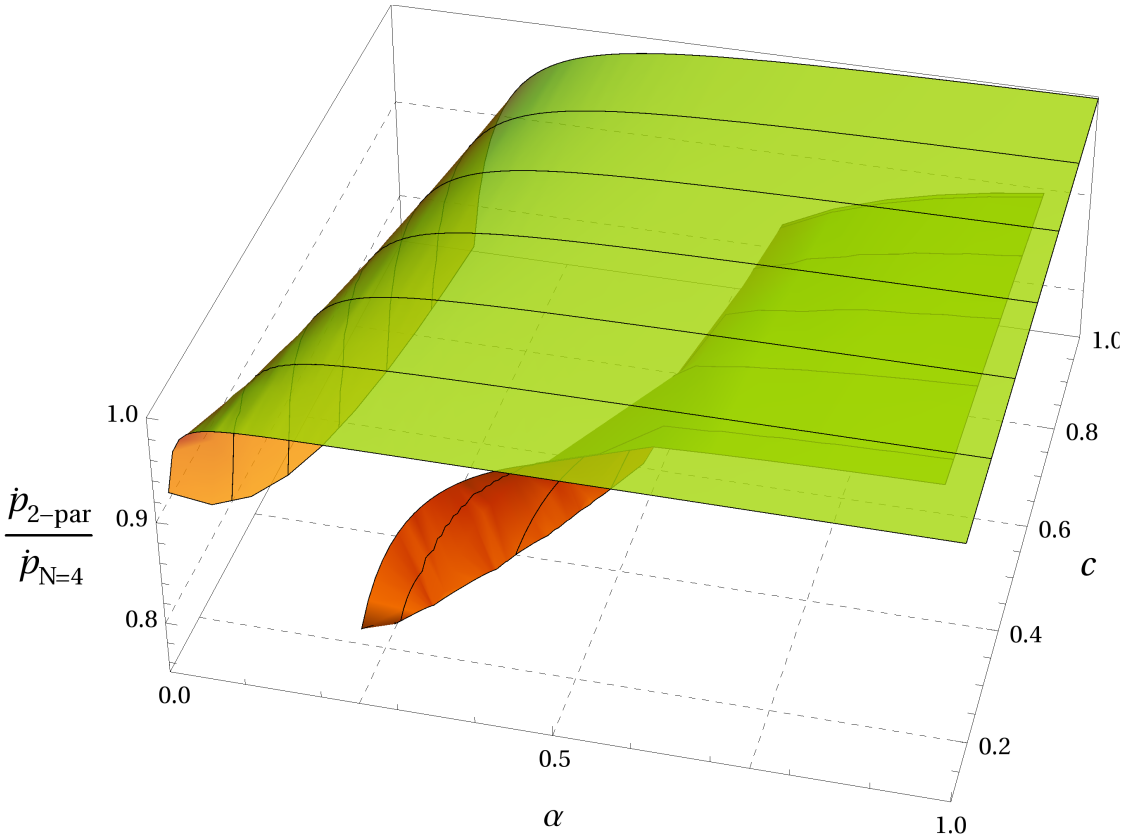


Figure 4.4: Ratio of the drag force in the Einstein frame of the 2-parameter model to the corresponding conformal result against the two deformation parameters $\alpha$ and $c$ for two different fixed temperatures $T$, $T = 0.3$ and 1. The smaller the temperature, the earlier occurs the decrease. This means that $T = 1$ is the upper surface and $T = 0.3$ the lower one.

$T > T_{\text{min}}$ are allowed. Here, a larger deformation ($\alpha \longrightarrow 0$ and/or $c \longrightarrow \infty$) leads to a higher minimal temperature $T_{\text{min}}$ and thus the drag force is not well-defined for a fixed temperature close to $\alpha = 0$ because the temperature we want to adjust is below the minimal temperature for this choice of parameters.

4. The drag force in the 2-parameter (Einstein frame) model is bounded from above by the conformal values. This is an indication for a general behaviour of the drag force. Unfortunately, the string frame computation (see Fig. 4.5) suggests a different behaviour.

As already indicated above, the drag force computations in the string frame of the 1- and 2-parameter model – see Fig. 4.5 for the 2-parameter results – show a different behaviour than the corresponding Einstein-frame computations. In this setup the drag force is larger than the $\mathcal{N} = 4$ computation for all values of the deformation. Similar results are shown for the 1-parameter model in Fig. 4.6. There, both frames are shown in one figure.

Although the results do not strongly deviate from the conformal result in a physically meaningful regime around $\alpha = 0.31$ and $c = 0.1\,\text{GeV}^2$, suggesting a robust behaviour, we can find certain limits where the drag force in the 1- or 2-parameter case is very different from the conformal result. To visualise this fact, we plot in Fig. 4.6 and 4.7 the ratio of the drag force in the respective model and the corresponding conformal value for the minimal temperature

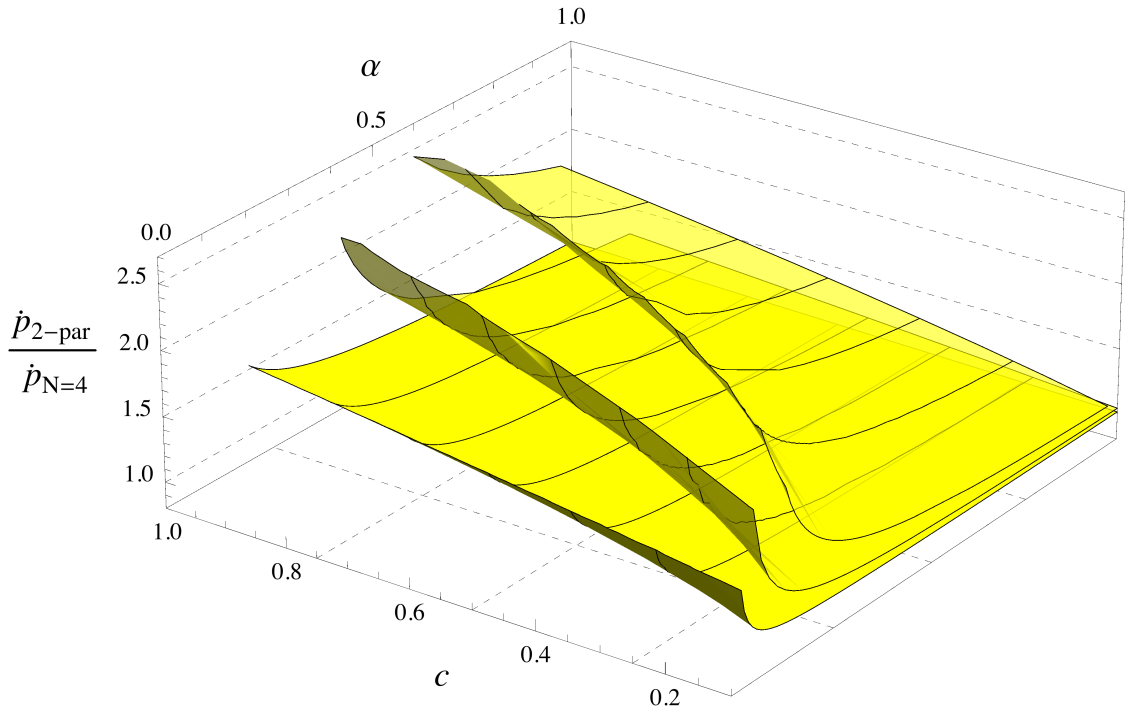


Figure 4.5: Drag force in the string frame of the 2-parameter model against the deformation parameters $\alpha$ and $c$ for three different fixed temperatures $T$, $T = 0.3$ (highest surface), 0.5 and 1 (lowest surface). The smaller the temperature the earlier occurs the increase. Due to the large numerical effort and some minor technical subtleties therein we could not generate arbitrarily smooth surfaces.

$T_{\min}$ of each parameter choice. These plots show the maximal deviation of the drag force from the conformal result for the given choice of deformation parameters since for a given choice of deformation parameters a temperature $T > T_{\min}$ would immediately lead to a more conformal result. The reason for this is the following: higher temperatures lead to the suppression of the deformation and in the limit $T \longrightarrow \infty$ all the results are conformal again. Thus the strongest influence of the deformation happens at the minimal temperature $T_{\min}$. Several interesting facts can be extracted from Figs. 4.6 and 4.7:

1. In the case of the 1-parameter model (Fig. 4.6) the strongest deviation from the conformal result is bounded from below in the Einstein frame and from above in the string frame. In particular, in the Einstein frame we have a very robust behaviour.

2. A higher velocity $v$ of the moving quark leads to a more conformal behaviour. In the 1-parameter model this effect is remarkably strong in the string frame case. But it is not only valid in the 1-parameter case. In Fig. 4.7 where the most strongly deviating drag force is shown in both frames of the 2-parameter model we observe the same behaviour. In Fig. 4.7(a) higher surfaces correspond to higher velocities and in Fig. 4.7(b) lower surfaces correspond to higher velocities.

3. In the 2-parameter case we find a peculiar behaviour of the most strongly deviating drag force. For more and more conformal values the strongest deviation goes either to zero (Einstein frame) or to infinity (string frame). This can be explained in the following

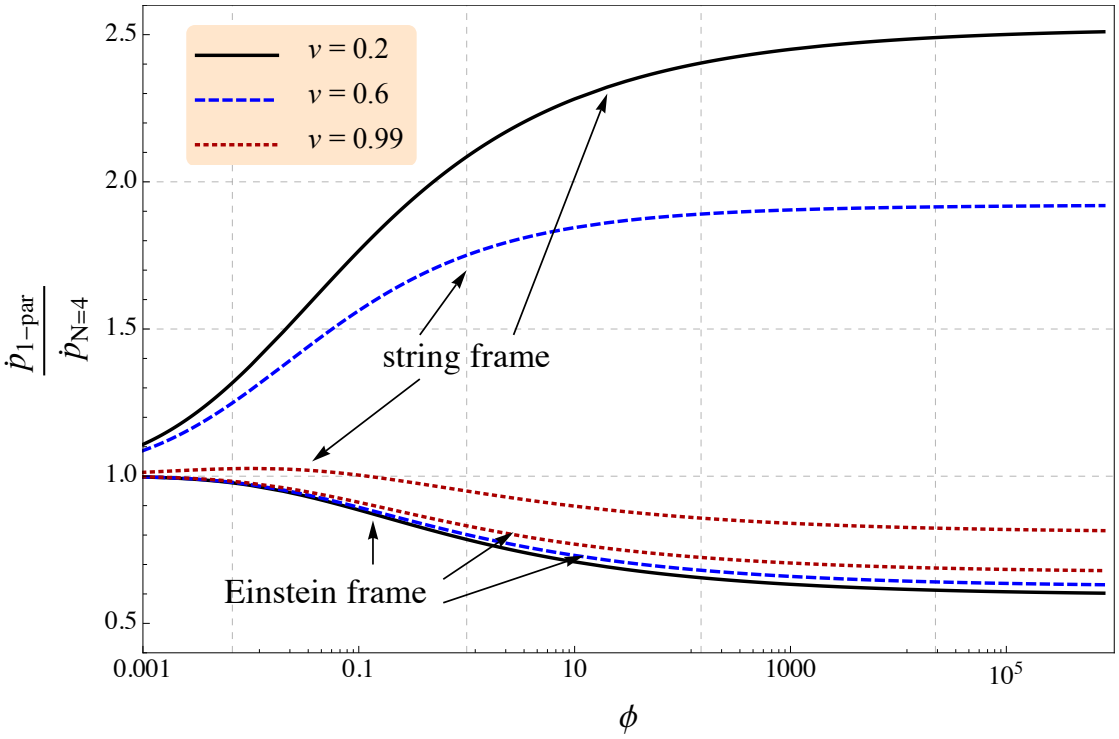


Figure 4.6: Ratio of the most strongly deviating drag force in the 1-parameter model to the conformal result against the corresponding deformation parameter $\phi$ for three different velocities $v$, $v = 0.2, 0.6$ and $0.99$. The three lower curves represent the Einstein- and the upper curves the string frame. The strongest deviation from $\mathcal{N} = 4$ occurs at the minimal temperature $T_{\text{min}}$ for a given deformation $\phi$.

way: if we go to smaller and smaller deformation parameters (closer to the conformal limit) we note a strong decrease in the minimal temperature $T_{\text{min}}$. This decrease is more dominant than the loss of non-conformality by taking the conformal limit. Thus, since a smaller temperature intensifies the effect of a given deformation, we see a stronger deviation from the conformal result.

In summary, we can state that the analysis of the drag force shows in each of the different models a consistent, systematic behaviour when a deformation is introduced and that for physically meaningful parameters only a small deviation from the conformal limit is observed. This is called a *robust* behaviour in the literature. However, we do not see a universal increase or decrease in the drag force for all models under investigation as it has been observed in the case of the screening distance in [75].

In the next section, we review the computational steps in the analysis of the quark-antiquark distance needed to derive a very interesting quantity that has not been calculated at all with the help of holographic methods in non-conformal theories. We focus on the running coupling $\alpha_{\text{Q}\bar{\text{Q}}}$ derived from the free energy of a quark-antiquark pair. There we hope to gain some additional insights about common properties of all our models. That this is indeed quite likely has been indicated in the analysis of thermodynamic properties in Chapter 3 as well as in the previous discussion of energy loss; in both cases a very robust behaviour is apparent. From the thermodynamic analysis in Chapter 3 we have learned for example that these models share many properties (e. g. the amplitude of the trace anomaly).

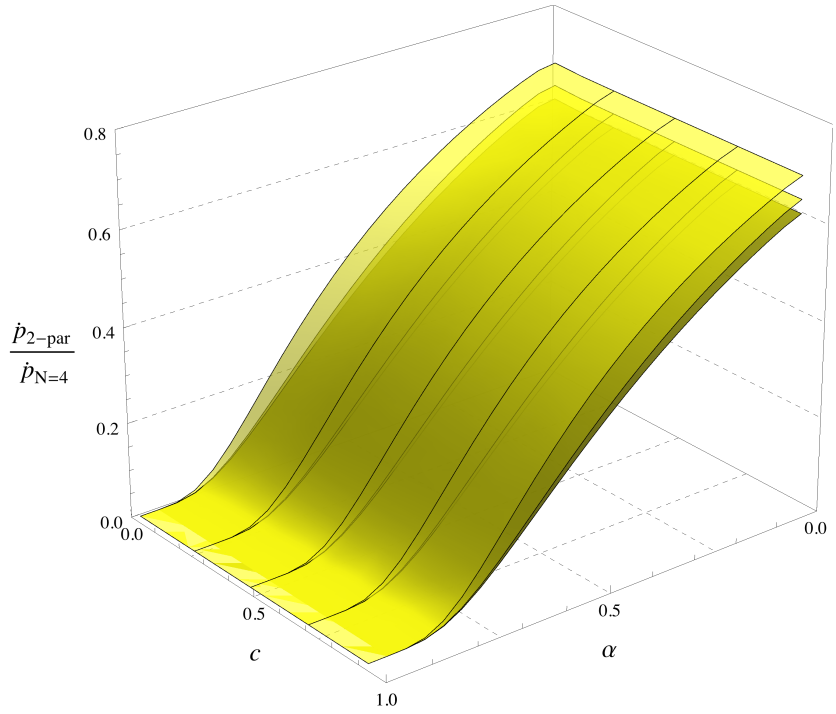


(a) Ratio of the most strongly deviating drag force in the Einstein frame of the 2-parameter model to the corresponding conformal value against the deformation parameters $\alpha$ and $c$. The lowest surface is for $v = 0.2$, the middle one for $v = 0.6$, and the highest surface for $v = 0.99$.

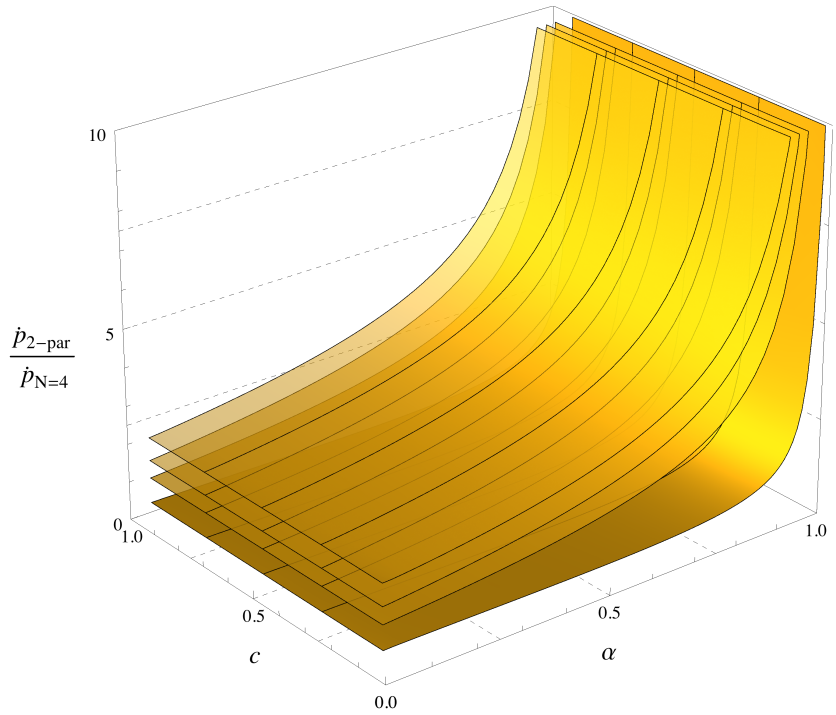


(b) Ratio of the most strongly deviating drag force in the string frame of the 2-parameter model to the corresponding conformal value against the deformation parameters $\alpha$ and $c$ for four different velocities $v$, $v = 0.2$ (highest surface), 0.6, 0.8 and 0.99 (lowest surface).

Figure 4.7: Ratio of the most strongly deviating drag force of the 2-parameter model to the corresponding conformal value against the deformation parameters.

## 4.3 Running Coupling $\alpha_{Q\bar{Q}}$

In this section we want to discuss the running coupling $\alpha_{Q\bar{Q}}$ in deformed *AdS*-models that correspond to non-conformal, strongly coupled plasmas at high temperature. This quantity can be derived with the help of the computation of the quark-antiquark distance $L$ and the corresponding free energy $F$. $\alpha_{Q\bar{Q}}$ is very important for the understanding of interactions between quarks and gluons in confined and deconfined phases of these theories.

On quite general grounds it is expected, that fundamental forces between quarks and gluons get modified at finite temperature. In particular the forces between static quarks are very sensitive to changes in the plasma because the gluons, which mediate the interaction between the static quarks, also interact with the constituents – $N_c^2 - 1$ different types of gluons due to the SU($N_c$) – of the thermal bath. We expect that above the deconfinement temperature $T_c$ the free energy is exponentially screened at large distances ($L \gg T^{-1}$). This can be understood in leading order perturbation theory due to the generation of a chromoelectric Debye mass. However, beyond leading order, all the different screening effects cannot be disentangled.

On the other hand, knowledge about the short and intermediate distances of static quark-antiquark pairs is required in order to understand the peculiar properties of hot and dense matter generated at the LHC and RHIC.

Unfortunately, the computation of the running coupling $\alpha_{Q\bar{Q}}$ at all length scales is very complicated and most progress has been achieved in the context of lattice simulations [147, 196–200] where the following definition of the running coupling is widely used:

$$\alpha_{Q\bar{Q}}(L) \equiv \frac{3}{4} L^2 \frac{\mathrm{d}V(L)}{\mathrm{d}L} \quad \text{or} \quad \alpha_{Q\bar{Q}}(L, T) \equiv \frac{3}{4} L^2 \frac{\mathrm{d}F(L, T)}{\mathrm{d}L} \,. \tag{4.27}$$

Here, $V$ denotes the potential at zero temperature, $F$ the free energy if the analysed model exhibits a temperature $T$, and $L$ is the distance between the quark-antiquark pair. The factor of 3/4 is the Casimir factor of QCD. This formula for $\alpha_{Q\bar{Q}}$ measures the deviation of the potential or the free energy from a pure coulombic behaviour where the running coupling would be a constant. Unfortunately, this definition has some caveats. In the case of deformed *AdS*-models it is questionable whether we can adapt the definition of a running coupling in (4.27) since the dual gauge theory and in particular its Casimir factor is unknown. In addition to this, the main and still not fully understood problem concerns the proper value of the 't Hooft coupling $\lambda$. Gubser proposed in [74] a value of $\lambda = 5.5$ by matching the finite temperature results in $\mathcal{N} = 4$ to lattice results of Kaczmarek *& al.* in [199, 200] and Cheng *& al.* in [147]. Since we are mainly interested in the qualitative behaviour and only briefly focus on quantitative agreement with QCD in Sec. 4.3.5 we leave the value of the 't Hooft coupling undetermined for the moment.

A necessary ingredient for this analysis is the computation of the quark-antiquark distance $L$ (Sec. 4.3.1) and of the free energy $F$ (Sec. 4.3.2). Many important results concerning quark-antiquark distances and free energies have been worked out in [75, 76] and, thus in the next sections, we will review only the main expressions which are necessary in order to study the running coupling.

Then, in Chapter 5 we will have a closer look at the screening distance $L_{\mathrm{max}}$. This observable has the remarkable property that $L_{\mathrm{max}}$ evaluated in $\mathcal{N} = 4$ is a lower bound for the screening distance in all non-conformal models. This has been studied numerically in our previous work [75, 76] and will be investigated analytically for small perturbations around the conformal limit.

### 4.3.1 $Q\bar{Q}$-Distance $L$

The computation of the free energy $F$ and the $Q\bar{Q}$-distance is well-posed in the framework of the $AdS$/CFT correspondence. As presented in the seminal work of Maldacena [47, 201] expectation values of rectangular Wilson loops – which provide gauge invariant information about the physics in non-abelian Yang–Mills theories – can be computed in the dual gravitational theory. More precisely it was argued that these expectation values correspond to the area of a macroscopic string worldsheet on the string theory side whose boundary is the loop in question. This has been derived with the help of the basic formula in $AdS$/CFT given in (2.3). The Wilson loop operator can be written as

$$\langle W(\mathcal{C})\rangle = \mathrm{e}^{-\mathrm{i}\,\mathcal{T}F(L)}\,, \quad \text{with} \quad W(\mathcal{C}) = \mathrm{Tr}\,\mathcal{P}\,\exp\left[\mathrm{i}\oint_{\mathcal{C}} \mathrm{d}x_\mu\, A^\mu(x)\right], \tag{4.28}$$

where $\mathcal{C}$ denotes a closed loop in space-time and the trace is over the fundamental representation. $A^\mu(x) \equiv A^\mu_a(x)\,T^a$ is the vector potential and can be expressed in terms of the generators $T^a$ of the corresponding representation. Finally, $\mathcal{P}$ denotes the path ordering. In the large-$\mathcal{T}$ limit the free energy $F$ and the quark-antiquark distance $L$ can be extracted. The particular shape of the Wilson loop is illustrated in Fig. 4.8. The properties of the medium, e. g. the

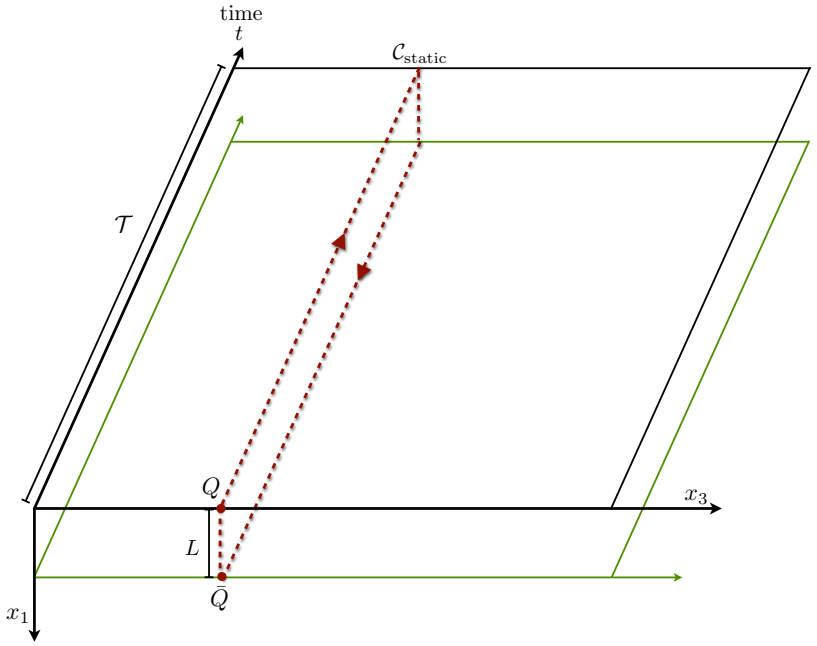


Figure 4.8: Shape of a rectangular Wilson loop. The quark-antiquark pair is aligned along the $x_1$-direction.

temperature $T$, enter into (4.28) via the expectation value $\langle\ldots\rangle$. This becomes more obvious on the gravity side. Maldacena showed in [201] that the expectation value of the Wilson loop is given by

$$\langle W(\mathcal{C})\rangle \propto \mathrm{e}^{-\mathrm{i}S}\,, \tag{4.29}$$

where $S$ is the extremal action of a macroscopic, fundamental string worldsheet bounded by the loop $\mathcal{C}$ at the boundary of the (deformed) $AdS$ space-time. This setup is shown in Fig. 4.9. The dynamics of the strings is governed by the same Nambu–Goto action $S_{\mathrm{NG}}$ that we have

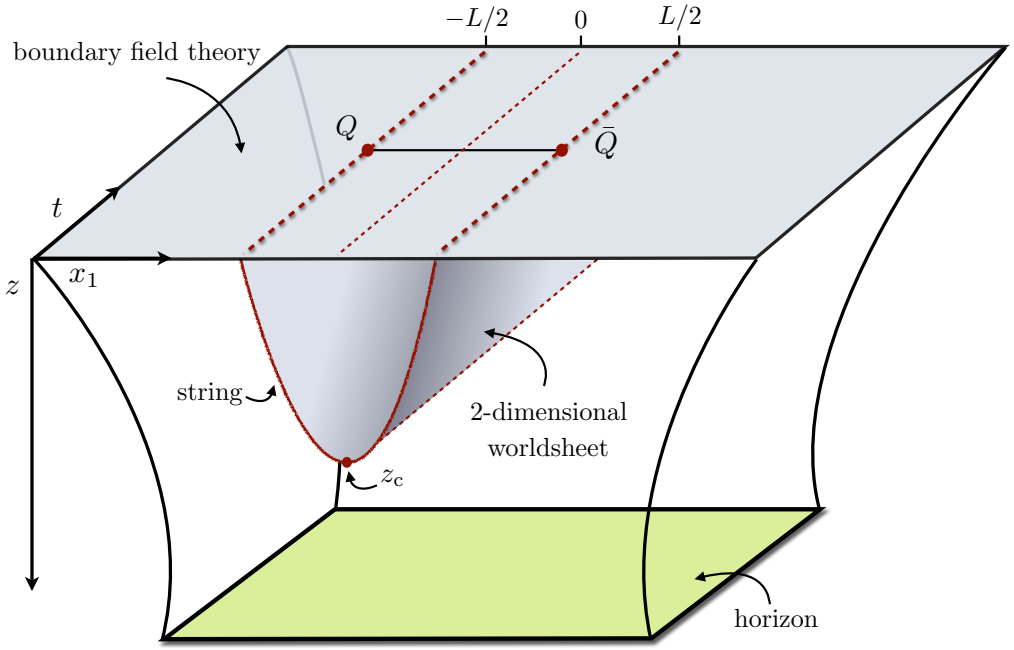


Figure 4.9: Sketch of a quark-antiquark pair at the boundary with the connecting string hanging into the bulk. The lowest point of the string in $z$-direction is denoted by $z_c$.

encountered in (4.14). We just have to adjust the parameterisation of the string worldsheet and the appropriate boundary conditions. As we will see in the following this Nambu–Goto action contains a contribution from the mass of the quarks and is therefore infinite since we assume infinitely heavy quarks. After subtracting this contribution we end up with a finite result given by

$$\langle W(\mathcal{C})\rangle \propto \mathrm{e}^{-\mathrm{i}(S-S_{\mathrm{mass}})}\,, \quad \text{with} \quad S \equiv S_{\mathrm{NG}} = \frac{1}{2\pi\alpha'}\int \mathrm{d}\sigma\mathrm{d}\tau\,\sqrt{-\det g_{ab}}\,,$$
$$\text{and} \quad g_{ab} = G_{\alpha\beta}\,\partial_a X^\alpha\,\partial_b X^\beta\,. \tag{4.30}$$

$g_{ab}$ is again the induced metric that describes the particular worldsheet of our problem. $S_{\mathrm{mass}}$ will be computed in Sec. 4.3.2. Therefore, finding the free energy of a quark-antiquark pair is equivalent to finding the extremal area of a classical string worldsheet. Within this computation the $Q\bar{Q}$-distance can be obtained as a byproduct.

We will derive the $Q\bar{Q}$-distance for our general metric ansatz. Because of the fact that the quark-antiquark distance will be discussed in detail in Chapter 5 we will concentrate on the free energy more intensively in this section. A detailed computation of the $Q\bar{Q}$-distance

and the free energy in $\mathcal{N} = 4_T$ and the $\mathrm{SW}_T$-model can be found in [73, 124], however, a computation in the consistently deformed models has not been worked out so far. We use the metric of (3.25) which we quote here for convenience:

$$\mathrm{d}s^2 = \mathrm{e}^{2A(z)}\left(-h(z)\mathrm{d}t^2 + \mathrm{d}\vec{x}^2\right) + \mathrm{e}^{2B(z)}\,\frac{\mathrm{d}z^2}{h(z)}\,. \tag{4.31}$$

The parameterisation, also visualised in Fig. 4.9 is given by

$$X^\mu \equiv \big(t = \tau,\, \sigma,\, 0,\, 0,\, z = z(\sigma)\big)\,, \quad \text{and} \quad \sigma \in \left[-\frac{L}{2}, \frac{L}{2}\right], \tag{4.32}$$

which is even simpler than in the trailing string setup (4.17) since we are dealing with a static configuration. Furthermore, we can make use of a mirror symmetry at $\sigma = 0$. We thus have to compute the string configuration only from $\sigma = 0$ to $L/2$ and take the result twice. Nevertheless certain boundary conditions for the endpoints of the string at the boundary have to be imposed because the differential equation is non-linear and first order in derivatives:

$$\begin{aligned} z\left(\frac{L}{2}\right) &\equiv 0\,, \\ z'(0) &\equiv z_{\mathrm{c}}\,, \end{aligned} \tag{4.33}$$

where $'$ denotes a derivative with respect to $\frac{\partial}{\partial\sigma}$. The second equation in (4.33) will be used to replace a free parameter of the problem by $z_{\mathrm{c}}$ which is the minimum value of the string in $z$-direction. By using (4.30), (4.31) and (4.32) we can compute the induced metric $g_{ab}$ leading to the following explicit expression of the Nambu–Goto action

$$S = \frac{\mathcal{T}}{2\pi\alpha'}\int_{-L/2}^{L/2}\mathrm{d}\sigma\mathcal{L} = \frac{\mathcal{T}}{2\pi\alpha'}\int_{-L/2}^{L/2}\mathrm{d}\sigma\left[h(z)\mathrm{e}^{2A}\left(\mathrm{e}^{2A} + \frac{\mathrm{e}^{2B}}{h(z)}\,z'^2\right)\right]^{1/2}, \tag{4.34}$$

where $\mathcal{T}$ is the time in the lab frame that is obtained by the $\mathrm{d}\tau$ integration and drops out of the computation when the free energy $F = S/\mathcal{T}$ is concerned. However, one should not forget that the large-$\mathcal{T}$ limit ensures the possibility to extract the free energy and the $\mathrm{Q}\bar{\mathrm{Q}}$-distance out of the vacuum expectation value of the rectangular Wilson loop. Since the Lagrangian is independent of $\sigma$ we have a conserved Hamiltonian given by

$$\mathcal{H}(z) \equiv \mathcal{L}(z) - \frac{\partial\mathcal{L}(z)}{\partial z'}\,z' = \frac{h(z)\mathrm{e}^{2A(z)}}{\mathcal{L}(z)} = q\,, \tag{4.35}$$

with $q$ denoting a constant. We can now use the second condition of (4.33) in order to replace $q$ by an expression in terms of $z_{\mathrm{c}}$:

$$\mathcal{H}(z_{\mathrm{c}}) = \sqrt{h(z_{\mathrm{c}})\,\mathrm{e}^{4A(z_{\mathrm{c}})}}\,. \tag{4.36}$$

The last computational step is to solve (4.35) together with (4.36) for $z'$ which leads to

$$z' = \sqrt{\frac{h(z)\,\mathrm{e}^{2A(z)}}{h(z_{\mathrm{c}})\,\mathrm{e}^{2B(z)+4A(z_{\mathrm{c}})}}\left(h(z)\,\mathrm{e}^{4A(z)} - h(z_{\mathrm{c}})\,\mathrm{e}^{4A(z_{\mathrm{c}})}\right)}\,. \tag{4.37}$$

The quark-antiquark distance given by $L\pi T$ in dimensionless units, where $\pi$ is multiplied just for convenience, can now be derived very easily by stating

$$L\pi T = 2\pi T \int_0^{L/2} \mathrm{d}\sigma = 2\pi T \int_0^{L/2} \frac{\mathrm{d}z}{z'} = 2\pi T \int_0^{z_c} \mathrm{d}z \sqrt{\frac{h(z_c)\,\mathrm{e}^{2B(z)+4A(z_c)-2A(z)}}{h(z)^2\,\mathrm{e}^{4A(z)} - h(z)\,h(z_c)\,\mathrm{e}^{4A(z_c)}}}\,. \tag{4.38}$$

In (4.38) we have used the above-mentioned symmetry so that we just have to integrate half the way, as well as a coordinate transformation between $\sigma$ and $z$. In Fig. 4.10 the string configurations are shown in the $\mathcal{N} = 4_T$ case for three different $Q\bar{Q}$-distances $L\pi T$, $L\pi T = 0.48$ (red), 0.7 (blue) and $(L\pi T)_{\max} = 0.869$ (black). Apart from the screening distance $(L\pi T)_{\max}$

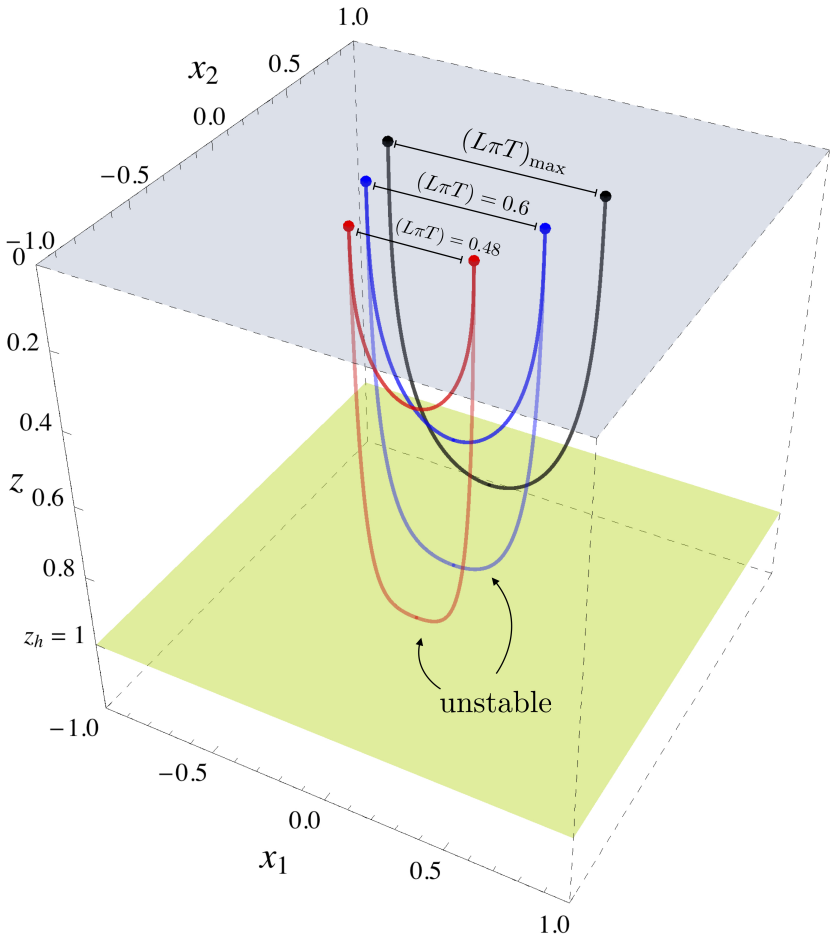


Figure 4.10: String configurations in $\mathcal{N} = 4$ for three different $Q\bar{Q}$-distances $L\pi T$, $L\pi T = 0.48$ (red), 0.6 (blue) and $(L\pi T)_{\max} = 0.869$ (black). The lower string configurations are unstable as a consequence of a higher free energy (see below).

all values of the quark-antiquark distance in Fig. 4.10 have two configurations: an unstable configuration closer to the horizon and a shorter, stable one. It is noteworthy that the unstable configurations do not touch the horizon for any choice of the parameters. Furthermore, a very interesting universal property arises when studying the screening distance in deformed metric models. With screening distance we denote the maximal $Q\bar{Q}$-distance $L_{\max}$. We showed in

[75, 76] numerically that the screening distance in $\mathcal{N} = 4$ is always a lower bound for a large class of metric models. In Chapter 5 an analysis will be presented where we prove this universal behaviour analytically for small deviations from the conformal background.

The reason for referring to the lower string configuration as an unstable one is based on the analysis of the free energy $F$ which can be computed with the help of the Nambu–Goto action. In addition to this, $F$ is the last quantity required to compute the running coupling. This will be the task of the next section.

### 4.3.2 Free Energy $F$

In principle we just have to substitute the result for $z'$ in (4.37) into the integral of the Nambu–Goto action $S$ in (4.34) and evaluate the resulting integral. This is given by

$$\begin{aligned} S &= \frac{\mathcal{T}}{2\pi\alpha'} \int_{-L/2}^{L/2} \mathrm{d}\sigma \sqrt{h\,\mathrm{e}^{2A}\left(\mathrm{e}^{2A} + \frac{\mathrm{e}^{2B}}{h}\,z'^2\right)} \\ &= \frac{\mathcal{T}\sqrt{\lambda}}{\pi L_{\mathrm{AdS}}^2} \int_0^{z_\mathrm{c}} \mathrm{d}z \sqrt{h\,\mathrm{e}^{2A}\left(\frac{\mathrm{e}^{2A}}{z'^2} + \frac{\mathrm{e}^{2B}}{h}\right)} \\ &= \frac{\mathcal{T}\sqrt{\lambda}}{\pi L_{\mathrm{AdS}}^2} \int_0^{z_\mathrm{c}} \mathrm{d}z \sqrt{\frac{\mathrm{e}^{2A(z)+2B(z)}}{1 - \frac{h(z_\mathrm{c})}{h(z)}\,\mathrm{e}^{4A(z_\mathrm{c})-4A(z)}}}\,. \end{aligned} \tag{4.39}$$

Here, $\alpha'$ has been substituted by $\alpha' = L_{\mathrm{AdS}}^2/\sqrt{\lambda}$. $L_{\mathrm{AdS}}$ appearing in the denominator of (4.39) is the $AdS$ length that should not to be confused with the $\mathrm{Q\bar{Q}}$-distance $L$.

As we have mentioned above the Nambu–Goto action $S$ in (4.39) does not converge irrespective of the chosen values of $z_\mathrm{c}$ since the free energy of the quark-antiquark pair includes the mass of the quarks which is infinite. This mass can be calculated by considering a string that is hanging down into the bulk and is connected to a certain point at the boundary. Thus, we can use our trailing string computation by setting the velocity $v$ equal 0. Then, the trailing-string Lagrangian (4.19) can be substituted back into the Nambu–Goto action (4.14) and evaluation at $v = 0$ leads to

$$\begin{aligned} 2S_{\mathrm{mass}} &= \frac{\mathcal{T}\sqrt{\lambda}}{\pi L_{\mathrm{AdS}}^2} \int_0^{z_\mathrm{h}} \mathrm{d}z \sqrt{\mathrm{e}^{4A(z)}\,h\,\xi'^2 - \frac{\mathrm{e}^{2A(z)+2B(z)}}{h}\,(v^2 - h)} \\ &\xrightarrow{v=0} \frac{\mathcal{T}\sqrt{\lambda}}{\pi L_{\mathrm{AdS}}^2} \int_0^{z_\mathrm{h}} \mathrm{d}z\,\mathrm{e}^{A(z)+B(z)}\,. \end{aligned} \tag{4.40}$$

Here, $S_{\mathrm{mass}}$ corresponds to the mass of a quark located at the boundary and the factor of 2 appears since we have to compensate twice the mass of a trailing string in the quark-antiquark scenario. In the second line of (4.40) we have used the fact that for a hanging string $x_3(z) \equiv \xi(z) = 0$ giving $\frac{\partial\xi(z)}{\partial z} = 0$ for all $z$. The final expression for the free energy $F$ – or

potential $V$ in the zero-temperature case – can be written as

$$\frac{F}{T\sqrt{\lambda}} = \frac{S - 2S_{\mathrm{mass}}}{T\sqrt{\lambda}\mathcal{T}} = \frac{1}{\pi T L_{\mathrm{AdS}}^2}\int_0^{z_{\mathrm{c}}} \left[\sqrt{\frac{\mathrm{e}^{2A(z)+2B(z)}}{1-\frac{h(z_{\mathrm{c}})}{h(z)}\,\mathrm{e}^{4A(z_{\mathrm{c}})-4A(z)}}} - \mathrm{e}^{A(z)+B(z)}\right]\mathrm{d}z$$
$$- \frac{1}{\pi T L_{\mathrm{AdS}}^2}\int_{z_{\mathrm{c}}}^{z_{\mathrm{h}}} \mathrm{e}^{A(z)+B(z)}\,\mathrm{d}z\,. \tag{4.41}$$

Here, we always consider the dimensionless quantity $F/T$ scaled with the square root of the 't Hooft coupling. Since all these integrals have to be evaluated numerically, it is not possible to derive the free energy $F$ in terms of the quark-antiquark distance $L$ analytically. This relation is the main ingredient for the running coupling defined in (4.27).

### 4.3.3 Running Coupling in $\mathcal{N} = 4_T$

The numerics thus work as follows: for every $\mathrm{Q\bar{Q}}$-string configuration parameterised by the minimal point $z_{\mathrm{c}}$ in the bulk we compute $L\pi T(z_{\mathrm{c}})$ and $\frac{F(z_{\mathrm{c}})}{T\sqrt{\lambda}}$. After collecting them in a table the `Interpolation` routine of MATHEMATICA® is used in order to obtain a functional relation of the table elements that allows for a derivation with respect to $L$. A plot of the free energy in the conformal $\mathcal{N} = 4$ case is shown in Fig. 4.11. This figure suggests to think of the black

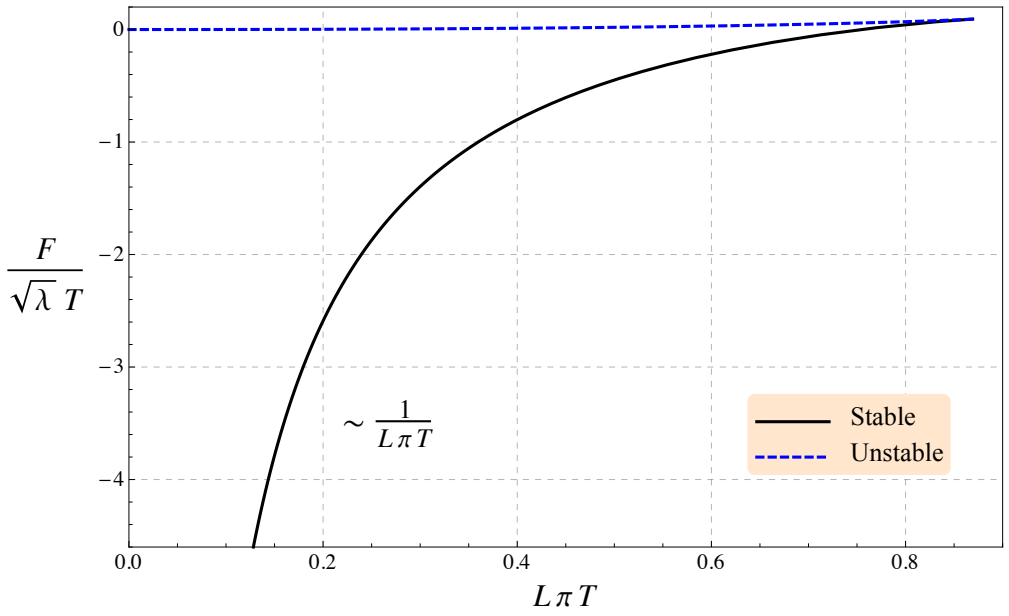


Figure 4.11: Free energy $\frac{F}{\sqrt{\lambda}T}$ against the quark-antiquark distance $L\pi T$ in the conformal $\mathcal{N} = 4$ case. The upper (blue) branch represents the unstable string configuration and the lower (black) branch the stable one.

branch as the stable string configuration due to the lower free energy which corresponds to the upper configuration in Fig. 4.10. Furthermore, the curve exhibits a coulombic shape for small separation distances of the two quarks but deviates from this form close to the cusp. This deviation will be measured as a function of the distance $L$ and will be called the running

coupling $\alpha_{Q\bar{Q}}$:

$$\alpha_{Q\bar{Q}}(L) \equiv \frac{3}{4} L^2 \frac{\mathrm{d}V(L)}{\mathrm{d}L} \quad \text{or} \quad \alpha_{Q\bar{Q}}(L,\, T) \equiv \frac{3}{4} L^2 \frac{\mathrm{d}F(L,\, T)}{\mathrm{d}L}\,. \tag{4.42}$$

There are different approaches known in the lattice community [147, 196–200] but we compare at the end of this section with lattice results by Kaczmarek *& al.* [196, 197] and thus focus on their conventions.

For sake of completeness we start with a brief discussion of the running coupling results for the conformal case with and without temperature. This will lead to a good understanding of many features the running coupling exhibits. In section 4.3.4 we try to apply these techniques to the deformed $AdS$-models.

The basic computation of the potential $V$ and the $Q\bar{Q}$-distance $L$ in $\mathcal{N} = 4$ at zero temperature has been known for a long time [201] and the final relation is given by

$$V(L) = -\frac{4\pi^2\sqrt{\lambda}}{\Gamma^4\left(\frac{1}{4}\right) L}\,. \tag{4.43}$$

A short calculation reveals that the running coupling in $\mathcal{N} = 4$ is given by

$$\alpha_{Q\bar{Q}}^{\mathcal{N}=4} = \frac{3\pi^2\sqrt{\lambda}}{\Gamma^4\left(\frac{1}{4}\right)}\,, \tag{4.44}$$

which is constant. This is obvious, since $\mathcal{N} = 4$ is a conformal theory where the coupling has to be constant.

In the case of $\mathcal{N} = 4_T$ we see a different behaviour. Although the energy-momentum tensor remains traceless by construction of the temperature (see Sec. 2.2.1) we break the scale invariance since $z_\mathrm{h}$ defines a length scale in the system. In order to understand the consequences we recall the necessary expressions needed to derive the running coupling $\alpha_{Q\bar{Q}}$ in finite temperature $\mathcal{N} = 4$ at strong coupling. Although a functional relation like in (4.43) is not available Avramis *& al.* found in [202, 203] analytic expressions for $F$ and $L$ given by

$$\begin{aligned} L(z_\mathrm{c},\, z_\mathrm{h}) &= \frac{2\sqrt{\pi} z_\mathrm{c}}{z_\mathrm{h}} \sqrt{1 - \frac{z_\mathrm{c}}{z_\mathrm{h}}}\, \frac{\Gamma\left(3/4\right)}{\Gamma\left(1/4\right)}\, {}_2F_1\left(\frac{1}{2}, \frac{3}{4}, \frac{5}{4}, \frac{z_\mathrm{c}^4}{z_\mathrm{h}^4}\right), \\ F(z_\mathrm{c},\, z_\mathrm{h}) &= \frac{\sqrt{2\pi^3}\,(z_\mathrm{c}^4 - z_\mathrm{h}^4)}{z_\mathrm{c}\, z_\mathrm{h}\, \Gamma\left(1/4\right)} \left[{}_2F_1\left(\frac{1}{2}, \frac{3}{4}, \frac{5}{4}, \frac{z_\mathrm{c}^4}{z_\mathrm{h}^4}\right) - 2\, {}_2F_1\left(\frac{3}{4}, \frac{3}{2}, \frac{5}{4}, \frac{z_\mathrm{c}^4}{z_\mathrm{h}^4}\right)\right], \end{aligned} \tag{4.45}$$

where ${}_2F_1(\dots)$ denotes the hypergeometric function.

By using the numerical routine mentioned above we end up with Fig. 4.12 for the running coupling at zero and finite temperature for several values of $T$, $T = 0, 2\,T_\mathrm{c}, 3\,T_\mathrm{c}$ and $4\,T_\mathrm{c}$. Here we have resubstituted dimensions to the temperature $T$ and have fixed the critical temperature $T_\mathrm{c}$ to be $T_\mathrm{c} = 176\,\mathrm{MeV}$ that we have taken from recent computation using particle ratios at RHIC in [145]. Although $\mathcal{N} = 4_T$ has no critical temperature this decrease of the running coupling as shown in Fig. 4.12 will reappear when we focus on non-conformal models. There the definition of $T_\mathrm{c}$ is meaningful as we have observed in the computation of the trace anomaly in Sec. 3.1.2. Thus, in order to estimate the influence of temperature in the deformed models we work with the same temperature definitions already in $\mathcal{N} = 4_T$. As we have expected from our previous considerations the running coupling in $\mathcal{N} = 4_T$ deviates from a constant due to

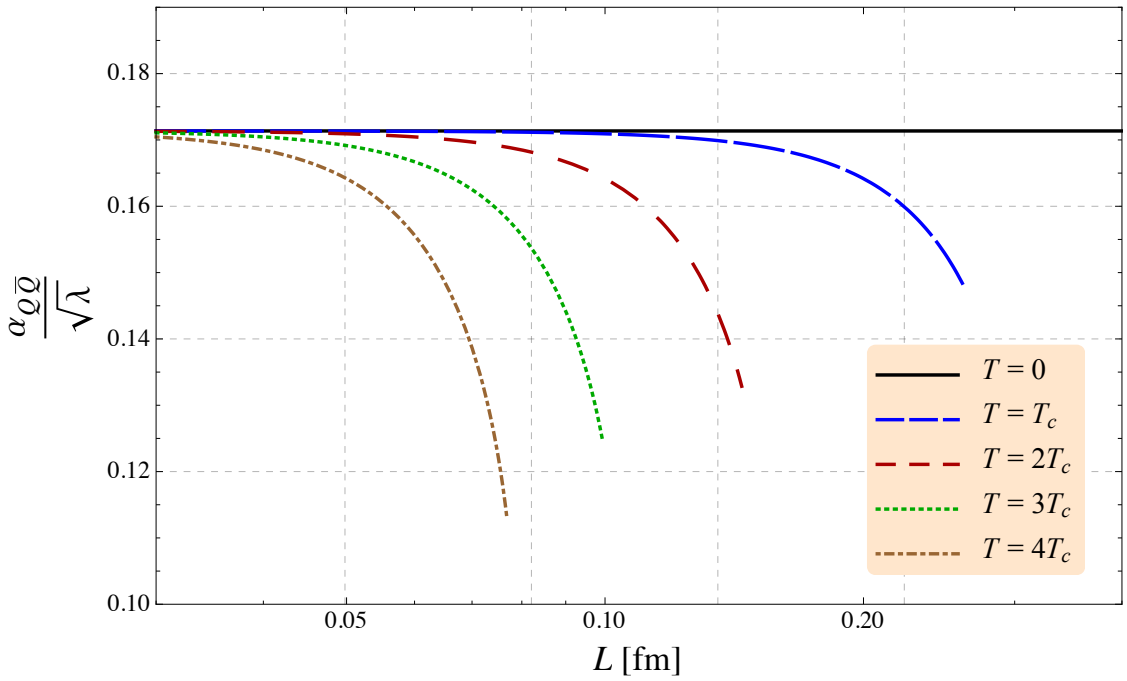


Figure 4.12: Running coupling $\alpha_{Q\bar{Q}}$ against the $Q\bar{Q}$-distance $L$ in $\mathcal{N} = 4$ at zero and finite temperature $T$, $T = 0, 2\,T_c, 3\,T_c$ and $4\,T_c$. The 't Hooft coupling remains undetermined. The constant line represents the value of (4.44).

the appearance of temperature. It is noteworthy that the deviation from a constant appears at a length scale $L \sim T^{-1}$ at which the corresponding temperature becomes important.

The fact that a decrease in the running coupling arises in general is obvious due to our discussion at the begin of this section where we argued that gluonic interactions with the plasma become more and more important at higher temperatures leading to a screening of the heavy, static quarks. In order to apply these results to heavy-ion collisions at the LHC we have at least three problems:

**'t Hooft coupling** In all the holographic models we are working in this thesis the 't Hooft coupling $\lambda$ is not specified. Gubser proposed a value of 5.5 by comparing $\mathcal{N} = 4_T$ with QCD. A derivation of $\lambda$ from first principles is, however, not possible.

**Casimir factor** We lose knowledge about the properties of the gauge theory when a deformation is included. Thus, the Casimir factor remains unknown in all our deformed models.

**$T_{\mathrm{SYM}} = T_{\mathrm{QFT}}$** It is not clear that the temperature of the supersymmetric Yang–Mills model is identical to the QCD temperature. This can be seen by comparing the energy density in 2-flavor QCD from perturbation theory and $\mathcal{N} = 4_T$. The $T^4$-proportionality – suggesting a measure for the degrees of freedom – is by a factor of three larger in $\mathcal{N} = 4_T$ than the corresponding QCD value [74].

Studying the running coupling in the case of non-conformal models within a holographic approach has not been done so far. This will be the task of the next section. Two question

serve as a guideline through the subsequent analysis:

1. Does the running coupling show a universal behaviour for arbitrarily chosen values of the deformation parameters?

2. Is there a regime of deformations mimicking QCD lattice results obtained by Kaczmarek *& al.* [196–199]?

### 4.3.4 Running Coupling in Non-Conformal Models

Since all the necessary computations have been done in the previous sections we can start by plotting the running coupling $\alpha_{\mathrm{Q\bar{Q}}}^{\mathrm{SW}_T}$ of the $\mathrm{SW}_T$-model in Fig. 4.13 for five temperatures $T$ in terms of the critical temperature $T_\mathrm{c} \approx 176\,\mathrm{MeV}$, $T/T_\mathrm{c} = 1, 1.1, 1.4, 2$ and 4. Recall that the

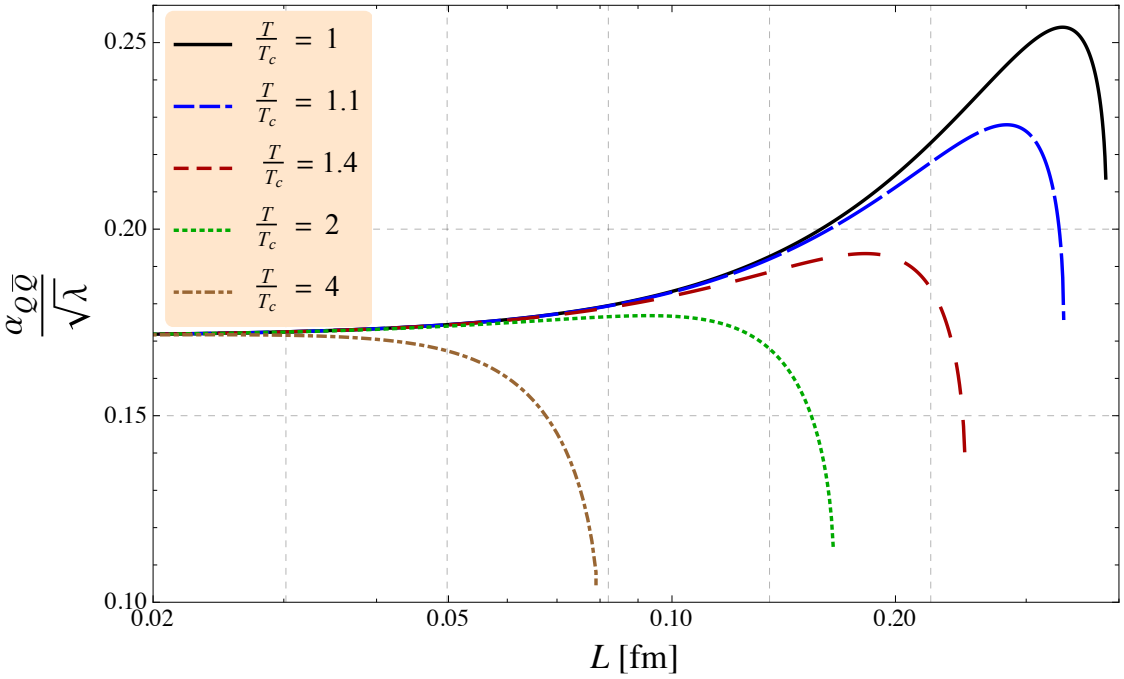


Figure 4.13: Running coupling $\alpha_{\mathrm{Q\bar{Q}}}^{\mathrm{SW_T}}$ in the $\mathrm{SW}_T$-model at finite temperature $T$ in terms of the critical temperature $T_\mathrm{c} \approx 176\,\mathrm{MeV}$, $T/T_\mathrm{c} = 1, 1.1, 1.4, 2$ and 4 against the $\mathrm{Q\bar{Q}}$-distance $L$. The deformation is fixed at the value $c = 0.127\,\mathrm{GeV}^2$. The 't Hooft coupling remains undetermined.

definition of a critical temperature was reasonable in this model. We adjusted the value of the deformation $c$ in a way the the increase of the trace anomaly in Fig. 3.1(a) matches with the critical temperature $T_\mathrm{c} = 176\,\mathrm{MeV}$. We identified $c = 0.127\,\mathrm{GeV}^2$ as the deformation leading to the most QCD-like $\mathrm{SW}_T$-model in Sec. 3.1.2. Before we start with a quantitative analysis in the consistently deformed models we need to understand the different curves in Fig. 4.13 qualitatively.

The overall scaling of all curves can be adjusted by a particular choice of the 't Hooft coupling $\sqrt{\lambda}$. However, for the moment the 't Hooft coupling remains undetermined in Fig. 4.13 because only qualitative properties are relevant.

The most remarkable fact observable in Fig. 4.13 is the universal increase of the running coupling until a maximum is reached. This rise of the coupling for intermediate distances $L_{\text{int}}$ – with $0 < L_{\text{int}} < T^{-1}$ – is in agreement with lattice QCD computations probing a regime above $T_c$ where confinement is still valid. There, the quark-antiquark pair feels a Cornell-type potential like in QCD in the confined phase in vacuum. This reflects the influence of the non-conformality in our models and is a strong hint that introducing deformations is an appropriate way to mimic QCD observables. However, one has to keep in mind that our models are not asymptotically free since the coupling reaches a constant for vanishing $Q\bar{Q}$-distances whereas the QCD coupling $\alpha_s$ vanishes. In the study of 1- and 2-parameter models we obtain the same universal behaviour for all deformations, e. g. in Fig. 4.16 for the 2-parameter model.

The fact that the running coupling reaches a maximum can be explained as follows. The decrease is a consequence of temperature as we have noticed already in Fig. 4.12. This is sufficient to understand the shape of the black, blue, red and green curves in Fig. 4.13. Furthermore, high temperature leads to more and more conformal models even in highly deformed metrics as we have seen in previous chapters. The effective influence of the deformation is thus weaker at high-$T$ and all these curves tend to looks like $\mathcal{N} = 4_T$. This nicely explains the shape of the brown curve in Fig. 4.13.

Let us focus in the following on the maximum value of each curve. The shift along the $L$-coordinate is due to temperature and can be quantified by plotting the running coupling $\alpha_{Q\bar{Q}}^{\text{SW}_T}$ against the $Q\bar{Q}$-distance for a fixed temperature and several values of the dimensionless deformation $c/T^2$, $c/T^2 = 0, 1, 2, 3$ and 4, in Fig. 4.14. The amplitude of the maximum is

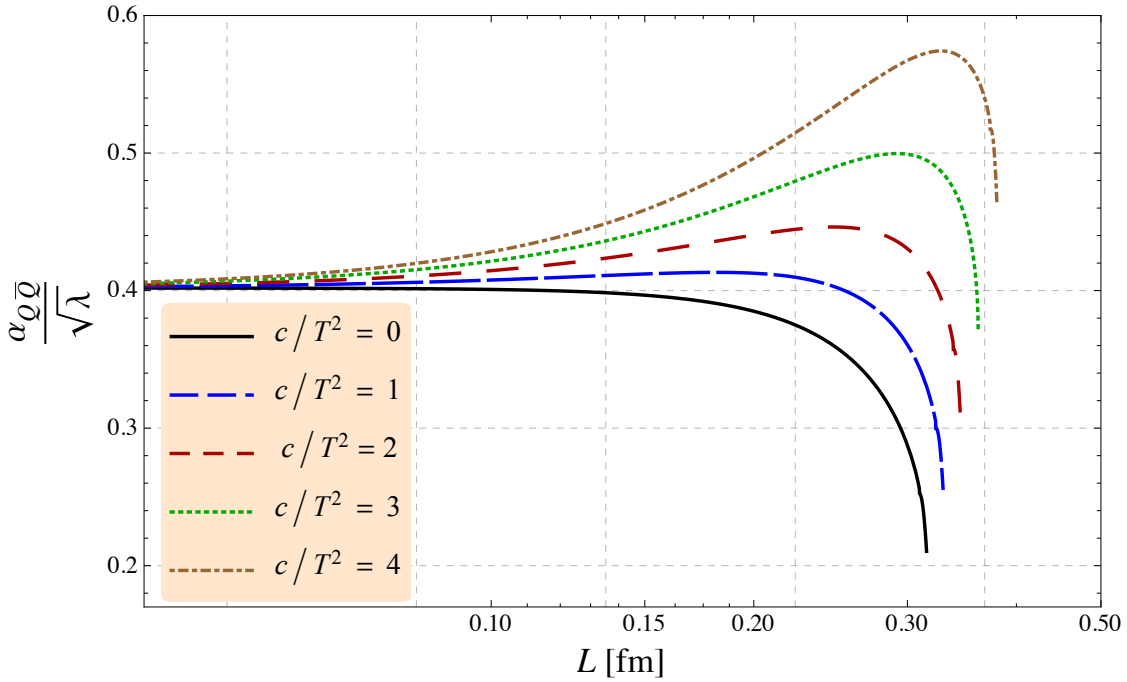


Figure 4.14: Running coupling $\alpha_{Q\bar{Q}}$ in the $\text{SW}_T$-model against the $Q\bar{Q}$-distance $L$ at a fixed temperature $T$ and several values of the deformation in dimensionless units $c/T^2$, $c/T^2 = 0, 1, 2, 3$ and 4.

defined by the amount of deformation in agreement with our expectations since the rise of the coupling is in general a consequence of non-conformality. However, it is rather remarkable that

even for high deformations the $Q\bar{Q}$-distance $L_{\max}$ of the maximum is almost stationary. A possible explanation is the dominance of temperature. The influence of the deformation on the shift of the $L$-value at the maximum is weak in comparison to temperature.

Although in Fig. 4.13 and 4.14 only $SW_T$ results are shown, the behaviour in 1- and 2-parameter models is identical.

The last thing we want to discuss concerns the different length scales that have appeared in the ongoing discussion. Four different length scales can be distinguished:

**$L_S$** The endpoint of each curve in the Figs. 4.13 and 4.14 is the maximal distance $L_S$ of each quark-antiquark pair for a given temperature $T$ and deformation $c$. This point has been denoted by *screening distance* in the last section.

**$L_{max}$** The value of $L$ at which the curve of our holographic computations reaches a maximum in the running coupling defines the length scale $L_{\max}$.

**$L^{Lat}_{max}$** Analogous to $L_{\max}$ a value of $L$ at which $\alpha_{Q\bar{Q}}$ reaches a maximum can be defined in lattice QCD computations. This point is denoted by $L^{\mathrm{Lat}}_{\max}$.

**$L_D$** In the literature the *screening length* $L_D$ is used extensively as the appropriate length scale where screening sets in. It is defined as the inverse Debye mass extracted from exponential fits to the free energy at large quark-antiquark distances $L$. Since the free energy $F$ in our holographic description has a sharp cut-off at finite $L$, this length scale cannot be obtained via this simple application of the $AdS$/CFT correspondence.

In Fig. 4.13 $L_S$ and $L_{\max}$ coincide at lower temperatures. This remains true in the more sophisticated non-conformal metric models. In order to reveal the relation of $L_S$ and $L_{\max}$ to a lattice QCD computation of $L^{\mathrm{Lat}}_{\max}$ we plot in Fig. 4.15 $L^{\mathrm{Lat}}_{\max}$ together with $L_S^{SW_T}$ and $L^{SW_T}_{max}$ for the most QCD-like deformation $c = 0.127\,\mathrm{GeV}^2$. The lattice curve has been taken from [197] and satisfies $L^{\mathrm{Lat}}_{\max}(T) = 0.48\,T_c/T$. In particular, at small and very large temperatures all length scales coincide. Furthermore, it is important to note that the lattice curve is above the screening distance curve of the $SW_T$-model. Thus our bound – that the screening distance in $\mathcal{N} = 4_T$ is a minimum for a large class of models – is satisfied for QCD-like theories. This nice agreement of the length scales is even more remarkable due to the independence of the 't Hooft coupling $\lambda$ and the Casimir factor. In the discussion of the maximum of the running coupling we have left the 't Hooft coupling undetermined. It is just a scale factor in the $\alpha_{Q\bar{Q}}$. The same is true for the unknown Casimir factors of the dual gauge theory of the deformed $AdS$ models. This means, that the two length scales (the screening distance as well as the maximum of the coupling) are independent of the free parameters providing us with an excellent observable to compare our models to QCD-like theories. This leads us to the last task of this chapter dealing with the following question:

*Is it possible to find an appropriate value of our deformations in the 2-parameter model in order to mimic QCD?*

### 4.3.5 Mimicking QCD?

Gubser *& al.* tried in [61, 62] to fix the dilaton potential and a specific deformation in order to approximate as much QCD thermodynamic observables as they can. Furthermore, they proposed a value of the 't Hooft coupling $\lambda = 5.5$ in the analysis of the running coupling in

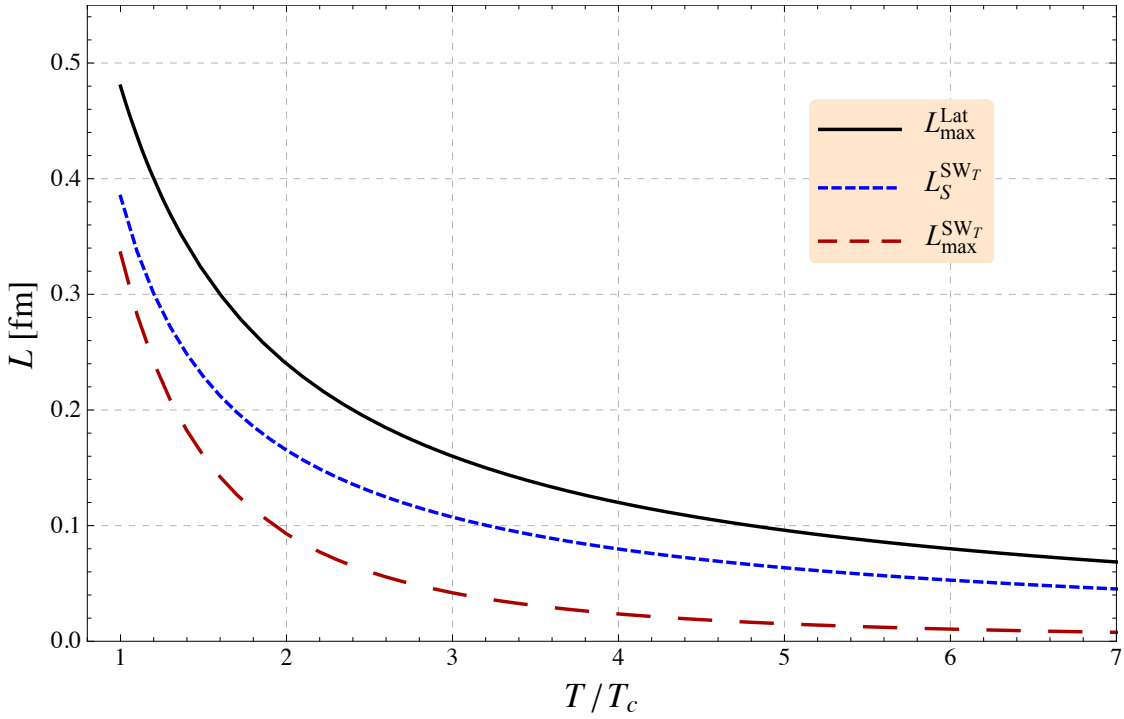


Figure 4.15: Different length scales against temperature $T$ in units of $T_c = 176\,\mathrm{MeV}$. The black solid curve represents $L^{\mathrm{Lat}}_{\mathrm{max}}(T)$ extracted from lattice QCD [197].

$\mathcal{N} = 4_T$ in [74] leading to models that incorporate many properties of QCD. The problem of the first approach is that they only studied thermodynamic observables which seem to be quite robust with respect to a large class of deformations. An observable that is much more sensitive to changes in the deformation seems to be more interesting. The second approach is insufficient since only conformal $\mathcal{N} = 4_T$ is under investigation which is getting closer to QCD only at large temperatures. That is why we follow a mixed approach.

The running coupling $\alpha_{Q\bar{Q}}$ is on one hand very sensitive to changes in the deformation whereas on the other hand the absolute value is sensitive to free parameters like the 't Hooft coupling. Thus, $\alpha_{Q\bar{Q}}$ is an excellent observable to test whether we can get closer to QCD by choosing appropriate deformations.

Before proceeding with the results, we briefly focus on the problem of a proper temperature comparison between QCD and $\mathcal{N} = 4_T$. In the previous chapters we compared $\mathcal{N} = 4$ with deformed models at fixed temperature. In order to be consistent we use the same approach in the following but want to note that Gubser suggested an alternative way [74]. In order to mimic QCD he compared QCD and $\mathcal{N} = 4_T$ at fixed energy density rather than fixed temperature. This suggestion is not without its own problems, but the resulting comparison scheme has some physical motivation which would lead to far beyond the current discussion.

Now, after applying our numerical method to the 2-parameter model and adjusting the values in order to get a reasonable fit we end up with the results in Fig. 4.16, where the running coupling $\alpha^{\mathrm{2p}}_{Q\bar{Q}}$ in the 2-parameter model is plotted against temperature with $T_c = 176$ MeV, $\alpha = 0.5$, $c = 0.3\,\mathrm{GeV}^2$ and $\lambda = 5.5$. The points represent lattice data taken from Kaczmarek *& al.* [197]. For small temperatures above $T_c$ the first two maxima of the lattice calculations

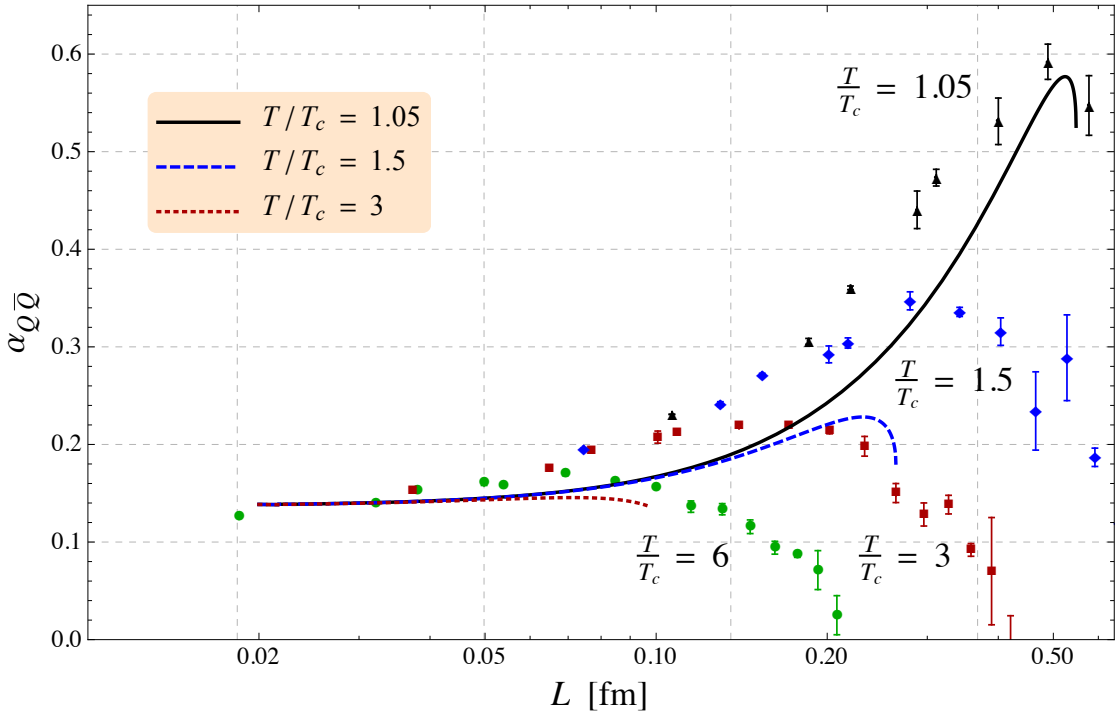


Figure 4.16: Running coupling $\alpha_{Q\bar{Q}}$ in the 2-parameter model against the $Q\bar{Q}$-distance $L$ for three different temperatures $T/T_c$, $T/T_c = 1.05, 1.5$ and 3. The deformation is fixed at $\alpha = 0.5$, $c = 0.3\,\mathrm{GeV}^2$. The 't Hooft coupling is given by $\lambda = 5.5$.

can be reproduced within 10%. However, at higher $T$, $\alpha_{Q\bar{Q}}^{2p}$ decreases faster. This strong dependence on the temperature has also been found in the $SW_T$-model and we can state that it emerges from the $c/T^2$ behaviour. A change in temperature leads to a quadratic change in the dimensionless ratio $c/T^2$ which is the ratio that appears in all our expressions. A last thing to note is that we found $\lambda$ to be 5.5 which is in very good agreement with the results of Gubser.

Although the best fit is within the preferred deformation parameter regime that we had fixed in the analysis of thermodynamic quantities, this model cannot reproduce a very sensitive QCD observable like the running coupling to high accuracy. To improve this, we suggest a change in how the deformation is introduced in the 2-parameter model. The metric function $A(z)$ where the $c$ deformation enters has the following form

$$A(z) = \frac{1}{2}\log\left(\frac{L^2}{z^2}\right) - \frac{1}{2}cz^2\,. \tag{4.46}$$

We now use a different metric function for the whole computation in order to come closer to QCD. The new metric function $\tilde{A}(z)$ can be written as:

$$\tilde{A}(z) = \frac{1}{2}\log\left(\frac{L^2}{z^2}\right) - \frac{1}{2}\tilde{c}z\,, \tag{4.47}$$

where we just have turned the quadratic deformation $cz^2$ into a linear one of the form $\tilde{c}z$. This

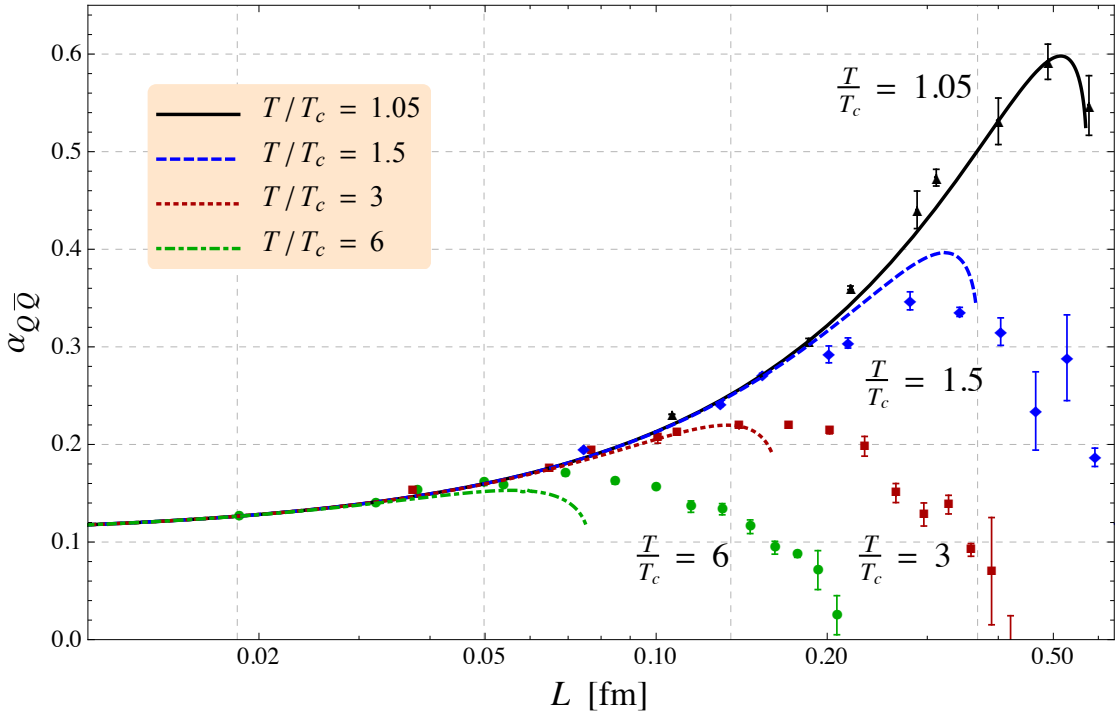


Figure 4.17: Running coupling $\alpha_{Q\bar{Q}}$ in the linear deformed 2-parameter model against the $Q\bar{Q}$-distance $L$ for four different temperatures $T/T_c$, $T/T_c = 1.05, 1.5, 3$ and 6. The deformation is fixed at $\tilde{\alpha} = 0.8$, $\tilde{c} = 1.2\,\text{GeV}$. The 't Hooft coupling is given by $\lambda = 0.39$.

new approach of $A(z)$ can now be used in order to compute the other metric functions as well as a new running coupling which is shown in Fig. 4.17 for $\tilde{\alpha} = 0.8$, $\tilde{c} = 1.2\,\text{GeV}$ and $\tilde{\lambda} = 0.39$. This plot now nicely resembles QCD lattice data over a large range of temperatures. However, a quadratic deformation has many advantages, e. g. the possibility to obtain Regge trajectories of the lowest lying mesons [60]. The fact that a linear combination of $\tilde{c}$ and $z$ is required to improve the plot will be discussed in the next section.

### 4.3.6 Different Length Scales

The main task of this subsection – which also leads to an explanation why a linear deformation improves the comparison to QCD – is to find the appropriate length scale in our holographic description that can be compared to $L^{\text{Lat}}_{\text{max}}$ which is the most important length scale in the lattice data. We have learned in Fig. 4.15 that $L^{\text{Lat}}_{\text{max}} \propto T^{-1}$. In Fig. 4.16 – where we studied the normal 2-parameter model – we saw a stronger decrease of $L^{\text{2p}}_{\text{max}}$ than the lattice results would suggest.

To quantify this result we compare in Fig. 4.18 the different length scales we can extract from the running coupling as a function of the temperature. Since the differences between our holographic models are in principle very small we take the values from the $\text{SW}_T$-model for simplicity. In Fig. 4.18 we can see that the screening distance (blue, dashed curve) $L_{\text{S}}^{\text{SW}_T}$ is the best length scale to compare with the $L^{\text{Lat}}_{\text{max}}$. Although there are small deviations at smaller temperatures because in this regime the deformation dominates temperature, we find a nearly

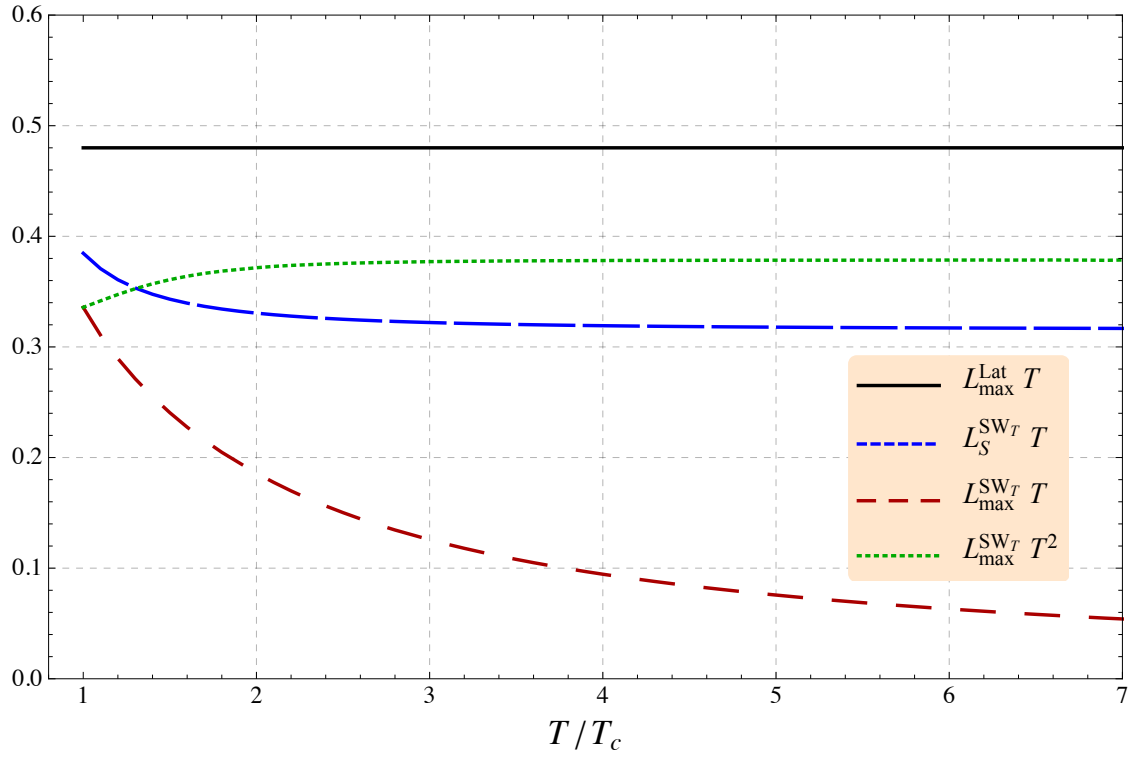


Figure 4.18: Different length scales $L_{\rm max}^{\rm Lat}\,T$, $L_{\rm S}^{{\rm SW}_T}\,T$, $L_{\rm max}^{{\rm SW}_T}\,T$ and $L_{\rm max}^{{\rm SW}_T}\,T^2$ against the temperature ratio $T/T_{\rm c}$ for a certain deformation $c$, $c = 0.127\,{\rm GeV}^2$ in the ${\rm SW}_T$-model.

perfect $1/T$ behaviour at high $T$. This is a consequence of the small distance between the horizon $z_{\rm h}$ and the boundary at $z = 0$ at large $T$ which restricts the expansion of the string into the bulk. Thus, the screening distance is exclusively determined by the temperature. This agrees nicely with the shape of the dashed blue line in Fig. 4.18.

Surprisingly, our values of $L_{\rm max}^{{\rm SW}_T}$ do not show any $1/T$ shape and – as we have seen in the 2-parameter case in Fig. 4.16 – are not in a good agreement with the lattice data. This is visualised by the dashed red line. Even more surprising is the fact that this quantity presents a rather good $1/T^2$ behaviour as indicated by the dotted green line. It seems that $L_{\rm max}^{{\rm SW}_T}$ is not fully determined by temperature but enjoys a large dependence on the deformation. That makes sense since the rise of the coupling is a consequence of the deformation only. Thus, choosing a deformation with linear dependence on the $5^{\rm th}$-dimension $z$ would lead to the dimensionless ratio $\tilde{c}/T$ rather than $c/T^2$ which is the only way how the deformation appears in almost all equations we have encountered in this analysis. This leads to a $1/T$-dependence $L_{\rm max}^{\rm 2p,Lin}$ as observed in Fig. 4.17. Besides, the screening distance in this linearly-deformed model is also very robust since this quantity still scales with temperature in the high-$T$ regime and is only weakly depending on the deformation in this regime. This nicely explains the good agreement in Fig. 4.17.

Finally, a third length scale was mentioned by Kaczmarek *& al.* in [197]. There the authors try to compute the non-perturbative screening mass $m_{\rm D}(T)$ by using the following ansatz

$$F(L,T) \simeq -\frac{4}{3}\,\frac{\alpha(T)}{L}\,{\rm e}^{-m_{\rm D}(T)\,L}\,, \tag{4.48}$$

to perform a best-fit analysis. As we have mentioned above, such a computation is not possible in our holographic approaches because the computation stops close to the point where the exponential drop-off sets in. For holographic theories the best approach to obtain the Debye mass was proposed by Bak, Karch and Yaffe in [204]. They used an analysis of the complete IIB supergravity spectrum on the *AdS* black-hole background and identified the mass of the lightest supergravity mode that can be sourced by the strings with the Debye mass $m_{\mathrm{D}}$. Such a computation is unfortunately not possible in deformed *AdS* models since we are not aware of the full spectrum. A full derivation of the *screening length* is thus still beyond the current state of the *AdS*/CFT correspondence. Other promising approaches how to implement meson melting in a holographic setup have been worked out by Peeters *& al.* in [205–209].

Let us pause for a moment and recall the main progress we have made in the current chapter. We started with the rather simple calculation of the drag force that measures the energy loss due to drag of a uniformly moving particle through a strongly coupled plasma. In each of the different models we found a consistent, systematic behaviour when a deformation is introduced, however, a general change in one particular direction independent of the studied model could not be observed. This is in contrast to the screening distance measuring the largest possible distance of a $Q\bar{Q}$-pair in our holographic setup.[3] That this quantity is a lower bound for a large class of theories has been shown numerically in a previous paper [75, 76] and will be discussed analytically in the next chapter.

The second part of this chapter has dealt with the analysis of the running coupling $\alpha_{Q\bar{Q}}$. Several remarkable facts have been observed for the first time:

1. The computation of a running coupling $\alpha_{Q\bar{Q}}$ in deformed *AdS* models reveals many features that are known for non-conformal, strongly coupled nonabelian gauge theories like QCD. The main properties are the rising of the coupling for intermediate distances of the $Q\bar{Q}$ pair, the development of a maximum for larger distances and a sharp decrease afterwards.

2. These properties are universal for all models we have studied, irrespective of the particular embedding of the dilaton.

3. The running coupling is an excellent quantity to check the possibility of mimicking QCD since it is very sensitive to changes in the deformation parameters and temperature but remains simple in arithmetical details.

4. A certain model linear in the deformation ($\tilde{c}z$) is suitable to mimic QCD for a large temperature range.

5. Furthermore, all the length scales we have encountered were below the corresponding QCD value. This is in particular true for the $\mathcal{N} = 4_T$ value of the screening distance $(L\pi T)_{\mathrm{S}} = 0.86912$ that has been conjectured to be a lower bound for a large class of non-conformal theories. Furthermore the screening distance $(L\pi T)_{\mathrm{S}}$ is the appropriate length scale to compare with the lattice QCD length scale $(L\pi T)^{\mathrm{Lat}}_{\mathrm{max}}$ used in this chapter.

The last statement will be investigated in the subsequent chapter. Although an extensive numerical study in [75, 76] has indicated that the screening distance in $\mathcal{N} = 4_T$ is a lower bound

[3] Above the distance $L$ where our $Q\bar{Q}$-computation breaks down a more sophisticated approach has to be worked out. In this regime we can only argue that a simple connection of the quark and the antiquark via a single string is not reliable anymore.

for a large class of nonconformal theories an analytic verification is still missing. To overcome this problem an analysis of slightly non-conformal theories with only a small deformation will be done with the help of linearised Einstein equations. Finally, in Chap. 6 we will focus on the energy loss of rotating quarks which is a quantity strongly correlated to the drag force.

Chapter 5

# Screening-Distance Conjecture

In this chapter we will focus entirely on the quark-antiquark distance $L$ and in particular on its maximum value $L_\mathrm{S}$ called *screening distance*. In 1998 Maldacena developed a formalism in [201] to study the free energy $F$ and the binding distance $L$ of a static $\mathrm{Q\bar{Q}}$-pair in the $\mathcal{N}=4$ SYM theory at zero temperature by evaluating vacuum expectation values of rectangular Wegner-Wilson loops with the help of the $AdS$/CFT correspondence. On the gravity side this corresponds to extremising the worldsheet area that connects the two boundary quarks via the Nambu–Goto action $S_\mathrm{NG}$. This procedure has been reviewed in Sec. 4.3.1. Liu *& al.* in [124] extended this computation to $\mathcal{N}=4$ at finite temperature[1] and included two kinematic parameters, i. e. the rapidity $\eta$ of the quark-antiquark pair with respect to the surrounding plasma and an orientation angle $\theta$ of the $\mathrm{Q\bar{Q}}$-pair with respect to the direction of the velocity. In a last step Liu *& al.* introduced, in [73], deformations of the $\mathrm{SW}_T$-type in order to study non-conformal metric models. This discussion has been systematically extended in our work [75, 76] to consistent deformations. There we found evidence for a universal increase of the screening distance $L_\mathrm{S}$ when a deformation is introduced. This led to the so-called *screening-distance conjecture* stating that the screening distance in $\mathcal{N}=4_T$,

$$(L\pi T)_\mathrm{S}^{\mathcal{N}=4_\mathrm{T}} = 0.86912\,, \tag{5.1}$$

is a lower bound for a large class of deformed, non-conformal theories. Here and in the following sections we always compute the dimensionless quark-antiquark distance $L\pi T$ where the factor of $\pi$ is included just for convenience. Currently, much effort is spend to include finite chemical potential $\mu$ and test the conjecture in this regime as well [77].

Unfortunately, the screening-distance conjecture could not be verified for all deformations since the corresponding equations (see (4.38)) are only solvable numerically except for the conformal $\mathcal{N}=4$ scenario at finite and zero temperature. The explicit, analytic solution in $\mathcal{N}=4_T$ is given by (4.45). In this chapter the task is now

*to prove analytically that the screening distance $L_\mathrm{S}$ for small perturbations around $\mathcal{N}=4_T$ is bounded from below by the corresponding conformal value.*

[1] The solutions in $\mathcal{N}=4$ at finite temperature will often be denoted as 'conformal' solutions for convenience although conformality is broken by introducing temperature as we have seen in the last chapter in the analysis of the running coupling.

This analysis is restricted to static ($\eta = 0$) quark-antiquark pairs at finite temperature $T$ and zero chemical potential ($\mu = 0$) in order to simplify the equations as much as possible. The subsequent analysis can then be divided into two parts:

1. By studying the expressions for the $\mathrm{Q\bar{Q}}$-distance in the $\mathrm{SW}_T$-model we expand the integral in (4.38) to 1$^{\mathrm{st}}$-order and try to solve the result analytically. There the question occurs whether we should rely on consistently deformed gravity theories only. An affirmative answer cannot be given in general since already the full $\mathrm{SW}_T$-model violates the conjectured bound for negative values of the deformation parameter $c$ as it was shown in [75]. Nevertheless, this discussion is very helpful in order to understand the general procedure of how to compute the linearised contribution to the maximum of the $\mathrm{Q\bar{Q}}$-distance.

2. By expanding the full Einstein equations derived from the Einstein–Hilbert-scalar action $E_{\mathrm{EHs}}$ in Sec. 3.2 to linear order along with a general, appropriate choice of the metric we compute an integral for the $\mathrm{Q\bar{Q}}$-distance for small perturbations around the conformal solution. This allows for an analytic proof of our conjecture.

In the following section we focus on the study of the screening distance $L_{\mathrm{S}}$ in the $\mathrm{SW}_T$-model and try to prove analytically that small negative values of the deformation parameter $c$, $c < 0$, lead to a decrease of $L_{\mathrm{S}}$ at first order.

## 5.1 $\mathrm{Q\bar{Q}}$-Distance for Small Deformations in the $\mathrm{SW}_T$-Model

From numerical studies in [75] we have learned that the $\mathrm{SW}_T$-model shows a universal increase of the screening distance for the physically meaningful regime of $c > 0$. We found this range of parameters appropriate due to the good agreement of thermodynamic quantities with lattice simulations (see Sec. 3.1.2). For negative values of $c$ this bound is violated. This behaviour had been expected because it is not a consistent implementation of non-conformality as the metric is not a solution to Einstein equations. This particular property should be reproducible by expanding the integral to 1$^{\mathrm{st}}$-order in the deformation, where we try to derive a linear correction to the conformal value. We hope to find an analytic solution to the integrals describing the $\mathrm{Q\bar{Q}}$-distance and gain some insights how this task can be accomplished in the consistent cases.

Let us recall the general form of the $\mathrm{Q\bar{Q}}$-distance for a general metric ansatz in the string frame given by (4.31):

$$L\pi T = 2\pi T \int_0^{L/2} \mathrm{d}\sigma = 2\pi T \int_0^{z_{\mathrm{c}}} \mathrm{d}z \sqrt{\frac{h(z_{\mathrm{c}})\, \mathrm{e}^{2B(z)+4A(z_{\mathrm{c}})-2A(z)}}{h(z)^2\, \mathrm{e}^{4A(z)} - h(z)\, h(z_{\mathrm{c}})\, \mathrm{e}^{4A(z_{\mathrm{c}})}}}\,, \tag{5.2}$$

This leads to the following expression in the case of the conformal $AdS_5$-BH (see (2.33)) model:

$$A(z) = B(z) = \log L - \log z\,, \quad h(z,\, z_\mathrm{h}) = 1 - \frac{z^4}{z_\mathrm{h}^4}\,, \quad T(z_\mathrm{h}) = \frac{1}{\pi\, z_\mathrm{h}}\,,$$

$$\begin{aligned}(L\pi\, T)_{\mathcal{N}=4_T}[y_\mathrm{c}] &= 2\pi\, T(z_\mathrm{h}) \int_0^{z_\mathrm{c}} \mathrm{d}z \sqrt{\frac{z^4(z_\mathrm{h}^4 - z_\mathrm{c}^4)}{(z_\mathrm{c}^4 - z^4)\,(z_\mathrm{h}^4 - z^4)}} = \int_0^{y_\mathrm{c}} \mathrm{d}y\, \frac{2y^2\sqrt{1-y_\mathrm{c}^4}}{\sqrt{1-y^4}\,\sqrt{y_\mathrm{c}^4 - y^4}} \\ &= \frac{(2\pi)^{3/2}\, y_\mathrm{c}}{\Gamma\big(\frac{1}{4}\big)^2}\, \sqrt{1-y_\mathrm{c}^4}\cdot {}_2F_1\left(\frac{1}{2}, \frac{3}{4}, \frac{5}{4}, y_\mathrm{c}^4\right). \end{aligned} \tag{5.3}$$

In the first line we used the substitution $y = z/z_\mathrm{h}$ and ${}_2F_1\big(\cdot,\cdot,\cdot,\cdot\big)$ denotes the hypergeometric function.

The SW$_T$-metric as it is written in (3.3) is formulated in the Einstein frame, but (5.2) requires the metric functions ($A$, $B$ and $h$) given in the string frame. The transformation between these two frames is not very difficult and has been worked out by Kajantie *& al.* in [64]. The string frame metric of the SW$_T$-model is given by

$$\begin{aligned}\mathrm{d}s^2 = \frac{L^2}{z^2}\, \mathrm{e}^{\frac{29}{20}c\,z^2} \left(-h(z,z_\mathrm{h})\,\mathrm{d}t^2 + \mathrm{d}\vec{x}^{\,2} + \frac{\mathrm{d}z^2}{h(z,z_\mathrm{h})}\right), \\ \text{with} \quad h(z,z_\mathrm{h}) = 1 - \frac{z^4}{z_\mathrm{h}^4}\,. \end{aligned} \tag{5.4}$$

Only the coefficient in the exponential of the deformation has changed due to the assumption that the dilaton in this model is quadratic in $z$. With (5.4) in our hand the expression for the QQ̄-distance can be expanded to first order in $c$:

$$\begin{aligned}(L\pi\, T)_{\mathrm{SW}_T}[y_\mathrm{c}] &= \int_0^{y_\mathrm{c}} \mathrm{d}y\, \frac{2y^2\,\sqrt{y_\mathrm{c}^4 - 1}}{\sqrt{y^4-1}} \left[y^4\,(y_\mathrm{c}^4 - 1) - \mathrm{e}^k\,(y^4-1)\,y_\mathrm{c}^4\right]^{-1/2} \\ &= \underbrace{\int_0^{y_\mathrm{c}} \mathrm{d}y\, \frac{2y^2\sqrt{1-y_\mathrm{c}^4}}{\sqrt{1-y^4}\,\sqrt{y_\mathrm{c}^4 - y^4}}}_{(L\pi T)_{\mathcal{N}=4_T}} - c \int_0^{y_\mathrm{c}} \mathrm{d}y\, \frac{29\,y^2\,y_\mathrm{c}^4\sqrt{1-y^4}\,\sqrt{1-y_\mathrm{c}^4}}{10\pi^2(y^2+y_\mathrm{c}^2)\,\sqrt{y_\mathrm{c}^4 - y^4}}\,. \end{aligned} \tag{5.5}$$

with $k = \frac{29}{10\,\pi^2 y_\mathrm{c}^2}$. The first term is the quark-antiquark distance of the conformal $\mathcal{N} = 4_T$ case. For sake of simplicity we have used the above-mentioned substitution $y = z/z_\mathrm{h}$ right from the beginning. After some massage we end up with the following expression for the 1$^\mathrm{st}$-order correction of the QQ̄-distance in the SW$_T$-model

$$\begin{aligned}(L\pi\, T)^{\mathrm{SW}_T}_{1^\mathrm{st}}[y_\mathrm{c}] = c\,\frac{y_\mathrm{c}^3\,\sqrt{1-y_\mathrm{c}^4}}{4\pi^{5/2}\sqrt{2}} \Bigg[\Gamma\left(-\frac{1}{4}\right)\Gamma\left(\frac{3}{4}\right)\Bigg((3\,y_\mathrm{c}^4 - 1)\,{}_2F_1\left(-\frac{1}{4}, \frac{1}{2}, \frac{1}{4}, y_\mathrm{c}^4\right) \\ - 2(y_\mathrm{c}^4 - 1)\,{}_2F_1\left(-\frac{1}{4}, \frac{3}{2}, \frac{1}{4}, y_\mathrm{c}^4\right)\Bigg) + \Gamma\left(\frac{1}{4}\right)^2\Bigg(-3\,{}_2F_1\left(-\frac{3}{4}, \frac{1}{2}, -\frac{1}{4}, y_\mathrm{c}^4\right) \\ + (4 + 3y_\mathrm{c}^4)\,{}_2F_1\left(\frac{1}{4}, \frac{1}{2}, \frac{3}{4}, y_\mathrm{c}^4\right)\Bigg)\Bigg]\,. \end{aligned} \tag{5.6}$$

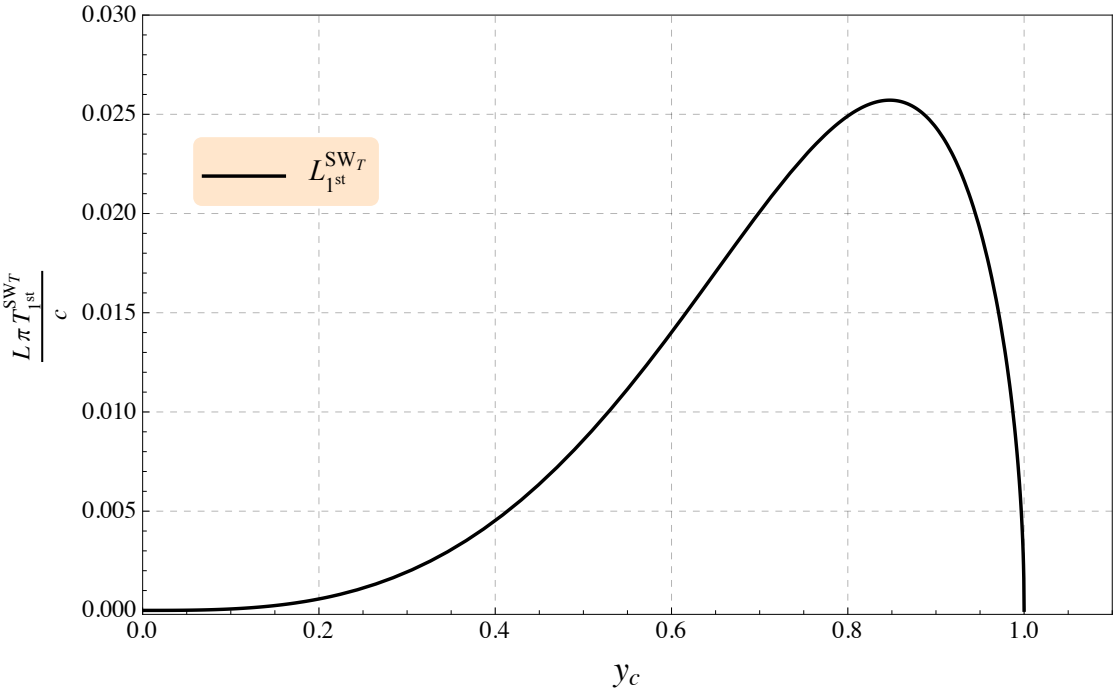


Figure 5.1: $1^{st}$-order correction of the $Q\bar{Q}$-distance against the maximal extension $y_c$ in the bulk given in dimensionless coordinates $y_c = \frac{z_c}{z_h}$. $y_c = 1$ is the location of the horizon.

Eq. (5.6) divided by $c$ is plotted in Fig. 5.1 and agrees with the expectation we had at the beginning of this section. The endpoint of the curve is precisely the location of the horizon $z = z_h$ which is given by $y_c = 1$ in dimensionless coordinates. The full screening distance is now the maximum value of the sum of the first-order contribution (5.6) and the conformal result (5.3). The $1^{st}$-order contribution is positive for positive values of $c$ leading to an overall increase of the screening distance with respect to the conformal result. Analogously, negative values of $c$ lead to a decrease of the screening distance disrespecting the bound as we have expected.

In the case of consistently deformed metric models (1- or 2-parameter scenario) the expression for the $1^{st}$-order correction in the deformation parameters cannot be calculated analytically. Thus, we want to follow a different path in the next section. We use the most general ansatz given by (3.25) satisfying the symmetry conditions expressed in Sec. 3.2.1 and linearise the Einstein equations in order to derive particular metric functions for $A$, $B$ and $h$ that allow for an analytic solution of the quark-antiquark distance.

## 5.2 Linearised Einstein-Equations Approach

The procedure in this section is as follows: we derive linearised Einstein equations by making use of our general 5D Einstein–Hilbert-scalar action (3.12). With the help of these, an analysis of small perturbations around the conformal $AdS_5$-BH solution will be done. The metric perturbation – denoted by $h_{\alpha\beta}$ with $\alpha, \beta \in \{t, \vec{x}, z\}$ – obeys the same symmetry conditions as the full metric since we do not want to break the Poincaré invariance. By specifying a particular ansatz for the metric functions we find solutions for $A$, $B$ and $h$ with which we are

able to compute an analytic expression for the $\mathrm{Q}\bar{\mathrm{Q}}$-distance.

First, let us recapitulate the unperturbed $\mathcal{N} = 4_T$ metric solution that is given by

$$G^0_{\alpha\beta} \equiv \mathrm{diag}\left(-\frac{L^2}{z^2}\,h(z,z_\mathrm{h}),\,\frac{L^2}{z^2},\,\frac{L^2}{z^2},\,\frac{L^2}{z^2},\,\frac{L^2}{z^2\,h(z,\,z_\mathrm{h})}\right), \quad \text{with} \quad h(z,\,z_\mathrm{h}) = 1 - \frac{z^4}{z_\mathrm{h}}\,, \tag{5.7}$$

which extremises the 5D Einstein–Hilbert action $S_\mathrm{EH}$

$$S_\mathrm{EH} = \frac{1}{16\pi G^{(5)}_\mathrm{N}} \int d^5x\sqrt{-G}\,\big(\mathcal{R} - 2\Lambda\big)\,, \quad \Lambda = -\frac{6}{L^2}\,. \tag{5.8}$$

In order to distinguish the conformal metric $G^0_{\alpha\beta}$ from the perturbed ones below, we add the superscript/subscript '0' to all unperturbed quantities.[2] In general, a perturbation of this metric should satisfy the equations of motion derived from the 5D Einstein–Hilbert-scalar action $S_\mathrm{EHs}$ (3.12) – written in Einstein frame – since these define the overall background we are interested in:

$$S_\mathrm{EHs} = \frac{1}{16\pi G^{(5)}_\mathrm{N}} \int \mathrm{d}^5x\,\sqrt{-G}\left(\mathcal{R} - \frac{1}{2}(\partial\Phi)^2 - V(\Phi)\right). \tag{5.9}$$

The full Einstein equations derived from this equation are the starting point for our further analysis and are given by

$$\begin{aligned} \mathcal{E}_{\alpha\beta} &\equiv \mathcal{G}_{\alpha\beta} - \mathcal{T}_{\alpha\beta} = 0\,, \\ \Box_{LB}\,\Phi &= V'(\Phi) \\ \text{with} \quad \mathcal{G}_{\alpha\beta} &\equiv \mathcal{R}_{\alpha\beta} - \frac{1}{2}\,\mathcal{R}G_{\alpha\beta}\,, \\ \text{and} \quad \mathcal{T}_{\alpha\beta} &\equiv \frac{1}{2}\,\partial_\alpha\Phi\partial_\beta\Phi - \frac{1}{4}G_{\alpha\beta}(\partial\Phi)^2 - \frac{1}{2}G_{\alpha\beta}V(\Phi)\,. \end{aligned} \tag{5.10}$$

Here, the Laplace–Beltrami operator can be written as

$$\Box_{LB}\Phi = \nabla_\alpha\nabla^\alpha\Phi = \frac{1}{\sqrt{-G}}\partial_\alpha\left(\sqrt{-G}\,G^{\alpha\beta}\partial_\beta\Phi\right), \tag{5.11}$$

where $G$ denotes the determinant of $G_{\alpha\beta}$. We are now interested in small perturbations around the conformal $AdS_5$ metric denoted by $G^0_{\alpha\beta}$ and want to derive a system of linearised differential equations from (5.10) that determine the perturbations. Thus, a decomposition of $G_{\alpha\beta}$ of the form

$$G_{\alpha\beta} \equiv G^0_{\alpha\beta} + h_{\alpha\beta}\,, \quad |h_{\alpha\beta}| \ll 1\,, \tag{5.12}$$

is a convenient way to proceed. Eq. (5.12) can now be substituted into (5.10) and will be evaluated to first order in $h_{\alpha\beta}$. In order to do so we have to specify the linearised form of the Christoffel symbols $\delta\Gamma^\gamma_{\alpha\beta}$, the Riemann tensor $\delta\mathcal{R}^\rho_{\alpha\sigma\beta}$, the Ricci tensor $\delta\mathcal{R}_{\alpha\beta}$ and the Ricci scalar $\delta\mathcal{R}$.

[2] The index '0' will be used as a subscript and superscript depending on the best position in the considered quantity.

By substituting (5.12) into the definition of the Christoffel symbols we end up with the following expression

$$\begin{aligned}\Gamma^{\gamma}_{\alpha\beta} &\equiv \frac{1}{2}\, G^{\gamma\eta}\left(\partial_\beta G_{\alpha\eta} + \partial_\alpha G_{\beta\eta} - \partial_\eta G_{\alpha\beta}\right), \quad \text{with} \quad G^{\alpha\beta} = G_0^{\alpha\beta} - h^{\alpha\beta} \\ &= \frac{1}{2}\, G_0^{\gamma\eta}\left(\partial_\beta G^0_{\alpha\eta} + \partial_\alpha G^0_{\beta\eta} - \partial_\eta G^0_{\alpha\beta}\right) + \delta\Gamma^{\gamma}_{\alpha\beta} \\ &\equiv \left(\Gamma^{\gamma}_{\alpha\beta}\right)_0 + \delta\Gamma^{\gamma}_{\alpha\beta}\,, \end{aligned} \tag{5.13}$$

with the variation of the Christoffel symbols $\delta\Gamma^{\gamma}_{\alpha\beta}$ given by

$$\delta\Gamma^{\gamma}_{\alpha\beta} = \frac{1}{2}\, G^{\gamma\eta}\left(\nabla_\beta h_{\alpha\eta} + \nabla_\alpha h_{\beta\eta} - \nabla_\eta h_{\alpha\beta}\right). \tag{5.14}$$

In (5.14) the covariant derivative is defined with respect to the unperturbed metric $G^0_{\alpha\beta}$ by

$$\nabla_\gamma h_{\alpha\beta} \equiv \partial_\gamma h_{\alpha\beta} - \left(\Gamma^{\kappa}_{\alpha\gamma}\right)_0 h_{\kappa\beta} - \left(\Gamma^{\kappa}_{\beta\gamma}\right)_0 h_{\alpha\kappa}\,. \tag{5.15}$$

In order to express the variation of the Einstein tensor we have to find the perturbed Ricci tensor $\delta\mathcal{R}_{\alpha\beta}$ and Ricci scalar $\delta\mathcal{R}$. For both quantities the variation of the Riemann tensor $\delta\mathcal{R}^{\rho}_{\alpha\sigma\beta} = \mathcal{R}^{\rho}_{\alpha\sigma\beta} - \left(\mathcal{R}^{\rho}_{\alpha\sigma\beta}\right)_0$ is required that can be calculated in the following way:

$$\mathcal{R}^{\rho}_{\alpha\sigma\beta} \equiv \partial_\sigma\Gamma^{\rho}_{\beta\alpha} - \partial_\beta\Gamma^{\rho}_{\sigma\alpha} + \Gamma^{\rho}_{\sigma\lambda}\,\Gamma^{\lambda}_{\beta\alpha} - \Gamma^{\rho}_{\beta\lambda}\,\Gamma^{\lambda}_{\sigma\alpha}\,, \tag{5.16}$$

leading to

$$\begin{aligned}\delta\mathcal{R}^{\rho}_{\alpha\sigma\beta} &= \partial_\sigma\delta\Gamma^{\rho}_{\beta\alpha} - \partial_\beta\delta\Gamma^{\rho}_{\sigma\alpha} + \delta\Gamma^{\rho}_{\sigma\lambda}\left(\Gamma^{\lambda}_{\beta\alpha}\right)_0 + \left(\Gamma^{\rho}_{\sigma\lambda}\right)_0\delta\Gamma^{\lambda}_{\beta\alpha} - \delta\Gamma^{\rho}_{\beta\lambda}\left(\Gamma^{\lambda}_{\sigma\alpha}\right)_0 - \left(\Gamma^{\rho}_{\beta\lambda}\right)_0\delta\Gamma^{\lambda}_{\sigma\alpha} \\ &= \nabla_\sigma\left(\delta\Gamma^{\rho}_{\beta\alpha}\right) - \nabla_\beta\left(\delta\Gamma^{\rho}_{\sigma\alpha}\right). \end{aligned} \tag{5.17}$$

In deriving the last line of (5.17) we have used the fact that the variation of the Christoffel symbols is a difference of two Christoffel symbols that form a tensor. Hence, we can apply the covariant derivative to this object that can be written as

$$\nabla_\lambda\delta\Gamma^{\rho}_{\beta\alpha} = \partial_\lambda\delta\Gamma^{\rho}_{\beta\alpha} + \left(\Gamma^{\rho}_{\sigma\lambda}\right)_0\delta\Gamma^{\sigma}_{\beta\alpha} - \left(\Gamma^{\sigma}_{\beta\lambda}\right)_0\delta\Gamma^{\rho}_{\sigma\alpha} - \left(\Gamma^{\sigma}_{\alpha\lambda}\right)_0\delta\Gamma^{\rho}_{\beta\sigma}\,. \tag{5.18}$$

By use of (5.14) and (5.17) we are able to compute the variation of the Ricci tensor in terms of the metric perturbation $h_{\alpha\beta}$

$$\begin{aligned}\delta\mathcal{R}_{\alpha\beta} &= \delta\mathcal{R}^{\rho}_{\alpha\rho\beta} = \nabla_\rho\left(\delta\Gamma^{\rho}_{\beta\alpha}\right) - \nabla_\beta\left(\delta\Gamma^{\rho}_{\rho\alpha}\right) \\ &= \frac{1}{2}\, G_0^{\rho\eta}\Big(\nabla_\rho\nabla_\alpha h_{\beta\eta} + \nabla_\rho\nabla_\beta h_{\alpha\eta} - \nabla_\rho\nabla_\eta h_{\beta\alpha} - \nabla_\beta\nabla_\alpha h_{\rho\eta} - \nabla_\beta\nabla_\rho h_{\alpha\eta} + \nabla_\beta\nabla_\eta h_{\rho\alpha}\Big) \\ &= \frac{1}{2}\Big(\nabla_\rho\nabla_\alpha h^{\rho}_{\beta} + \nabla_\rho\nabla_\beta h^{\rho}_{\alpha} - \nabla^2 h_{\alpha\beta} - \nabla_\alpha\nabla_\beta h\Big), \end{aligned} \tag{5.19}$$

with $h \equiv h^{\eta}_{\eta}$. The analogous computation is possible for the variation of the Ricci scalar which reads

$$\delta\mathcal{R} = \delta\big(G^{\alpha\beta}\mathcal{R}_{\alpha\beta}\big) = \mathcal{R}_{\alpha\beta}\,\delta G^{\alpha\beta} + G^{\alpha\beta}\,\delta\mathcal{R}_{\alpha\beta}\,. \tag{5.20}$$

In order to linearise (5.10) we have to apply our results to the Einstein tensor $\mathcal{G}_{\alpha\beta}$ that is given by

$$\begin{aligned}
\delta\mathcal{G}_{\alpha\beta} &= \delta\mathcal{R}_{\alpha\beta} - \frac{1}{2}h_{\alpha\beta}\,\mathcal{R}_0 - \frac{1}{2}G^0_{\alpha\beta}\left(\delta G^{\mu\nu}\,\mathcal{R}^0_{\mu\nu} + G^{\mu\nu}_0\delta R_{\mu\nu}\right)\\
&= \frac{1}{2}\big(\nabla_\rho\nabla_\alpha\,h^\rho_\beta + \nabla_\rho\nabla_\beta\,h^\rho_\alpha - \nabla^2\,h_{\alpha\beta} - \nabla_\alpha\nabla_\beta\,h\big)\\
&\quad - \frac{1}{2}\,G^0_{\alpha\beta}\left(G^{\mu\nu}\,\frac{1}{2}\big[\nabla_\rho\nabla_\mu\,h^\rho_\nu + \nabla_\rho\nabla_\nu\,h^\rho_\mu - \nabla^2\,h_{\mu\nu} - \nabla_\mu\nabla_\nu\,h\big]\right)\\
&\quad - \frac{1}{2}\,h_{\alpha\beta}\,\mathcal{R}_0 + \frac{1}{2}G_{\alpha\beta}\,h^{\mu\nu}\,R^0_{\mu\nu}\\
&= \frac{1}{2}\left(2\,\nabla^\rho\nabla_{(\alpha}h_{\beta)\rho} - \nabla^2\,h_{\alpha\beta} - \nabla_\alpha\nabla_\beta\,h - G^0_{\alpha\beta}\left(\nabla_\mu\nabla_\nu\,h^{\mu\nu} - \nabla^2\,h\right)\right.\\
&\quad \left. - h_{\alpha\beta}\,\mathcal{R}_0 + G^0_{\alpha\beta}\,h^{\mu\nu}\,\mathcal{R}^0_{\mu\nu}\right).
\end{aligned} \tag{5.21}$$

The vanishing of the last line in (5.21) gives the linearised equations of motion for a 5D Einstein–Hilbert action without a cosmological constant $\Lambda$ and any further scalar fields. By assuming the explicit form of the 5D Einstein–Hilbert action in the unperturbed case in (5.8), with $\Lambda = -\frac{6}{L^2}$ being the cosmological constant, we can compute the unperturbed Ricci scalar $\mathcal{R}_0$ and Ricci tensor $\mathcal{R}^0_{\alpha\beta}$ that are given by

$$\mathcal{R}_0 = -\frac{20}{L^2}\,, \tag{5.22}$$

and

$$h^{\alpha\beta}\,\mathcal{R}^0_{\alpha\beta} = h^{\alpha\beta}\left(\frac{1}{2}\,G^0_{\alpha\beta}\,\mathcal{R}_0 + G^0_{\alpha\beta}\,\frac{6}{L^2}\right) = -\frac{4}{L^2}\,h\,. \tag{5.23}$$

In (5.23) we have used the unperturbed Einstein equations without scalar fields. The contribution of $\Lambda$ to the linearised equations is covered by the variation of the stress-energy tensor which will be the next quantity we consider.

The unperturbed stress-energy tensor $\mathcal{T}_{\alpha\beta}$ is shown in (5.10). Similar to the metric we can decompose the full scalar $\Phi$ into the constant, unperturbed part $\Phi_0$ and the small perturbation $\delta\Phi$:

$$\Phi = \Phi_0 + \delta\Phi\,. \tag{5.24}$$

The unperturbed solution is set to zero ($\Phi_0 \equiv 0$) since any constant value can be absorbed by the fields in our action. The stress-energy tensor can thus be written to linear order as

$$\begin{aligned}
\delta\mathcal{T}_{\alpha\beta} &= -\frac{6}{L^2}\,h_{\alpha\beta} + \frac{1}{2}\underbrace{\partial_\alpha\delta\Phi\,\partial_\beta\delta\Phi}_{\mathcal{O}(\delta\Phi^2)} - \frac{1}{4}\underbrace{\left(\partial\delta\Phi\right)^2 h_{\alpha\beta}}_{\mathcal{O}(\delta\Phi^2)} - \frac{1}{2}h_{\alpha\beta}\,V(\delta\Phi)\\
&= -\frac{6}{L^2}\,h_{\alpha\beta}\,,
\end{aligned} \tag{5.25}$$

where we assume $V(\delta\Phi)$ to be at least quadratic in $\delta\Phi$ since the constant term is the cosmological constant $\Lambda$ and a linear one does not arise in general as we have seen in the full metric solution in Sec. 3.2.

Finally, we end up with the complete linearised Einstein equations of the 5D-Einstein–Hilbert-scalar action

$$0 = 2\,\nabla^\rho \nabla_{(\alpha} h_{\beta)\rho} - \nabla_\alpha \nabla_\beta\, h + G^0_{\alpha\beta}\left(\nabla^2\, h - \nabla^\mu \nabla^\nu\, h_{\mu\nu} - \frac{4}{L^2}\, h\right) - \nabla^2\, h_{\alpha\beta} + \frac{8}{L^2}\, h_{\alpha\beta}\,,$$
$$\nabla^\alpha \nabla_\alpha\, \delta\Phi = \frac{1}{\sqrt{\text{-}G^0}}\, \partial_\alpha\big(\sqrt{\text{-}G^0}\, G_0^{\alpha\beta}\, \partial_\beta\, \delta\Phi\big) = \frac{\partial V}{\partial \delta\Phi}\,. \tag{5.26}$$

This system of differential equations has the nice property of being decoupled at first order which simplifies the computation dramatically.

In the next section we choose a general metric ansatz that we have already used in Sec. 3.2.1 and try to solve (5.26) for $h_{\alpha\beta}$. The scalar equation of motion is not important for the computation of the screening distance. However, knowledge about the scalar potential $V$ is important to estimate, inter alia, the stability of the physical solution by evaluating the mass squared $M_\Phi^2$ of the scalar.

## 5.3 Solutions of the Linearised Einstein Equations

With the help of the general, full metric given by

$$\mathrm{d}s^2 = \mathrm{e}^{2A(z)}\left(\text{-}h(z)\mathrm{d}t^2 + \mathrm{d}\vec{x}^{\,2}\right) + \mathrm{e}^{2B(z)}\,\frac{\mathrm{d}z^2}{h(z)}\,, \tag{5.27}$$

we are able to extract a $1^{\text{st}}$-order perturbation which can be substituted into the linearised Einstein equations. We use the following expansion of the full metric functions around the conformal $AdS_5$-BH solution

$$e^{2A} \approx \frac{L^2}{z^2}\left(1 + \delta A(z)\right),$$
$$e^{2B} \approx \frac{L^2}{z^2}\left(1 + \delta B(z)\right),$$
$$h(z) \approx h_0(z) + \delta h(z) = 1 - \frac{z^4}{z_{\text{h}}^4} + \delta h(z)\,. \tag{5.28}$$

In Chapter 3 two boundary conditions were used in order to ensure the consistency of the model. In the limit $z \longrightarrow 0$ the metric functions should become asymptotically $AdS_5$ and the horizon function has to reach unity. This translates into conditions for the perturbations $\delta A(z)$, $\delta B(z)$ and $\delta h(z)$:

$$\delta A(0) = \delta B(0) = \delta h(0) \equiv 0\,. \tag{5.29}$$

By looking at the full metric we see that there is in principle one last gauge freedom left. We can use reparameterisation invariance of $z$ in order to gauge the $B(z)$ function away. A possible choice for a new coordinate $\tilde{z}$ would be

$$\mathrm{d}\tilde{z} = \frac{\mathrm{e}^B}{\mathrm{e}^A}\,\mathrm{d}z\,. \tag{5.30}$$

However, the details of this transformation are given after solving the full Einstein equations. This is very difficult to ensure in the linearised case since we do not know at this stage whether

this transformation possesses any singularities or not. Therefore, we use the ungauged solution including $\delta B(z)$ for the main part of the computation.

Now, let us turn back to solutions of the linearised Einstein equations. By introducing a deformation $\delta A(z)$ and $\delta B(z)$ we cannot assume that the horizon is still identical to that in the conformal scenario. There are two ways to derive this fact. Firstly, a look at the full solution in a numerical study reveals that turning on a deformation immediately leads to a change in the corresponding horizon. Secondly, we can set $\delta h(z)$ to zero and check the results of the linearised Einstein equations. We will do this in Sec. 5.3.1.

But first, let us substitute (5.28) into the full metric (5.27) and collect first order terms. This calculation leads to

$$\begin{aligned}
\mathrm{d}s^2_{\mathrm{Lin}} &= \frac{L^2}{z^2}\left(1+\delta A(z)\right)\left(-\left(h_0(z)+\delta h(z)\right)\mathrm{d}t^2+\mathrm{d}\vec{x}^2\right)+\frac{L^2}{z^2}\left(1+\delta B(z)\right)\frac{\mathrm{d}z^2}{h_0(z)+\delta h(z)} \\
&= \left(-\frac{L^2}{z^2}\,h_0-\frac{L^2}{z^2}\,\delta h-\frac{L^2}{z^2}\delta A\,h_0-\underbrace{\frac{L^2}{z^2}\delta A\,\delta h}_{\mathcal{O}(\delta^2)}\right)\mathrm{d}t^2+\frac{L^2}{z^2}\left(1+\delta A\right)\mathrm{d}\vec{x}^2 \\
&\quad+\left(\frac{L^2}{z^2}\,\frac{1}{h_0}-\frac{L^2}{z^2}\,\frac{\delta h}{h_0^2}+\frac{L^2}{z^2}\,\frac{\delta B}{h_0}-\underbrace{\frac{L^2}{z^2}\,\frac{\delta B\delta h}{h_0^2}}_{\mathcal{O}(\delta^2)}\right)\mathrm{d}z^2 \\
&= \mathrm{d}s^2_{AdS_5}+\frac{L^2}{z^2}\left(-\left(\delta h+\delta A\,h_0\right)\mathrm{d}t^2+\delta A\,\mathrm{d}\vec{x}^{\,2}\right)+\frac{L^2}{z^2}\left(\frac{\delta B}{h_0}-\frac{\delta h}{h_0^2}\right)\mathrm{d}z^2\,,
\end{aligned} \tag{5.31}$$

where $\mathrm{d}s^2_{AdS_5}$ is the line element of the conformal $AdS_5$-BH space and second order terms have been neglected. In addition, we use the following expansion

$$\frac{1}{h_0+\delta h}=\frac{1}{h_0}-\frac{\delta h}{h_0^2}+\mathcal{O}(\delta h^2)\,. \tag{5.32}$$

With the help of (5.31) we can now specify the metric perturbation $h_{\alpha\beta}$

$$h_{\alpha\beta}=\begin{pmatrix}
-\frac{L^2}{z^2}\left(\delta h(z)+\delta A(z)\,h_0(z)\right) & 0\cdot\mathbb{1}_{1\times 3} & 0 \\
0\cdot\mathbb{1}_{3\times 1} & \left(\frac{L^2}{z^2}\,\delta A(z)\right)\cdot\mathbb{1}_{3\times 3} & 0\cdot\mathbb{1}_{3\times 1} \\
0 & 0\cdot\mathbb{1}_{1\times 3} & \frac{L^2}{z^2}\left(\frac{\delta B(z)}{h_0}-\frac{\delta h(z)}{h_0^2}\right)
\end{pmatrix} \tag{5.33}$$

This can be plugged into the linearised Einstein equations (5.26).

Keeping this in mind we can answer the question whether a small perturbation in $A(z)$ and $B(z)$ is possible by simultaneously leaving $h(z)$ unchanged. In this case the equations are very simple. Then, we proceed with the perturbation of all three metric functions and derive the formulae for the horizon function $h(z)$ and temperature $T$.

### 5.3.1 Unperturbed Horizon Solution

In the case of a vanishing horizon perturbation ($\delta h(z)=0$) the line element in (5.31) can be written as

$$\mathrm{d}s^2=\mathrm{d}s_0^2+\frac{L^2}{z^2}\left(-\delta A\,h_0\,\mathrm{d}t^2+\delta A\,\mathrm{d}\vec{x}^{\,2}\right)+\frac{L^2}{z^2}\,\delta B\,\frac{\mathrm{d}z^2}{h_0}\,. \tag{5.34}$$

By substituting (5.34) into the linearised Einstein equations (5.26) the following system of second order differential equations can be obtained

$$\begin{aligned}
\frac{z_\mathrm{h}^8\, z^2}{z^4 - z_\mathrm{h}^4}\,\mathcal{E}_{00} - z^2\, z_\mathrm{h}^4\,\mathcal{E}_{ii} &= 4\,\delta A'(z) - \delta B'(z) = 0 \\
\frac{z_\mathrm{h}^8\, z^2}{z^4 - z_\mathrm{h}^4}\,\mathcal{E}_{00} + (z^6 - z^2\, z_\mathrm{h}^4)\,\mathcal{E}_{44} &= \delta A'(z) + \delta B'(z) + z\,\delta A''(z) = 0 \\
z^2\, z_\mathrm{h}^4\,\mathcal{E}_{ii} + (z^6 - z^2\, z_\mathrm{h}^4)\,\mathcal{E}_{44} &= (-11\, z^4 + 3\, z_\mathrm{h}^4)\,\delta A'(z) - (z^4 - 3\, z_\mathrm{h}^4)\,\delta B'(z) \\
&\quad + 3\, z\,(-z^4 + z_\mathrm{h}^4)\,\delta A''(z) = 0\,.
\end{aligned} \tag{5.35}$$

Here, $\mathcal{E}_{\alpha\alpha}$, $\alpha = 0, 1, 2, 3, 4$ are the diagonal matrix elements of the tensor defined in (5.26) with $\mathcal{E}_{ii}$, $i = 1, 2, 3$ being identical due to the global symmetries of the metric. In this particular case with a unperturbed horizon function $h(z) = h_0(z)$ the horizon $z_\mathrm{h}$ has still its physical meaning of being related to the temperature $T \sim z_\mathrm{h}^{-1}$.

This system can be treated exactly by solving the first equation of (5.35) for $\delta B'$ and substituting this into the second equation of (5.35). We end up with

$$5\,\delta A'(z) + z\,\delta A''(z) = 0 \quad \text{with} \quad \delta B'(z) = 4\,\delta A'(z)\,, \tag{5.36}$$

which can now be solved easily by using standard integration techniques

$$\begin{aligned}
-\frac{5}{z} = \frac{\delta A''}{\delta A'} \quad &\Longrightarrow \quad -5\,\log z = \log \delta A'(z) + \mathcal{C} \\
&\Longrightarrow \quad \delta A(z) = \frac{1}{4}\, z^{-4}\,\mathcal{C}' + \mathcal{C}''\,.
\end{aligned} \tag{5.37}$$

The solution for $\delta B$ is then simply given by

$$\delta B = \mathcal{C}'\, z^{-4} + \mathcal{C}'''\,, \tag{5.38}$$

where all $\mathcal{C}$s are integration constants. Finally, we still have to impose our boundary conditions, meaning that we assume the whole system to approach the conformal limit in the UV. This corresponds to a vanishing $\delta A$ and $\delta B$ for $z \longrightarrow 0$. From (5.37) and (5.38) we conclude that the deformations do increase dramatically for small values of $z$ in order to cancel possible fluctuations in the horizon function. This contradicts our general assumption and thus only the trivial solution

$$\delta A = 0\,, \quad \delta B = 0\,, \tag{5.39}$$

is left in accordance with our general consideration at the beginning of this chapter. In the next paragraph we then start the complete metric in (5.31) and solve for the metric perturbations.

### 5.3.2 Solutions Including Horizon Perturbations

After substituting the complete perturbed metric (5.31) into the linearised Einstein equations (5.26) and working out the covariant derivatives and Christoffel symbols we end up with a

system of second order differential equations that is given by

$$\begin{aligned}
\frac{z_\mathrm{h}^8\, z^2}{z^4 - z_\mathrm{h}^4}\,\mathcal{E}_{00} - z^2\, z_\mathrm{h}^4\,\mathcal{E}_{ii} &= -8\, z^4\,\delta A'(z) + 2\, z^4\,\delta B'(z) + z_\mathrm{h}^4\,(-3\,\delta h'(z) + z\,\delta h''(z)) = 0 \\
\frac{z_\mathrm{h}^8\, z^2}{z^4 - z_\mathrm{h}^4}\,\mathcal{E}_{00} + (z^6 - z^2\, z_\mathrm{h}^4)\,\mathcal{E}_{44} &= \delta A'(z) + \delta B'(z) + z\,\delta A''(z) = 0 \\
z^2\, z_\mathrm{h}^4\,\mathcal{E}_{ii} + (z^6 - z^2\, z_\mathrm{h}^4)\,\mathcal{E}_{44} &= (-11\, z^4 + 3\, z_\mathrm{h}^4)\,\delta A'(z) - (z^4 - 3\, z_\mathrm{h}^4)\,\delta B'(z) - 3\, z_\mathrm{h}^4 \delta h'(z) \\
&\quad - 3z^5\,\delta A''(z) + 3\, z\, z_\mathrm{h}^4\,\delta A''(z) + z\, z_\mathrm{h}^4\,\delta h''(z) = 0\,. \qquad (5.40)
\end{aligned}$$

These equations are not algebraically independent which can be seen by subtracting the first equation of (5.40) from the last ending up with an expression of the second equation. Thus – analogous to the full, numerical solutions – we specify an ansatz for $\delta A(z)$ and solve for the other functions. In order to stay close to the full solutions where an ansatz of the form $A(z) \approx \frac{L^2}{z^2}\,(1 + cz^2)$ is used we choose

$$\delta A(z) = \alpha\, z^k\,. \qquad (5.41)$$

with $k$ being an arbitrary positive real number and $\alpha \in \mathbb{R}$. $\alpha$ should not be confused with the $\alpha$ given in the 2-parameter model. Both values are completely unrelated. Negative values of $k$ are not allowed since the perturbation would become dominant in the limit $z \to 0$ where we expect to recover the conformal result. This ansatz is of course only valid in a linearised approximation if $\alpha\, z_\mathrm{h}^k$ is much smaller than 1. It is noteworthy that we cannot argue that (5.41) is a unique choice. In principle, we have to allow for all kinds of functions that vanish in the limit $z \longrightarrow 0$ limit. However, a proof for all monomials with positive values of $k$ would be a satisfying statement.

After substituting (5.41) into the second equation of (5.40) we have to solve the following equation for $\delta B$:

$$k^2\, z^{k-1}\,\alpha + \delta B'(z) = 0 \quad \Longrightarrow \quad \delta B(z) = -k\, z^k\,\alpha + \mathcal{C}\,, \qquad (5.42)$$

where the integration constant can be set to zero ($\mathcal{C} \equiv 0$) by using the boundary condition $\delta B(0) = 0$. With this solution for $\delta B$ we solve the first equation of (5.40) for $\delta h(z)$ that leads to

$$\begin{aligned}
0 &= -2\, k\,(4 + k)\, z^{3+k}\,\alpha - 3\, z_\mathrm{h}^4\,\delta h'(z) + z\, z_\mathrm{h}^4\,\delta h''(z)\,, \quad \text{with } \delta h(0) = 0\,, \\
\delta h(z) &= \frac{2\, z^{4+k}\,\alpha}{z_\mathrm{h}^4} + \frac{1}{4}\, z^4\,\kappa\,. \qquad (5.43)
\end{aligned}$$

Since we have a second order equation for $\delta h$ and only one boundary condition, an additional parameter $\kappa$ arises that can be absorbed into the new horizon $z_\mathrm{nh}$ which has to obey

$$\begin{aligned}
h(z_\mathrm{nh}) = 1 - \frac{z_\mathrm{nh}^4}{z_\mathrm{h}^4} + \delta h(z_\mathrm{nh}) \equiv 0 \quad &\Longrightarrow \quad \kappa = -\frac{4\left(z_\mathrm{h}^4 - z_\mathrm{nh}^4 + 2\, z_\mathrm{nh}^{4+k}\,\alpha\right)}{z_\mathrm{h}^4\, z_\mathrm{nh}^4} \\
h(z, z_\mathrm{h}, z_\mathrm{nh}, k, \alpha) &= 1 + \frac{2\, z^{4+k}\,\alpha}{z_\mathrm{h}^4} + z^4\left(-\frac{1}{z_\mathrm{nh}^4} - \frac{2\, z_\mathrm{nh}^k\,\alpha}{z_\mathrm{h}^4}\right). \qquad (5.44)
\end{aligned}$$

Equation (5.44) and the full expression for the other metric functions $A$ and $B$, are given by

$$A(z,\,\alpha,\,k) = \frac{L^2}{z^2}\left(1+\delta A(z,\,\alpha,\,k)\right) = \frac{L^2}{z^2}\left(1+\alpha z^k\right),$$
$$B(z,\,\alpha,\,k) = \frac{L^2}{z^2}\left(1+\delta B(z,\,\alpha,\,k)\right) = \frac{L^2}{z^2}\left(1-\alpha\,k\,z^k\right). \tag{5.45}$$

These expressions define the metric functions which are required to prove the screening-distance conjecture in first order.

Altogether, four parameters ($\alpha$, $k$, $z_\mathrm{h}$, $z_\mathrm{nh}$) appear in this analysis of small perturbations around the conformal solution. This seems to be a real mess, but we will find a relation at the end of this analysis between our primary deformation parameter $\alpha$ and the new horizon $z_\mathrm{nh}$. Such a relation has to exist since in the limit of vanishing deformation ($\alpha \longrightarrow 0$) we should arrive at the conformal $AdS_5$-BH solution. This is the case for $\delta B(z)$ by looking at (5.42). However, the horizon function $h(z)$ in (5.44) reduces to

$$\lim_{\alpha\to 0} h(z, z_\mathrm{h}, z_\mathrm{nh}, k, \alpha) = 1 - \frac{z^4}{z_\mathrm{nh}^4} \neq 1 - \frac{z^4}{z_\mathrm{h}^4}\,. \tag{5.46}$$

Thus, $\alpha$ is a kind of a *primary* deformation parameter, since it determines the validity of the linearisation as well as the deviation of the new horizon $z_\mathrm{nh}$ from the original one $z_\mathrm{h}$. This means that a small value of $\alpha$, $\alpha\, z_\mathrm{h}^k < 1$, is related to a value of $z_\mathrm{nh}$ which has to be even closer to conformality, $\frac{z_\mathrm{nh}-z_\mathrm{h}}{z_\mathrm{h}} \ll 1$, in order to stay within the linearisation. To get a feeling for these deformations we analyse the horizon function $h(z)$ and the temperature in the following and try to figure out which parameter ranges are physically meaningful. In Sec. 5.4 we then derive appropriate relations (5.58) and (5.68) between $\alpha$ and the corresponding most non-conformal, value of $z_\mathrm{nh}^{\max/\min}$ in the Einstein and string frame, respectively.

In Fig. 5.2 the horizon function $h(z)$ given by (5.44) is plotted against the $5^\mathrm{th}$-dimensional coordinate $z$ for a large range of $\alpha$, $-0.4 < \alpha < 0.4$ (in arbitrary units) and four different values of the new horizon $z_\mathrm{nh}$, $z_\mathrm{nh} = 0.8$, 0.9, 1 and 1.1. For all choices of parameters we obtain a horizon function $h(z)$ that fulfils the necessary condition of exhibiting a zero which is the new horizon $z_\mathrm{nh}$. In the following computations we set the free parameter $z_\mathrm{h} = 1$ since it is just a rescaling of the other quantities and has no further physical relevance anymore. For the temperature $T_\mathrm{Lin}$ that is given by the general temperature formula

$$T = \mathrm{e}^{A(z_\mathrm{h})-B(z_\mathrm{h})}\,\frac{|h'(z_\mathrm{h})|}{4\pi}\,, \tag{5.47}$$

the new horizon $z_\mathrm{nh}$ is now the dominant length scale and replaces $z_\mathrm{h}$ but has to be close to this value because the main deformation parameter $\alpha$ has to be small in general. These values of $z_\mathrm{nh}$ are not allowed to exceed the ranges of validity set by $\alpha$ as we have mentioned above. With the full metric functions $A$, $B$ (5.45) and $h$ (5.44) in our hand we can now compute the perturbed temperature $T_\mathrm{Lin}$. The answer can be written as

$$T_\mathrm{Lin} = \frac{\sqrt{1+z_\mathrm{h}^k\,\alpha}\left(4z_\mathrm{h}^4 - 2k\,z_\mathrm{nh}^{4+k}\,\alpha\right)}{\sqrt{1-k\,z_\mathrm{h}^k\,\alpha}\,4\pi z_\mathrm{h}^4\,z_\mathrm{nh}}\,,$$
$$\xrightarrow{\alpha z_\mathrm{h}^k \ll 1} \quad \frac{1}{\pi\,z_\mathrm{nh}} + \alpha\,\frac{(1+k)z_\mathrm{h}^{4+k} - k\,z_\mathrm{nh}^{4+k}}{2\pi\,z_\mathrm{h}^4\,z_\mathrm{nh}}\,. \tag{5.48}$$

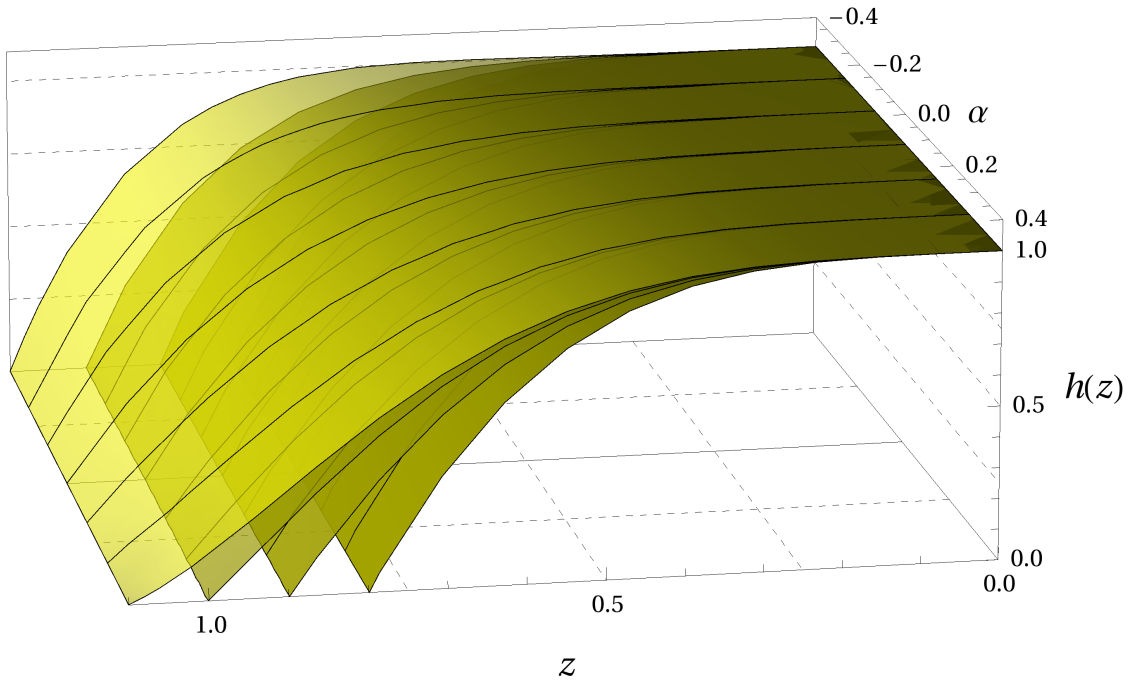


Figure 5.2: Horizon function $h(z)$ for a large range of $\alpha$ values, $-0.4 < \alpha < 0.4$ (in arbitrary units) and four different values of the new horizon $z_{\mathrm{nh}}$, $z_{\mathrm{nh}} = 0.8$ (lowest surface), 0.9, 1 and 1.1 (highest surface). The old horizon is fixed at $z_{\mathrm{h}} = 1$ and we used $k = 2$ for simplicity. Other values of $k$ result in similar plots.

The temperature $T_{\mathrm{Lin}}$ is visualised in Fig. 5.3 for a large range of $\alpha$ values, $-0.5 < \alpha < 0.5$ (in arbitrary units) and $k = 2$. The original horizon is fixed at $z_{\mathrm{h}} = 1$. The transparent surface located at the back is the small-$\alpha$ expansion and the front surface is the first line in (5.48). For negative values of $\alpha$ the temperature has the same shape as all our unperturbed, consistent models (see Figs. 3.2 and 3.5) and assumes a minimal temperature $T_{\mathrm{min}}$ for all values. For $\alpha = 0$ we obtain the conformal result, $T = (\pi z_{\mathrm{nh}})^{-1}$, and for positive values of $\alpha$ we can find a horizon $z_{\mathrm{nh}}$ for every chosen temperature. However, at $\alpha > 0.5$ for $k = 2$ the temperature is not well-defined anymore since the square root in the denominator of (5.48) becomes negative and our approximation is not valid anymore. This interesting behaviour around $\alpha = 0.5$ provides us with a good estimate of where the linearisation finally loses its validity. Remember, that $z_{\mathrm{h}}$ is set to unity, which defines a scale in our model. Thus, we will restrict our analysis to values of $|\alpha| < 0.5$ although we always plot in the subsequent figures a slightly larger $\alpha$-range for sake of completeness.

The results up to now seem to be very promising and we start in the next two sections (5.4 and 5.4.2) with the derivation of an analytic solution of the QQ̄-distance for small perturbations around the conformal solution.

## 5.4 Linearised QQ̄-Distance $L^{\mathrm{Lin}}$

In the following computations$A$, $B$ and $h$ always refer to the linearised metric functions specified in (5.45) and (5.44). By using the general expression for the QQ̄-distance given in (4.38) we can write down a formula of the quark-antiquark distance in the perturbed metric

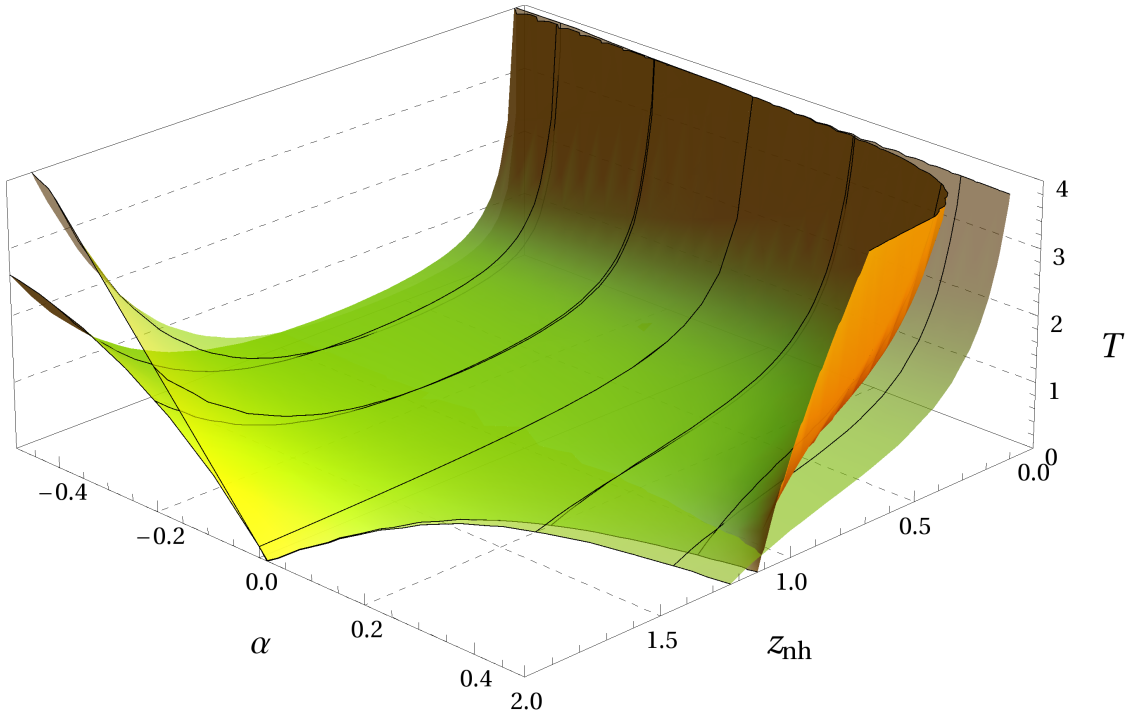


Figure 5.3: Temperature $T_{\text{Lin}}$ (top surface) and small $\alpha$-approximation (back surface) against $z_{\text{nh}}$ for a large range of $\alpha$ values, $-0.5 < \alpha < 0.5$ (in arbitrary units) and $k = 2$. The old horizon is fixed at $z_{\text{h}} = 1$. For large positive values of $\alpha$ the root in the denominator of (5.48) becomes negative which indicates a breakdown of the linearised theory.

scenario. Furthermore, our computation is only valid to linear order in the perturbation which is measured by the parameter $\alpha$. Hence, we use a Taylor expansion of the integrand in $\alpha$ around $\alpha = 0$ in order to obtain the $1^{\text{st}}$-order correction to the conformal quark-antiquark distance. $(L\pi T)_{\text{Lin}}$ can then be written as

$$(L\pi T)_{\text{Lin}} = (L\pi T)_{\mathcal{N}=4} + \alpha \int_0^{z_{\text{c}}} \mathrm{d}z\, \mathcal{I} + \mathcal{O}\big(\alpha^2\big)\,, \tag{5.49}$$

with

$$\begin{aligned}
\mathcal{I} = \frac{z^2}{z_{\text{nh}}} \sqrt{\frac{z_{\text{nh}}^4 - z_{\text{c}}^4}{(z_{\text{c}}^4 - z^4)\,(z_{\text{nh}}^4 - z^4)}} \Bigg[ & (1+k)\, z_{\text{h}}^k + \frac{1}{(z^4 - z_{\text{c}}^4)\, z_{\text{h}}^4\, (z^4 - z_{\text{nh}}^4)\, (z_{\text{c}}^4 - z_{\text{nh}}^4)} \\
& \cdot \Bigg( - 2 z_{\text{c}}^{8+k}\, (z^4 - z_{\text{nh}}^4)^2 - (z^4 - z_{\text{c}}^4) z_{\text{nh}}^{4+k} \Big( k z^4 z_{\text{c}}^4 - \big((2+k) z^4 \\
& + (k-2) z_{\text{c}}^4\big) z_{\text{nh}}^4 + k z_{\text{nh}}^8 \Big) + 2 z^{4+k}\, (z_{\text{c}}^4 - z_{\text{nh}}^4) \Big( z^4\, (z_{\text{c}}^4 - z_{\text{nh}}^4) - 2 z_{\text{c}}^4 z_{\text{nh}}^4 \Big) \Bigg) \\
& + \frac{1}{(z^4 - z_{\text{c}}^4)\, z_{\text{nh}}^4} \Bigg( 2 z_{\text{c}}^{4+k}\, (z^4 - z_{\text{nh}}^4) + z^k \Big( (3+k) z_{\text{c}}^4 z_{\text{nh}}^4 \\
& - z^4 \big( 2 z_{\text{c}}^4 + (1+k) z_{\text{nh}}^4 \big) \Big) \Bigg) \Bigg]\,.
\end{aligned} \tag{5.50}$$

The nice fact about (5.49) is the possibility to integrate this analytically for all values of $k$. The primitive of the linearised part can be found very easily although it is quite lengthy. It is given in full detail in Appendix D.

By inserting the integration limits some problems occur. The primitive at the lower limit ($z = 0$) vanishes whereas at the upper limit ($z = z_{\mathrm{c}}$) we find two putatively divergent terms in the primitive that cancel each other up to a finite remainder. We focus on these two divergent terms later on and denote them by $\mathcal{F}_{\mathrm{II}}$. The other summands in the primitive are finite in the limit $z \to z_{\mathrm{c}}$ and can be collected in the expression $\mathcal{F}_{\mathrm{I}}$. Thus, we can express the integral in (5.49) in the form

$$\alpha \int_0^{z_{\mathrm{c}}} \mathrm{d}z\, \mathcal{I} = \alpha\Big(\mathcal{F}_{\mathrm{I}} + \mathcal{F}_{\mathrm{II}}\big|_{z=z_{\mathrm{c}}} - 0\Big)\,, \tag{5.51}$$

with $\mathcal{F}_{\mathrm{I}}$ given by

$$\begin{aligned}
\mathcal{F}_{\mathrm{I}} = \alpha\, \frac{\sqrt{\pi}\, z_{\mathrm{c}}}{42\,(3+k) z_{\mathrm{h}}^4\, z_{\mathrm{nh}}^7 \sqrt{z_{\mathrm{nh}}^4 - z_{\mathrm{c}}^4}} \Bigg\{ & -14\,(3+k)\, z_{\mathrm{nh}}^4 \Big( z_{\mathrm{c}}^k\, z_{\mathrm{h}}^4\, z_{\mathrm{nh}}^4 - (1+k)\, z_{\mathrm{h}}^{4+k}\, z_{\mathrm{nh}}^4 \\
& + k\, z_{\mathrm{nh}}^{8+k} + z_{\mathrm{c}}^{4+k} \left(z_{\mathrm{nh}}^4 - z_{\mathrm{h}}^4\right) + (1+k) z_{\mathrm{c}}^4 \left(z_{\mathrm{h}}^{4+k} - z_{\mathrm{nh}}^{4+k}\right) \Big) \frac{\Gamma(7/4)}{\Gamma(5/4)} \\
& \cdot {}_2F_1\left(\frac{1}{2}, \frac{3}{4}, \frac{5}{4}, \frac{z_{\mathrm{c}}^4}{z_{\mathrm{nh}}^4}\right) + 3\Bigg[ -6\,(3+k) z_{\mathrm{c}}^4 \left( z_{\mathrm{nh}}^{8+k} + z_{\mathrm{c}}^k \left( z_{\mathrm{c}}^4\, z_{\mathrm{h}}^4 - \left(z_{\mathrm{c}}^4 + z_{\mathrm{h}}^4\right) z_{\mathrm{nh}}^4 \right) \right) \\
& \cdot \frac{\Gamma(11/4)}{\Gamma(9/4)}\, {}_2F_1\left(\frac{1}{2}, \frac{7}{4}, \frac{9}{4}, \frac{z_{\mathrm{c}}^4}{z_{\mathrm{nh}}^4}\right) + \frac{7 z_{\mathrm{c}}^k\, z_{\mathrm{nh}}^4\, \Gamma\left(\frac{7+k}{4}\right)}{\Gamma\left(\frac{5+k}{4}\right) \Gamma\left(\frac{9+k}{4}\right)} \Bigg( -2(1+k)\, z_{\mathrm{h}}^4\, z_{\mathrm{nh}}^4\, \Gamma\left(\frac{9+k}{4}\right) \\
& \cdot {}_2F_1\left(-\frac{1}{2}, \frac{3+k}{4}, \frac{5+k}{4}, \frac{z_{\mathrm{c}}^4}{z_{\mathrm{nh}}^4}\right) + z_{\mathrm{c}}^4\, \Gamma\left(\frac{5+k}{4}\right) \Bigg\{ (1+k)\, z_{\mathrm{h}}^4 \\
& \cdot {}_2F_1\left(\frac{1}{2}, \frac{3+k}{4}, \frac{9+k}{4}, \frac{z_{\mathrm{c}}^4}{z_{\mathrm{nh}}^4}\right) + 2 z_{\mathrm{nh}}^4\, {}_2F_1\left(\frac{3}{2}, \frac{3+k}{4}, \frac{9+k}{4}, \frac{z_{\mathrm{c}}^4}{z_{\mathrm{nh}}^4}\right) \Bigg\} \Bigg) \Bigg] \Bigg\}\,.
\end{aligned} \tag{5.52}$$

The other part reads

$$\begin{aligned}
\mathcal{F}_{\mathrm{II}}\big|_{z=z_{\mathrm{c}}} = & -\frac{z_{\mathrm{c}}^3 \left( (z_{\mathrm{c}}^4 + z_{\mathrm{h}}^4) z_{\mathrm{nh}}^4 - z_{\mathrm{c}}^4 z_{\mathrm{h}}^4 \right)}{(3+k) z_{\mathrm{h}}^4 z_{\mathrm{nh}}^5 \sqrt{z_{\mathrm{nh}}^4 - z_{\mathrm{c}}^4}} \lim_{z \to z_{\mathrm{c}}} \Bigg[ (3+k) z_{\mathrm{c}}^k \sqrt{\frac{z^4 - z_{\mathrm{nh}}^4}{z^4 - z_{\mathrm{c}}^4}} \\
& + 2 \frac{z^k z_{\mathrm{nh}}^2}{z_{\mathrm{c}}^2}\, F_1\left(\frac{3+k}{4}, \frac{3}{2}, -\frac{1}{2}, \frac{7+k}{4}, \frac{z^4}{z_{\mathrm{c}}^4}, \frac{z^4}{z_{\mathrm{nh}}^4}\right) \Bigg]\,,
\end{aligned} \tag{5.53}$$

where $F_1(\cdot,\cdot,\cdot,\cdot,\cdot,\cdot)$ is the *Appell function* of the first kind. For $z \to z_{\mathrm{c}}$ the result of $\mathcal{F}_{\mathrm{II}}$ is finite which has been verified by a numerical computation. However, this finite remainder in (5.53) could not be extracted analytically. In summary, the quark-antiquark distance for the linearised case for a general perturbation around the conformal solution reads

$$(L\pi T)_{\mathrm{Lin}} = (L\pi T)_{\mathcal{N}=4} + \alpha\Big(\mathcal{F}_{\mathrm{I}} + \lim_{z \to z_{\mathrm{c}}} \mathcal{F}_{\mathrm{II}}\Big)\,. \tag{5.54}$$

In the next subsection we discuss (5.54) and try to deduce whether the screening-distance conjecture holds for small perturbations. This means that the sum of the $0^{\text{th}}$- and $1^{\text{st}}$-order of the screening distance $(L\pi T)_{\text{S}}$ has to be larger than the conformal value (5.1). We have seen in previous chapters that there is the possibility to interpret the scalar field $\Phi$ as the dilaton (string frame computation) or not (Einstein frame computation). In the latter case, we have a scalar field $\Phi$ in our model and the dilaton vanishes. We discuss the latter frame first since there we do not need to care about the scalar $\Phi$ because it has decoupled from the linearised Einstein equations (5.26). In Sec. 5.4.2 the dilaton case will be considered and a new – and definitely the last – parameter $\phi$ appears in the derivation.

### 5.4.1 Einstein-Frame Computation

We have to cope with a bunch of parameters with some of them being more important than the others. At the beginning of this chapter we argued that the old horizon $z_{\text{h}}$ represents a scaling but does not change the physics in general. Therefore, we set $z_{\text{h}} = 1$ again for sake of simplicity. An analogous argument can be found for the parameter $k$ measuring the power of $z$ in the metric function perturbation $\delta A$. Larger values of $k$ lead to stronger deformations but do not introduce further qualitative changes. Thus, in order to stay close to the metric ansatz chosen when solving full Einstein equations in Chapter 3 we set $k = 2$ and show plots for different values of $k$ at the end of this section in Figs. 5.6 and 5.9(a). We end up with two parameters that are important for this computation:

**$z_{\text{nh}}$:** which is the root of the horizon function $h = h_0 + \delta h$ representing the location of the black-hole horizon. Furthermore, it is the most dominant parameter in the temperature formula.

**$\alpha$:** which measures the strength of the perturbation. $\alpha = 0$ is the conformal limit. In this case the new horizon $z_{\text{nh}}$ has to coincide with $z_{\text{h}} \equiv 1$.

The main question we have to pose now is the following:

*How can we decide analytically that the screening distance in the linearised case is larger than the conformal value?*

In addition to this, we have to determine the appropriate $\alpha$- and $z_{\text{nh}}$-regime. The answer to the first question is very easy. The quantity $(L\pi T)^{\mathcal{N}=4_T}_{\text{max}}$ is a universal number in $\mathcal{N} = 4_T$ that reads

$$(L\pi T)^{\mathcal{N}=4_T}_{\text{max}} = 0.86912015361\,. \tag{5.55}$$

Thus, we compute the maximum of the linearised $\text{Q}\bar{\text{Q}}$-distance $(L\pi T)^{\text{Lin}}_{\text{max}}$ and compare the result with (5.55). If $(L\pi T)^{\text{Lin}}_{\text{max}} > (L\pi T)^{\mathcal{N}=4_T}_{\text{max}}$ the bound is satisfied for the chosen parameters. In order to find the appropriate regime of validity we recall that the main perturbation parameter is $\alpha$. Thus, the deviation of the new horizon $z_{\text{nh}}$ from the old one expressed in appropriate units should always be smaller than the corresponding value of $\alpha$. We do not expect the bound to be fulfilled for large $z_{\text{nh}}$ and small $\alpha$ because this perturbation is not small and our approximation is not valid.

For every value of $\alpha$ we have to find a small real number $\delta > 0$ so that $(L\pi T)^{\text{Lin}}_{\text{max}}[\alpha\,, z_{\text{nh}}] \geq (L\pi T)^{\mathcal{N}=4_T}_{\text{max}}$ for every $z_{\text{nh}}$ with $|z_{\text{nh}} - z_{\text{h}}| < \delta$. This statement ensures that we are always in the valid limit of our linearisation. Furthermore, we have to assume $\alpha\, z_{\text{h}}^k$ to be small.

The proof goes as follows:

1. The increase of the screening distance will be proven for fixed $\alpha = \pm 0.5$, $k = 2$ and $z_{\rm nh} = z_{\rm h} = 1$ first.

2. Then, the focus is on fixed $\alpha = \pm 0.5$, $k = 2$ but we allow for $z_{\rm nh} \neq z_{\rm h} = 1$.

3. Finally the discussion will be extended to arbitrary values of $\alpha$ and $z_{\rm nh} \neq z_{\rm h}$ for fixed $k = 2$.

To this end we plot in Fig. 5.4 the 1st-order correction in $\alpha$ for fixed $\alpha = \pm 0.5$ and various values of the new horizon $z_{\rm nh}$, $z_{\rm nh} = 0.99$, 1 and 1.01. The black solid curve represents the conformal curve divided by a factor of 2 for $z_{\rm nh} = 1$. Some important facts have to be noted.

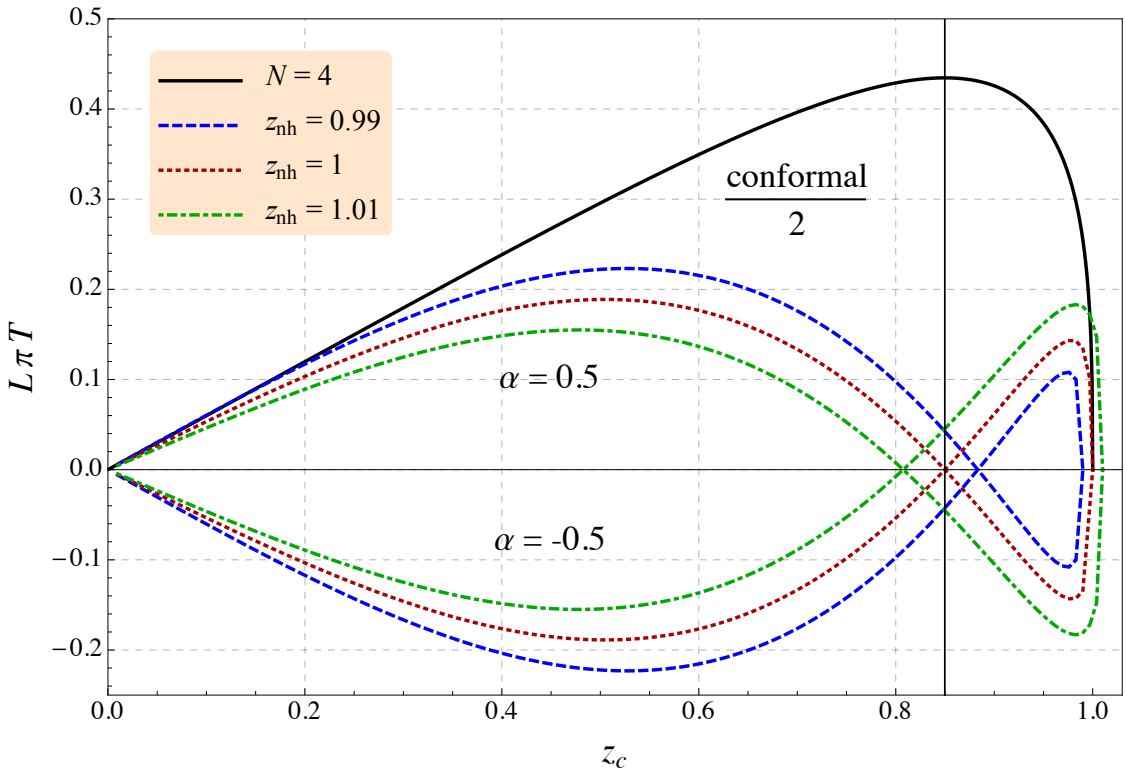


Figure 5.4: 1st-order correction in $\alpha$ against the conformal quark-antiquark distance for fixed $\alpha = \pm 0.9$ and various values of the new horizon $z_{\rm nh}$, $z_{\rm nh} = 0.99, 1$ and 1.01. The black solid curve represents the conformal curve divided by a factor of 2 for $z_{\rm nh} = 1$. The thin vertical line illustrates the fact that the $z_{\rm c}$-value of the zero-crossing of the red dotted line coincides precisely with the particular $z_{\rm c}$-value where the conformal curve assumes the the maximum QQ̄-distance $(L\pi T)^{\mathcal{N}=4_T}_{\rm max}$.

Firstly, for all values of $\alpha$ the 1st-order correction given by (5.51) has a positive and a negative part. This allows in principle for the possibility that positive and negative values of $\alpha$ lead to an increase of the screening distance $(L\pi T)^{\rm Lin}_{\rm max}$ in opposition to the SW$_T$-model in Sec. 5.1 where negative values of $c$ inexorably led to a decrease of the screening distance. Secondly, all curves end precisely at the horizon which is defined by $z_{\rm nh}$ in this discussion. The QQ̄-distance $(L\pi T)^{\rm Lin}$ to first order in $\alpha$ is just the sum of twice the conformal black line and one of the

dashed 1st-order corrections. Thirdly, the red dotted curves that obey $z_{\rm nh} = z_{\rm h} = 1$ cross zero at a specific value for $z_{\rm c} = z_{\rm c}^*$ given by

$$z_{\rm c}^* = 0.8498\,. \tag{5.56}$$

$z_{\rm c}^*$ is identical to the $z_{\rm c}$-value where the conformal curve assumes the maximum $\mathrm{Q}\bar{\mathrm{Q}}$-distance $(L\pi T)^{\mathcal{N}=4_T}_{\rm max}$. The $z_{\rm c}$ value of this to happen is denoted by $z_{\rm c}^{\rm max}$ and in the particular case of $z_{\rm nh} = z_{\rm h}$ we find that the following condition holds:

$$z_{\rm c}^* = z_{\rm c}^{\rm max}\,. \tag{5.57}$$

This is indicated by the thin vertical line in Fig. 5.4.

The last property is a necessary condition to prove the conjecture. Let us focus now on this particular case (red dotted line) with $\alpha = 0.5$ and $z_{\rm nh} = z_{\rm h} = 1$. Here, it should be obvious that the new maximum of the linearised $\mathrm{Q}\bar{\mathrm{Q}}$-distance is larger than the pure conformal solution; we just have to add the black solid curve and the red dotted one. The slope of the conformal curve (black line) goes to zero close to the maximum whereas the slope of the 1st-order correction (red dotted line) is non-zero in the limit $z_{\rm c} \longrightarrow z_{\rm c}^*$, where $z_{\rm c}^*$ is again the point where the red line crosses zero. Therefore, we can argue that in a small region close to $z_{\rm c}^*$ we find points in the sum of the conformal and 1st-order correction $(L\pi T)^{\rm Lin}$ that are larger than the conformal screening distance (5.55). Thus, for $\alpha = 0.5$ we have a new maximum at $z_{\rm max}^{\rm new} < z_{\rm c}^*$ and for $\alpha = -0.5$ we find a new maximum at $z_{\rm max}^{\rm new} > z_{\rm c}^*$.

Up to now, we have shown that at least for $z_{\rm nh} = z_{\rm h}$ and $\alpha = \pm 0.5$ the screening-distance conjecture is satisfied. We continue with the second step of our proof and choose values for $z_{\rm nh}$ that slightly differ from $z_{\rm h}$. This is also visualised in Fig. 5.4 for $z_{\rm nh} = 0.99$ (blue dashed line) and $z_{\rm nh} = 1.01$ (green dot-dashed line). In this case we encounter the problem that the $z_{\rm c}^*$-value of the zero-crossing is not equal to $z_{\rm c}^{\rm max}$ anymore. If we go for $\alpha = 0.5$ to $z_{\rm nh} < z_{\rm h}$, the increase in the screening distance is obvious. The same happens for $\alpha = -0.5$ and $z_{\rm nh} > z_{\rm h}$. Thus, the number $\delta$ which determines the range of possible new horizons has to be fixed by studying $z_{\rm nh} > z_{\rm h}$ for $\alpha = 0.5$ and $z_{\rm nh} < z_{\rm h}$ for $\alpha = -0.5$.

By focusing on the green, dot-dashed line in Fig. 5.4 and $\alpha = 0.5$ we can argue in this case that the absolute value of the slope of the 1st-order correction at $z_{\rm c}^*$ is much steeper than the corresponding slope of the conformal black curve at $z_{\rm c}^*$. Thus, if the difference of the conformal $\mathrm{Q}\bar{\mathrm{Q}}$-distance value at $z_{\rm c}^*$ and the conformal screening distance $(L\pi T)^{\mathcal{N}=4_T}_{\rm max}$ is not too large, the stronger increase of the 1st-order correction than the decrease of the conformal curve ensures an overall increase in the screening distance of the linearised model. On the other hand, if the difference is too large, we choose a $z_{\rm nh}$ closer to $z_{\rm h}$ which pushes $z_{\rm c}^*$ closer to $z_{\rm c}^{\rm max}$ leading to a smaller slope of the conformal curve whereas this choice of $z_{\rm nh}$ has almost no influence on the slope at $z_{\rm c}^*$ of the 1st-order correction. In an analogous way, an overall increase in the screening distance can be achieved for $\alpha = -0.5$. In summary, we can state that a $\delta$ can be found so that every $z_{\rm nh}$ with $|z_{\rm nh} - z_{\rm h}| < \delta$ leads to $(L\pi T)^{\rm Lin}_{\rm max} \geq (L\pi T)^{\mathcal{N}=4_T}_{\rm max}$ for $\alpha = \pm 0.5$.

An extension to arbitrary values of $\alpha$ is now straightforward by plotting in Fig. 5.5 the 1st-order correction in $\alpha$ against the conformal quark-antiquark distance for fixed $z_{\rm nh} = 1.01$ and various values of the deformation $\alpha$, $\alpha = \pm 0.6$, $\pm 0.5$, $\pm 0.4$, and $\pm 0.3$. The black solid curve represents the conformal curve for $z_{\rm nh} = 1.01$. We find that for fixed value of the new horizon $z_{\rm nh}$ all curves intersect at one particular point $z_{\rm c}^*$ which is independent of $\alpha$. Thus, our discussion about how to choose $z_{\rm nh}$ in order to obtain an increase of the overall screening distance is nearly independent of the chosen $\alpha$. A different value of $\alpha$ leads – according to

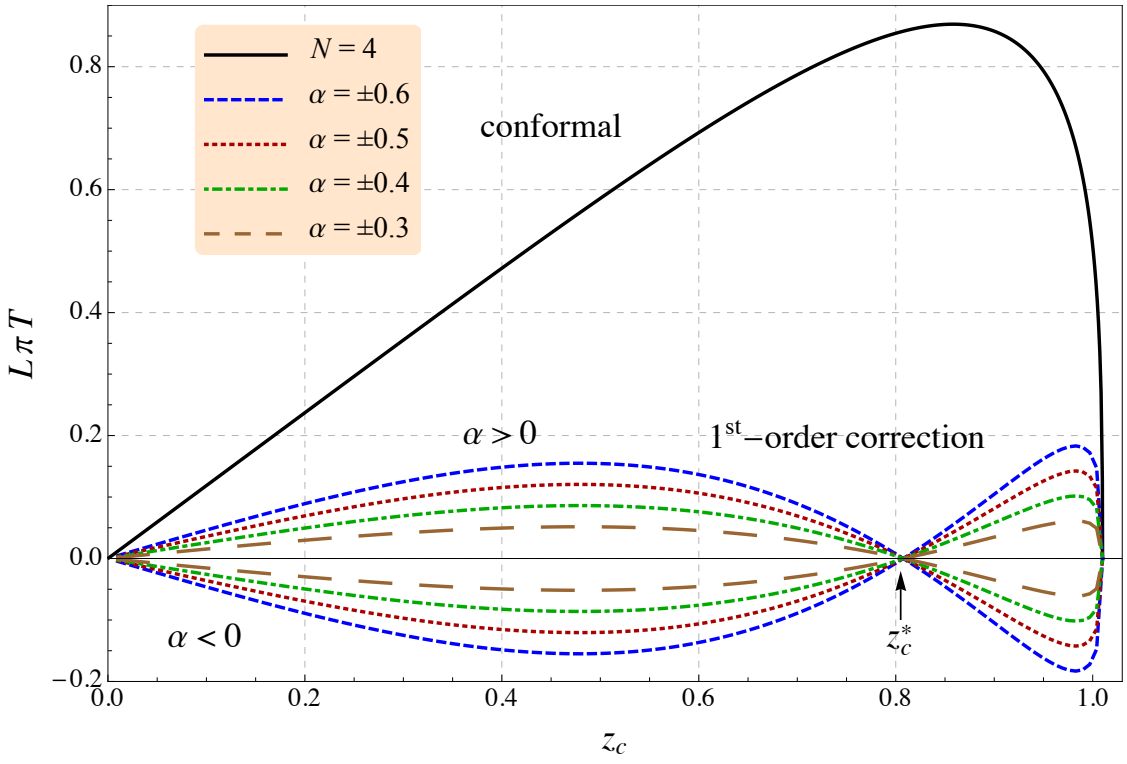


Figure 5.5: 1st-order correction in $\alpha$ against the conformal quark-antiquark distance for fixed $z_{\mathrm{nh}} = 1.01$ and various values of the deformation $\alpha$, $\alpha = \pm 0.6$, $\pm 0.5$, $\pm 0.4$, and $\pm 0.3$. The black solid curve represents the conformal curve for $z_{\mathrm{nh}} = 1.01$.

Fig. 5.5 – to different slopes at $z_{\mathrm{c}}^*$ but all of them being non-zero which is sufficient to find a $\delta$ that satisfies above-mentioned condition.

Finally, this allows us to conclude that we can find for every value of $\alpha$ a small $\delta > 0$ so that $(L\pi T)^{\mathrm{Lin}}_{\mathrm{max}}[\alpha\,, z_{\mathrm{nh}}] \geq (L\pi T)^{\mathcal{N}=4_T}_{\mathrm{max}}$ for every $z_{\mathrm{nh}}$ with $|z_{\mathrm{nh}} - z_{\mathrm{h}}| < \delta$.

Nevertheless, a numerically study for very small values of $\alpha$ is computationally quite intensive since $z_{\mathrm{nh}}$ has to be much smaller and we have to increase the precision of the whole computation dramatically. The results of the previous discussion are shown in Fig. 5.6 and Fig. 5.7. The first one is a 3D plot of the screening distances in the linearised framework for $k = 2$, 3 and 4 together with the conformal bound normalised to 1. The second figure consists of two contour plots of the full linearised screening distance $(L\pi T)^{\mathrm{Lin}}_{\mathrm{max}}$ against the deformation $\alpha$ and the new horizon $z_{\mathrm{nh}}$ for $k = 2$ as well as a sketch of this contour plot that illustrates the discussion from above once more. Fig. 5.6 agrees perfectly with our analytic discussion before. For every $\alpha$ we find a small regime in $z_{\mathrm{nh}}$ in which the screening distance is larger than the conformal value. In addition, the tough numerical computations become visible, especially close to the conformal point $z_{\mathrm{nh}} = z_{\mathrm{h}} = 1$. A last interesting result in this plot is the universality for other values of $k$. The surfaces become steeper for higher values of $k$ but do not change qualitatively as we have mentioned already at the beginning of this discussion.

The last missing part of this analysis is a proper relation between the largest deviating $z_{\mathrm{nh}} = z_{\mathrm{nh}}^{\mathrm{max/min}}$ from $z_{\mathrm{h}}$ and the corresponding $\alpha$. This is now visualised in Fig. 5.7(a) using a contour plot for fixed $k = 2$. It reveals again the numerical problems since not all edges are as smooth as they should. In Fig. 5.7(b) we have included the black $L^{\mathcal{N}=4_T}_{\mathrm{max}}$ contour lines

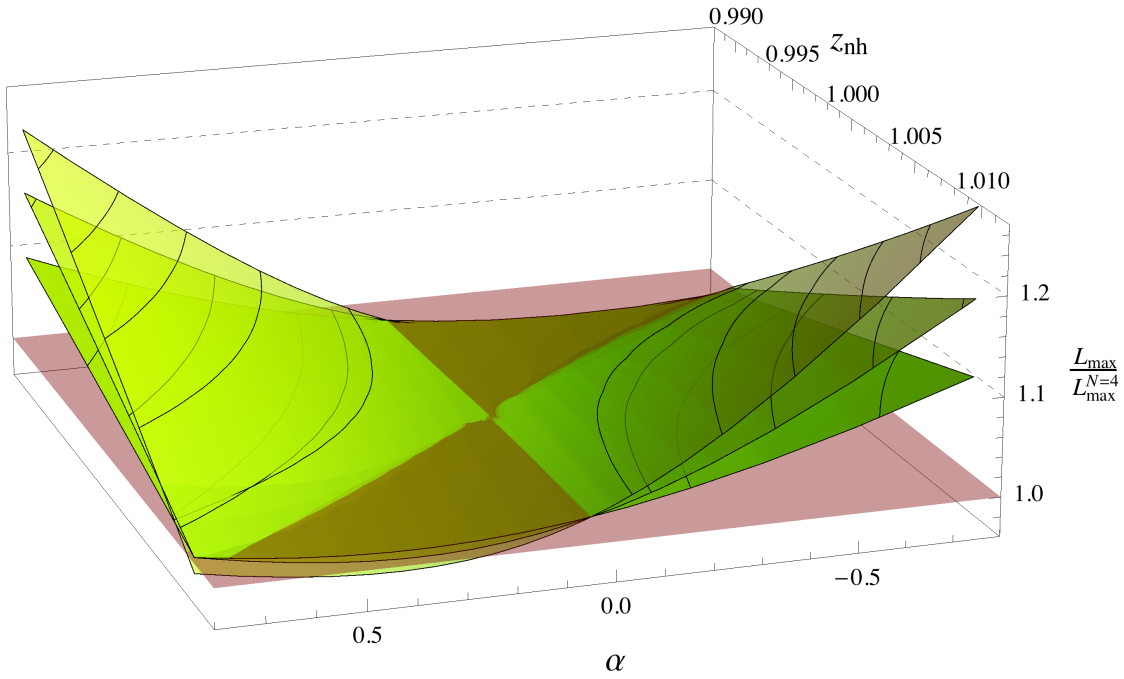


Figure 5.6: Full linearised screening distance $(L\pi T)^{\rm Lin}_{\rm max}$ against the deformation $\alpha$ and the new horizon $z_{\rm nh}$ for three values of $k$, $k = 2$ (lowest surface at negative $\alpha$), 3 and 4 (highest surface at negatie $\alpha$).

which are not accessible in the numerics. It is demonstrated for six choices of $\alpha$ (brown dots) how to choose the maximal regime of $z_{\rm nh}$ with $(L\pi T)^{\rm Lin}_{\rm max} \geq (L\pi T)^{\mathcal{N}=4_T}_{\rm max}$. Two facts are quite remarkable by studying Fig. 5.7(b). Firstly, for $\alpha > 0$ the regime of possible new horizons $z_{\rm nh}$ that still obey the screening-distance conjecture can be extended to arbitrary small values of $z_{\rm nh} > 0$. However, we cannot assume that all of these values are still valid within our approximation. The range of possible $z_{\rm nh}$ is limited by the values larger one since there we find a sharp point where the screening distance falls below the conformal value indication the breakdown of the approximation. We have the analogous effect for negative values of $\alpha$ where the valid range is limited by the positive values of $z_{\rm nh}$. This behaviour has been explained in full detail in the preceding discussion. It was a direct consequence of the slope at $z_{\rm c}^*$ of the $1^{\rm st}$-order correction $(L\pi T)^{\rm Lin}_{1^{\rm st}}$. By changing $z_{\rm nh}$ we move more or less the whole $1^{\rm st}$-order correction of the $\mathrm{Q}\bar{\mathrm{Q}}$-distance along the $z_{\rm c}$-coordinate. If we move in a direction where the conformal maximum $(L\pi T)^{\mathcal{N}=4_T}_{\rm max}$ is at the same $z_{\rm c}$-value as a positive contribution of the $1^{\rm st}$-order correction, we have an immediate increase of the screening distance.

Secondly, at the beginning of Sec. 5.3.2 we expected the valid regime of the new horizons to be linear in $\alpha$. However, we could not find a concrete relation analytically since we only know how $z_{\rm nh}$ behaves for vanishing $\alpha$ (see (5.46)). By using our numerical study we can now use the maximal (minimal) value of the new horizon $z_{\rm nh}^{\rm max/min}$ for positive (negative) $\alpha$ in order to find a relation between these two quantities. Fig. 5.7(b) already suggests a linear relation which we want to specify in the following.

By extracting the maximal (minimal) values of $z_{\rm nh}^{\rm max/min}$ that still satisfies the screening-distance conjecture numerically for several values of $\alpha$ and fixed $k = 2$ and $z_{\rm h} = 1$, we can use

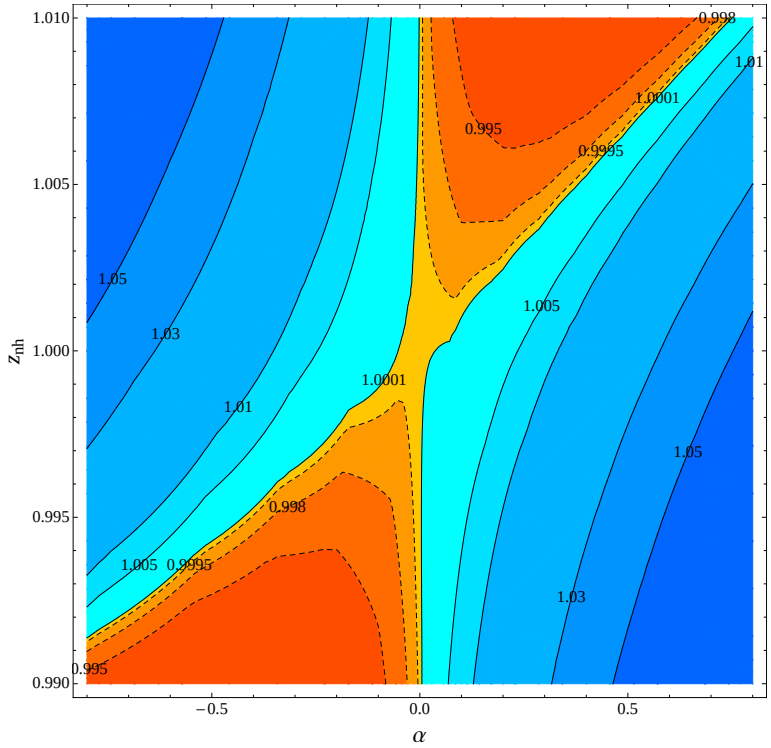


(a) Contour plot of the full linearised screening distance $(L\pi T)^{\mathrm{Lin}}_{\mathrm{max}}$ against the deformation $\alpha$ and the new horizon $z_{\mathrm{nh}}$ for $k = 2$.

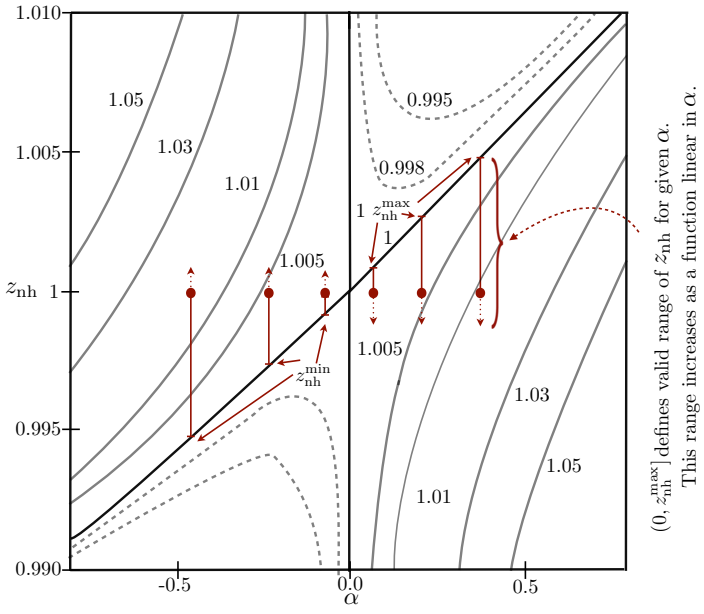


(b) Contour plot sketch of the full linearised screening distance $(L\pi T)^{\mathrm{Lin}}_{\mathrm{max}}$ against the deformation $\alpha$ and the new horizon $z_{\mathrm{nh}}$ for $k = 2$. The ranges shown along the $z_{\mathrm{nh}}$-axis obey the screening-distance conjecture for the corresponding value of $\alpha$.

Figure 5.7: Visualisation of the analytic discussion with the help of two contour plots.

a fitting routine to compute the functional relation $z_{\mathrm{nh}}^{\mathrm{max/min}}(\alpha)$. The result can be written as

$$z_{\mathrm{nh}}^{\mathrm{max/min}}(\pm\alpha,\, z_{\mathrm{h}},\, k) = z_{\mathrm{h}}\left(1 \pm \mathrm{const}\cdot|\alpha|\cdot z_{\mathrm{h}}^{k}\right) \quad \text{with} \quad \mathrm{const} \approx 0.0123 \quad \text{for} \quad k = 2\,. \tag{5.58}$$

For different values of $k$ similar linear relations between $\alpha$ and $z_{\mathrm{nh}}^{\mathrm{max/min}}$ can be found. This completes the proof of the screening-distance conjecture for small perturbations around the conformal solution in Einstein frame.

In the next section we will extend our discussion to the string frame case since the screening-distance conjecture holds numerically in this regime as well. This has been verified in [75, 76].

### 5.4.2 String-Frame Computation

Most of the computations in the string frame are analogous to the preceding calculations. After implementing the changes due to the dilaton in the perturbed metric functions we derive the linearised $\mathrm{Q\bar{Q}}$-distance function at first order in $\alpha$ and introduce a new parameter $\phi$ characterising the dilaton profile. The integrals can be calculated analytically and are presented along with some plots in full detail at the end of this section. Furthermore, we will show that the parameter describing the dilaton is not independent of $\alpha$ and that we can find a relation between these two quantities similar to the Einstein-frame case.

In the full solution we have implemented a dilaton of the form

$$\Phi = \sqrt{\frac{3}{2}}\,\phi\, z^2\,, \tag{5.59}$$

with $\phi$ being the same parameter we have encountered in all the previous chapters. This definition of the dilaton will be used in the following as well. The freedom to choose the dilaton arbitrarily becomes clear by recalling the linearised scalar equation (5.26). The differential equation has two unknown functions ($\Phi$ and $V$). Before we proceed with the discussion of the screening length in the string frame we have to show that the dilaton potential does not lead to tachyonic instabilities. Thus, we have to compute the mass which has to satisfy the Breitenlohner–Freedman bound given in (3.42). By substituting the conformal metric $G^{0}_{\alpha\beta}$ into the linearised scalar equation (5.26) we end up with the following differential equation

$$-\frac{2\sqrt{6}\, z^2\left(z^4 + z_{\mathrm{h}}^4\right)\phi}{L^2\, z_{\mathrm{h}}^4} = -\frac{4\Phi\left(\Phi^2 + \Phi_{\mathrm{h}}^2\right)}{L^2\,\Phi_{\mathrm{h}}^2} = \frac{\partial V}{\partial \Phi}\,. \tag{5.60}$$

The dilaton potential $V(\Phi)$ is then given by

$$V(\Phi) = -\frac{2\Phi^2}{L^2} - \frac{\Phi^4}{L^2\,\Phi_{\mathrm{h}}^2}\,. \tag{5.61}$$

Since we have separated the cosmological constant $\Lambda$ from the dilaton potential the first contribution in (5.61) is a $\Phi^2$ term. The mass $M_{\Phi}^2$ is equal to $-\frac{4}{L^2}$ and satisfies the Breitenlohner–Freedman bound.

According to our discussion in Sec. 4.2 a dilaton quadratic in the $5^{\mathrm{th}}$-dimension has some neat features when computing Regge trajectories [60]. Implementing the string frame is then

very easy since we just have to transform the Einstein frame metric via

$$\begin{aligned} G^{\mathrm{s}}_{\alpha\beta} &\equiv G^{\mathrm{E}}_{\alpha\beta}\, \mathrm{e}^{\sqrt{\frac{2}{3}}\,\Phi(z)} \\ \Longrightarrow \quad G^{\mathrm{s,Lin}}_{\alpha\beta} &= G^{\mathrm{E,Lin}}_{\alpha\beta}\left(1+\phi\, z^2\right). \end{aligned} \tag{5.62}$$

Thus, we have to multiply our solutions for $A$ and $B$ in (5.45) just by $(1+\phi\, z^2)$ and we end up with the metric functions in the string frame

$$\begin{aligned} A_{\mathrm{dil}}(z,\, \alpha,\, \phi,\, k) &= \frac{1}{z^2}\left(1+\alpha\, z^k\right)\cdot\left(1+\phi\, z^2\right), \\ B_{\mathrm{dil}}(z,\, \alpha,\, \phi,\, k) &= \frac{1}{z^2}\left(1-\alpha\, k\, z^k\right)\cdot\left(1+\phi\, z^2\right). \end{aligned} \tag{5.63}$$

It is worth mentioning that the parameter $\phi$ exhibits an analogous asymptotic behaviour as the new horizon $z_{\mathrm{nh}}$ meaning that it has to vanish for $\alpha \longrightarrow 0$. The vanishing of the parameter $\phi$ is equivalent to the vanishing of the whole scalar $\Phi$ which is necessary in the $\alpha \to 0$ limit since we have to recover the pure Einstein–Hilbert action $S_{\mathrm{EH}}$ where no scalar is included. Thus, we have to prove that we find for small $\alpha$ – with 'small' we mean $\alpha\, z_{\mathrm{h}}^k \ll 1$ – a $\phi$-neighbourhood around 0 such that every maximum of the QQ̄-distance is larger than the conformal value $(L\,\pi T)^{\mathcal{N}=4_T}_{\mathrm{max}}$. It is important to notice that the horizon function $h(z)$ as well as the temperature $T$ are identical to the Einstein frame case.

With these assumptions we can start with the expansion of the integral of the full quark-antiquark distance in (4.38) in the string frame for small values of $\alpha$ and $\phi$. This can be written as

$$(L\pi T)^{\mathrm{Lin}}_{\mathrm{dil}} = (L\pi T)_{\mathcal{N}=4} + \alpha \int_0^{z_{\mathrm{c}}} \mathrm{d}z\, \mathcal{I} + \phi \int_0^{z_{\mathrm{c}}} \mathrm{d}z\, \mathcal{J} + \mathcal{O}\big(\alpha\,\phi,\, \alpha^2,\, \phi^2\big), \tag{5.64}$$

with $\mathcal{I}$ being identical to (5.50) and $\mathcal{J}$ given by

$$\mathcal{J} = -\frac{2 z_{\mathrm{c}}^4\, z^2\, \sqrt{z^4 - z_{\mathrm{nh}}^4}\sqrt{z_{\mathrm{c}}^4 - z_{\mathrm{nh}}^4}}{\left(z^2+z_{\mathrm{c}}^2\right)^{3/2} z_{\mathrm{nh}}^5\, \sqrt{z_{\mathrm{c}}^2 - z^2}}. \tag{5.65}$$

Since $\alpha$ and $\phi$ are small, contributions of order $\alpha\,\phi$ are of second order and can be neglected in the expansion in (5.64). It is noteworthy that our result is the same as the linearised expression in Einstein frame plus a small contribution from the $\mathcal{J}$-term in (5.64). By use of the following two substitutions

$$\begin{aligned} &1.: \quad y \equiv \frac{z_{\mathrm{nh}}}{z}, \quad \text{and} \quad y_{\mathrm{c}} \equiv \frac{z_{\mathrm{nh}}}{z_{\mathrm{c}}}, \\ &2.: \quad u \equiv \frac{y^2}{y_{\mathrm{c}}^2}, \end{aligned} \tag{5.66}$$

MATHEMATICA® can solve the $\mathcal{J}$-integral in (5.64) leading to

$$\begin{aligned}\phi \int_0^{z_c} \mathrm{d}z\, \mathcal{J} = -\phi\, \frac{z_c^7 \sqrt{z_{nh}^4 - z_c^4}}{3\sqrt{2\pi}\, z_{nh}^7} \sqrt{\frac{z_{nh}^4}{z_c^4} - 1} \Bigg[ \frac{3 z_n^4}{z_c^4} \Bigg( 12\, \Gamma\Big(\frac{5}{4}\Big)^2\, {}_2F_1\Big(-\frac{3}{4}, \frac{1}{2}, -\frac{1}{4}, \frac{z_c^4}{z_{nh}^4}\Big) \\ + \Gamma\Big(\frac{3}{4}\Big)^2\, {}_2F_1\Big(-\frac{1}{4}, \frac{1}{2}, \frac{1}{4}, \frac{z_c^4}{z_{nh}^4}\Big)\Bigg) - 12\Big(3 + \frac{4 z_{nh}^4}{z_c^4}\Big)\, \Gamma\Big(\frac{5}{4}\Big)^2\, {}_2F_1\Big(\frac{1}{4}, \frac{1}{2}, \frac{3}{4}, \frac{z_c^4}{z_{nh}^4}\Big) \\ + \Gamma\Big(-\frac{1}{4}\Big)\, \Gamma\Big(\frac{7}{4}\Big)\, {}_2F_1\Big(-\frac{1}{2}, \frac{3}{4}, \frac{5}{4}, \frac{z_c^4}{z_{nh}^4}\Big)\Bigg], \end{aligned} \tag{5.67}$$

where we resubstituted our old coordinates. The 1st-order correction in $\phi$ given by (5.67) is shown in Fig. 5.8 for four values of the new horizon $z_{nh}$, $z_{nh} = 0.8$, 1, 1.3 and 1.5. It is an

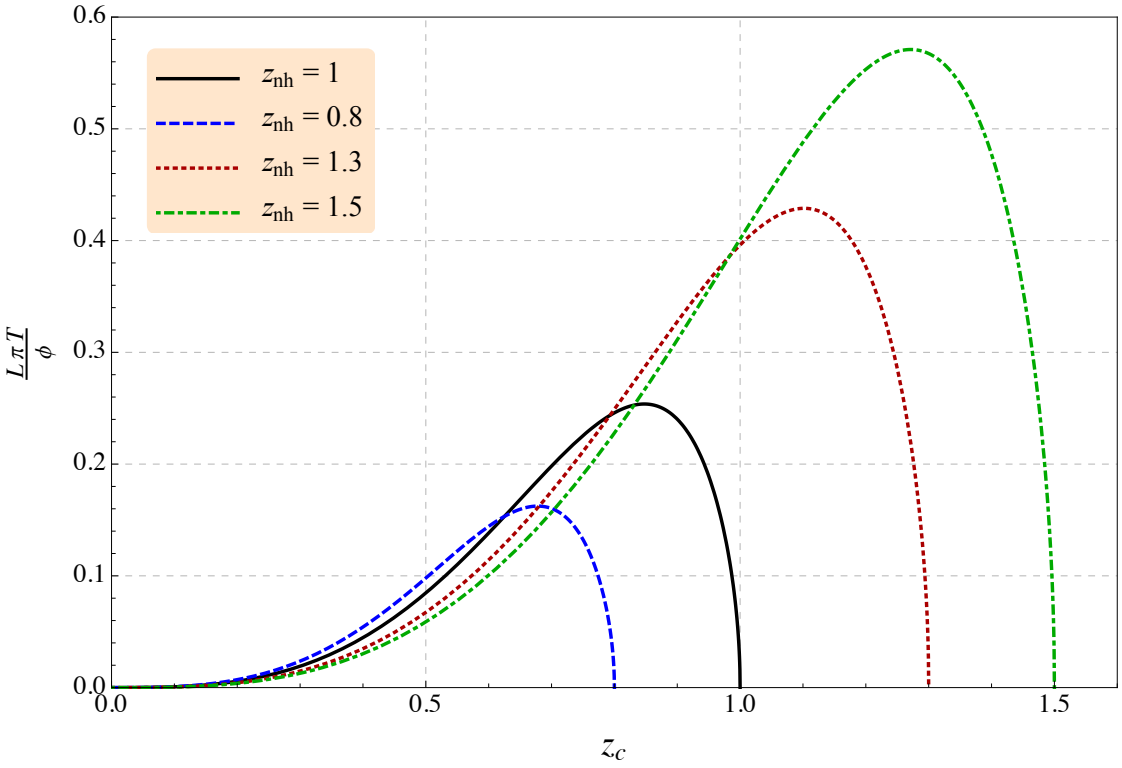


Figure 5.8: 1st-order correction term in $\phi$ against $z_c$ for four values of the new horizon $z_{nh}$, $z_{nh} = 0.8$, 1, 1.3 and 1.5. The function does not depend on $z_h$ and $k$. The endpoints are precisely the location of the new black-hole horizon $z_{nh}$.

interesting result that the dilaton contribution has no change in the sign when varying $z_{nh}$. Thus the overall sign of $\phi$ matters and we have to divide the analysis into two parts:

1. For all sufficiently small values of $\alpha$ that satisfy the linearisation we have to find a $\delta > 0$ and a $\phi > 0$ so that $(L\pi T)^{\text{Lin}}_{\text{dil,max}}[\alpha\,\phi,\, z_{nh}] \geq (L\pi T)^{\mathcal{N}=4_T}_{\text{max}}$ for every $z_{nh}$ with $|z_{nh} - z_h| < \delta$.

2. The same has to be proven for negative values of $\phi$.

It is important to recall once more that $\phi$ is not independent of $\alpha$ since the scalar has to vanish in the limit $\alpha \to 0$ as mentioned above. At the end of this discussion we try to derive a relation between $\phi$ and $\alpha$ analogous to the Einstein-frame case.

The proof is trivial for $\phi > 0$ as indicated in Fig. 5.8 since every choice of $\phi$ leads to a positive contribution to the screening distance irrespective of the chosen value for $\alpha$, $z_{\mathrm{nh}}$ and $k$. We have to focus, therefore, exclusively on the $\phi < 0$ case of the full, linearised screening distance $(L\pi T)^{\mathrm{Lin}}_{\mathrm{dil,max}}$ in the string frame.

Our argumentation is now as follows. For a given choice of $\alpha$ we use the Einstein-frame discussion in order to find an appropriate value for $\delta$ that satisfies the screening-distance conjecture and focus then on the $\phi$-contribution which leads to a smaller value of $\delta$. This is a reasonable way to proceed since the string frame computation just adds a particular $\phi$-dependant contribution to the well-known Einstein-frame expression (5.49) of the $\mathrm{Q\bar{Q}}$-distance. In addition to this we do not have to focus on the other parameters $z_{\mathrm{h}}$ and $k$ due to the fact that the $\mathcal{J}$-integral (5.67) is independent of $z_{\mathrm{h}}$ and $k$. For a given choice of $\alpha$ and $\delta$ in the Einstein-frame case we can now find a $\phi < 0$ with $|\phi|$ being small enough that the negative contribution due to the $\mathcal{J}$-integral is smaller than the prior increase of the screening distance $(L\pi T)^{\mathrm{Lin}}_{\mathrm{max}}$ given by the $\mathcal{I}$-integral in (5.49) by virtue of the appropriate choice of $\delta$. That such a sufficiently small value of $|\phi|$ has to exist is ensured by the vanishing of the whole $\mathcal{J}$-integral in the limit of vanishing $\phi$.

In summary, we can state that for every $\alpha$ that satisfies the linearisation and every $k$ a $\delta > 0$ and $\phi < 0$ can be found so that $(L\pi T)^{\mathrm{Lin}}_{\mathrm{dil,max}}[\alpha\,\phi,\, z_{\mathrm{nh}}] \geq (L\pi T)^{\mathcal{N}=4_T}_{\mathrm{max}}$ for every $z_{\mathrm{nh}}$ with $|z_{\mathrm{nh}} - z_{\mathrm{h}}| < \delta$. This is visualised in Fig. 5.9(a) where a 3D plot of the screening distance $(L\pi T)^{\mathrm{Lin}}_{\mathrm{dil,max}}$ in the linearised string frame against the main deformation parameter $\alpha$ and the dilaton parameter $\phi$ for several values of $k$, $k = 2$, 3 and 4, for fixed $z_{\mathrm{nh}} = z_{\mathrm{h}} = 1$ is shown. There we have normalised all values to the conformal screening distance $(L\pi T)^{\mathcal{N}=4_T}_{\mathrm{max}}$. In Fig. 5.9(b) the data for $k = 2$ is shown in a contour plot. In analogy to the Einstein-frame case we can argue that different values of $k$ do not change the results qualitatively.

One last task of this section is to find the explicit relation between $\alpha$ and the absolute value of the smallest possible dilaton measured by $|\phi_{\mathrm{min}}|$ that still obeys the conjecture. We focus entirely on $\phi < 0$ since the other case is trivial. For every $\alpha$ such a value has to exist due to the fact that the string frame computation is just the Einstein frame computation of Sec. 5.4.1 including an additional $\phi$-dependent contribution. The exact coefficients of this relation may vary since the $\delta$ is not unique for a given choice of $\alpha$, $z_{\mathrm{h}}$ and $k$. We can always go to smaller $\delta$ which results in a smaller value for the smallest possible dilaton $|\phi_{\mathrm{min}}|$. For a fixed choice of parameters $z_{\mathrm{h}} = z_{\mathrm{nh}} = 1$ and $k = 2$ we extract the relation between $\alpha$ and the smallest possible dilaton $|\phi_{\mathrm{min}}|$ from the data in Fig. 5.9(a). The figure already suggests an $\alpha^2$-dependence which can be stated precisely in the following form:

$$|\phi_{\mathrm{min}}(\alpha,\, z_{\mathrm{h}},\, k)| = \mathcal{C}(k) \cdot \alpha^2 \cdot z_{\mathrm{h}}^{2k-2}\,, \quad \text{with} \quad \mathcal{C}(2) \approx 0.322\,, \tag{5.68}$$

that nicely reproduces the data. $\mathcal{C}(k)$ is a constant for each choice of $k$. An $\alpha^2$-relation is a priori not a bad sign. Our linearisation in $\alpha$ only concerns the quark-antiquark distance integrals. The screening distance $(L\pi T)_{\mathrm{max}}$ is a totally different quantity and it is obvious in all of the 3D plots (Fig. 5.6 and Fig. 5.9(a)) that the relation between $(L\pi T)_{\mathrm{max}}$ and $\alpha$ is at least quadratic. This is indeed a necessary condition for the conjecture to be valid.

Let us summarise what we have achieved in this chapter. We have started with an explicit, analytic check of the small-perturbation regime of the inconsistent $\mathrm{SW}_T$-model where we argued that the screening-distance conjecture ($(L\pi T)^{\mathrm{Def}}_{\mathrm{max}} > (L\pi T)^{\mathcal{N}=4_T}_{\mathrm{max}}$) cannot be fulfilled for

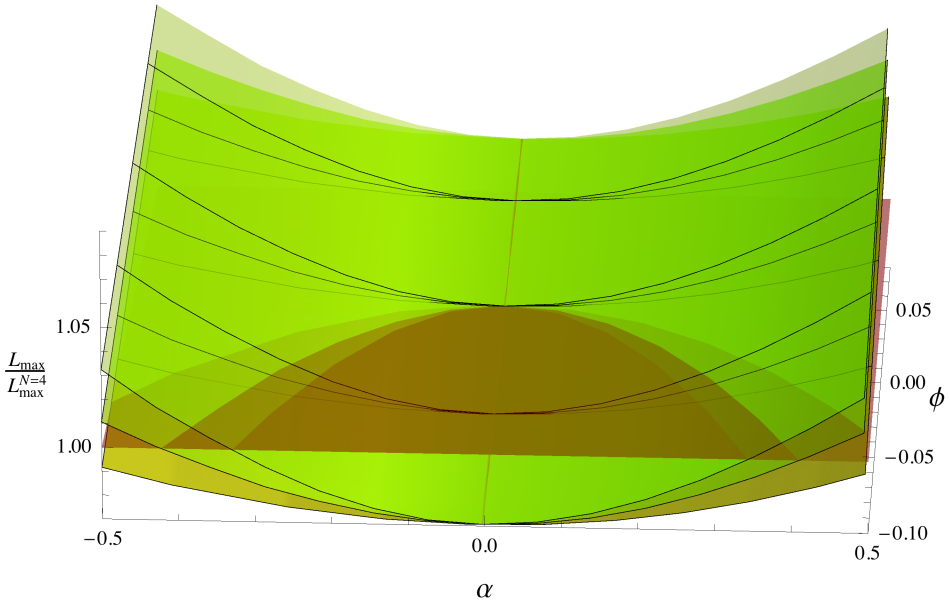


(a) 3D plot of the screening distance $(L\pi T)^{\text{Lin}}_{\text{dil,max}}$ in the linearised string frame against the main deformation parameter $\alpha$ and the dilaton parameter $\phi$ for several values of $k$, $k = 2$, 3 and 4 for fixed $z_{\text{nh}} = z_{\text{h}} = 1$.

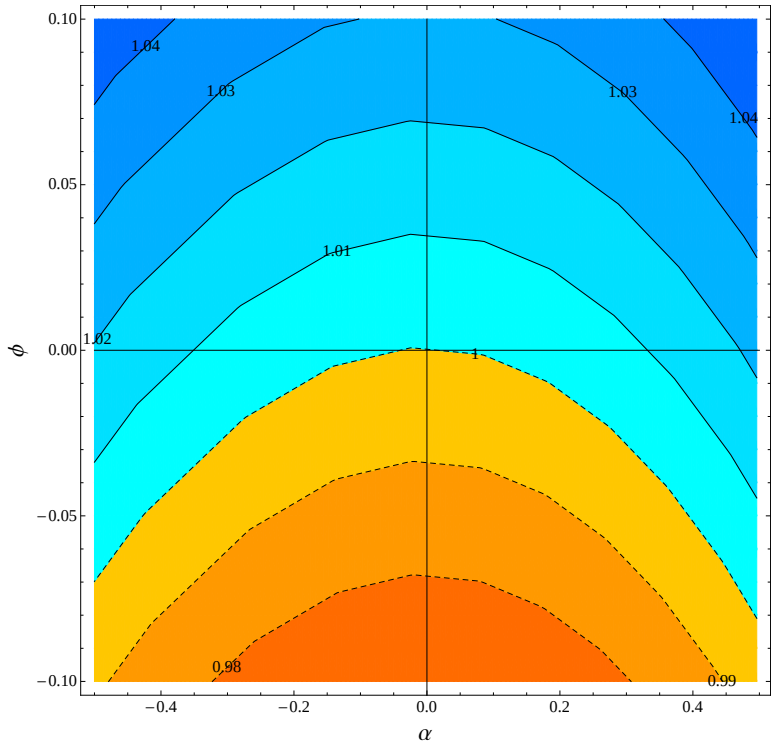


(b) Contour plot of the full linearised screening distance $(L\pi T)^{\text{Lin}}_{\text{dil,max}}$ in string frame against the deformation $\alpha$ and the dilaton parameter $\phi$ for $k = 2$.

Figure 5.9: Visualisation of the linearised screening distance in string frame.

negative values of the deformation. After that, we have investigated small perturbations around the conformal $\mathcal{N} = 4_T$ solution including a non-trivial dilaton with the help of a consistent approach based on the linearisation of Einstein equations derived from a 5D Einstein–Hilbert-scalar action $S_{\mathrm{EHs}}$. Our main goal – the proof of the screening-distance conjecture – has been achieved for a large class of solutions in Einstein and string frame. Some subtleties have been worked out, e. g. the regime of validity of our linearised Einstein equations, measured by the parameter $\alpha$. This choice of $\alpha$ has large influence on the other parameters $z_{\mathrm{nh}}$ and $\phi$.

There are many other possibilities how to extend our well-defined setting, e. g. by implementing higher dimensional branes or including gauge fields in the 5D Einstein–Hilbert action. In these scenarios it is, a priori, not clear whether the screening distance is higher than the conformal value. Furthermore, a rigorous proof to all orders in the deformation is still not possible in the case of our models. Nevertheless, the current state of the screening-distance conjecture can be used for physical interpretations. We have argued – by looking at Fig. 4.15 – that the length scale of the melting of a quark-antiquark pair in QCD from lattice computations is comparable to the length scale we obtain in our computations and that, even better, the conformal screening distance $(L\pi T)^{\mathcal{N}=4_T}_{\mathrm{max}}$ in $\mathcal{N} = 4_T$ is lower. This statement nicely agrees with the above-mentioned conjecture.

In the last main chapter – before summarising what has been achieved – we focus on another observable related to the drag force. By analysing rotating quarks we want to study the energy loss of accelerated partons in a strongly coupled plasma. We will extend the computation from the well-known conformal case to deformed metric models where we analyse the $\mathrm{SW}_T$-, 1- and 2-parameter models as possible examples.

Chapter 6

# Rotating Quarks

In Chapter 4 we focused on the behaviour of the energy loss of a quark moving through a non-abelian plasma and on the running coupling $\alpha_{Q\bar{Q}}$ in non-conformal metric models. We found a universal increase of the coupling when a deformation is introduced and a robust behaviour of the energy loss over a large parameter range.

However, a direct comparison to experiments at the LHC is still very difficult. The most important problems that are related to our current work are listed in the following:

1. It is often very complicated for experimental physicists to extract the appropriate observable (e. g. the energy loss) out of the data. Thus, a comparison to our computation of the energy loss of a fast moving, heavy parton is a challenging task.

2. In the gravity dual, a computation of a heavy parton moving through a strongly coupled plasma has been accomplished at fixed velocity and it was shown that the energy loss occurs via drag. However, an analysis of the energy loss would be more reliable if there were no external force keeping the parton at constant velocity since deceleration leads to larger gluon-bremsstrahlung, especially at high velocities. This important radiative contribution is not included in the drag force computation.

In the following discussion we would like to analyse a non-trivial angular acceleration/deceleration $a$ by forcing the quark at the boundary to move on a circle. This is visualised in Fig. 6.1. According to Fadafan *& al.* [190], two energy regimes can be distinguished:

As already indicated in Sec. 4.2 the dominant contribution to the energy loss of a relativistic particle at high energies is gluon bremsstrahlung (synchrotron radiation and QCD-bremsstrahlung) which can be tackled by using perturbative QCD techniques [179, 210–214]. In addition to this, we have interactions of the particle with the coloured, finite temperature medium. These interactions should involve small momentum transfers, of order of the temperature, that have to be described non-perturbatively since the coupling constant is large.

In the limit of lower energies we have already mentioned in Sec. 4.2 that for example collisional energy loss due to drag via elastic interactions is important. By analysing a rotating quark which circulates at the boundary with a certain radius $R_0$ and angular velocity $\omega$, we can smoothly explore the regime of slowly moving quarks – where drag is dominant – and a regime of highly rotating quarks where deceleration-induced radiative energy loss (synchrotron

radiation and gluon bremsstrahlung) should be favoured. In addition to this, the intermediate regime is accessible where interferences between energy loss via drag and radiation-induced energy loss occur.

The guiding task that leads us through this analysis is the behaviour (robustness, universality) of the energy loss of a rotating quark in these different regimes when a deformation of the metric is involved. This discussion will be similar to the trailing string analysis in Sec. 4.2 although the string configuration in the bulk is now slightly different (see Fig. 6.1). Therefore,

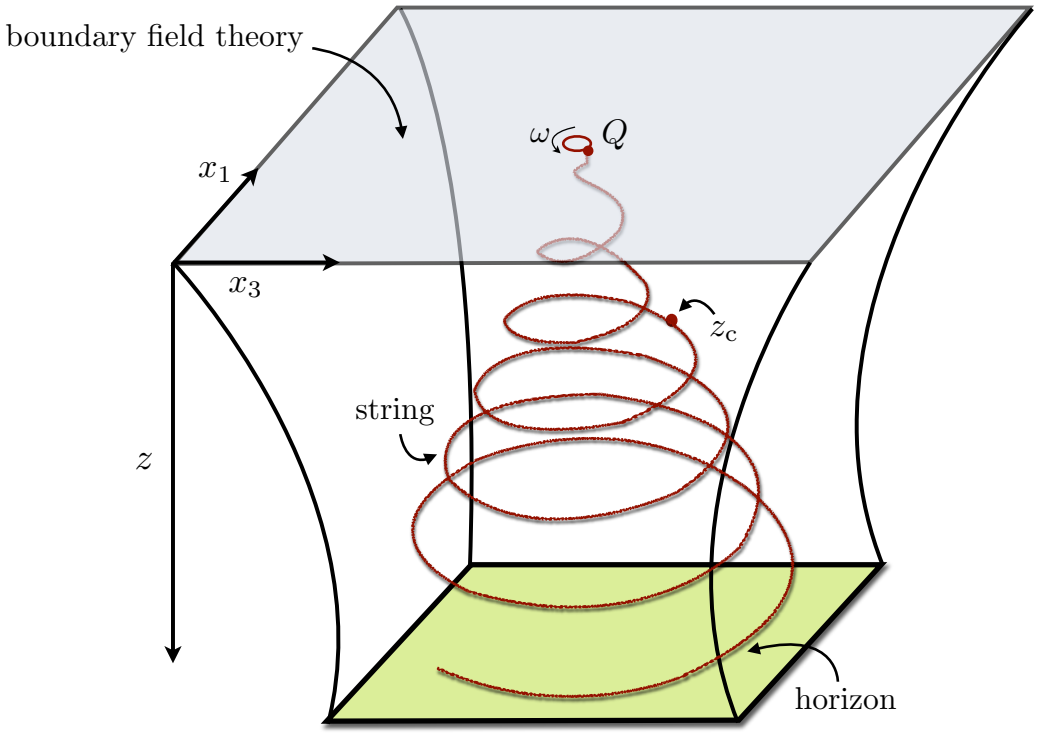


Figure 6.1: Schematic picture of a rotating quark moving at constant angular velocity $\omega$ through a hot plasma including the dual gravity scenario of a string forming spirals in the bulk. $z_c$ denotes again the point where the string exceeds the local speed of light in the bulk.

we begin with the a review of the computation of the string configuration of a rotating quark in the well-known and analytically tractable regime of $\mathcal{N} = 4$ at zero temperature (Sec. 6.1) [215] and proceed with finite temperature in Sec. 6.2 [190]. Then this observable will be analysed in non-conformal models in Sec. 6.3. A discussion of non-conformal theories has not been worked out before in the context of rotating quarks. The knowledge of the string configuration is the main ingredient in order to study the energy loss in all the aforementioned models in Sec. 6.4 leading to the identification of two regimes, one in which energy loss due to linear drag (Sec. 6.4.1) is dominant and a second one where energy loss can be explained in terms of vacuum radiation (see Sec. 6.4.2). This has been studied for the conformal case in [190].

## 6.1 Conformal $AdS_5$ Metric

In the next two sections we review the $\mathcal{N} = 4$ computation at zero and finite temperature of a rotating quark [215]. Thus, the well-known $AdS_5$ and $AdS_5$ black-hole metric in the $z$-parameterisation will be used which are given by

$$\mathrm{d}s^2 = \frac{L^2}{z^2}\left(-h(z)\,\mathrm{d}t^2 + \mathrm{d}\vec{x}^{\,2} + \frac{\mathrm{d}z^2}{h(z)}\right), \tag{6.1}$$

with

$$\begin{aligned} \mathcal{N} = 4\text{:} \quad & h(z) = 1\,, \\ \mathcal{N} = 4_T\text{:} \quad & h(z) = 1 - \frac{z^4}{z_\mathrm{h}^4}\,. \end{aligned} \tag{6.2}$$

We start with the zero-temperature computation first. It can be solved analytically (see [215]) and consists of a straightforward computation which will be helpful in order to understand the more complicated, non-conformal analysis. Since there is no plasma on the field theory side, we expect to find pure vacuum radiation.

We place a rotating quark with radius $R_0$ and angular velocity $\omega$ at the three-dimensional boundary and compute the classical configuration of a string hanging into the bulk (see Fig. 6.1) that obeys the boundary conditions specified in the gauge theory at $z = 0$. The metric perturbations that this string creates are small in the large-$N_\mathrm{c}$ limit so that we can neglect their backreaction on the shape of the string itself. Thus, we start with deriving the shape of the rotating string in pure $AdS_5$, in the absence of any metric perturbations. The Nambu–Goto action of the string, which we have to extremise, reads

$$S_\mathrm{NG} = \frac{\sqrt{\lambda}}{2\pi L^2}\int \mathrm{d}\tau\,\mathrm{d}\sigma\sqrt{-\det g_{ab}}\,. \tag{6.3}$$

which is the same formula as in the previous chapters. Before we can write down the induced metric, we have to fix the parameterisation of the system. The string embedding functions are given by

$$X^\alpha(t,z) = \big(t, \vec{r}_s(t,z), z\big)\,, \tag{6.4}$$

where the three-vector $\vec{r}_s$ is given in spherical coordinates $(r,\theta,\varphi)$:

$$\vec{r}_s(t,z) \equiv \left(R(z), \frac{\pi}{2}, \varphi = \phi(z) + \omega t\right). \tag{6.5}$$

Here, the rotating character of our configuration becomes apparent. $\phi(z)$ denotes the $z$-dependent angular function and should not be confused with the scalar parameter of the dilaton $\phi$. This approach has the property that the angular velocity $\omega$ is constant for all values of $z$. It is not clear whether other ansätze – including a $z$-depending angular-velocity function $\omega(z)$ – lead to valid string configurations of a moving quark at the boundary. In any case, computations are much more involved.

The special dependence on $z$, $t$ and $\omega$ shown in (6.4) is everything we have to put into this computation at this stage. In the later part we just have to specify the radius of the circle on which the quark is moving at the boundary. The further computation of the induced metric is

now similar to the previous cases in Sec. 4.2 and Sec. 4.3.1 and leads to a Lagrangian of the following form:

$$\mathcal{L}_{\mathcal{N}=4} = \sqrt{-\det g_{ab}} = \frac{L^2}{z^2}\sqrt{\left(1-\omega^2 R(z)^2\right)\left(1+R'(z)^2\right)+R(z)^2\phi'(z)^2}\,. \tag{6.6}$$

Here, L is again the $AdS$ length. Due to the fact that we have to deal with two unknown functions $\phi(z)$ and $R(z)$ in (6.6) we compute equations of motion for $\phi(z)$ and $R(z)$ by extremising the Nambu–Goto action (6.3). Following Athanasiou *& al.* in [215] we obtain a constant of motion $\Pi$ by noting that (6.6) is independent of $\phi(z)$:

$$\Pi \equiv -\frac{\partial\mathcal{L}}{\partial\phi'}\,, \tag{6.7}$$

where $'$ means $\frac{\partial}{\partial z}$. The minus sign in front of (6.7) is needed to have positive momenta for positive angular velocities $\omega$ leading to a more physical configuration. This means that the string always trails behind the quark.

In total, two parameters have to be adjusted: the radius $R_0$ of the rotating quark and its angular velocity $\omega$ which can be related to the quantity $\Pi$. Equation (6.7) can be solved for $\phi'(z)$ giving

$$\phi'(z) = \frac{z^2\Pi\sqrt{1-\omega^2R(z)^2}\,\sqrt{1+R'(z)^2}}{R(z)\sqrt{R(z)^2-z^4\Pi^2}}\,, \tag{6.8}$$

which will be used to eliminate the $\phi(z)$-dependence in the final differential equation for $R(z)$. The Euler–Lagrange equation for $R(z)$ reads

$$\frac{\partial\mathcal{L}}{\partial R} - \frac{\partial}{\partial z}\frac{\partial\mathcal{L}}{\partial R'} = 0\,, \tag{6.9}$$

and can be transformed by using (6.8) into the following form

$$\begin{aligned} &R'' + \frac{\left(z^5\Pi^2 - z\omega^2R^4 + 2R^3R' - 2\omega^2R^5R'\right)\left(1+R'^2\right)}{z\left(1-\omega^2R^2\right)\left(z^4\Pi^2R - R^3\right)} = 0 \\ \iff\quad &R'' + \frac{R\left(z+2RR'\right)\left(1+R'^2\right)}{z\left(z^4\Pi^2-R^2\right)} + \frac{1+R'^2}{R\left(1-\omega^2R^2\right)} = 0\,. \end{aligned} \tag{6.10}$$

From the first to the second line we have used a partial fraction decomposition to separate the two diverging parts of the second order differential equation. One expects that (6.10) requires two initial conditions to specify a unique solution. As shown in a numerical study of a rotating quark in $\mathcal{N}=4$ at non-zero temperature by [190], which we will briefly discuss in section 6.2, this kind of differential equations are fully determined by only one external, initial condition. The other one can be fixed by studying the differential equation itself. This can be understood in the following way. Firstly, we note that (6.10) is singular when $1-\omega^2R(z)^2=0$ or when $R(z)^2-z^4\Pi^2=0$. In analogy to the case of the drag force we would like to maintain reality of (6.8) and thus both divergent parts have to vanish at the same value of $z$, $z\equiv z_\mathrm{c}$. This gives us a condition for the special values $z_\mathrm{c}$ and $R(z_\mathrm{c})$:

$$z_\mathrm{c} \equiv \frac{1}{\sqrt{\Pi\omega}}\,, \quad R(z_\mathrm{c}) = R_\mathrm{c} \equiv \frac{1}{\omega}\,. \tag{6.11}$$

$z_c$ has many interesting properties one of them being that it is the point where the second, intrinsic, initial condition can be extracted from. Furthermore, as the notation already indicates, it is again the point where the velocity of the string exceeds the local speed of light[1]. For the current computation we still need in principle a second initial condition for $R'(z_c)$ in order to determine the shape of the rotating string in the bulk. This condition will be extracted from (6.10) in the following. We solve (6.10) in the vicinity of $z = z_c$ by using an expansion of $R(z)$ given by

$$R(z) \equiv R_c + R'_c\,(z - z_c) + \frac{1}{2}R''_c(z - z_c)^2 + \mathcal{O}\big((z - z_c)^2\big) \tag{6.12}$$

In (6.12) we can substitute what we know about $R_c$ in (6.11). Since the second and third terms of (6.10) are divergent at $z = z_c$ whereas $R''$ is finite, we can collect powers of $z - z_c$ and observe that they do not involve any factors of $R''_c$ but lead to an equation for $R'_c$. This means that the equation of motion itself determines $R'_c$. This was shown in [215]. After substituting (6.12) into (6.10) and collecting powers of $z - z_c$ we obtain

$$\frac{1 + R'^2_c}{\omega^2 z_c^4}\left(z(z + z_c)(z^2 + z_c^2) - 4z_c^4\,R'_c\,(R_c + z\,\omega)\right)(z - z_c) + \mathcal{O}\big((z - z_c)^2\big) = 0 \tag{6.13}$$

The coefficient of $(z - z_c)$ has to vanish for all $z$. By taking the limit $z \to z_c$ we find an equation for $R'_c$ that reads

$$\begin{aligned} R'_c &= \frac{1}{2}\left(-z_c\,\omega + \sqrt{4 + z_c^2\,\omega^2}\right) \\ &= \frac{1}{2}\left(\sqrt{\frac{\omega}{\Pi} + 4} - \sqrt{\frac{\omega}{\Pi}}\right). \end{aligned} \tag{6.14}$$

As far as we know, the differential equation in (6.10) with the given initial conditions in (6.11) and (6.14) cannot in general be solved analytically. In the particular case of $\mathcal{N} = 4$ at zero temperature we can use the series expansion of $R(z)$ (see (6.12)) and recognise that this can be analytically continued for all values of $z$ leading to the following function:

$$R(z) = \frac{1}{2\sqrt{z_c}\omega}\sqrt{\left(-z_c\,\omega + \sqrt{4 + z_c^2\,\omega^2}\right)\left(2z^2\,\omega + z_c\big(-z_c\,\omega + \sqrt{4 + z_c^2\,\omega^2}\big)\right)}\,. \tag{6.15}$$

In the final expression we just want to have $R_0$ and $\omega$ as parameters. Therefore, we express $z_c$ as given in (6.11) in terms of $\Pi$ and $\omega$. $\Pi$ itself can now be related to $R_0$ by calculating the value of $R(0)$ in (6.15) which can be written in the form

$$R_0 \equiv R(0) = \frac{-z_c\,\omega + \sqrt{4 + z_c^2\,\omega^2}}{2\omega}\,. \tag{6.16}$$

With the help of (6.16) the function of the string configuration $R(z)$ in (6.15) gets simplified and is given by

$$R(z) = \sqrt{\frac{R_0^2\,\omega^2}{1 - R_0^2\,\omega^2}\,z^2 + R_0^2} = \sqrt{v^2\gamma^2 z^2 + R_0^2}\,, \tag{6.17}$$

where we used the definition of the velocity $v = R_0\,\omega$ and the Lorentz boost factor $\gamma \equiv 1/\sqrt{1 - v^2}$ in the second step. This compact form was presented for the first time in [215]. In Fig. 6.2 we show the radial function in $\mathcal{N} = 4$ at zero temperature for a fixed radius $R_0 = 1$ at the boundary and four values of the angular velocity $\omega$, $\omega = 0.2$, 0.5, 0.8 and 0.9. As in

[1] These important properties of $z_c$ are derived for the rotating quark in Appendix C.

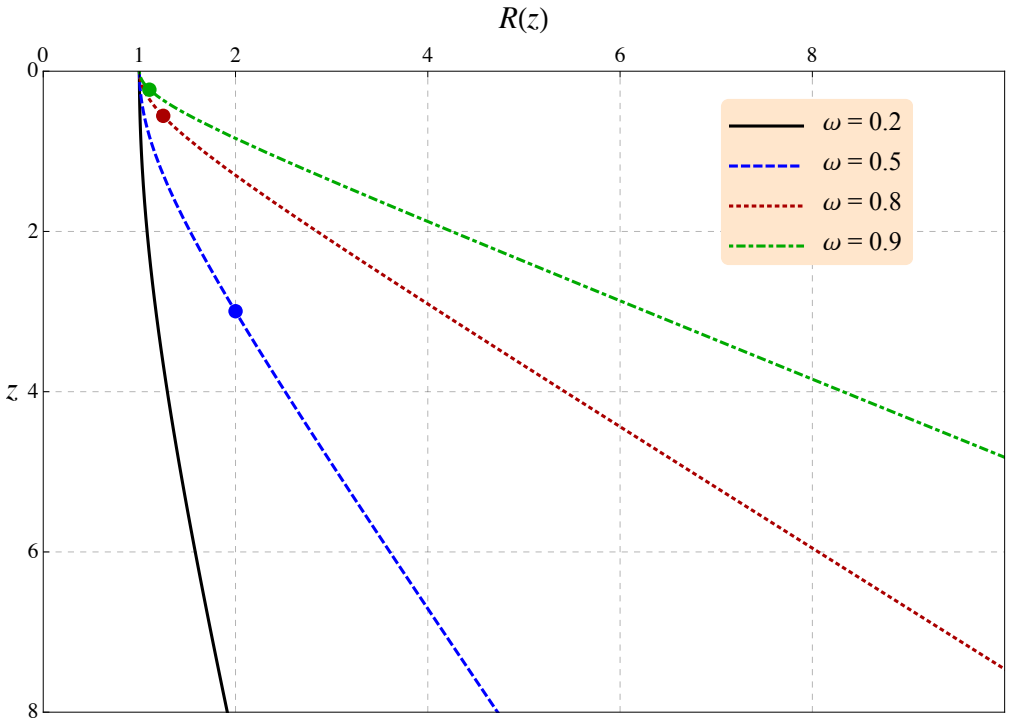


Figure 6.2: Radial string configuration in $\mathcal{N} = 4$ at zero temperature for a rotating quark with radius $R_0 = 1$ and four angular velocities $\omega$, $\omega = 0.2$, 0.5, 0.8 and 0.9 in dimensionless units. The $AdS$ length $L$ is set to 1 for simplicity. The coloured dots denote the point $z_c$ where the upper and lower parts of the string are causally disconnected. The black dot is behind the plotting range.

the previous chapter we use arbitrary units. By fixing the unit for one observable the units for all other quantities are determined. For larger values of the angular velocity $\omega$ the radial extension in the bulk increases monotonously. This is an interesting behaviour because in finite temperature models the horizon is reached at a certain value $z = z_h$ and the radial extension into the bulk will be finite.

Since $v = R_0\,\omega$, we have a maximum angular velocity of $\omega = 1$ for $R_0 = 1$. The closer we are to this limiting velocity the closer is the special point $z_c$ to the boundary. Physically, $z_c$ marks the point where the upper and lower string parts are causally disconnected [216].

In order to obtain a final three-dimensional (3D) visualisation of the rotating string configuration we need to integrate the first derivative of the angular function $\phi(z)$ given in (6.8) which leads to

$$\phi(z) = -z\gamma\,\omega + \arctan(z\gamma\,\omega)\,. \tag{6.18}$$

This leads to the following form of the angular shape of the rotating string

$$\varphi(t, z) = \omega(t - z\gamma) + \arctan(z\gamma\,\omega)\,. \tag{6.19}$$

In Fig. 6.3 we plot the string configuration of a rotating quark and the moving string in the bulk at radius $R_0 = 1$ and angular velocity $\omega$, $\omega = 0.3$ (blue) and 0.7 (black). A higher angular velocity $\omega$ leads to broader spirals and higher winding numbers which agrees with our discussion of the radial function.

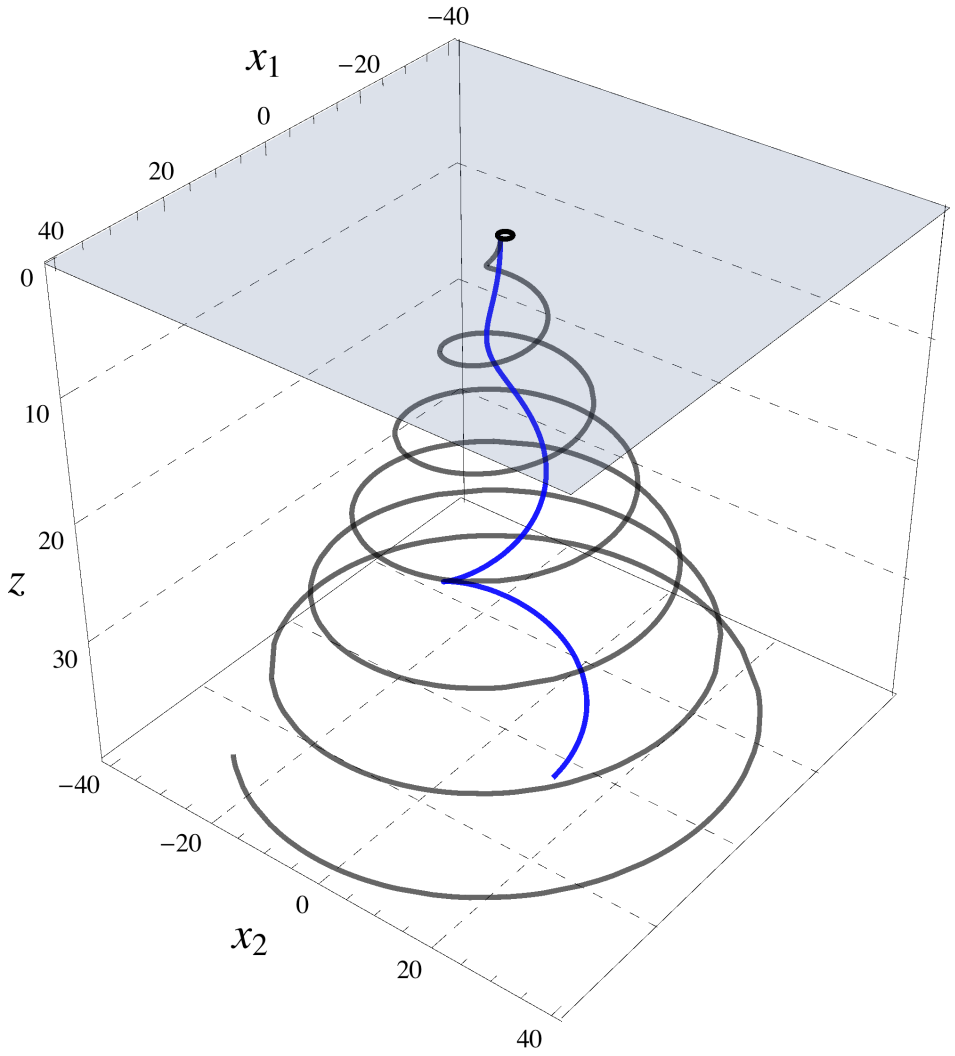


Figure 6.3: 3D plot of a string configuration of a rotating quark in $\mathcal{N} = 4$ at zero temperature and radius $R_0 = 1$ and angular velocity $\omega$, $\omega = 0.3$ (blue) and 0.7 (black). The small black circle at the top represents the trajectory of the rotating quark.

We postpone the computation of the energy loss $\mathrm{d}E/\mathrm{d}t$ until Sec. 6.4 and focus in the next section on the calculation of the string configuration in finite temperature models. The easiest one is $\mathcal{N} = 4_T$ which will be discussed now.

## 6.2 Conformal $AdS_5$ Black-Hole Metric

We review now the string configuration of a rotating quark in $\mathcal{N} = 4$ at finite temperature. This analysis has been done by Fadafan *& al.* in [190] for the first time in the literature. The basic metric is now $AdS_5$-BH which is given in (6.1) but with $h(z) = 1 - \frac{z^4}{z_\mathrm{h}^4}$. As we have learned in Sec. 2.2.2 temperature is given by

$$T = \frac{1}{\pi z_\mathrm{h}} \,. \tag{6.20}$$

We can use the same parameterisation (6.4) as in the previous section and obtain a Lagrangian of the form

$$\mathcal{L}_{\mathcal{N}=4_T} = \frac{L^2}{z^2}\sqrt{\Big(h(z)-\omega^2 R(z)^2\Big)\left(\frac{1}{h(z)}+R'(z)^2\right)+h(z)R(z)^2\phi'(z)^2}\,. \tag{6.21}$$

Although this equation is very similar to the previous case we have to cope with the problem that the equations of motion cannot be solved analytically. The calculation of the Euler–Lagrange equation for the derivative of the angular function $\phi_{\mathcal{N}=4_T}(z)$ leads to

$$\phi'_{\mathcal{N}=4_T}(z) = \frac{z^2\Pi\sqrt{h(z)-\omega^2R(z)^2}\,\sqrt{1+h(z)R'(z)^2}}{h(z)R(z)\sqrt{z^4\,\Pi^2-h(z)R(z)^2}}\,, \tag{6.22}$$

and the equation of motion for the radial function $R(z)$ – after using a partial fraction decomposition – is given by

$$\begin{aligned} R'' &+ \frac{R\big(1+hR'^2\big)\big(-4hRR'+z\big(-2+Rh'R'\big)\big)}{2z\big(z^4\,\Pi^2-hR^2\big)} \\ &+ \frac{\big(2+Rh'R'+2hR'^2+\omega^2R^3h'R'^3\big)}{2R\big(h-\omega^2R^2\big)} = 0\,. \end{aligned} \tag{6.23}$$

In order to find a solution for $R(z)$ we have to specify the initial conditions. Again, two singularities appear that have to be located at the same point due to the reality condition of (6.22). Fortunately, it is possible to solve for $z_\mathrm{c}$ and $R_\mathrm{c}$ analytically:

$$\begin{aligned} h(z_\mathrm{c})-\omega^2R(z_\mathrm{c})^2=0 \quad &\Longrightarrow \quad R(z_\mathrm{c}) = \frac{\sqrt{h(z_\mathrm{c})}}{\omega} \\ z_\mathrm{c}^4\,\Pi^2\,\omega^2-h(z_\mathrm{c})^2=0 \quad &\Longrightarrow \quad z_\mathrm{c} = \frac{1}{\sqrt{2}}\sqrt{z_\mathrm{h}^2\left(-z_\mathrm{h}^2\,\Pi\,\omega+\sqrt{4+z_\mathrm{h}^4\,\Pi^2\,\omega^2}\right)}\,. \end{aligned} \tag{6.24}$$

Before proceeding with the computation of the radial string shape we focus on the behaviour of $z_\mathrm{c}$. This point reflects the causal disconnection between the upper and lower part of the string. To compute the boundary radius $R_0$ it is sufficient to start an upward integration process at this point. This means that a value of $z_\mathrm{c}$ close to the boundary leads to a physical configuration which is nearly insensitive to the properties of the bulk since the boundary physics is determined by the part of the string above $z_\mathrm{c}$ only. We observed in the zero-temperature case that high velocity $v = R_0\,\omega$ leads to small $z_\mathrm{c}$. In (6.24) we can note that $z_\mathrm{c}$ strongly depends on the horizon $z_\mathrm{h}$:

$$\begin{aligned} z_\mathrm{c} &\xrightarrow{z_\mathrm{h}\text{ large}} \frac{1}{\sqrt{\Pi\omega}}\,, \\ z_\mathrm{c} &\xrightarrow{z_\mathrm{h}\text{ small}} 0\,, \end{aligned} \tag{6.25}$$

Thus, large values of $z_\mathrm{h}$ lead to the zero-temperature limit whereas $z_\mathrm{c}$ vanishes for small values of $z_\mathrm{h}$. Thus the high-temperature regime (small $z_\mathrm{h}$) is similar to a regime where $\omega$ is very large since $z_\mathrm{c}$ is very small in both cases which reduces the volume where the boundary is sensitive to the bulk. This interesting behaviour will be relevant when we focus on the energy loss in

different models in Sec. 6.4. In order to find the full expansion of $R(z)$ in powers of $z - z_\mathrm{c}$ we need the relation between $\Pi\,\omega$ and $z_\mathrm{c}$ which is simply the second condition in (6.24):

$$\Pi\,\omega = \frac{h(z_\mathrm{c})}{z_\mathrm{c}^2}\,. \tag{6.26}$$

With these formulae in our hand we can now fix $R'(z_\mathrm{c})$ by expanding $R(z)$ in powers of $z - z_\mathrm{c}$ as in (6.12) and substituting this into the differential equation (6.23). We focus here only on the coefficient in front of the $z - z_\mathrm{c}$ term since no $R''(z_\mathrm{c})$ is involved anymore. The vanishing of this coefficient determines again the second initial condition $R'_\mathrm{c}$ which is required to solve the differential equation in (6.23). The condition on $R'_\mathrm{c}$ can then be written in the form

$$-2R_\mathrm{c}\,z_\mathrm{c}\,\omega^2 + 2\omega\sqrt{h(z_\mathrm{c})} - 2R_\mathrm{c}'^2\omega h(z_\mathrm{c})^{3/2} + R_\mathrm{c}\,h(z_\mathrm{c})h'(z_\mathrm{c}) = 0\,. \tag{6.27}$$

In (6.27) we have used the relation between $\Pi\,\omega$ and $z_\mathrm{c}$ and have taken the limit $z \to z_\mathrm{c}$. The solution to this expression can be given analytically by

$$\begin{aligned} R'_\mathrm{c} &= \frac{-2z_\mathrm{c}\,\omega^2 + h(z_\mathrm{c})h'(z_\mathrm{c}) + \sqrt{16\omega^2 h(z_\mathrm{c})^2 + \big(-2z_\mathrm{c}\,\omega^2 + h(z_\mathrm{c})h'(z_\mathrm{c})\big)^2}}{4\omega\,h(z_\mathrm{c})^{3/2}} \\ &\xrightarrow{T=0} \quad \frac{1}{2}\left(-z_\mathrm{c}\,\omega + \sqrt{4 + z_\mathrm{c}^2\,\omega^2}\right), \end{aligned} \tag{6.28}$$

where we take the positive root which leads to positive values of $R'(z_\mathrm{c})$. This is physically meaningful because we want the string to trail and curl behind the quark. Furthermore, if we set $h = 1$ representing the zero-temperature case this condition nicely reproduces what we have found in (6.14). The remaining parameters are again $\omega$, $\Pi$ and the horizon $z_\mathrm{h}$ representing the temperature.

We could not find an analytic solution to the differential equation for the radial function $R(z)$ in (6.23) with the given initial conditions (6.24) and (6.28). Thus, the `NDSolve` routine of MATHEMATICA® was used. It is important to note that the start of the integration process has to be slightly above the singular point $z_\mathrm{c}$ in order to integrate towards the boundary. The integration upwards allows for the computation of the boundary radius $R_0$ of the rotating quark. The numerical relation between $R_0$ and $\Pi$ will be explained in subsection 6.2.1. In a second step a downward integration has been done and the full radial extension of the string for fixed angular velocity $\omega = 0.2$ and boundary radius $R_0 = 4$ is shown in Fig. 6.4 for several values of the temperature $T$, $T = 0$, 0.05, 0.07, 0.09, 0.1 and 0.15. Again the temperatures are given in arbitrary units.

A few things are noteworthy: the lower the temperature the closer is the radial function to the zero-$T$ case. This can be seen analytically be setting $h = 1$ in the differential equation (6.23) and in the initial conditions (6.24) and (6.28).

The endpoint of each curve is the location of the horizon and in fact each string has a finite radial extension at the horizon. This is indeed a very interesting observation indicating that the energy is deposited in the medium up to a finite radius and not up to infinity as in the zero-temperature case.

In order to see that the string has nevertheless an infinite length we must compute the angular function $\phi(z)$. It will be obvious that the winding number of the string diverges at the horizon. For higher temperatures, the radial extension into the bulk is smaller due to the stronger interaction of the plasma with the rotating string. A full 3D picture of a certain string configuration will be shown in Sec. 6.2.2.

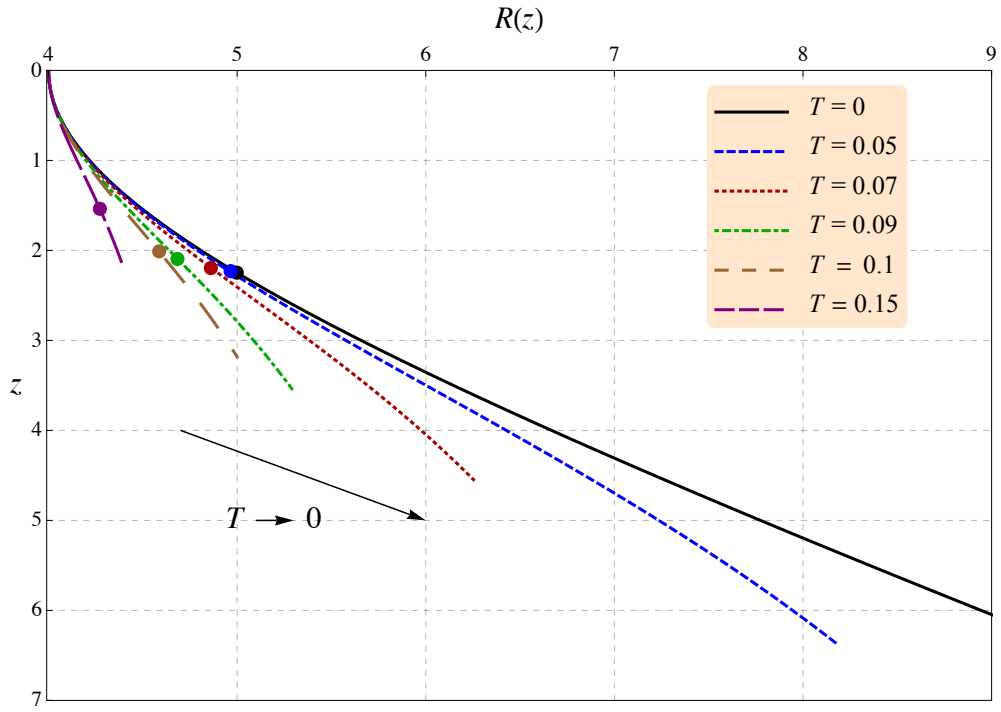


Figure 6.4: Radial function $R(z)$ in $\mathcal{N} = 4_T$ for fixed angular velocity $\omega = 0.2$, boundary radius $R_0 = 4$ and several values of the temperature $T$, $T = 0$, 0.05, 0.07, 0.09, 0.1 and 0.15. The points mark the value $z_c$ where the upper part of the string is causally disconnected from the lower one. Each curve ends at the respective horizon.

### 6.2.1 Π–$R_0$ Relation

Since we have to insert Π in our initial conditions, it is not easy to fix the boundary radius $R_0$ right from the beginning of the calculation. In the zero-temperature case we could find an analytic relation between these two parameters. However, here and in the following models, we have to choose Π and integrate upwards to the boundary in order to find the boundary radius. In $\mathcal{N} = 4$ at zero temperature the equation that relates Π and $R_0$ has the form:

$$\Pi = \frac{R_0^2\,\omega^3}{(1 - R_0^2\,\omega^2)^2} = \gamma^4\,v^2\,\omega\,. \tag{6.29}$$

For fixed angular velocity $\omega = 0.1$ we have plotted the Π–$R_0$ relation in Fig. 6.5. For small temperatures the relation approaches the zero-$T$ computation. Furthermore, we can state that small values of Π lead to small radii. For larger values of Π an upper limit is reached since we are limited by the speed of light $v = 1$. This means that for fixed $\omega = 0.1$ we can reach a maximum radius of $R_0 = v/\omega = 10$. Thus, we can state that Π has the meaning of a scaled velocity which can be seen in (6.29). A similar plot (Fig. 6.6) can be drawn for fixed temperature but varying angular velocity $\omega$. Again, we encounter a monotonous relation between Π and $R_0$ for all values of the angular velocity $\omega$. The flat regime for high angular velocities arises due to the small values of allowed radii; thus, the change in $R_0$ is small when Π increases since the kinematics dominate this regime.

Before we proceed with more advanced metric models we will compute the angular function in the next paragraph and show finally the string configuration for the finite temperature case.

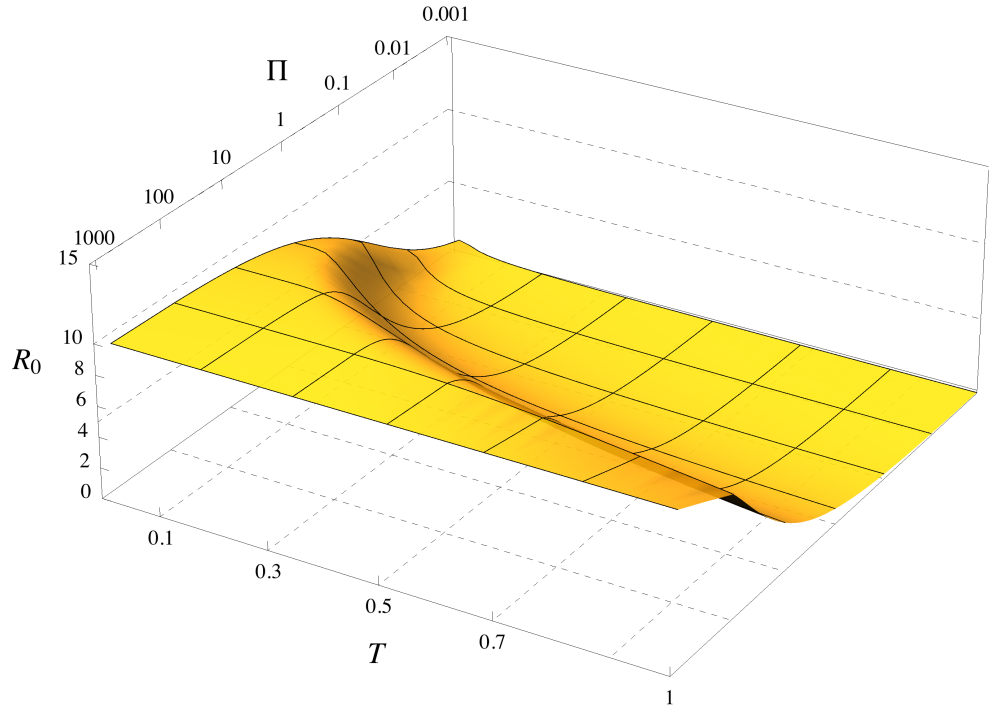


Figure 6.5: $\Pi$–$R_0$ relation in $\mathcal{N} = 4_T$ against the temperature $T$ for fixed angular velocity $\omega = 0.1$.

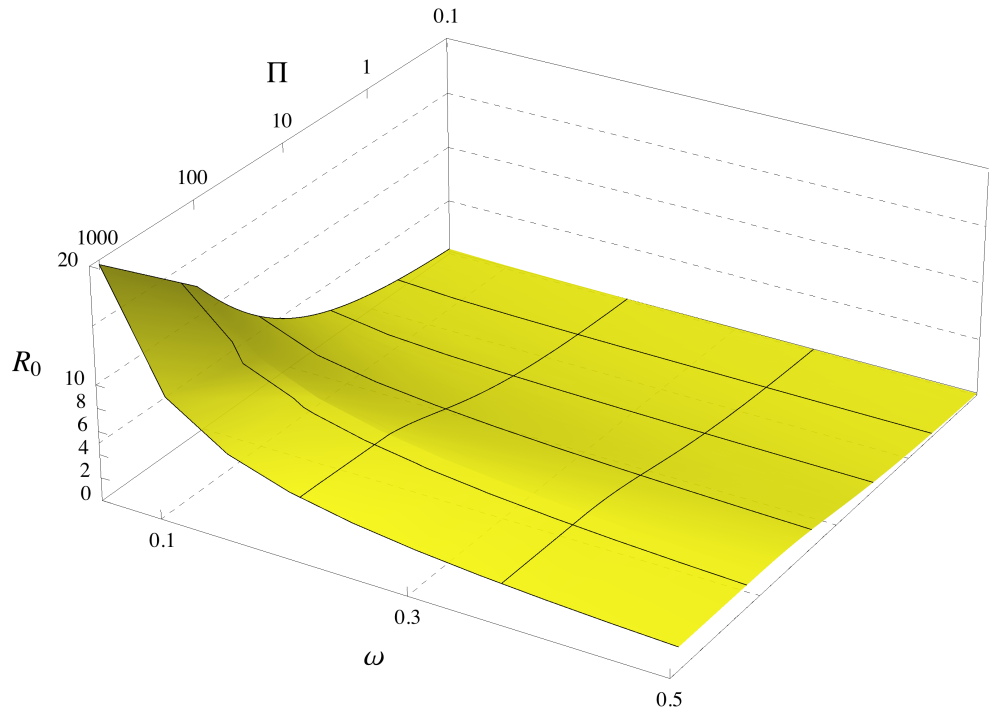


Figure 6.6: $\Pi$–$R_0$ relation in $\mathcal{N} = 4_T$ against the angular velocity $\omega$ for fixed temperature $T = 1$ in arbitrary units. The high-$\Pi$ regime represents the highest possible values for $R_0$

### 6.2.2 String Configuration in $\mathcal{N} = 4_T$

A problem that occurred in the previous discussion is the finiteness of the radial extension $R(z)$ although we know that the string has to have infinite length. If we substitute the numerical solution of the differential equation for $R(z)$ (6.23) into the integral representation of $\phi(z)$ (6.22) we can solve for $\phi(z)$ numerically. Here, one has to be careful since two integrations have to be worked out in order to obtain the full $R(z)$. An upward[2] integration of the differential equation in (6.23) starting at $z_\mathrm{c}$ leads to $R_<(z)$ for $z < z_\mathrm{c}$ and a downward integration leads to $R_>(z)$ for $z > z_\mathrm{c}$. The angular function $\phi(z)$ then reads

$$\begin{aligned}\phi(z_) &= \int_0^z d\tilde{z} \frac{\tilde{z}^2 \Pi \sqrt{-h(\tilde{z}) + \omega^2 R(\tilde{z})^2}\,\sqrt{1 + h(\tilde{z}) R'(\tilde{z})^2}}{h(\tilde{z}) R(\tilde{z}) \sqrt{z^4\,\Pi^2 - h(\tilde{z}) R(\tilde{z})^2}} \equiv \int_0^z d\tilde{z}\, \mathcal{F}\big(\tilde{z}, R(\tilde{z})\big) \\ &= \int_0^{z_\mathrm{c}-\varepsilon} d\tilde{z}\, \mathcal{F}\big(\tilde{z}, R_<(\tilde{z})\big) + \int_{z_\mathrm{c}+\varepsilon}^{z} d\tilde{z}\, \mathcal{F}\big(\tilde{z}, R_>(\tilde{z})\big)\,. \end{aligned} \tag{6.30}$$

$z$ denotes the point in the bulk where we want to compute the angle of the string. It can be chosen in the range of 0 to $z_\mathrm{h}$. For every value of the free parameters $R_0$, $\omega$ and $T$ we have interpolated the radial function $R(z)$ and have computed the angular function $\phi(z)$ with the help of the `NIntegrate` routine of MATHEMATICA®. The second line ensures that the correct radial functions are used: $R_<$ for $z < z_\mathrm{c}$ and $R_>$ for $z > z_\mathrm{c}$. In addition to this, the numerical integration requires a slight shift of the initial value $z_\mathrm{c}$ by a small $\varepsilon > 0$ in order to specify the direction of integration.

The results are shown in Fig. 6.7 where we plot the angular function $\phi(z)$ versus $z$ for two angular velocities $\omega$, $\omega = 0.3$ and 0.7 and three different temperatures $T$, $T = 0.01, 0.015$ and 0.02. For small values of $z$ we see an approximately linear increase of the angle. This can be verified in Fig. 6.3 where the distance between two spirals is always constant. The introduction of temperature leads to a strong increase in the angle close to the horizon $z_\mathrm{h}$ which is indicated by the small thin black lines at the $z$-axis. Thus, we can argue that the string has infinite length since the number of windings diverges close to the horizon. Furthermore, a larger increase in the angle can be achieved by higher values of the angular velocity but this effect is only noticeable if we consider regions far away from the boundary.

If we now put all the details together we obtain a 3D plot (Fig. 6.8) of a rotating quark in $\mathcal{N} = 4$ at finite temperature. The blue circle at the boundary is the circle on which the quark is moving in the three-dimensional space.

We saw in this chapter that temperature has a huge impact on the shape of the string and we will figure out in the Sec. 6.4 that this behaviour is true for other physical observables like the energy loss. Thus it is interesting if a more reliable and realistic model shows a similar effect in the shape of the string. Unfortunately, the energy loss cannot be extracted directly from the string configuration. We will discuss these problems in Secs. 6.3 and 6.4.

[2] In this context upwards means towards the boundary.

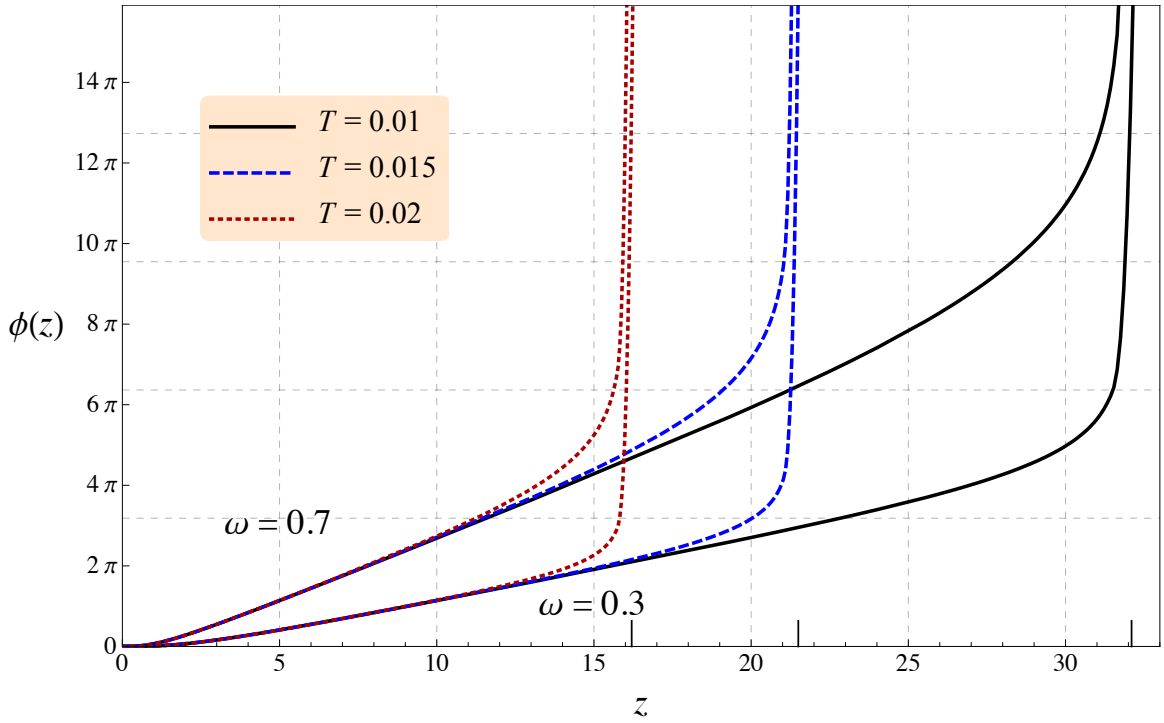


Figure 6.7: Angular function $\Phi(z)$ in $\mathcal{N}=4_T$ against $z$ for two angular velocities $\omega$, $\omega = 0.3$ and $0.7$ and three different temperatures $T$, $T = 0.01, 0.015$ and $0.02$ in arbitrary units.

## 6.3 Non-Conformal Metric Models

In this section we focus on the non-conformal extensions of the basic $\mathcal{N}=4$ model that we have derived in Chap. 3. On one hand we want to see whether the changes from conformal to non-conformal models are small and on the other hand we want to find similarities to QCD-like observables. The computation is in principle analogous to the last section. We will consider the same three models as before: the $\mathrm{SW}_T$-model which does not solve any supergravity equations of motion and the consistent 1- and 2-parameter models. With the detailed knowledge of the configuration of the string which is attached to the quark in the dual description we will finally compute the energy loss in Sec. 6.4.

### 6.3.1 $\mathrm{SW}_T$-Model

The basic parameterisation of the string worldsheet is again the same as in the previous sections. The metric has the following form

$$\mathrm{d}s^2 = e^{c\,z^2}\,\frac{L^2}{z^2}\left(-h(z)\,\mathrm{d}t^2 + \mathrm{d}\vec{x}^{\,2} + \frac{\mathrm{d}z^2}{h(z)}\right), \tag{6.31}$$

and the Lagrangian reads

$$\mathcal{L}_{\mathrm{SW}_T} = e^{c\,z^2}\,\frac{L^2}{z^2}\sqrt{\left(h(z)-\omega^2 R(z)^2\right)\left(\frac{1}{h(z)}+R'(z)^2\right)+h(z)R(z)^2\phi'(z)^2}\,. \tag{6.32}$$

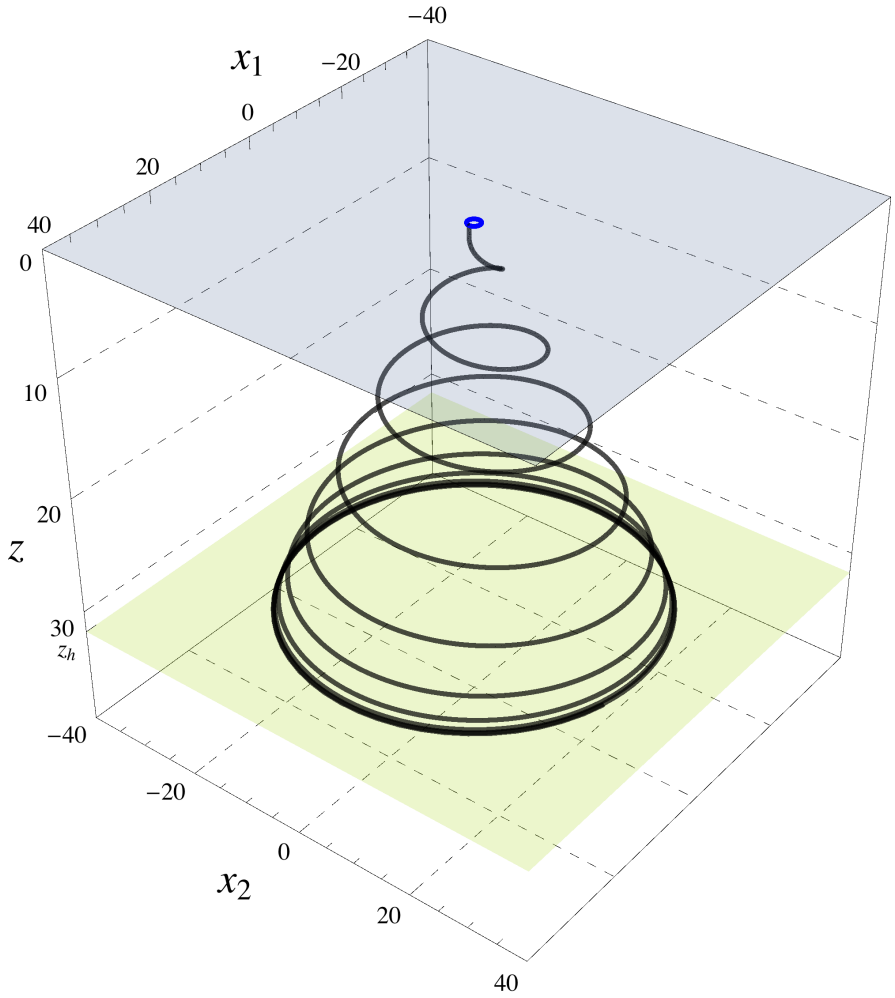


Figure 6.8: Full 3D string configuration in $\mathcal{N} = 4_T$ at $T = 1^{-2}$ in arbitrary units and angular velocity $\omega = 0.7$ with boundary radius (blue circle) $R_0 = 1.4$.

Since we just inserted an exponential factor into the metric the computational steps change only slightly compared to the $\mathcal{N} = 4_T$ case. However, this model is very interesting due to the simplicity and the fact that it includes non-conformality. The problem of not solving any equations of motion might lead to some inconsistencies which we hope to solve be studying more reliable models in the next subsection. Nevertheless, any universal behaviour that might occur by studying this model should be observable in the more reliable models as well. Although the equations are in principle simple we are not able to solve analytically the differential equations for the angular function $\phi(z)$

$$\phi'_{\mathrm{SW}_T}(z) = \frac{z^2\,\Pi\sqrt{-h(z)+\omega^2 R(z)^2}\,\sqrt{1+h(z)R'(z)^2}}{h(z)R(z)\sqrt{z^4\,\Pi^2 - e^{2cz^2}h(z)R(z)^2}}\,, \tag{6.33}$$

and for the radial function $R(z)$

$$R'' + \frac{-e^{2c\,z^2}\,R\big(1+hR'^2\big)\Big[4(-1+c\,z^2)hRR' + z\big(-2+Rh'R'\big)\Big]}{2z\big(z^4\,\Pi^2 - e^{2c\,z^2}\,hR^2\big)} + \frac{\Big(2+Rh'R'+2hR'^2+\omega^2R^3h'R'^3\Big)}{2R\big(h-\omega^2R^2\big)} = 0\,. \tag{6.34}$$

Again we fix the initial conditions with the help of the singular point $z_c$ which has to satisfy the following equation:

$$z_c^4\Pi^2\,\omega^2 - e^{2c\,z_c^2}\,h(z_c)^2 = 0 \quad \Longrightarrow \quad \xi(z_c) \equiv \frac{e^{c\,z_c^2}\,h(z_c)}{z_c^2} - \Pi\,\omega = 0\,, \tag{6.35}$$

$$R_c \equiv R(z_c) = \frac{\sqrt{h(z_c)}}{\omega}\,. \tag{6.36}$$

Here, we have introduced the function $\xi(z)$ that has to be solved numerically and that defines $z_c$ as its first zero. If we now naively choose $\Pi$, $\omega$ and $T$ and vary the deformation $c$ we encounter the problem that $z_c$ is not defined for all values of $c$. For large $c$ the $z_c$-defining equation $\xi(z) = 0$ has no solution if we assume a particular range of boundary radii $R_0$. This is illustrated in Fig. 6.9 for fixed $R_0 = 4.6$, $\omega = 0.2$ and $T = 0.02$ and several values of the deformation $c$, $c = 0$, 0.1, 0.2, 0.3, 0.6 and 1. Here, we observe that $z_c$ is very robust for a

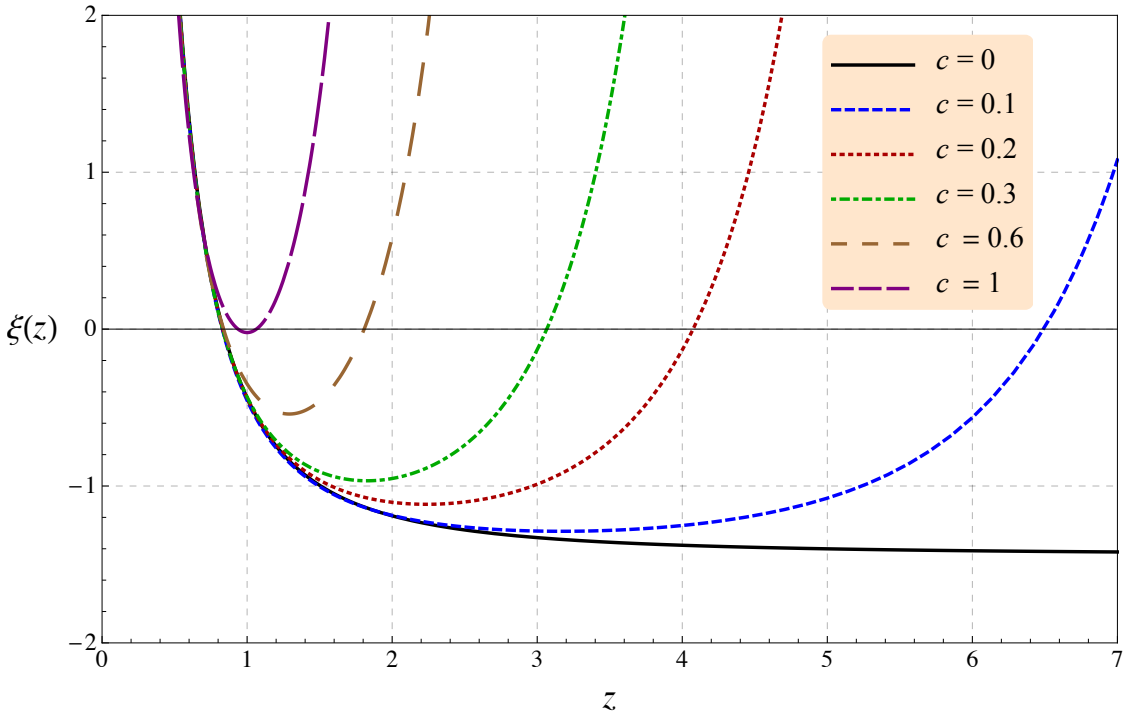


Figure 6.9: Function $\zeta(z)$ defining $z_c$ against $z$ for fixed $R_0 = 4.6$, $\omega = 0.2$ and $T = 0.02$ and various values of the deformation $c$, $c = 0, 0.1, 0.2, 0.3, 0.6$ and 1. The value of $z_c$ is the first zero of this function. For deformations larger than $c \sim 1.05$ no $z_c$ can be found.

large range of deformations $c$. It is not easy to fix $R_0$ in $\xi(z)$ given by (6.35). $R_0$ has to be

adjusted dynamically by computing $R(0)$ with the help of the full differential equation for $R(z)$ (6.34) for a large range of $\Pi$ until the particular $\Pi$-value is found that leads to $R_0 = 4.6$. We see that $z_c$ is well-defined for a large range of deformations $c$ but at a certain critical value $c \approx 1.05$ the computation breaks down. An analogous behaviour can be found in the case of the drag force in the $SW_T$ model. There the results become physically inconsistent above a certain value of the deformation $c$ [77]. In both cases these results are just an artefact due to the inconsistency concerning the supergravity equations of motion that will be discussed in the next section when we consider consistent models. There we will show that $z_c$ is well-defined for all values of the deformation.

In order to calculate $R_c$ we make use of the expansion in (6.12) and evaluate the function $R(z)$ at $z = z_c$. This leads to the following expression

$$\begin{aligned} 0 &= -\frac{R_c\, z_c\, \omega^2}{1 - c\, z_c^2} + \omega \sqrt{h(z_c)} - R_c'^2 \omega\, h(z_c)^{3/2} + \frac{1}{2} R_c\, h(z_c) h'(z_c)\,, \\ \Longrightarrow \quad R_c' &= \frac{2 z_c\, \omega^2 - (1 - c\, z_c^2)\, h(z_c) h'(z_c)}{4(-1 + c\, z_c^2)\, \omega h(z_c)^{3/2}} \\ &\quad - \frac{\sqrt{16(1 - c\, z_c^2)^2\, \omega^2 h(z_c)^2 + \left(-2 z_c\, \omega + (1 - c\, z_c^2)\, h(z_c) h'(z_c)\right)^2}}{4(c\, z_c^2 - 1)\, \omega h(z_c)^{3/2}}\,. \end{aligned} \tag{6.37}$$

The radial function for several values of the deformation $c$, $c = 0$, 0.1, 0.2 and 0.4 is plotted in Fig. 6.10. We find many similarities to the conformal case that will be noted briefly. However,

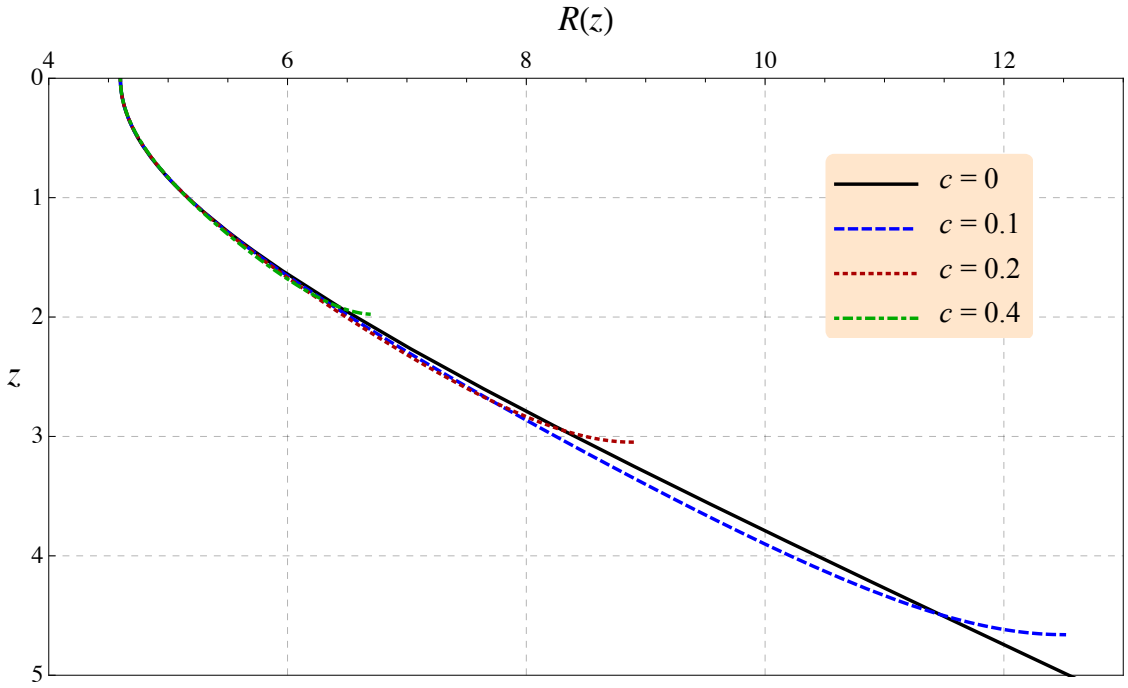


Figure 6.10: Radial function $R(z)$ in the $SW_T$ model against $z$ for fixed temperature $T = 0.02$, angular velocity $\omega = 0.2$ and boundary radius $R_0 = 4.6$ and several values of the deformation $c$, $c = 0$, 0.1, 0.2 and 0.4. Each curve shows an abrupt ending before the horizon ($z_h = 15.9$) is reached. Since such a behaviour is not apparent in consistent models, it seems to be a consequence of the inconsistency concerning supergravity equations of motion.

some qualitative changes arise that have to be discussed in greater detail. This model has the advantage that the temperature $T = (\pi z_\mathrm{h})^{-1}$ is independent of the deformation parameter $c$. Thus, we can fix the temperature and study different regimes of $c$. Even for large values of the deformation the shape of the radial function is similar to the conformal case. Since $z_\mathrm{c}$ is always below 1 in the curves shown, we state that the string shape is almost unchanged in the physically meaningful regime. This regime is called physically meaningful due to the causal disconnection between the part of the string with $z$ values larger than $z_\mathrm{c}$ and values smaller $z_\mathrm{c}$. The boundary field theory only probes the regime of $z < z_\mathrm{c}$.

In all curves in Fig. 6.10 the numerical computation collapses at certain values of $z$ above the horizon ($z_\mathrm{h} = 15.9$). The higher the deformation the shorter are the curves. Since this behaviour disappears in the consistently deformed models, it seems to be an artefact due to the inconsistency of the model concerning the supergravity equations of motion.

In the next subsections we focus on consistently deformed models. The expressions are more complicated but still numerically tractable. In addition, we have to distinguish between the string- and Einstein frame. After that discussion we compute the energy loss for all models and explain the differences.

### 6.3.2 1-Parameter Deformation

The 1-parameter model has the big difference to the $\mathrm{SW}_T$-model that we now change the temperature if we choose different values of the deformation parameterised by $\phi$. The temperature is quoted here for convenience and has the form

$$T = \frac{z_\mathrm{h}^3\,\phi^2}{4\pi\left(1 - e^{-\frac{z_\mathrm{h}^4\,\phi^2}{4}}\right)}\,. \tag{6.38}$$

Thus, we have to be more careful when comparing different deformations for fixed values of the angular velocity $\omega$, temperature $T$ and the radius $R_0$. In the following discussion we will focus on both, Einstein and string frame, and discuss the differences therein.

#### 1-Parameter Model: Einstein Frame

If we use again the parameterisation in (6.4) the Lagrangian in the Nambu–Goto action of this model can be written as

$$\mathcal{L}_\mathrm{1p} = e^{2A(z)}\sqrt{\left(h(z) - \omega^2\,R(z)^2\right)\left(\frac{e^{2B(z)}}{h(z)\,e^{2A(z)}} + R'(z)^2\right) + h(z)\,R(z)^2\,\phi'_\mathrm{1p}(z)^2}\,, \tag{6.39}$$

where $A(z)$, $B(z)$ and $h(z)$ are the metric functions in the Einstein frame which have been derived in (3.36) and (3.37) and are quoted here for convenience:

$$\begin{aligned} A(z) &= \frac{1}{2}\,\log\left(\frac{L^2}{z^2}\right), \\ B(z) &= \frac{1}{4}\big(-z^4\,\phi^2 - 4\log(z)\big) + \log L \\ h(z) &= \frac{1 - e^{\frac{1}{4}\left(z_\mathrm{h}^4 - z^4\right)\phi^2}}{1 - e^{\frac{z_\mathrm{h}^4\,\phi^2}{4}}}\,. \end{aligned} \tag{6.40}$$

The angular function will be denoted by $\phi_{1\mathrm{p}}(z)$ in the following since the deformation parameter of the 1-parameter model is also called $\phi$. By using the Euler–Lagrange equation for $\phi_{1\mathrm{p}}(z)$ we end up with a differential equation given by

$$\phi'_{1\mathrm{p}}(z) = \frac{\Pi\sqrt{e^{-2A(z)}\left(\omega^2\,R(z)^2 - h(z)\right)\left(e^{2B(z)} + e^{2A(z)}\,h(z)\,R'(z)^2\right)}}{R(z)\,h(z)\,\sqrt{\Pi^2 - e^{4A(z)}\,h(z)\,R(z)^2}}\,. \tag{6.41}$$

The computation of the equation of motion for $R(z)$ leads to the following differential equation

$$\begin{aligned} R'' &+ \frac{e^{2A-2B}\,R\big(2e^{2B} - 4e^{2A}\,h\,R\,A'\,R' - e^{2A}\,R\,h'\,R'\big)\left(e^{2B} + e^{2A}\,h\,R'^2\right)}{2\big(\Pi^2 - e^{4A}\,h\,R^2\big)} \\ &+ \frac{e^{-2(A+B)}}{2R\left(h - \omega^2\,R^2\right)}\Bigg[2e^{4B} + e^{2(A+B)}\,R\Big(2\big(h - \omega^2\,R^2\big)\left(A' - B'\right) + h'\Big) \\ &+ 2e^{2(A+B)}\,h\,R'^2 + e^{4A}\,\omega^2\,R^3\,h'\,R'^3\Bigg] = 0\,. \end{aligned} \tag{6.42}$$

Together with the two expressions for the initial conditions $R_\mathrm{c}$ and $R'_\mathrm{c}$ evaluated at $z_\mathrm{c}$ given by

$$\begin{aligned} \Pi^2\,\omega^2 - e^{4A(z_\mathrm{c})}\,h(z_\mathrm{c})^2 \equiv 0 \quad\Longrightarrow\quad \xi(z_\mathrm{c}) &\equiv e^{2A(z_\mathrm{c})}\,h(z_\mathrm{c}) - \Pi\,\omega = 0\,, \\ R(z_\mathrm{c}) &\equiv \frac{\sqrt{h(z_\mathrm{c})}}{\omega}\,, \end{aligned} \tag{6.43}$$

and

$$\begin{aligned} 0 &= -2e^{4A+2B}\,z_\mathrm{c}^5\,\omega^2\,R_\mathrm{c} + 2e^{2B}\,\omega\,\sqrt{h} + 2e^{6A}\,z_\mathrm{c}^5\,\omega\,h^{3/2}\,A'\,R'^2_\mathrm{c} + e^{2A}\,h\,h'\,R_\mathrm{c} \\ \Longrightarrow\quad R'_\mathrm{c} &= \frac{e^{-6A}}{4z_\mathrm{c}^5\,\omega\,h^{3/2}\,A'}\Bigg[2\,e^{4A+2B}\,z_\mathrm{c}^5\,\omega^2 - e^{2A}\,h\,h' \\ &\quad - \sqrt{-16e^{6A+2B}\,z_\mathrm{c}^5\,\omega^2\,h^2\,A' + \left(-2e^{4A+2B}\,z_\mathrm{c}^5\,\omega^2 + e^{2A}\,h\,h'\right)^2}\Bigg]\,, \end{aligned} \tag{6.44}$$

we can now compute the string configuration of a rotating quark in a non-conformal metric model in the Einstein frame. We want to note that (6.41) – (6.44) are expressed by general $A(z)$,$B(z)$ and $h(z)$ functions. These equations will be also used for the string frame case and the whole 2-parameter model where a relabelling to $\Phi$-coordinates has to happen. Before computing the string configuration for various parameters $\omega$, $\Pi$ and $T$ in the Einstein frame of the 1-parameter model we have to make sure that a configuration exists. There are two subtleties due to which this computation may break down.

As we have seen in Sec. 3.2.3 we can find a minimal temperature for each value of the deformation $\phi$. In other words, a fixed temperature determines the highest possible deformation $\phi_\mathrm{max}$. Furthermore, we want to compare to the behaviour of the $\mathrm{SW}_T$-model where the condition on $z_\mathrm{c}$ given by (6.35) does not lead to physical results for certain values of the deformation. Thus, the function $\xi(z)$ given in (6.43) is plotted in Fig. 6.11 in the 1-parameter Einstein frame for fixed values of the temperature $T = 1$, angular velocity $\omega = 0.2$, boundary radius $R_0 = 4$ for and several values of the deformation $\phi$, $\phi = 0$, 1, 1.5, 2, 5 and $\phi_\mathrm{max}$. Here, we note that for every deformation we have chosen, a zero in $\xi(z)$ exists leading to the existence of $z_\mathrm{c}$. Since

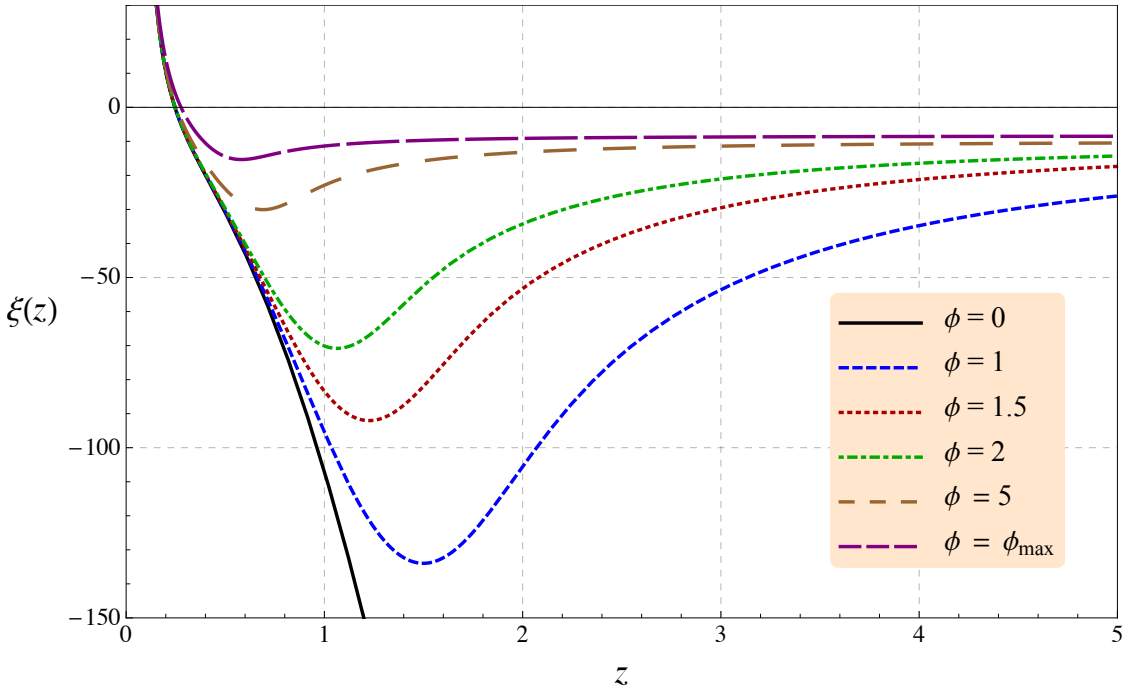


Figure 6.11: $z_c$-defining function $\xi(z)$ against $z$ for fixed values of the temperature $T = 1$, angular velocity $\omega = 0.2$ and boundary radius $R_0 = 4$ and various deformation parameters $\phi$, $\phi = 0, 1, 1.5, 2, 5, \phi_{\max}$. The conformal case (black line) has no turning point and extends to minus infinity.

this is not the case in the $SW_T$-model, this seems to be a consequence of the consistency of this model which is now a solution to Einstein equations.

In order to obtain the boundary radius $R_0$ for a given value of $\Pi$ we have to go through the numerical calculation of $R(z)$ (6.42) and evaluate this at $R(0)$. This procedure has to be done until we find the value of $\Pi$ which leads to the appropriate value of $R_0$. In Fig. 6.11 it is obvious that every possible value of $\phi$ results in a crossing of the curve with zero. For fixed temperature $T = 1$ the upper limit of the deformation is $\phi_{\max} \approx 8.6$ as visualised in Fig. 3.2. The existence of a minimal temperature $T_{\min}$, or equivalently, a maximal deformation $\phi_{\max}$ is a property that appeared as a consequence of the consistent implementation of non-conformality as explained in Sec. 3.

With all the initial conditions in our hand we can now compute and plot the radial function $R(z)$ in the 1-parameter model in the Einstein frame by using again the `NIntegrate` routine of MATHEMATICA®. This is shown in Fig. 6.12 for fixed temperature $T = 1$, angular velocity $\omega = 0.2$ and boundary radius $R_0 = 4$ for three different values of the deformation $\phi$, $\phi = 0, 5, \phi_{\max}$. First, we can state that the string configuration of a rotating quark in the 1-parameter model in the Einstein frame is very robust in comparison to the conformal case. The dotted, red curve shown in Fig. 6.12 is the maximal deformation possible at this temperature and differs only slightly from the solid, black conformal curve. This robust behaviour can be found in nearly all figures in this chapter. When the focus is on the energy loss we have to focus on the point $z_c$ where the upper part is causally disconnected from the lower part since only the upper part is relevant for the energy-loss discussion.

After introducing a deformation the string tends to rotate at larger radii for a fixed set

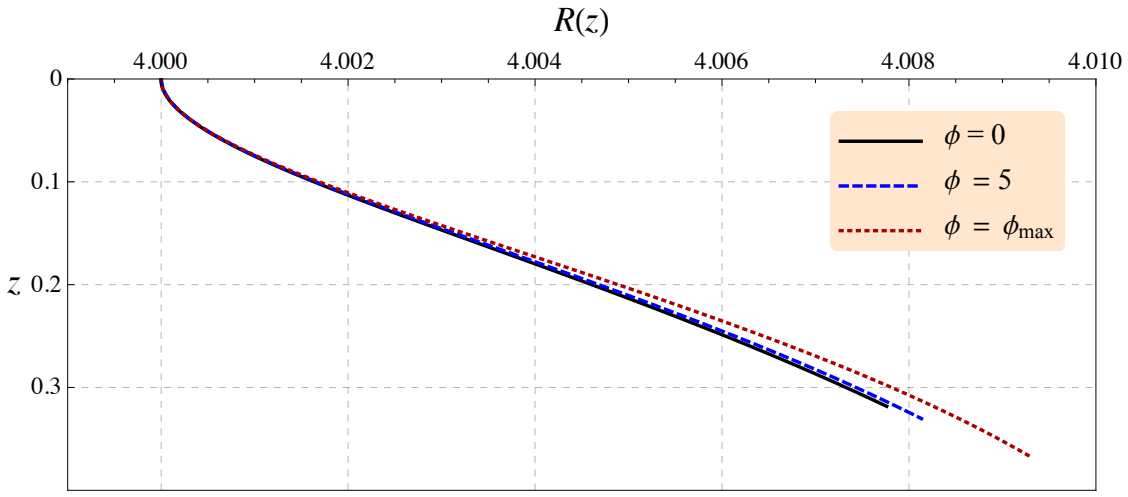


Figure 6.12: Radius function $R(z)$ in the 1-parameter (Einstein frame) model against the $5^{\text{th}}$-dimension coordinate $z$ for fixed temperature $T = 1$, angular velocity $\omega = 0.2$ and boundary radius $R_0 = 4$ for three different values of the deformation $\phi$, $\phi = 0, 5, \phi_{\text{max}}$. The endpoints of the string represent the horizon $z_{\text{h}}$ of each string configuration.

of our free parameters. The value of $z_{\text{c}}$ where the string velocity exceeds the local speed of light is between $z_{\text{c}} = 0.24$ for the conformal case and $z_{\text{c}} = 0.27$ for the deformed case with $\phi = \phi_{\text{max}}$. At these small values of $z$ below $z_{\text{c}} \approx 0.3$ both string configurations (the conformal and highly deformed one) are nearly identical. Thus, physical observables – like the energy loss – may be robust with respect to these range of parameters. A last thing we have to note is the different length of each curve. Since the temperature is not solely a function of the horizon but $\phi$-dependent, we have to adjust the horizon $z_{\text{h}}$ after choosing the deformation. In principle, a larger deformation leads to a larger horizon for constant temperature.

The shape of the curves we have seen in Fig. 6.12 is very robust, which means that it is similar for a large range of temperatures, angular velocities, boundary radii and possible deformations. In opposition to the $\text{SW}_T$-model, the 1-parameter case has string configurations that are valid up to the horizon for every choice of parameters. This agrees nicely with our previous result indicating that we should favour a consistent model being a solution to supergravity equations of motion.

### 1-Parameter Model: String Frame

Before we proceed with the analysis of the 2-parameter model in section 6.3.3 a brief description of the string frame computation is helpful. Although many observables are robust concerning the interchange of string and Einstein frame[3], we found in Sec. 4.2 that the energy loss of trailing string decreases in the latter but rises in the former. Thus we have to discuss both frames in the context of rotating quarks more carefully. However, we will not go through all the computational details and just explain the changes in the metric functions together with some plots.

[3]The temperature $T$ and the horizon function $h(z)$ is independent of the frame. Thus the values $T_{\text{min}}$ and $\phi_{\text{max}}$ are identical for a given choice of parameters.

Switching to the string frame leads to a change in the metric functions $A$ and $B$ which can now be written as

$$A_{\rm s} = \frac{1}{2}\left(\log\left(\frac{L^2}{z^2}\right) + \phi\, z^2\right),$$
$$B_{\rm s} = \frac{1}{4}\left(-z^4\,\phi^2 - 4\log\, z\right) + \frac{1}{2}\,\phi\, z^2 + \log L\,. \tag{6.45}$$

The horizon function $h$ and the temperature $T$ remain unchanged. Although the temperature is quadratic in $\phi$ the linear $\phi$-contribution in (6.45) allows for choosing negative deformations with different physical properties than its positive counterparts. Thus, we have to make sure that the subtleties occurring in the $\mathrm{SW}_T$-model are still not possible here and plot $\xi_{\rm s}(z)$ defined by

$$\Pi^2\,\omega^2 - e^{4A_{\rm s}(z_{\rm c})}\,h(z_{\rm c})^2 \equiv 0 \quad\Longrightarrow\quad \xi_{\rm s}(z_{\rm c}) \equiv e^{2A_{\rm s}(z_{\rm c})}\,h(z_{\rm c}) - \Pi\,\omega = 0\,,$$
$$R_{\rm s}(z_{\rm c}) \equiv \frac{\sqrt{h(z_{\rm c})}}{\omega}\,, \tag{6.46}$$

in Fig. 6.13 for the same fixed parameters ($\omega = 0.2$, $R_0 = 4$) but negative and positive values of $\phi$, $\phi = -8$, $-5$, 0, 1.5, 2 and 5. The curves with negative $\phi$ show a behaviour similar to the

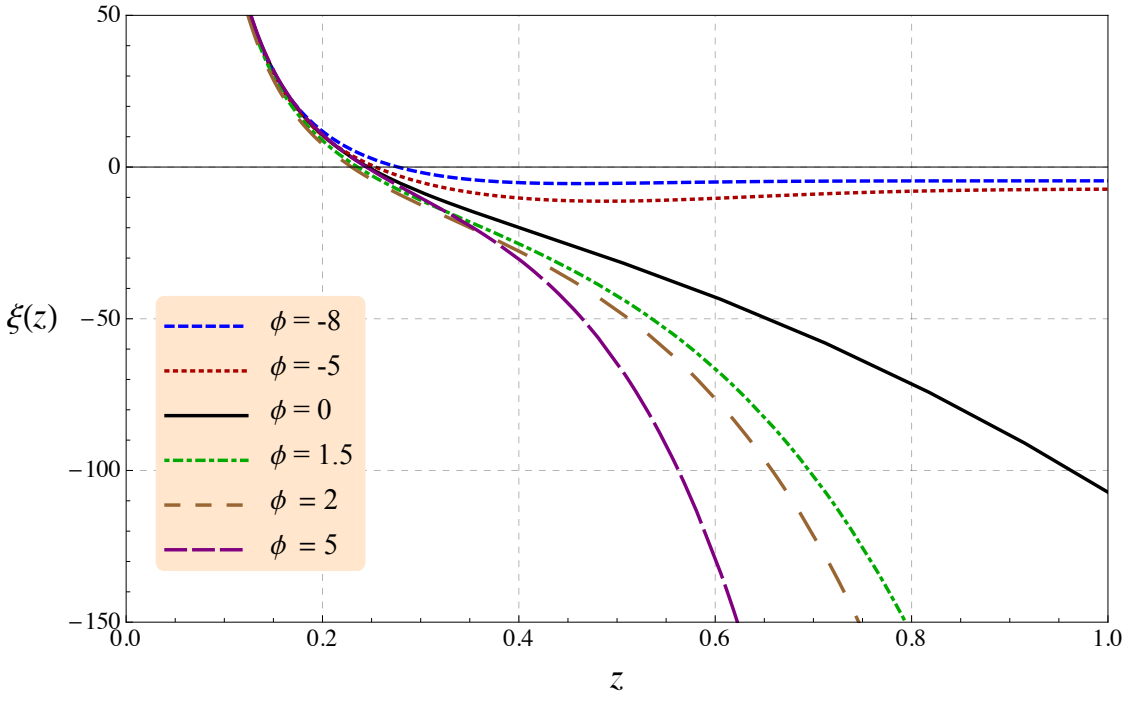


Figure 6.13: $z_{\rm c}$-defining function $\xi(z)$ in the string frame of the 1-parameter model against $z$ for fixed values of the temperature $T = 1$, angular velocity $\omega = 0.2$ and boundary radius $R_0 = 4$ and various deformation parameters $\phi$, $\phi = -8$, $-5$, 0, 1.5, 2 and 5.

previous Einstein frame case. The curves with positive values of $\phi$ are decreasing faster than the $\mathcal{N} = 4_T$ case, but all of them cross zero at some particular value of $z = z_{\rm c}$. Due to the fact that the function of the temperature remains unchanged the valid regime for the deformation is still $|\phi| < 8.6$ for $T = 1$.

The radial function can now be computed numerically and is plotted for fixed $T = 1$, $\omega = 0.2$ and $R_0 = 4$ and various deformations $\phi$, $\phi = -8, -5, 0, 1.5, 2$ and 5 in Fig. 6.14. Again,

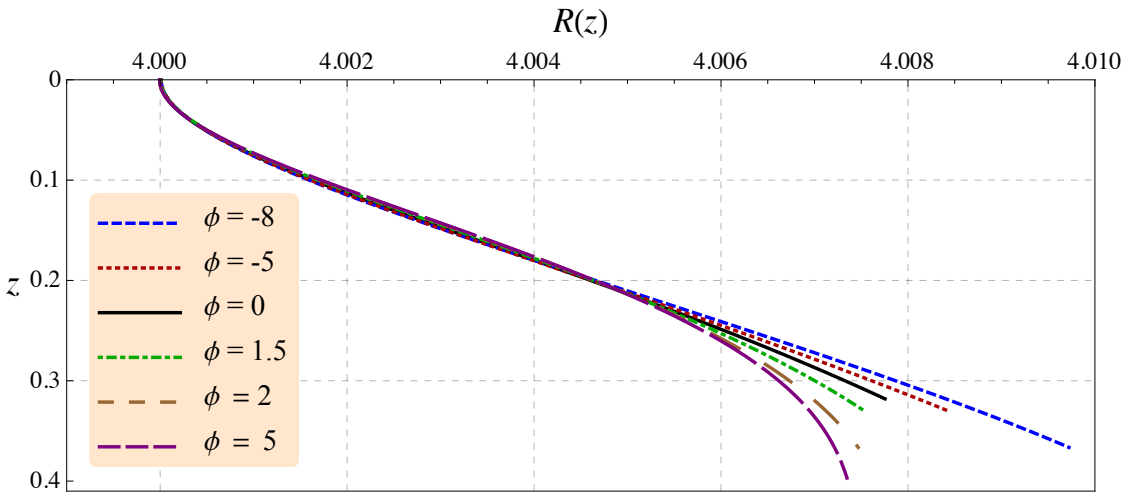


Figure 6.14: Radius function $R(z)$ in the string frame of the 1-parameter model against the $5^{\text{th}}$-dimension coordinate $z$ for fixed temperature $T = 1$, angular velocity $\omega = 0.2$ and boundary radius $R_0 = 4$ for six different values of the deformation $\phi$, $\phi = -8, -5, 0, 1.5, 2$ and 5

the string configuration is very robust, although we have small deviations at large $z$ close to the horizon. Furthermore, we have to mention that all curves cross the $\mathcal{N} = 4_T$ one. Whereas the Einstein frame has a universal increase of the radial function towards larger radii when a deformation is introduced, this behaviour cannot be reproduced in the string frame due to the crossing of the conformal curve. This is analogous to the drag force where we did not find a universal behaviour either. These drag force results will become important when focusing on the energy loss because a slowly rotating quark can be interpreted as a linearly dragged quark and should lead to the same expressions and physical results.

Now we turn to the 2-parameter model and try to verify the results we found in this section. The string configuration should be very robust again, although we have an additional free parameter. There, we will plot the total 3D string configuration of a deformed model.

### 6.3.3 2-Parameter Deformation

To keep things as simple as possible we will not quote the differential equation (6.42) which is applicable to the 2-parameter model without restrictions again and again since we just need to change the metric functions. In the 2-parameter model we have functions that depend on the scalar (dilaton) $\Phi$ which will be used as the $5^{\text{th}}$-dimensional coordinate. This has been defined in (3.48). The metric functions of this model are given in eqs. (3.47) and (3.49). The $5^{\text{th}}$-dimensional coordinate $\Phi$ should not be confused with the deformation parameter $\phi$. The deformation parameters in this case are $c$ and $\alpha \equiv c/\phi$, where $\phi$ is the deformation parameter of the last section. In the following we will derive the string configuration in the Einstein- and string frame.

### 2-Parameter Model: Einstein Frame

The initial conditions are given by the following expressions:

$$\begin{aligned}\Phi_{\rm c}\ :\quad & \xi(\Phi_{\rm c}) \equiv e^{2\,A(\Phi_{\rm c},\,\alpha,\,c)}\,h(\Phi_{\rm c},\alpha,\Phi_h) - \Pi\,\omega = 0\,,\\ R_{\rm c}\ :\quad & R_{\rm c} \equiv R(\Phi_{\rm c}) = \frac{\sqrt{h(\Phi_{\rm c},\,\alpha,\,\Phi_h)}}{\omega}\,,\end{aligned} \tag{6.47}$$

and

$$\begin{aligned}R_{\rm c}'\ :\quad & -8\,e^{2\sqrt{\frac{2}{3}}\,\alpha\,\Phi_{\rm c}+4A_{\rm c}+2B_{\rm c}}\,\alpha^2\,\Phi_{\rm c}^3\,\omega^2\,R_{\rm c} + 2c^2\,e^{2B_{\rm c}}\left(3+\sqrt{6}\,\alpha\,\Phi_{\rm c}\right)\omega\sqrt{h_{\rm c}}\\ & + 8\,e^{2\,\sqrt{\frac{2}{3}}\,\alpha\Phi_{\rm c}+6A_{\rm c}}\,\alpha^2\,\Phi_{\rm c}^3\,\omega\,h_{\rm c}^{3/2}\,A_{\rm c}'\,R_{\rm c}'^2 + c^2 e^{2\,A_{\rm c}}\left(3+\sqrt{6}\,\alpha\Phi_{\rm c}\right)h_{\rm c}\,h_{\rm c}'\,R_{\rm c} = 0\\ \Longrightarrow\quad & R_{\rm c}' = \frac{e^{-2\sqrt{\frac{2}{3}}\,\alpha\Phi_{\rm c}-6A_{\rm c}}}{16\alpha^2\,\Phi_{\rm c}^3\,\omega\,h_{\rm c}^{3/2}\,A_{\rm c}'}\left[K(\Phi_{\rm c}) - \sqrt{M(\Phi_{\rm c})+K(\Phi_{\rm c})^2}\right].\end{aligned} \tag{6.48}$$

Here, we have used the following definitions:

$$\begin{aligned}A_{\rm c} \equiv A(\Phi_{\rm c},\alpha,c)\,,\quad B_{\rm c} \equiv B(\Phi_{\rm c},\alpha,c)\,,\quad h_{\rm c} \equiv h(\Phi_{\rm c},\alpha,c)\,,\\ K(\Phi_{\rm c}) \equiv 8\,e^{2\sqrt{\frac{2}{3}}\,\alpha\,\Phi_{\rm c}+4A_{\rm c}+2B_{\rm c}}\,\alpha^2\,\Phi_{\rm c}^3\,\omega^2 - c^2\,e^{2A_{\rm c}}\left(3+\sqrt{6}\,\alpha\,\Phi_{\rm c}\right)h_{\rm c}\,h_{\rm c}'\,,\\ M(\Phi_{\rm c}) \equiv -64\,c^2\,e^{2\sqrt{\frac{2}{3}}\,\alpha\,\Phi_{\rm c}+6A_{\rm c}+2B_{\rm c}}\,\alpha^2\,\Phi_{\rm c}^3\left(3+\sqrt{6}\,\alpha\,\Phi_{\rm c}\right)\omega^2\,h_{\rm c}^2\,A_{\rm c}'\,,\end{aligned} \tag{6.49}$$

and the $'$ denotes derivatives with respect to $\Phi$. The special value $\Phi = \Phi_{\rm c}$ corresponds to $z_{\rm c}$ which we have defined in the SW$_T$-model (6.35) and in the 1-parameter model (6.43). It defines the point where the singularities in the differential equation for $R(\Phi)$ (6.42) appear.

By plotting the $\Phi_{\rm c}$-defining function $\xi(\Phi)$ we check whether the 2-parameter model contains a range of parameters that do not allow for a definition of $\Phi_{\rm c}$. Furthermore, we have again a maximal deformation for a given temperature $T$ in this model as visualised in Fig. 3.5. The results for $\xi(\Phi)$ are shown in Fig. 6.15 for fixed values of the temperature $T = 1$, angular velocity $\omega = 0.2$, deformation $\alpha = 0.2$ and boundary radius $R_0 = 4$ and various deformation parameters $c$, $c = 0.1, 0.4, 0.8, 1$ and 2. Several things have to be mentioned. Since every new choice of the deformation parameters $\alpha$ and $c$ changes the coordinates via the formula,

$$\Phi_{\rm c} \equiv \sqrt{\frac{3}{2}}\,\frac{c}{\alpha}\,z_{\rm c}^2\,, \tag{6.50}$$

we cannot compare the $\mathcal{N} = 4_T$ result with all of these curves. In principle, we should plot each of the deformed curves together with the corresponding conformal one. This is a disadvantage of the $\Phi$ gauge. By using this gauge choice every conformal $\mathcal{N} = 4_T$ curve, which has only a $T$ dependence in $z$-coordinates, is $c$ and $\alpha$ dependant due to the coordinate transformation.

For the sake of clarity, only the conformal curve for the dashed, blue line with deformation $c = 0.1$ is shown in Fig. 6.15. We can state by studying this figure that for each combination of parameters the initial value $\Phi_{\rm c}$ is perfectly determined. Some combinations are forbidden due to the lack of a well-defined temperature. This behaviour stays the same if we change $\alpha$ over a wide range of parameters. We choose $c = 2$ as the highest deformation in Fig. 6.15 because for this given set of parameters we have a maximal deformation of $c_{\rm max} = 2.45$. The existence of a

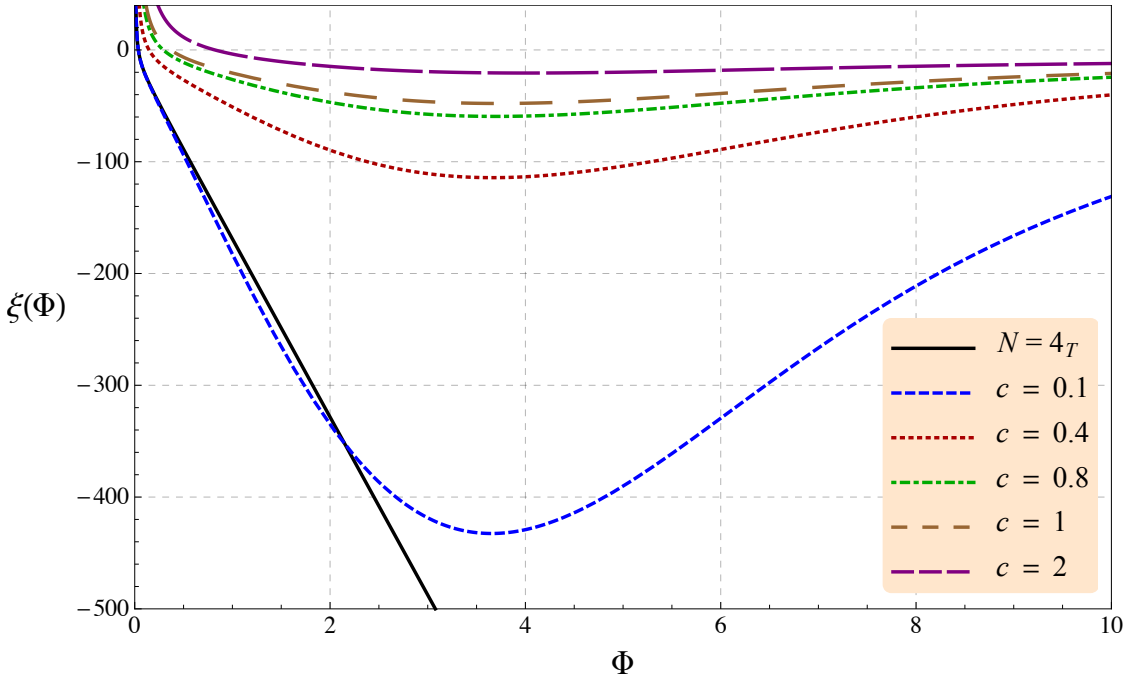


Figure 6.15: $z_c$-defining function $\xi(z)$ in the Einstein frame of the 2-parameter model against $z$ for fixed values of the temperature $T = 1$, angular velocity $\omega = 0.2$, deformation $\alpha = 0.2$ and boundary radius $R_0 = 4$ and various deformation parameters $c$, $c = 0.1, 0.4, 0.8, 1$ and 2. The solid, black line represents the $\mathcal{N} = 4_T$ computation.

maximal deformation $c_{\max}$ and $\alpha_{\max}$ for every temperature is analogous to the 1-parameter case and can be reviewed in Fig. 3.5.

In summary, we can finally argue that the non-existence of $z_c$ for several sets of parameters in the $SW_T$-model is just an artefact due to its inconsistency.

The numerical solution of the radial function $R(z)$ can now easily be computed and is shown in Fig. 6.16 in the Einstein frame of the 2-parameter model for fixed temperature $T = 1$, angular velocity $\omega = 0.2$, deformation parameter $\alpha = 0.2$ and boundary radius $R_0 = 4$ and three different values of the deformation $c$, $c = 0.4, 1$ and 2. In contrast to Fig. 6.15 all the curves are transformed into the $z$-coordinate and we can now compare all curves with each other. In particular, in this $z$-parameterisation there is only one universal $\mathcal{N} = 4_T$ curve. We argue that higher deformations lead to larger extensions in the radial direction of the string. However, the largest possible deformation is around $c_{\max} = 2.45$ and the model is, as shown in the figure, quite robust, especially if we are in the regime $0 < z < z_c$ which is physically meaningful. $z_c$ is in this figure around $z_c \approx 0.3$.

The endpoints of each curve are exactly at the respective $z_h$. The fact that they do not coincide can again explained by the $c$- and $\alpha$-dependence of the temperature leading to different values $z_h$ of the horizon.

Before we use the previous computations in order to compute the energy loss we finally focus on the string-frame computation where we just show the final results.

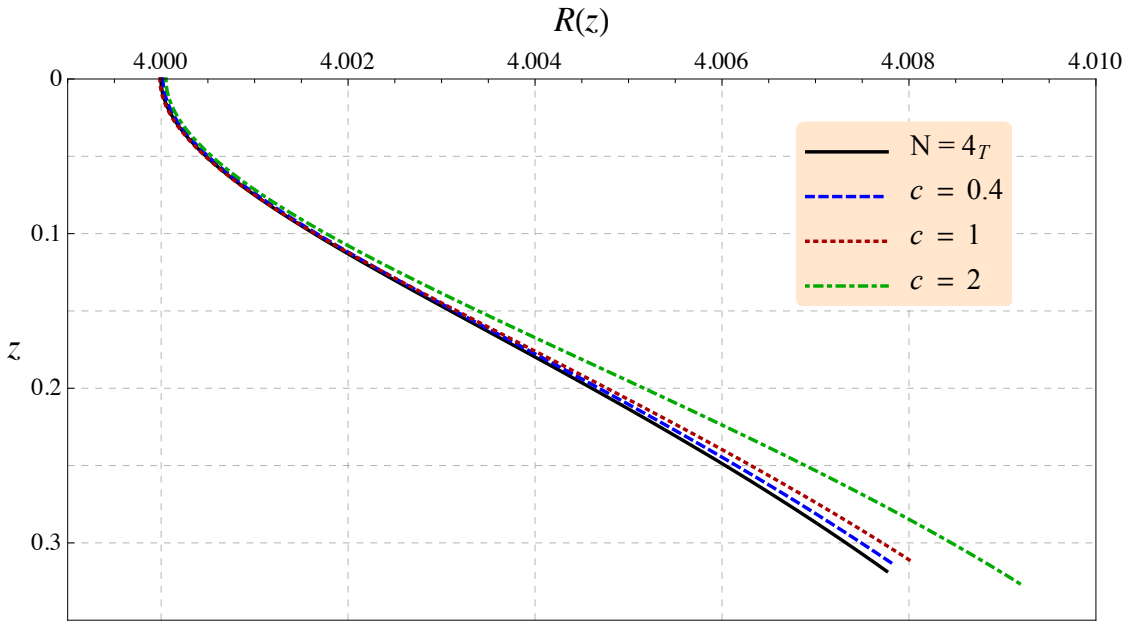


Figure 6.16: Radius function $R(z)$ in the Einstein frame of the 2-parameter model against the $5^{\text{th}}$-dimension coordinate $z$ for fixed temperature $T = 1$, angular velocity $\omega = 0.2$, deformation parameter $\alpha = 0.2$ and boundary radius $R_0 = 4$ for three different values of the deformation $c$, $c = 0.4, 1$ and 2. The black solid line represents the conformal $\mathcal{N} = 4_T$.

### 2-Parameter Model: String Frame

In the string frame the metric functions can be written as

$$A_{\text{s}} = \frac{1}{2}\log\left(\sqrt{\frac{3}{2}}\,c\frac{L^2}{\alpha}\right) - \frac{1}{2}\log\Phi + \frac{1-\alpha}{\sqrt{6}}\,\Phi\,,$$
$$B_{\text{s}} = \log\frac{L}{2} + \frac{1+2\alpha^2}{2\alpha^2}\,\log\left(1+\alpha\sqrt{\frac{2}{3}}\,\Phi\right) - \log\Phi - \frac{\Phi}{\alpha\sqrt{6}} + \frac{1}{\sqrt{6}}\,\Phi\,. \tag{6.51}$$

The initial conditions $\Phi_{\text{c}}, R_{\text{c}}, R'_{\text{c}}$ that can be computed by substituting (6.51) into (6.43) and (6.44) are well-defined and we can immediately solve the differential equation (6.42) where the metric functions of (6.51) are used. The horizon function $h(\Phi)$ and the temperature $T$ remain unchanged with respect to the Einstein frame. After transforming back into the $z$-parameterisation we plot in Fig. 6.17 the radial function $R(z)$ in the string frame of the 2-parameter model for fixed temperature $T = 1$, angular velocity $\omega = 0.2$, deformation parameter $\alpha = 0.2$ and boundary radius $R_0 = 4$ for three different values of the deformation $c$, $c = 1, 2$ and 2.44. The results are very similar to the 1-parameter case in Fig. 6.14. The curves seem again to oscillate around the conformal one. The length of each string is determined by the horizon value $z_{\text{h}}$ which reaches values lower than the $\mathcal{N} = 4_T$ one. Although many other observables that we investigated in previous chapters presented a strong deviation from the conformal values, the radial string configuration is very robust. This can also be verified by plotting the full 3D string configuration of the maximally distorted curve and $\mathcal{N} = 4_T$ in Fig. 6.18. This plot visualises the similarities of the different models. For sake of clarity we have chosen a higher angular velocity $\omega = 0.7$ than in the previous figures, a smaller temperature $T = 0.01$ and the largest possible deformation $\alpha = 0.2$ and $c = c_{\text{max}} = 0.00024$ for the chosen

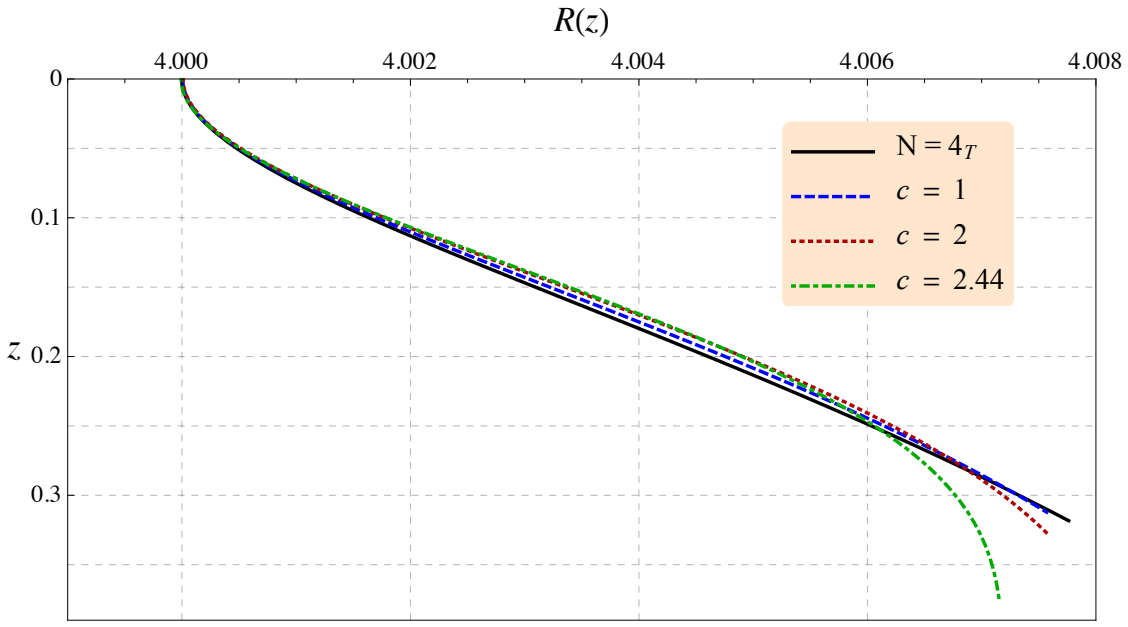


Figure 6.17: Radial function $R(z)$ in the string frame of the 2-parameter model against the $5^{\text{th}}$-dimension coordinate $z$ for fixed temperature $T = 1$, angular velocity $\omega = 0.2$, deformation parameter $\alpha = 0.2$ and boundary radius $R_0 = 4$ for three different values of the deformation $c$, $c = 1, 2$ and 2.44. The solid black line is representing the conformal $\mathcal{N} = 4_T$ result.

temperature. The small blue circle at the top is again the trajectory which the quark describes at the boundary. Although we choose almost the strongest deformation in $c$ and $\alpha$ we can barely see a deviation from the $\mathcal{N} = 4_T$ curve for small values of the $5^{\text{th}}$-dimension coordinate $z$. Furthermore, boundary quantities can only be influenced by deviations up to $z_{\text{c}}$ which is close to $z_{\text{c}} \approx 3$. The main difference between the conformal computation and the deformed case is a consequence of the different horizons $z_{\text{h}}^{\mathcal{N}=4_T}$ and $z_{\text{h}}^{\text{def}}$. They have to be different since the deformation has an impact on the temperature which has to be equal in both case. Thus, the horizon has to be adjusted.

These results give a hint for the energy loss which should be – according to this discussion – very robust in this consistent 2-parameter model. For larger values of $z$ we clearly see larger differences due to the different horizons these models define. However, the overall radial and angular deviation still remains small.

With this detailed knowledge of the string configurations in the four different models in our hand we can now derive an expression for the energy loss and try to figure out relevant deviations in comparison to the conformal case.

## 6.4 Energy Loss at High and Low Velocities

In this section we want to focus on the energy loss of a rotating quark. While a constant, linear motion is very easy to describe, it is more difficult to analyse accelerated motion, especially in non-conformal metric models. Thus, we want to tackle two main problems:

1. What are the properties of the energy loss of a moving quark with non-zero angular acceleration?

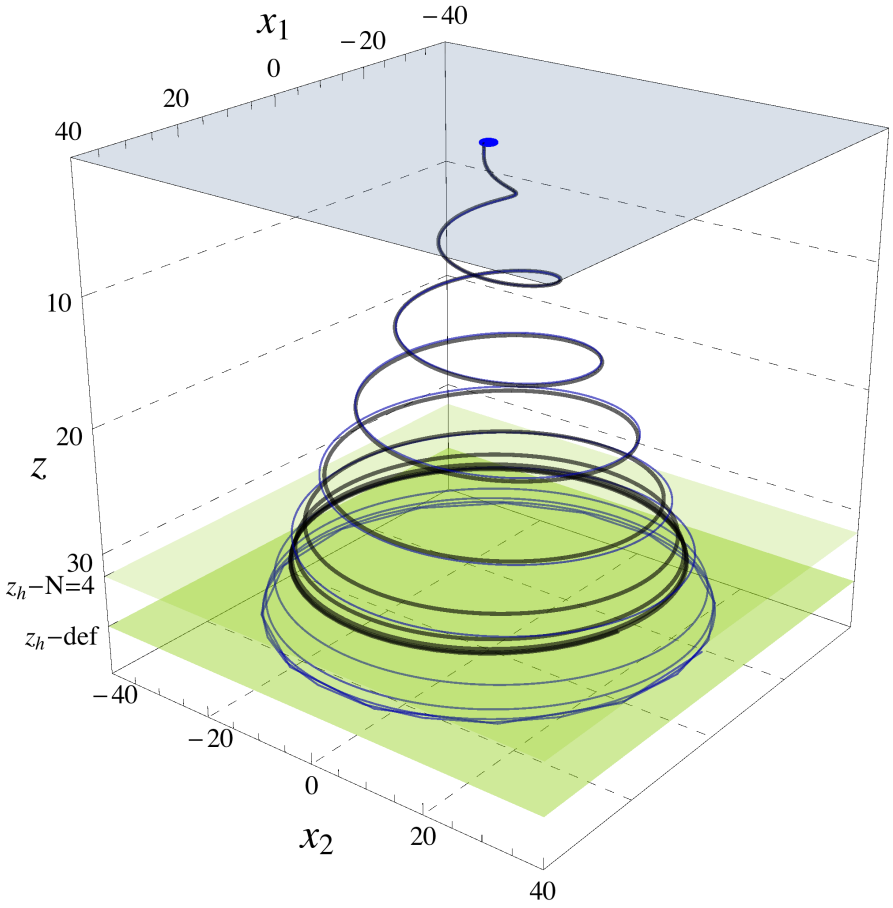


Figure 6.18: Full 3D string configuration of a 2-parameter model system (blue line) in string frame with $\alpha = 0.2$ and $c = c_{\max} = 0.00024$ together with the corresponding $\mathcal{N} = 4_T$ computation (black line) at $T = 0.01$, $R_0 = 1$ and $\omega = 0.7$.

2. How strong is the deviation in the energy loss in the transition from dragging to fast rotating quarks in non-conformal models?

A very interesting question is whether the energy loss of a highly rotating test particle can be interpreted as synchrotron radiation in vacuum although it is moving in a high-temperature plasma.

First, we derive the equation for the energy loss in a general formulation for all our metric models. The basic expression was derived by Herzog *& al.* [168] and Gubser [165] for the case of a quark moving in a straight line with constant velocity. This can be extended to other motions once the string configuration has been determined. It is in principle the same formula that we have derived in Sec. 4.2 for the trailing string. Then, an expression for the energy deposited in the medium per unit time can be given by

$$\frac{\mathrm{d}E}{\mathrm{d}t} = \mathcal{M}_t^\sigma \,, \tag{6.52}$$

where

$$\begin{aligned}\mathcal{M}_t^\sigma &= \frac{1}{2\pi\,\alpha'}\,\frac{\partial\mathcal{L}}{\partial\big(\partial_\sigma X^t\big)} \\ &= -G_{t\beta}\,\frac{\big[\partial_z X\cdot\partial_t X\big]\,\partial_t X^\beta - \big[\partial_t X\big]^2\,\partial_z X^\beta}{2\pi\,\alpha'\,\sqrt{-g}}\,. \end{aligned} \tag{6.53}$$

From the first to the second line we used the property of the Lagrangian $\mathcal{L}$ in the Nambu–Goto action of being the negative determinant of the induced two-dimensional worldsheet metric $g_{ab}$:

$$\mathcal{L} = \sqrt{-\det g_{\alpha\beta}}\,, \qquad \text{where} \qquad g_{ab} \equiv G_{\alpha\beta}\,\partial_a X^\alpha\,\partial_b X^\beta\,. \tag{6.54}$$

In (6.53) and (6.54) $G_{\alpha\beta}$ denotes the five-dimensional space-time metric which we now have to determine explicitly. In addition, the appropriate parameterisation of our rotating string has to be used. This description is equivalent to the power deposited by an external agent pulling the quark through the plasma. According to our discussion in the last sections we use the same general metric ansatz (3.25) that has been derived in Sec. 3.2.1 and which can be written as

$$\begin{aligned} \mathrm{d}s^2 &= e^{2A}\left(-h\,\mathrm{d}t^2 + \mathrm{d}\vec{x}^{\,2}\right) + \frac{e^{2B}}{h}\,\mathrm{d}z^2\,, \\ \text{with} \qquad \mathrm{d}\vec{x}^{\,2} &= \mathrm{d}R^2 + R^2\,\mathrm{d}\theta^2 + R^2\sin^2\theta\,\mathrm{d}\varphi^2\,. \end{aligned} \tag{6.55}$$

The parameterisation of the string coordinates is again given by (6.4) which we quote here for convenience:

$$X^\mu \equiv \Big(t,\, R(z),\, \frac{\pi}{2},\, \phi(z) + \omega\,t,\, z\Big)\,. \tag{6.56}$$

After computing the Lagrangian $\mathcal{L}$ we can substitute this into (6.53) and derive a compact expression for the energy loss of a rotating quark

$$\begin{aligned}\frac{\mathrm{d}E}{\mathrm{d}t} = \mathcal{M}_t^\sigma &= \frac{h(z)\,e^{2A(z)}}{2\pi\,\alpha'\,\sqrt{-g}}\,\phi'(z)\,\omega\,R^2(z)\,e^{2A(z)} \\ &= \frac{1}{2\pi\,\alpha'}\,\Pi\,\omega\,, \\ &= \frac{1}{2\pi\,\alpha'}e^{2A(z_\mathrm{c})}\,h(z_\mathrm{c})\,, \end{aligned} \tag{6.57}$$

where we used the fact that $\partial_z X^t \equiv 0$ since the $t$-component of the coordinates $X^\mu$ has no $z$-dependence. From the first to the second line we used the explicit form of the Lagrangian (6.39) and the equation of motion for the $\phi$-derivative (6.41). In the last step of the derivation in (6.57) the relationship between $\Pi\,\omega$ and $z_\mathrm{c}$ is used which has been derived in (6.43) and (6.47). The derivation of the energy loss of a rotating quark has been worked out explicitly for the $\mathcal{N} = 4_T$ case in [190] and we have extended it in (6.57) to a wider class of metric models. It is very important to note that the energy loss of a rotating quark is mainly determined by $\Pi$; for fixed angular velocity $\omega$, temperature $T$ and boundary radius $R_0$ only $\Pi$ has to be computed.

In the case of the conformal model we can simplify (6.57) even further and derive a well-known expression. By making use of

$$e^{2A(z_c)} = \frac{L^2}{z_c^2}\,, \quad h(z_c) = 1 - \frac{z_c^4}{z_h^4}\,, \quad R_c = \frac{\sqrt{h(z_c)}}{\omega}\,, \quad z_c^4\,\Pi^2 - L^4\,h(z_c)\,R(z_c) = 0\,,$$
$$\implies \quad z_c = \frac{1}{\sqrt{2}L}\sqrt{z_h^2\left(-z_h^2\,\Pi\,\omega + \sqrt{4L^4 + z_h^4\,\Pi^2\,\omega^2}\right)}\,, \tag{6.58}$$

the energy loss can be further simplified and has the form of

$$\begin{aligned}\frac{\mathrm{d}E}{\mathrm{d}t} &= \frac{1}{2\pi\,\alpha'}\,\frac{R^2(z_c)\,\omega^2\,L^2}{z_h^2\,\sqrt{1 - R^2(z_c)\,\omega^2}} \\ &= \frac{1}{2\pi\,\alpha'}\,\frac{v_c^2}{\sqrt{1-v_c^2}}\,L^2\pi^2T^2\,, \quad \text{with} \quad R_c\,\omega \equiv v_c \quad \text{and} \quad T = \frac{1}{\pi\,z_h} \\ &= \frac{\sqrt{\lambda}\,\pi}{2}\,T^2\,\frac{v_c^2}{\sqrt{1-v_c^2}}\,, \quad \text{with} \quad \alpha' = L^2\,\sqrt{\lambda}\,.\end{aligned} \tag{6.59}$$

The last line in (6.59) is exactly the energy loss of a linearly moving particle with constant velocity due to drag. However, this time the expression is not evaluated at the boundary velocity $v = R_0\,\omega$ but at the velocity $v_c = R_c\,\omega$ of the special point $z_c$ in the bulk. Thus, wherever $v_c \simeq v$, the standard linear drag result for $\mathrm{d}E/\mathrm{d}t$ is obtained. For non-conformal models we have to rely on the numerical relation between $\Pi$ and $R_0$ since no explicit expression for $z_c(\Pi,\,\omega)$ can be derived. Then we can calculate for each combination of parameters $(R_0,\,\omega,\,T)$ the corresponding energy loss.

The above result for the energy loss in $\mathcal{N} = 4_T$ leads us to the question if we can take a certain limit of our kinematic parameters in order to reach the pure drag regime. That this is indeed possible at least for the conformal case was shown in [190]. We can extend their procedure to all our non-conformal metric models. Let us start with a short review of the $\mathcal{N} = 4_T$ computation.

### 6.4.1 Linear Drag Limit

In order to obtain a purely dragging quark we should take the limit of $v = R_0\,\omega = \text{const}$ and $a = v\,\omega \to 0$. This means we keep the velocity fixed by simultaneously decreasing the angular velocity $\omega$ and increasing the boundary radius $R_0$. Thus, $R_0$ has to be proportional to $\frac{1}{\omega}$ in order not to exceed the speed of light, $c_{\text{light}} = 1$. An $\omega$-expansion of $R(z)$ and $v(z)$ has then the following form

$$\begin{aligned}R(z) &= \frac{R_0(z)}{\omega} + R_1(z) + R_2(z)\,\omega + \mathcal{O}(\omega^2)\,, \\ v(z) &= v_0(z) + v_1(z)\,\omega + v_2(z)\,\omega^2 + \mathcal{O}(\omega^3)\,, \quad \text{with} \quad v(z) = \omega\,R(z)\,.\end{aligned} \tag{6.60}$$

By substituting (6.60) into the differential equation for $R(z)$ in the conformal finite temperature case (6.23) we can extract an expression for $v_0$ in the limit $\omega \longrightarrow 0$ that is given by

$$\frac{h(z)\left(-4h(z) + 4v_0^2(z) + z\,h'(z)\right)v_0'^3(z)}{z\left(h(z) - v_0^2(z)\right)} = 0\,. \tag{6.61}$$

A solution to this equation is $v_0'(z) = 0$ for all $z$. This means that in the limit $\omega \longrightarrow 0$ the velocity is constant at all points in the bulk, in particular for $z = z_c$ leading to the final form of the energy loss in $\mathcal{N} = 4_T$:

$$v(z=0) = v_c \equiv v\,,$$
$$\left.\frac{\mathrm{d}E}{\mathrm{d}t}\right|_{\mathrm{RotQ}} = \frac{\sqrt{\lambda}\,\pi}{2}\,T^2\,\frac{v_c^2}{\sqrt{1-v_c^2}} = \frac{\sqrt{\lambda}\,\pi}{2}\,T^2\,\frac{v^2}{\sqrt{1-v^2}} = \left.\frac{\mathrm{d}E}{\mathrm{d}t}\right|_{\mathrm{Drag}}. \tag{6.62}$$

This can be visualised by taking a closer look at the radial functions $R(z)$ in all of our models. For small angular velocities $\omega$ the string is hanging almost straight down into the bulk and is curved slightly outwards close to the horizon.

The same analysis can now be done for the other metric models under investigation. We recall the general form of the drag force (4.25) which can be written as

$$\left.\frac{\mathrm{d}E}{\mathrm{d}t}\right|_{\mathrm{Drag}} = \frac{1}{2\pi\,\alpha'}\,e^{2A(z_*)}\,v^2\,, \tag{6.63}$$

where $v$ is the velocity of the moving quark at the boundary and $z_*$ is the point in the bulk where the following condition is satisfied

$$z_*: \quad h(z_*) = v^2\,. \tag{6.64}$$

By recalling the condition for $z_c$:

$$z_c: \quad h(z_c) = v_c^2\,, \tag{6.65}$$

we already see that if we could prove that $v_c = v$, then both regimes coincide. Therefore, we just have to verify again that the velocity function $v(z)$ has to have the same behaviour in the small-$\omega$ limit as the conformal model. Since the discussion in the last section showed the robustness of the string configuration in strongly deformed models, we expect that the substitution of $v(z)$ (6.60) into the differential equation (6.42) leads to a condition similar to the conformal case (6.61). And indeed, we find

$$e^{2A(z)-2B(z)}\,\frac{h(z)\left(4h(z)A'(z) - 4v_0^2(z)A'(z) + h'(z)\right)v_0'^3(z)}{2\left(h(z)-v_0^2(z)\right)} = 0\,. \tag{6.66}$$

Here, $A(z)$ and $B(z)$ represent general metric functions which can be identified for example with (6.40) and (6.45) for the 1-parameter model in Einstein and string frame or with (3.47) and (3.49) for the 2-parameter model in each frame.

We note by studying (6.66) that the exact form of the metric functions is not relevant and that the unique solution is again $v(z) = \text{const}$ for all values of $z$. Thus, we can state that in systems with a non-conformal metric the linear-drag regime of each model can be obtained by taking the limit $\omega \longrightarrow 0$ and $R_0 \longrightarrow \infty$ keeping $v = R_0\,\omega$ constant.

Fadafan *& al.* mentioned in [190] for the conformal $\mathcal{N} = 4_T$ case that it is not sufficient to take just the limit of angular acceleration going to zero because they could find a deviation from the drag result for fixed angular velocity at very low radii, although the angular acceleration $a = R_0\,\omega^2$ should be very small at this point. That these limits are not sufficient remains true after including deformations which can be verified in Fig. 6.19 where we plotted the ratio $\Pi/\Pi_{\mathrm{Drag}}$ versus $R_0$ for a fixed deformation $\phi = 8$ and temperature $T = 1$ in the 1-parameter

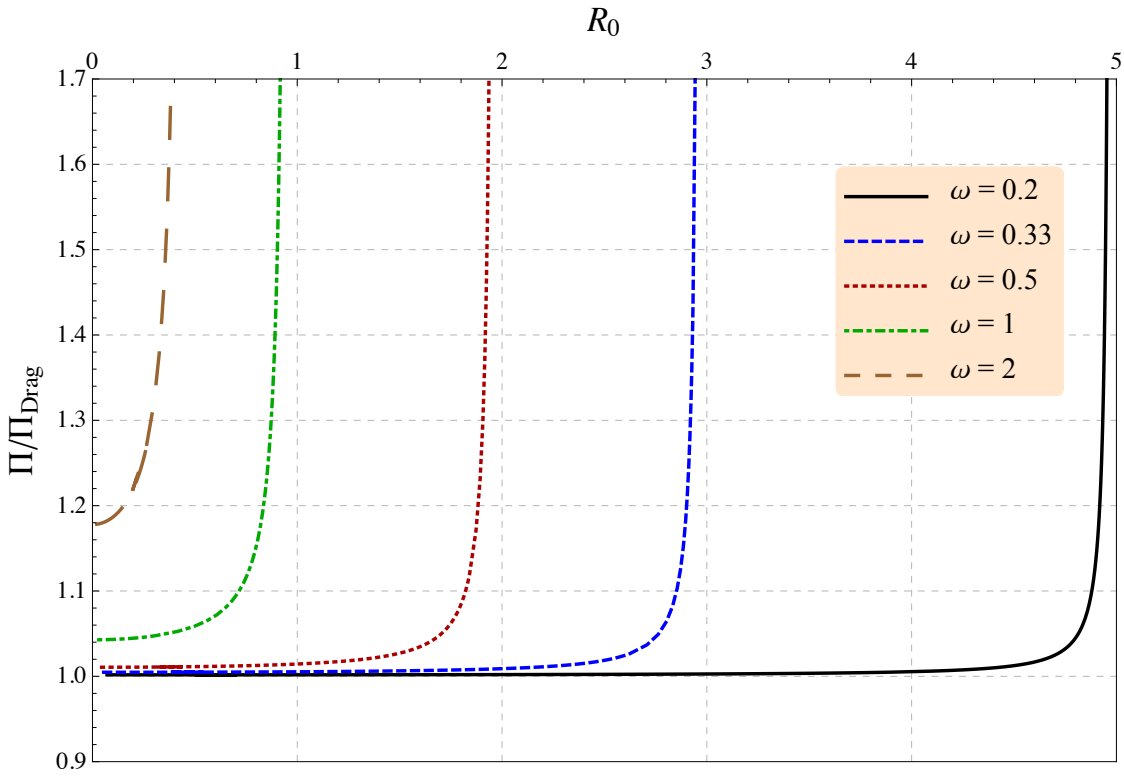


Figure 6.19: Ratio $\Pi/\Pi_{\text{Drag}}$ against $R_0$ in the Einstein frame of the 1-parameter model for a fixed deformation $\phi$, $\phi = 8$ and temperature $T$, $T = 1$ and several values of $\omega$, $\omega = 0.2, 0.33, 0.5, 1$ and 2.

model and several values of $\omega$, $\omega = 0.2, 0.33, 0.5, 1$ and 2. Here, $\Pi_{\text{Drag}}$ is just the drag force in the 1-parameter model. For convenience it is presented again in (6.67). Remember that (6.57) told us that the knowledge of $\Pi$ is enough to determine the energy loss for fixed angular velocity.

The computation of $\Pi/\Pi_{\text{Drag}}$ is not very complicated in the 1-parameter case. For given parameters ($\Pi$, $\omega$, $T$, $\phi$) we can use our numerical routine to calculate $R_0$. The denominator which is essentially (6.63) can be simplified in the 1-parameter model and has the following form

$$\begin{aligned} \left.\frac{\mathrm{d}E}{\mathrm{d}t}\right|_{\text{Drag}} &\equiv \frac{1}{2\pi\alpha'}\,\Pi_{\text{Drag}}\,\omega \equiv \frac{1}{2\pi\alpha'}\,e^{2A(z_*)}\,v^2 \\ &= \frac{L^2}{2\pi\alpha'}\,\frac{v^2}{z_*^2}\,, \quad \text{with} \quad v^2 = h(z_*)\,. \end{aligned} \tag{6.67}$$

The defining condition for $z_*$ can be solved analytically for $z_*$ and thus we have

$$\frac{\Pi}{\Pi_{\text{Drag}}} = \frac{\Pi\,\omega}{\phi\,(R_0\,\omega)^2}\,\sqrt{z_{\text{h}}^4\,\phi^2 - 4\log\left[1 + \left(-1 + \mathrm{e}^{\frac{z_{\text{h}}^4\,\phi^2}{4}}\right)(R_0\,\omega)^2\right]}\,. \tag{6.68}$$

Now we can understand the different curves in Fig. 6.19. In the case of small $\omega$ the ratio is 1 for nearly all values of $R_0$. This means that the energy loss of a rotating quark is identical to the energy loss of uniformly moving quark. This has been derived analytically at the beginning of this section.

For $\omega > 1$ (green and brown curve) it is not possible to decrease $R_0$ that far in order to reach the pure drag regime. This is indeed a very peculiar behaviour since the acceleration $a = R_0\,\omega^2$ goes to zero in the limit of $R_0 \to 0$. In addition, we see in Fig. 6.19 that at large radii for all values of $\omega$ we are definitely not in the drag regime anymore because the quark is now rotating on a circle with nearly the speed of light. This explains the sharp increase of all curves at large $R$.

We have to figure out in the next subsection if the regime at very large $R$ can be explained by synchrotron radiation. The problem of not being in the drag regime for $a$ going to zero while keeping $v$ fixed can be solved in $\mathcal{N} = 4_T$ – according to Fadafan *& al.* – by imposing a new condition that defines a new valid drag regime. We will focus on this condition after taking a closer look at the naive vacuum radiation regime (large $\omega$, small $R_0$) and try to figure out if it remains true in non-conformal models. A last thing we want to discuss is the robustness of the vacuum-radiation regime with respect to the deformation parameter $\phi$. Variation over the whole possible range of $\phi$-values will not lead to a visible change in the ratio $\frac{\Pi}{\Pi_{\text{VacRad}}}$. Here, $\Pi_{\text{VacRad}}$ denotes the energy loss of $\mathcal{N} = 4$ at zero temperature. This will be explained in full detail in the next section.

### 6.4.2 Vacuum-Radiation Limit

In this subsection we want to investigate if the fast moving regime $a = v\,\omega \longrightarrow \infty$, or equivalently, $R_0 \longrightarrow 0$ and $\omega \longrightarrow \infty$ can be described in terms of synchrotron radiation in vacuum of $\mathcal{N} = 4$. This is the case in finite temperature $\mathcal{N} = 4$ which has been shown by Fadafan *& al.* in [190].

In order to compare our computation with vacuum-synchrotron radiation we use the $\mathcal{N} = 4$ result at zero temperature of Mikhailov [217] which can be written in a very compact form given by

$$\left.\frac{\mathrm{d}E}{\mathrm{d}t}\right|_{\text{VacRad}} \equiv \frac{\sqrt{\lambda}}{2\pi}\,\frac{\vec{a}^{\,2} - (\vec{a}\times\vec{x})^2}{(1-v^2)^3}\,. \tag{6.69}$$

This expression is true for arbitrary accelerations and is indeed equivalent to Liénard's result for electromagnetic radiation from an accelerating charge [218] upon replacing $2e^2/3$ – with $e$ being the electric charge – in the latter by $\sqrt{\lambda}/(2\pi)$. For the case of circular motion (6.69) is given by

$$\left.\frac{\mathrm{d}E}{\mathrm{d}t}\right|_{\text{VacRad}} = \frac{\sqrt{\lambda}}{2\pi}\,\Pi_{\text{VacRad}}\,\omega = \frac{\sqrt{\lambda}}{2\pi}\,\frac{\vec{a}^{\,2}\,(1-v^2)}{(1-v^2)^3} = \frac{\sqrt{\lambda}}{2\pi}\,a^2\,\gamma^4\,, \tag{6.70}$$

where

$$\gamma = \frac{1}{\sqrt{1-v^2}}\,, \quad \text{and} \quad a = v\,\omega = R_0\,\omega^2\,. \tag{6.71}$$

With the help of (6.70) we are now in the position to define the ratio $\frac{\Pi}{\Pi_{\text{VacRad}}}$ in the high-$\omega$ regime that can be written as

$$\frac{\Pi}{\Pi_{\text{VacRad}}} = \frac{\Pi}{(R_0\,\omega)^2\,\omega}\left(1-(R_0\,\omega)^2\right)^2\,. \tag{6.72}$$

Again, we compute $\Pi$ for a given choice of our parameters ($R_0$, $\omega$, $T$) in the 1-parameter model and plot the ratio $\frac{\Pi}{\Pi_{\text{VacRad}}}$ for the 1-parameter model in Einstein frame in Fig. 6.20 for fixed

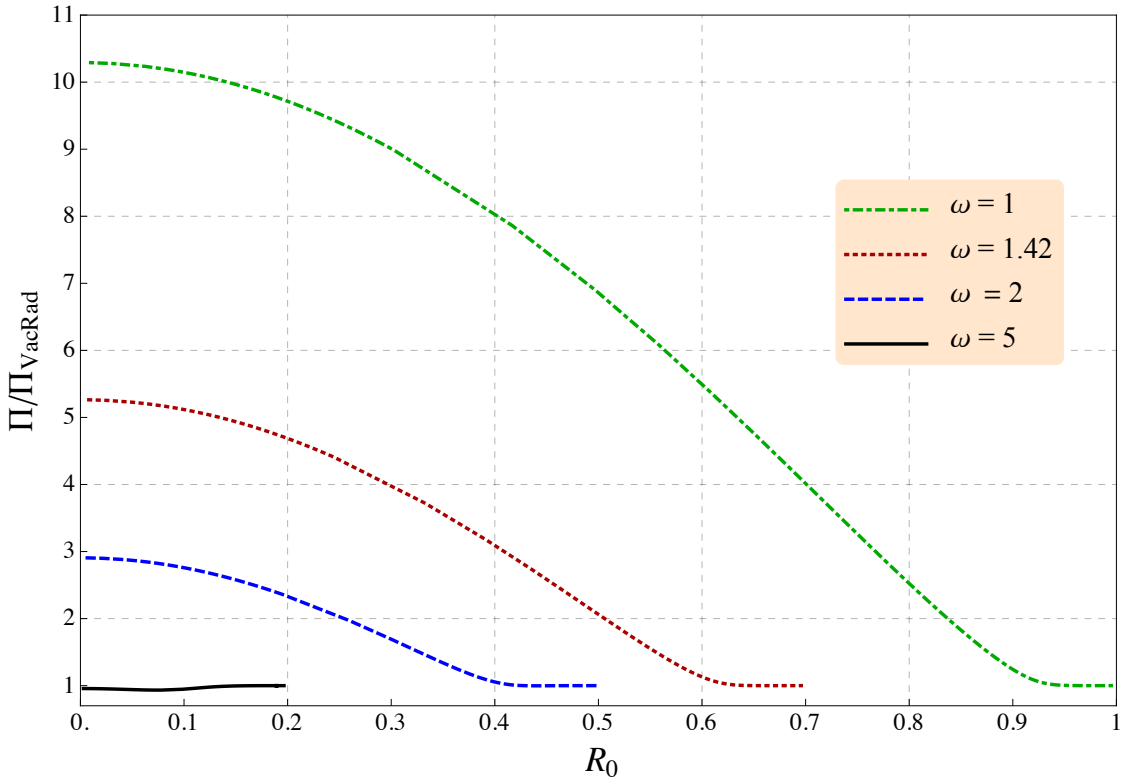


Figure 6.20: Ratio $\Pi/\Pi_{\rm VacRad}$ against $R_0$ in the Einstein frame of the 1-parameter model for a fixed deformation $\phi$, $\phi = 8$ and temperature $T$, $T = 1$ and several values of $\omega$, $\omega = 1, 1.42, 2$ and 5.

deformation $\phi = \phi_{\rm max}$, temperature $T = 1$ and several values of $\omega$, $\omega = 1, 1.42, 2$ and 5. We have tested all the computations in the other non-conformal metric models but the results are qualitatively the same. Thus, for sake for clarity we focus on the 1-parameter model in Einstein frame only.

For large values of $\omega$ we note that the ratio is close to 1 for all values of the boundary radius $R_0$. This means that the energy loss in the highly deformed model is identical to the energy loss due to vacuum-synchrotron radiation in a conformal $\mathcal{N} = 4$ computation at zero temperature. This is a very peculiar behaviour that leads to the following questions:

1. Why does the energy loss of a rotating quark show a vacuum-radiation behaviour although we are in the regime of finite temperature? Is this behaviour also true at high $T$?

2. Why is this ratio $\phi$-independent? $\Pi$ is computed at very high deformations in the 1-parameter model but $\Pi_{\rm VacRad}$ is the $\mathcal{N} = 4$ value at zero temperature.

Before we try to answer these questions we further note that – according to Fadafan *& al.* [190] – the limit of high acceleration $a = v\,\omega$ is not enough to produce pure vacuum radiation because for small values of $\omega$ ($\omega \sim 1$) the green curve is not close to unity although we are at sufficiently high $R_0$. This can be observed in Fig. 6.20. Only close to the speed of light $v = 1$ the energy loss is due to vacuum radiation. Thus, a new condition is needed to distinguish the drag- and vacuum-radiation regimes. After answering the above questions we will address this

issue in section 6.4.3 which will not only give us the right description of the validity of both limits, but furthermore allows us to access the cross-over regime.

We give now a partial explanation for the phenomenon that in the acceleration-dominated regime, $\mathrm{d}E/\mathrm{d}t$ is as it would be in vacuum although a high deformation is considered. To this end, we plot in Fig. 6.21(a) the radial function $R(z)$ against $z$ in the Einstein frame of the 1-parameter model for two different temperatures $T$, $T = 1$ and 5 and two deformations $\phi$, $\phi = 0$ ($\mathcal{N} = 4_T$) and $\phi_{\max}$. To ensure that our setup is located deeply in the vacuum-radiation regime we used $R_0 = 0.2$ and $\omega = 4$ which leads to a $\Pi/\Pi_{\mathrm{VacRad}}$ ratio close to unity as visualised in Fig. 6.20. Here, we can argue that the energy loss of the finite temperature, conformal $\mathcal{N} = 4_T$ case (solid, black line) is equal to the highly deformed configuration (dashed, blue line) since the depth $z_{\mathrm{c}}$ in the bulk up to which we have to integrate in order to determine the energy loss is almost identical. This is remarkable since both string configurations are quite different, especially, when we consider the string configuration at large $z > z_{\mathrm{c}}$. However, up to $z_{\mathrm{c}}$ the dashed, blue string in Fig. 6.21(a) has not yet developed its deviation from $\mathcal{N} = 4_T$ and thus leads to the same result for the energy loss. This discussion nicely explains the $\phi$-independence of the vacuum-radiation regime. So, the kinematic effect that higher rotation leads to a smaller value of $z_{\mathrm{c}}$ decreases the influence of any kind of deformation. This behaviour is indeed universal and can be seen in the 2-parameter model as well.

That this universal behaviour does not appear in the linear drag regime is visualised in Fig. 6.21(b) where the radial function $R(z)$ is plotted against $z$ in the Einstein frame of the 1-parameter model for the maximal deformation $\phi_{\max}$ and in the conformal $\mathcal{N} = 4$ case for fixed boundary radius $R_0 = 4$, angular velocity $\omega = 0.2$ and two different temperatures $T$, $T = 1$ and 5. The black and blue points denote again the value of $z_{\mathrm{c}}$ up to which the bulk influences the boundary. This choice of $\omega$ and $R_0$ is located deep in the linear-drag regime as shown in Fig. 6.19. In contrast to the vacuum-radiation discussion, $z_{\mathrm{c}}$ is now totally different in the conformal $\mathcal{N} = 4_T$ case and the deformed scenario. Thus, the energy loss noticeably differs in both models in the linear-drag regime. In addition to this, we note that at high enough temperatures the effect of deformations weakens since the horizon is now very close to the boundary and the string cannot develop any deviation from the conformal scenario.

After we have explained the $\phi$-independence of the vacuum-radiation regime and the strong $\phi$-sensitivity of the linear-drag regime, we can now address the first question raised at the beginning of this subsection. In Fig. 6.21(c) the radial function $R(z)$ is plotted against $z$ for $\mathcal{N} = 4$ at finite (coloured lines) and zero temperature (black, solid line) for fixed values of the angular velocity $\omega$, $\omega = 4$, and boundary radius $R_0$, $R_0 = 0.2$. So we are deep in the vacuum-radiation regime but without any deformation switched on.

Here, we can argue that for small temperatures ($\mathrm{T} \sim 1$) the energy loss is indeed due to vacuum-radiation because both curves and the corresponding values of $z_{\mathrm{c}}$ are nearly identical at least up to $z_{\mathrm{c}}$ which is enough in order to compute the energy loss. However, we have to admit that for very high temperatures ($T \approx 5$) the energy loss is not like vacuum radiation. The agreement between $\mathcal{N} = 4$ vacuum radiation and (deformed), high-$T$ computations is better for higher angular velocities $\omega$ since $z_{\mathrm{c}}$ is closer to the boundary. Thus, there has to be a relation between $\omega$ and $T$ that allows us to specify whether our string is located in the vacuum-radiation regime or not. This will be derived in the next section (6.4.3) and the relation we are looking for is given in (6.76). A comparison of $\mathcal{N} = 4$ with and without temperature in the linear drag regime is illustrated in Fig. 6.4.

In summary, we can state that the deformation can be neglected if the quark is deep in the regime of vacuum radiation. This seems to be true for all models ($\mathrm{SW}_T$, 1- and 2-parameter)

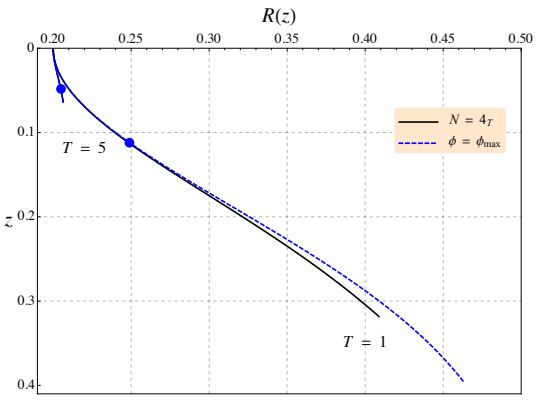


(a) Radial function $R(z)$ against $z$ for two different temperatures $T$, $T = 1$ and 5 in a conformal and highly deformed configuration in the Einstein frame of the 1-parameter model with $R_0 = 0.2$ and $\omega = 4$. The $T = 5$ curves almost overlap. All these strings are deep in the vacuum radiation regime. The black and blue dots – which are lying nearly on top of each other – denote the special point $z_c$ where the upper and lower parts of the string are causally disconnected.

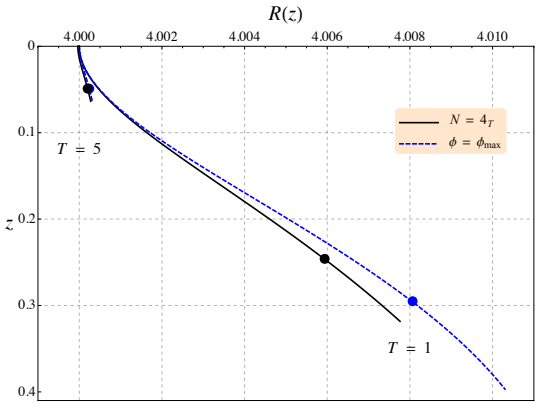


(b) Radial function $R(z)$ against $z$ for two different temperatures $T$, $T = 1$ and 5 in a conformal and highly deformed configuration in the Einstein frame of the 1-parameter model with $R_0 = 4$ and $\omega = 0.2$. This string is deep in the linear drag regime.

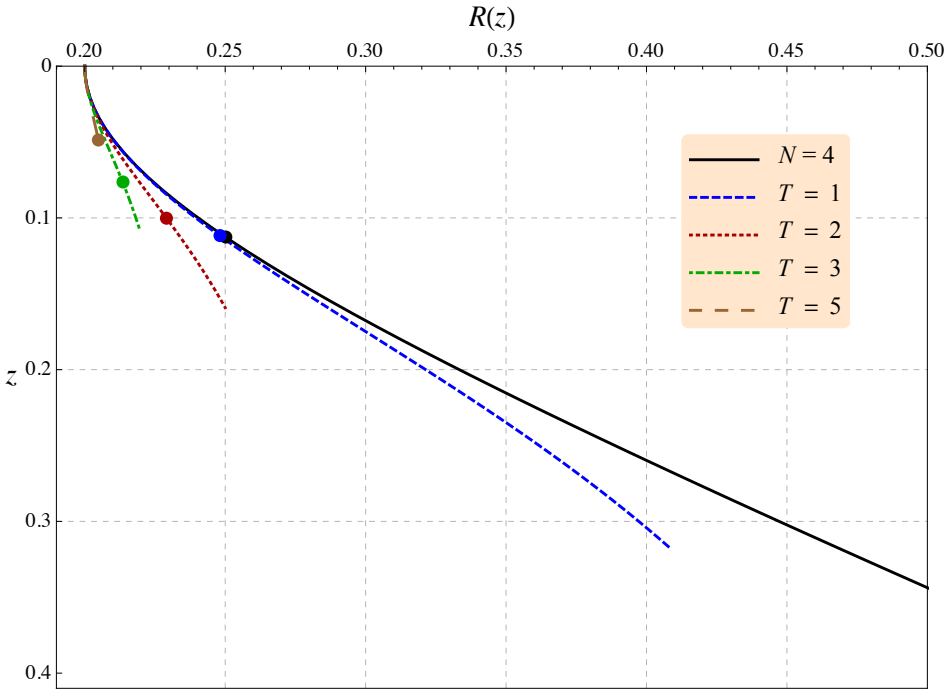


(c) Radial function $R(z)$ against $z$ for $\mathcal{N} = 4$ at finite (coloured lines) and zero temperature (black, solid line) for a fixed values of the angular velocity $\omega$, $\omega = 4$ and boundary radius $R_0$, $R_0 = 0.2$ These string configurations are deep in the vacuum radiation regime.

Figure 6.21: Comparison of the vacuum radiation and the linear drag regime at different temperatures and deformations. The coloured dots denote the values of $z_c$ where the upper and lower parts of the string are causally disconnected.

we have studied. Nevertheless, the linear drag regime gets strongly shifted by a deformation. In the next section we now focus on the problem which limit has to been taken in order to enter the linear drag or vacuum radiation regime. This finally leads to a $\omega$-$T$ relation.

### 6.4.3 Crossover Regime

The criterion for the validity of the vacuum-radiation approximation applied to our non-conformal models for the energy loss of the rotating quark is not simply $a \longrightarrow \infty$. It turns out that we should directly relate the angular velocity $\omega$ to the velocity $v$ or the boundary radius $R_0$. The question we should ask is which of the two processes of energy loss $\mathrm{d}E/\mathrm{d}t$ is dominant.

It turns out that

$$\left.\frac{\mathrm{d}E}{\mathrm{d}t}\right|_{\mathrm{VacRad}} \gg \left.\frac{\mathrm{d}E}{\mathrm{d}t}\right|_{\mathrm{Drag}}, \tag{6.73}$$

leads to an appropriate relation between $\omega$, $T$ and $R_0$ telling us when we are located in each of the different regimes. This has been figured out in the conformal $\mathcal{N} = 4_T$ case by Fadafen *& al.* in [190] and as we will show in the following this relation is also valid in the case of highly deformed metric models. The notation in (6.73) can be related to the corresponding values of $\Pi$ as we have derived in (6.57). Equation (6.73) then reads in a general deformed metric model

$$\begin{aligned} \Pi_{\mathrm{VacRad}} \gg \Pi_{\mathrm{Drag}} \quad &\Longleftrightarrow \quad v^2\,\omega\,\gamma^4 \gg \frac{v^2}{z_*^2\,\omega} \\ \text{Vacuum radiation}: \quad &\gamma^2\,\omega\,z_* \gg 1\,, \\ \text{Linear drag}: \quad &\gamma^2\,\omega\,z_* \ll 1\,. \end{aligned} \tag{6.74}$$

Here, $z_*$ denotes again the point where the velocity $v$ of the string in the drag-force computation reaches the local speed of light $c_{\mathrm{bulk}}$ at that depth in the bulk. $z_*$ was defined in (6.67).

Relation (6.74) is the natural generalisation of the $\mathcal{N} = 4_T$ computation of Fadafen *& al.* in [190] to non-conformal metric models with arbitrary metric functions $A$ and $B$. In order to see that (6.74) reduces to the known $\mathcal{N} = 4_T$ case we take the conformal limit of $\phi \longrightarrow 0$. Then (6.74) for the vacuum-radiation regime reads

$$\begin{aligned} z_* \xrightarrow{\phi\to 0} (1-v^2)^{1/4}\,z_{\mathrm{h}} &= \frac{\gamma^{-1/2}}{\pi T} \\ \Longrightarrow \quad \frac{\omega^2\,\gamma^3}{\pi^2 T^2} &\gg 1\,, \end{aligned} \tag{6.75}$$

which is exactly the conformal expression that has been derived in [190]. Although the deformation has in general an influence on the shape of the string and on the linear drag regime of the energy loss, we discussed in the last paragraph that the vacuum radiation regime is $\phi$-independent. Thus, we can take the limit in (6.75) and state that this condition for being in the vacuum-radiation regime should be valid in the case of highly deformed metric models as well. We end up with the desired relation between $T$ and $\omega$. Equation (6.75) can be rewritten in the form

$$\omega \gg \left(1-v^2\right)^{3/4}\pi\,T\,. \tag{6.76}$$

Therefore, we can state that $\omega \gg \pi T$ or $\omega \gg \left(1-v^2\right)^{3/4}$ is a good condition for vacuum radiation even in the highly deformed models. To fulfil this condition a large value of $R_0$ or a large $\omega$ in comparison to $T$ directly leads into the vacuum radiation regime. This is confirmed in our Figs. 6.19, 6.20 and 6.21(c).

Let us now turn back to the visualisation of both regimes in one figure. We plot $\frac{\Pi\,\omega\,z_*^2}{v^2}$ over $\gamma^4\,\omega^2\,z_*^2$ in Fig. 6.22 in the Einstein frame of the 1-parameter model for fixed temperature $T$, $T=1$ and deformation $\phi$, $\phi=8$ and several values of $\omega$, $\omega=0.02, 0.2$ and 2. This is nothing else than a plot of $\Pi_{\text{Rot}}/\Pi_{\text{Drag}}$ over $\Pi_{\text{VacRad}}/\Pi_{\text{Drag}}$. Thus it is clear that in the drag regime

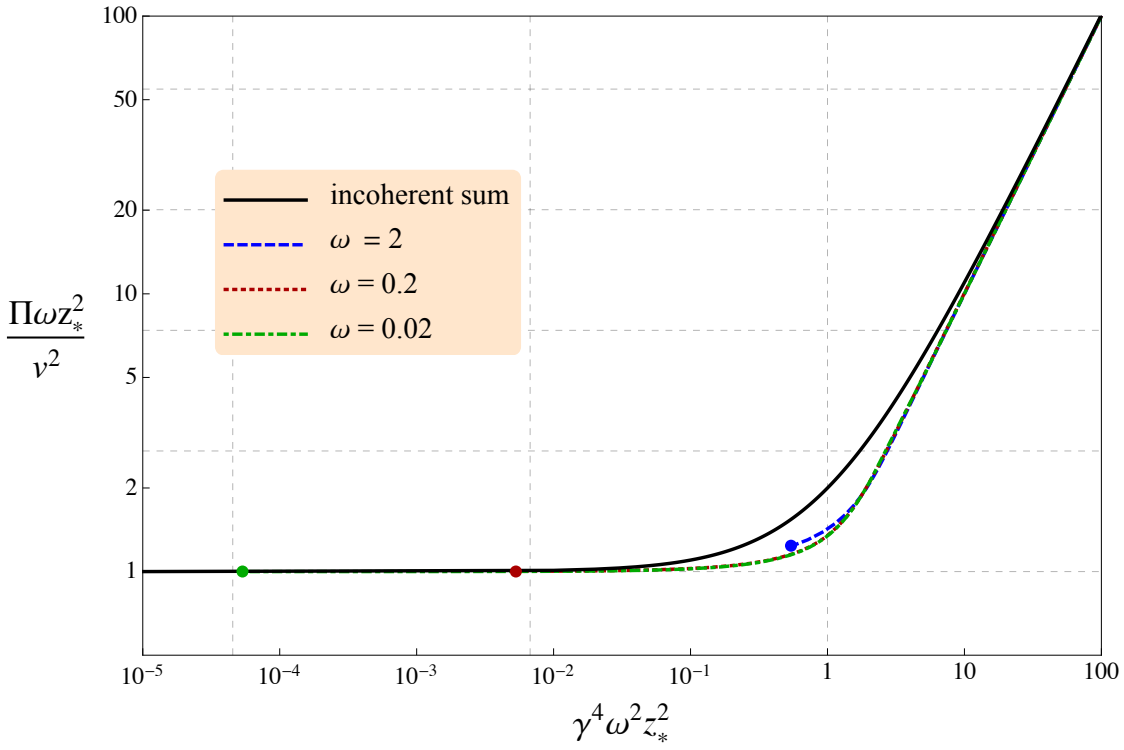


Figure 6.22: Combination $\Pi\,\omega\,z_*^2/v^2$ against $\gamma^4\,\omega^2\,z_*^2$ in the Einstein frame of the 1-parameter model for fixed temperature $T$, $T=1$ and deformation $\phi$, $\phi=8$ and several values of $\omega$, $\omega=0.02, 0.2$ and 2. The solid line represents the incoherent sum of the drag and vacuum-radiation regime.

the function $\Pi\,\omega z_*^2/v^2$ is 1 and linear in the radiation dominated regime, since in the first case $\Pi_{\text{Rot}}$ is almost $\Pi_{\text{Drag}}$ and in the latter case it is almost $\Pi_{\text{VacRad}}$.

The solid black line in Fig. 6.22 denotes the incoherent sum $\Pi\omega\big|_{\text{IncSum}} = \Pi\omega\big|_{\text{Drag}} + \Pi\omega\big|_{\text{VacRad}}$ that has been plotted in [190] for the first time. As in the conformal case we can state that general deformations lead to negative interference. In addition to this, our results illustrate that the analysis of the energy loss of rotating quarks in hot non-conformal plasmas allows us to study the crossover from a linear drag dominated to an acceleration dominated regime in a computation that is valid in both regimes. The main point is that we cannot only derive each regime but we have full control of the cross-over regime. We clearly see that the energy loss is dominated by linear drag when $\gamma^2\,\omega\,z_* \ll 1$ and by radiation as if in vacuum when $\gamma^2\,\omega\,z_* \gg 1$. Furthermore all curves are very robust when different values of the angular velocity $\omega$ are chosen.

Two interesting points have to be stated. First, we observe that all the curves for different

$\omega$ come very close to lying on a single universal scaling curve even in the crossover regime. This is still not fully understood in a conformal system and remains very complicated in a highly non-conformal model. For the sake of clarity we did not plot other curves with the deformation parameter $\phi$ changed in this figure because the deviation is not visible. The endpoints of each curve can be understood as the points where the velocity $v$ is zero and $\gamma = 1$ for a fixed angular velocity $\omega$. Each curve then extends arbitrarily far to the right as $\gamma$ increases. Similar to the change of deformation a change of temperature within a certain regime would not dramatically change the curves. Thus, we find another argument for the robustness of the energy loss of rotating quarks in hot, non-conformal plasmas.

Fadafan *& al.* [190] have tried to give a more physically motivated explanation for the fact that in the acceleration-dominated regime $\mathrm{d}E/\mathrm{d}t$ is as it would be in vacuum. In QED one would expect that the spectrum of synchrotron radiation rises for larger frequencies $\omega$ until a critical value of $\omega = \omega_\mathrm{c}$ is reached and falls off exponentially for even larger $\omega$. The critical frequency is given by

$$\omega_\mathrm{c} = 3\gamma^3\,\omega\,. \tag{6.77}$$

This can interpreted as follows: Small frequencies do not contribute to the radiative energy loss since almost all energy is carried by radiation modes $\omega$ of order $\omega_\mathrm{c}$. Thus, in QED, a plasma with temperature $T$ has no influence on the radiation whenever $\omega_\mathrm{c} \gg \pi T$ [190]. This condition is fulfilled in the acceleration-dominated regime as shown in (6.76) and tempts us to argue that $\mathrm{d}E/\mathrm{d}t$ for a rotating quark is as it would be in vacuum. However, it is questionable whether we can apply QED results to our strongly coupled plasma that contains coloured excitations. Although the differences between Liénard's result in QED and Mikhailov's one (6.70) for radiation of an accelerating charge in $\mathcal{N} = 4$ is only the coupling constant, we have on one hand a weakly coupled plasma (QED) and on the other hand a strongly coupled one ($\mathcal{N} = 4$). The radiation in the weakly coupled QED plasma consists neutral photons, whereas the latter has a synchrotron radiation which is composed of coloured excitations. Since the plasma carries colour as well the coloured excitations will not propagate for times large compared to the inverse of the temperature due to a strong quenching by the plasma. Fortunately, this is exactly what we see. Although the rotating quark is emitting synchrotron radiation as in vacuum, in the acceleration-dominated regime, the energy that the quark deposits in the plasma is different than that of synchrotron radiation in vacuum. By going back to Fig. 6.2 where $\mathcal{N} = 4$ at zero temperature is shown we note that the rotating string extends out to $R \longrightarrow \infty$ indicating that the radiated energy propagates to infinity. In the finite temperature regime – with or without deformation – the string approaches the horizon and coils on top of itself over and over and the radius remains finite. Thus, the energy is deposited in the plasma within a certain, finite radius. This nicely agrees with the physical interpretation of Fadafan *& al.* [190] we have mentioned above.

With the results derived in the current chapter we close the computational paragraphs in this thesis and draw some conclusions in the last chapter. There, we summarise the different behaviours (universality and robustness) of the observables under investigation.

Chapter 7

# Summary and Conclusions

Before concluding what this thesis has achieved we have to summarise the main results of the last chapters first. Therefore, we have to recall the three main questions this work was driven by which have been posed at the beginning:

1. RHIC and the LHC provide us with data of a strongly coupled, expanding, hot quark-gluon plasma and many standard methods are insufficient to explain all the phenomena that arise in the experiments. Is there a way to apply the theoretical framework of gauge/gravity dualities in order to gain insights into how matter behaves under these extreme conditions?

2. Gauge/gravity dualities are very helpful in various fields. In the realm of relativistic, strongly coupled, finite temperature systems many realisations of the holographic principle are known. They can be applied to several physical systems from ultracold atomic gases to hot, dense plasmas. Do many of these different systems share the same collective phenomena and is there a way to extract a universal behaviour by studying gauge/gravity dualities?

3. Is there a way to mimic QCD in the regime of strong coupling and finite temperature and maybe even finite density by finding appropriate holographic models?

As the second question already states, the range of physical systems that can be tackled with a gauge/gravity approach is considerably large. Apart from the prototype realisation of the holographic principle that we are using in order to study strongly coupled gauge theories at finite temperatures, $AdS$/CFT frameworks have been developed to study e. g. superconductors [219–223], non-relativistic systems [216, 224–229], relativistic fluids [127, 128, 230, 231] and holographic neutron stars [232]. Within our particular field of interest we restricted ourselves to a class of models that can be described on the gravitational side by metric solutions of a 5D Einstein–Hilbert-scalar action $S_{\mathrm{EHs}}$. The pure $AdS_5$ space-time is dual – according to the Maldacena conjecture – to conformal $\mathcal{N} = 4$ SYM, whereas deformed $AdS_5$ space-times that are solutions to $S_{\mathrm{EHs}}$ introduce non-conformalities right from the beginning. These deformed metric models are then mapped onto gauge theories that are non-conformal as well. In doing so, we lose knowledge about the exact dual gauge theory as we have mentioned in Chap. 3.

Since the string theory dual to QCD has not been found up to now, it is not sufficient to choose a particular deformation and claim that this choice is the best way to study real-world physics. More promising is to proceed by searching for universal behaviour in a large class of deformed $AdS_5$ space-times.

In the class of models under investigation in this thesis we have tried to be as complete as possible by choosing a very general metric ansatz in Sec. 3.2.1 that satisfies basic symmetries like Poincaré symmetry. After a general introduction in Chap. 2 to gauge/gravity dualities, we introduced the following three different deformed models in Chap. 3 that are representatives of our class of theories.

**SW$_T$-model** A simple overall deformation factor of the form $\mathrm{e}^{c\,z^2}$ in front of the pure $AdS_5$-BH metric leads to this non-conformal metric. The model has been proposed by Kajantie *& al.* in [64] and a similar approach is due to [63]. The computation of various physical quantities like the Q$\bar{\text{Q}}$-distance, drag force and trace anomaly is very similar to the conformal $AdS_5$-BH case. However, the model has some general disadvantages since it is not a solution to Einstein equations derived from any kind of 5D Einstein–Hilbert-scalar action.

**1-parameter model** A simple but very useful consistent deformation of the $AdS_5$-BH case has been studied as well. This model has not been analysed in the literature so far. It is the model which is closest to the conformal configuration with the scalar (dilaton) playing the dominant rôle in this deformation. No other deformations have been included by hand. The deformation parameter is called $\phi$.

**2-parameter model** A more complicated deformation of the conformal case has been used that has two parameters $c$ and $\phi$. It was proposed by Gubser *& al.* in [62]. Apart from the parameter $\phi$ due to the scalar it includes another deformation $c$ similar to the SW$_T$-model. These two parameters can be expressed in terms of dimensionless ratios $c/T^2$ and $\alpha = c/\phi$, where $T$ is the temperature. One can assume the scalar $\Phi \propto \phi\, z^2$ to be the string theory dilaton (string frame) or as a simple scalar of the theory (Einstein frame). Within this framework we have studied various observables and compared them to the other deformed models and the conformal case in order to extract conditions when a universal behaviour becomes apparent.

By using these metric models we have analysed the applicability – according to the first question – of holographic approaches to heavy-ion collisions. All of them contain strong coupling, non-conformality and finite temperature but lack for example fundamental quarks. This has the advantage that the class of our models incorporates a considerable amount of QCD properties but remains computationally simple for a large range of parameters.

We have been able to find, as was asked in the second question, that certain observables are either very robust or show a universal change in a certain direction. These results – most of them obtained for the first time in this thesis – will be summarised in the following. In order to study experimental results from RHIC and LHC several observables have been studied. Three of them, the quark-antiquark distance $L\pi T$ in Sec. 4.3.1 and Chap. 5, the drag force $\mathrm{d}p/\mathrm{d}t$ in Sec. 4.2 and the energy loss of rotating quarks $\mathrm{d}E/\mathrm{d}t$ in Chap. 6 are well-known in the conformal $AdS_5$-BH background[1] and the analysis has been systematically extended in

[1] For the drag force see [74, 165], for the Q$\bar{\text{Q}}$-distance see [124], for the energy loss of rotating quarks see [190, 215].

this work to the large class of deformed, non-conformal metric models specified above.

In the case of the quark-antiquark distance various studies are known even in non-conformal metric models in the literature [64, 65, 73]. However, a systematic analysis has only been done in our previous work [75, 76] where a universal behaviour was revealed numerically. There, we conjectured that the maximal value $(L\pi T)_{\mathrm{S}}$ of the $\mathrm{Q\bar{Q}}$-distance is in consistently deformed metric models always larger than the corresponding conformal $\mathcal{N}=4_T$ value $(L\pi T)^{\max}_{\mathcal{N}=4_T}$. In Chap. 5, this has now been proven analytically for a general class of small perturbations around the conformal solution by using linearised Einstein equations derived from the overall 5D Einstein–Hilbert-scalar action $S_{\mathrm{EHs}}$. Here, 'general' means that the perturbations have to obey the same symmetries as the full solution. The conjecture has been verified in Einstein- (Sec. 5.4.1) and string frame models (Sec. 5.4.2). The proof of this screening-distance conjecture confirms nicely the expectation expressed in the second question above. Based on these results it is now much simpler to consider, in a next step, additional kinematic parameters like the rapidity $\eta$ of the $\mathrm{Q\bar{Q}}$-pair as well as a possible orientation $\theta$ with respect to the rapidity that have also been studied numerically in [75, 76].

A similar systematic increase of an observable after introducing deformations has been found in the case of the running coupling $\alpha_{\mathrm{Q\bar{Q}}}$ derived from the free energy of a static $\mathrm{Q\bar{Q}}$-pair in Sec. 4.3. The analysis of this quantity that has hitherto been studied only in a conformal $\mathcal{N}=4_T$ plasma has been extended to all our non-conformal metric models. There it exhibits a universal increase for larger $\mathrm{Q\bar{Q}}$-distances up to a maximum value that defines a length scale $L_{\max}$. This in turn can be compared to the maximum $\mathrm{Q\bar{Q}}$-distance $L_S$ and both quantities are in the ballpark of a length scale $L^{\mathrm{Lat}}_{\max}$ obtained from lattice simulations [196–199]. These results that we have obtained by studying the running coupling address the last question raised at the beginning of this chapter.

Thermodynamic observables like the energy density, pressure and trace anomaly have been studied in Chap. 3 and have reproduced QCD results[2] known from lattice simulations [159, 160]. However, they are in principle not very useful to compare particular properties of several non-conformal models with QCD. This is due to their robust behaviour. It was shown that large deformations only lead to small changes in these observables. They resemble QCD irrespective of the chosen deformation. On the other hand the running coupling is very sensitive to a change of the deformation and it was possible in Sec. 4.3.5 to find a particular non-conformal, deformed $AdS_5$ model that mimics QCD even on a quantitative level. Driven by these promising results it might be possible to improve the agreement with QCD lattice results even more by using more advanced string-theoretic models that include for example asymptotic freedom. This would be advantageous since all our theories have a constant running coupling in the limit of very small $\mathrm{Q\bar{Q}}$-distances. However, due to the higher amount of complexity those models incorporate, a computation of $\alpha_{\mathrm{Q\bar{Q}}}$ has not been accomplished so far.

Although the other observables analysed in this thesis do not exhibit a systematic change in a certain direction when a deformation is implemented, they nevertheless show a universal behaviour that we have called robustness. In a large class of deformed metric models these observables deviate only slightly from the conformal $\mathcal{N}=4$ value or even do not change at all. The property of being robust is very prominent for example in the case of the drag force that has been analysed in Sec. 4.2. This quantity is very robust in the Einstein frame of the

[2] The best-fit values are: $c = 0.127\,\mathrm{GeV}^2$ for the $\mathrm{SW}_T$-model, $\phi = 0.02\,\mathrm{GeV}^2$ for the 1-parameter and $\phi = 0.32\,\mathrm{GeV}^2$, $c = 0.1\,\mathrm{GeV}^2$ for the 2-parameter model.

1-parameter model[3] for all values of the parameters as shown in Fig. 4.6. In the string frame robustness can be found in the regime of $\phi < 1$ for the 1-parameter model and $\alpha > 0.3$ and $c < 0.5$ for the 2-parameter model as we have presented in Sec. 4.2. These regimes include the physically meaningful, best-fit values mentioned above.

The robust behaviour of the drag force is in good agreement with the results that we have found in the case of the energy loss of rotating quarks in Chap. 6. In the conformal finite-temperature case that has been studied extensively in [190] this observable can be divided into three different regimes (drag, radiation-dominated and crossover). We have worked out that the same distinction between these different regimes is possible in deformed non-conformal models that have not been applied to the energy loss of a rotating quark so far in the literature. It was shown analytically that for certain limits of the radius at the boundary $R_0$ and the angular velocity $\omega$ pure energy loss due to drag or due to radiation can be recovered. The energy loss is in general very robust which has been visualised in Fig. 6.18. Furthermore, in the radiation-dominated regime of highly deformed models we obtained almost the same results as in the vacuum of $\mathcal{N} = 4$ at zero temperature. The important condition for this to happen is

$$\omega \gg \left(1 - v^2\right)^{3/4} \pi T \,, \tag{7.1}$$

where $v = R_0\,\omega$ is the velocity of the rotating quark, $T$ is the temperature and $\omega$ the angular velocity. This states for example that we enter the regime of almost pure vacuum radiation by choosing the angular velocity $\omega$ very large in comparison to the temperature. In addition to this, deformation does not matter in the vacuum-radiation regime. Furthermore, the crossover regime has been explored in non-conformal models for the first time and turns out to deviate only slightly from the conformal case. These robust results are very remarkable in the sense that it is not relevant for many observables if we do our computations in a conformal or highly non-conformal system, or equivalently, the energy loss of a rotating quark is not affected by the implementation of non-conformality.

The main problem in comparing the results of our computations with RHIC or LHC data is that these observables cannot be measured directly in the experiment. The energy loss of a rotating or a decelerated quark is encoded deeply in the data. The same is true for the screening distance of a fast-moving quark-antiquark pair. However, if QCD at strong coupling and high temperature is not that far away from what we have done, we can use our results in order to gain more insights into how such systems behave. The crossover regime for rotating quarks in Sec. 6.22, for example, tells us about the destructive interference of energy loss via drag and via vacuum radiation. In addition to this, Fig. 4.15 illustrates that all the length scales ($L_{\rm S}$, $L_{\rm max}$, $L_{\rm max}^{\rm Lat}$) that could be extracted from the $\mathrm{Q\bar{Q}}$-pair analysis in lattice QCD and holographic approaches are only slightly above the conformal $\mathcal{N} = 4$ result,

$$(L\pi T)_{\rm S}^{\mathcal{N}=4_{\rm T}} = 0.86912 \,, \tag{7.2}$$

indicating that the screening-distance conjecture is satisfied in real-world physics.

There are already some approaches where holography-driven computations are applicable to measurements in the experiments at the LHC and RHIC. A famous example is the measurement of the elliptic flow in terms of the coefficient $v_2$ that can be used in hydrodynamic simulations in order to compute the shear viscosity over entropy ratio $\eta/s$ being close to the value that $AdS/\mathrm{CFT}$ suggests [233]. It will be very interesting whether further agreement between

[3] There the maximal deviation from the conformal results is around 30 %.

theory and experiment for other observables can be achieved. But this is not the end of the applicability of the holographic principle to non-abelian gauge theories at strong coupling. By including gauge fields $A_\mu$ into the 5D Einstein–Hilbert-scalar action [155] it is possible to describe physical systems at non-zero chemical potential. It would be desirable to apply our discussion to this even larger class of theories. As far as recent computations by Samberg [77] are concerned, there is already strong evidence that these systems behave similarly to the models we have analysed in this work.

Further, more elaborate theories have been developed that incorporate higher-dimensional string theory input (D4, D7 branes) as studied for example by Erdmenger *& al.* in [129], Klebanov, Witten and Strassler in [55, 234–236] or by Sakai and Sugimoto in [57]. Some of these approaches include fundamental quarks and reproduce confinement leading to more QCD-like theories. However, these approaches are not without their own problems. The large amount of complexity impedes applications to the observables we have studied. Thus, our approach is well balanced between complexity and applicability.

In summary, we can state that the analysis performed in this thesis provides us with a better understanding of how strongly coupled, non-abelian gauge theories behave at high temperatures. Nearly all observables under investigation exhibit universal or robust behaviour for a large class of theories and it was even possible to take some steps in the direction of exploring QCD-like theories. But many issues still remain to be resolved. There are fundamental ones like the mathematical proof of the $AdS/$CFT-conjecture and more specific issues like the search for the exact gravity dual to QCD and it is very likely that the principle of holography will also lead to many new and interesting applications to various other physical systems in the near future. Thus, not only in high-energy experiments but also in the particular field of theoretical physics where issues at strong coupling are addressed, life is currently very exciting, and even more fascinating and groundbreaking days are ahead of us.

Appendix A

# Variation of Einstein–Hilbert action

Let us derive the general Einstein equations by varying an action of the Einstein–Hilbert form. Since this thesis deals with two different types of actions we derive the precise form of the Einstein equations in both cases. At the beginning of this work we stumbled over the basic Einstein–Hilbert action with a negative cosmological constant in Sec. 2.1.1 when the $AdS_5$ metric has been derived. Then, an extension of this action including a scalar (that might be the dilaton) has been studied in Sec. 3.2 with an action given by (3.12). Thus, this chapter is divided into two parts, each dealing with one of the two above-mentioned actions.

## A.1 Derivation of $AdS_5$ Metric

We recall the Einstein–Hilbert action (2.10) that leads to the $AdS_5$ metric:

$$S_{\mathrm{EH}} = \frac{1}{16\pi G_{\mathrm{N}}^{(5)}} \int d^5x \sqrt{-G} \left(\mathcal{R} - 2\Lambda\right), \quad \Lambda = -\frac{6}{L^2}, \tag{A.1}$$

with $\mathcal{R}$ being the Ricci scalar and $G_{\alpha\beta}$ being the five-dimensional space-time metric. The Ricci scalar is defined by

$$\mathcal{R} = \mathcal{R}^{\alpha}{}_{\alpha} = G^{\alpha\beta}\,\mathcal{R}^{\rho}_{\alpha\rho\beta} = G^{\alpha\beta}\,2\Gamma^{\rho}_{\alpha[\beta,\rho]} + 2\Gamma^{\rho}_{\lambda[\rho}\Gamma^{\lambda}_{\beta]\alpha}, \tag{A.2}$$

where $\mathcal{R}^{\rho}_{\alpha\mu\beta}$ is the Riemann tensor and $\Gamma^{\rho}_{\alpha\beta}$ are the Christoffel symbols. The only unknown field in this action is the metric. Thus, the variation of the action with respect to the metric $G_{\alpha\beta}$ has to vanish:

$$\begin{aligned}\frac{\delta S_{\mathrm{EH}}}{\delta G^{\alpha\beta}} &= 0 \\ &= \frac{1}{16\pi G_{\mathrm{N}}^{(5)}} \int \mathrm{d}^5x \left[\frac{\delta\sqrt{-G}}{\delta G^{\alpha\beta}}\,\mathcal{R} + \sqrt{-G}\,\frac{\delta\mathcal{R}}{\delta G^{\alpha\beta}} - \frac{\delta\sqrt{-G}}{\delta G^{\alpha\beta}}\,2\Lambda\right].\end{aligned} \tag{A.3}$$

By using basic relations in general relativity

$$\delta\sqrt{-G} = -\frac{1}{2\sqrt{-G}}\,\delta G = \frac{1}{2}\,\sqrt{-G}\,G^{\alpha\beta}\,\delta G_{\alpha\beta} = -\frac{1}{2}\sqrt{-G}\,G_{\alpha\beta}\,\delta G^{\alpha\beta}\,,$$
$$\frac{\delta\mathcal{R}}{\delta G^{\alpha\beta}} = \mathcal{R}_{\alpha\beta}\,, \tag{A.4}$$

(A.3) can be simplified in order to obtain Einstein equations in five dimensions including a negative cosmological constant $\Lambda$ that are given by

$$\int \mathrm{d}^5x \left[-\frac{1}{2}\sqrt{-G}\,G_{\alpha\beta}\,\mathcal{R} + \sqrt{-G}\,R_{\alpha\beta} + \frac{1}{2}\sqrt{-G}\,G_{\alpha\beta}\,2\Lambda\right] = 0$$
$$\implies \quad R_{\alpha\beta} - \frac{1}{2}\,\mathcal{R}\,G_{\alpha\beta} + \lambda\,G_{\alpha\beta} = 0\,. \tag{A.5}$$

We derived the $AdS_5$-BH metric in (2.33) which reads

$$\mathrm{d}s^2 = G_{\alpha\beta}\,\mathrm{d}X^\alpha \mathrm{d}X^\beta = \frac{L^2}{z^2}\left(-h(z,z_\mathrm{h})\,\mathrm{d}t^2 + \mathrm{d}\vec{x}^{\,2} + \frac{\mathrm{d}z^2}{h(z,z_\mathrm{h})}\right),$$
$$\text{with} \quad h(z,z_\mathrm{h}) = 1 - \frac{z^4}{z_\mathrm{h}^4}\,. \tag{A.6}$$

Thus, by using MATHEMATICA® to compute the Ricci tensor $\mathcal{R}_{\alpha\beta}$ and Ricci scalar $\mathcal{R}$ we end up with the following expressions

$$\mathcal{R}_{00} = \frac{4}{z^2} - \frac{4z^2}{z_\mathrm{h}}\,,$$
$$\mathcal{R}_{ii} = -\frac{4}{z^2}\,, \quad \text{with} \quad i \in \{x_1,\, x_2,\, x_3\}\,,$$
$$\mathcal{R}_{44} = \frac{4z_\mathrm{h}^4}{z^6 - z^2\,z_\mathrm{h}^4}\,,$$
$$\mathcal{R} = -\frac{20}{L^2}\,. \tag{A.7}$$

By substituting (A.7) into (A.5) it can be shown immediately that the Einstein equations are satisfied. Note that they are also satisfied if we go to zero temperature ($z_\mathrm{h} = \infty$). In the second part of this appendix we turn to the more sophisticated approach where the Einstein–Hilbert action has an additional dilaton term.

## A.2 Variation of Extended Einstein–Hilbert Action

The action $S_\mathrm{EHs}$ which will be analysed in this section is given by (3.12) and reads

$$S_\mathrm{EHs} = \frac{1}{16\pi G_\mathrm{N}^{(5)}} \int \mathrm{d}^5x\,\sqrt{-G}\left(\mathcal{R} - \frac{1}{2}(\partial\Phi)^2 - V(\Phi)\right). \tag{A.8}$$

In this action two fields ($G_{\alpha\beta}$ and $\Phi$) have to be determined. Therefore, we have to vary (A.8) with respect to the metric $G_{\alpha\beta}$ and the scalar field $\Phi$. The first variation leads to the following

expression

$$\begin{aligned}\frac{\delta S_{\text{EHs}}}{\delta G^{\alpha\beta}} &= \frac{1}{16\pi\, G_{\text{N}}^{(5)}} \int \mathrm{d}^5x \left[\frac{\delta\sqrt{\text{-}G}}{\delta G^{\alpha\beta}} \left(\mathcal{R} - \frac{1}{2}(\partial\Phi)^2 - V(\Phi)\right)\right. \\ &\quad \left. + \sqrt{\text{-}G}\Big(\frac{\delta\mathcal{R}}{\delta G^{\alpha\beta}} - \frac{1}{2}\,\frac{\delta(\partial\Phi)^2}{\delta G^{\alpha\beta}}\Big)\right] \\ &= \frac{1}{16\pi\, G_{\text{N}}^{(5)}} \int \mathrm{d}^5x \left[\text{-}\frac{1}{2}\,\sqrt{\text{-}G}\, G_{\alpha\beta}\left(\mathcal{R} - \frac{1}{2}\,(\partial\Phi)^2 - V(\Phi)\right)\right. \\ &\quad \left. + \sqrt{\text{-}G}\left(\mathcal{R}_{\alpha\beta} - \frac{1}{2}\partial_\alpha\Phi\,\partial_\beta\Phi\right)\right]. \end{aligned} \tag{A.9}$$

In the last line we used the identity

$$(\partial\Phi)^2 = \partial_\alpha\Phi\,\partial^\alpha\Phi = (\partial_\alpha\Phi)\,(\partial_\beta\Phi)\,G^{\alpha\beta}\,. \tag{A.10}$$

The variation with respect to $\Phi$ can be written as

$$\begin{aligned}\frac{\delta S_{\text{EHs}}}{\delta\Phi} &= \frac{1}{16\pi\, G_{\text{N}}^{(5)}} \int \mathrm{d}^5x\,\sqrt{\text{-}G}\left[\text{-}\frac{1}{2}\,\frac{\delta(\partial\Phi)^2}{\delta\Phi} - \frac{\delta V(\Phi)}{\delta\Phi}\right] \\ &= \frac{1}{16\pi\, G_{\text{N}}^{(5)}} \int \mathrm{d}^5x\,\sqrt{\text{-}G}\left[\Box_{\text{LB}}\Phi - V'(\Phi)\right], \end{aligned} \tag{A.11}$$

where $'$ denotes the derivative with respect to $\Phi$ and $\Box_{\text{LB}}$ the Laplace–Beltrami operator. In order to obtain the last line of (A.11) two integrations by parts have been used

$$\begin{aligned}\text{-}\frac{1}{2}\,\frac{\delta\big(\nabla_\alpha\Phi\,\nabla_\beta\Phi\,G^{\alpha\beta}\big)}{\delta\Phi} &= \text{-}\frac{1}{2}\left[\nabla_\beta\Phi\,\frac{\delta\nabla_\alpha\Phi}{\delta\Phi} + \nabla_\alpha\Phi\,\frac{\delta\nabla_\beta\Phi}{\delta\Phi}\right]G^{\alpha\beta} \\ &= \nabla_\alpha\nabla_\beta\Phi G^{\alpha\beta} = \nabla_\alpha\nabla^\alpha\Phi = \Box_{\text{LB}}\Phi\,, \end{aligned} \tag{A.12}$$

that are well-defined under the integral in (A.11). Furthermore, we can neglect the boundary terms that arise in the integration by parts since $\Phi$ is supposed to vanish identically at large $X^\alpha$.

In summary, the variation of (A.8) with respect to $G^{\alpha\beta}$ and $\Phi$ leads to the following equations of motion

$$\begin{aligned}\mathcal{R}_{\alpha\beta} - \frac{1}{2}\mathcal{R}\,G_{\alpha\beta} = \mathcal{T}_{\alpha\beta}\,, \quad \text{with} \quad \mathcal{T}_{\alpha\beta} &= \frac{1}{2}\,\partial_\alpha\Phi\,\partial_\beta\Phi - \frac{1}{4}\,(\partial\Phi)^2\,G_{\alpha\beta} - \frac{1}{2}\,V(\Phi)G_{\alpha\beta}\,, \\ \Box_{\text{LB}}\Phi = V'(\Phi)\,, \quad \text{with} \quad \Box_{\text{LB}}\Phi &= \frac{1}{\sqrt{\text{-}G}}\partial_\alpha\Big(\sqrt{\text{-}G}\,G^{\alpha\beta}\partial_\beta\Phi\Big)\,. \end{aligned} \tag{A.13}$$

In the last line of eq. (A.13) we recall the definition of the Laplace–Beltrami operator $\Box_{\text{LB}}$ which is a generalisation of the common d'Alembert operator. These coupled, non-linear differential equations in (A.13) have to be solved with an appropriate ansatz for the metric. This is discussed in detail in Sec. 3.2.

## A.3 Curvature Properties

By specifying to the general metric ansatz derived in Sec. 3.2.1 the metric reads

$$\mathrm{d}s^2 = \mathrm{e}^{2A(z)}\left(-h(z)\mathrm{d}t^2 + \mathrm{d}\vec{x}^{\,2}\right) + \mathrm{e}^{2B(z)}\,\frac{\mathrm{d}z^2}{h(z)}\,. \tag{A.14}$$

With the help of MATHEMATICA® we quote in the following the expressions for the Christoffel symbols $\Gamma^{\gamma}_{\alpha\beta}$, Riemann tensor $\mathcal{R}^{\rho}_{\alpha\beta\gamma\delta}$, Ricci tensor $\mathcal{R}_{\alpha\beta}$ and Ricci scalar $\mathcal{R}$. The Christoffel symbols are then given by

$$\begin{aligned}
&\Gamma^t_{zt} = A'(z) + \frac{h'(z)}{2h(z)}\,, \quad \Gamma^i_{zi} = A'(z)\,, \quad \Gamma^z_{ii} = -\mathrm{e}^{2A(z)-2B(z)}\,h(z)\,A'(z)\,,\\
&\Gamma^z_{tt} = \frac{1}{2}\,\mathrm{e}^{2A(z)-B(z)}\,h(z)\left(2h(z)\,A'(z) + h'(z)\right), \quad \Gamma^z_{zz} = B'(z) - \frac{h'(z)}{2h(z)}\,,
\end{aligned} \tag{A.15}$$

with $i \in \{x_1, x_2, x_3\}$. The elements of the Riemann tensor can be written as

$$\begin{aligned}
\mathcal{R}^t_{iit} &= \frac{1}{2}\,\mathrm{e}^{2A(z)-2B(z)}\,A'(z)\left(2h(z)\,A'(z) + h'(z)\right),\\
\mathcal{R}^t_{zzt} &= \frac{1}{2h(z)}\left[3A'(z)\,h'(z) - B'(z)h'(z) + 2h(z)\big(A'(z)^2 - A'(z)\,B'(z) + A''(z)\big) + h''(z)\right],\\
\mathcal{R}^i_{tit} &= \frac{1}{2}\,\mathrm{e}^{2A(z)-2B(z)}\,h(z)\,A'(z)\left(2h(z)\,A'(z) + h'(z)\right),\\
\mathcal{R}^{x_1}_{x_2x_2x_1} &= \mathcal{R}^{x_1}_{x_3x_3x_1} = \mathcal{R}^{x_2}_{x_3x_3x_2} = \mathrm{e}^{2A(z)-2B(z)}\,h(z)\,A'(z)^2\,,\\
\mathcal{R}^{x_2}_{x_1x_2x_1} &= \mathcal{R}^{x_3}_{x_1x_3x_1} = \mathcal{R}^{x_3}_{x_2x_3x_2} = -\mathrm{e}^{2A(z)-2B(z)}\,h(z)\,A'(z)^2\,,\\
\mathcal{R}^i_{zzi} &= A'(z)^2 + A'(z)\left(-B'(z) + \frac{h'(z)}{2h(z)}\right) + A''(z)\,,\\
\mathcal{R}^z_{tzt} &= -\frac{1}{2}\mathrm{e}^{2A(z)-2B(z)}\,h(z)\Big[3A'(z)\,h'(z) - B'(z)h'(z) + 2h(z)\left(A'(z)^2\right.\\
&\qquad \left. - A'(z)B'(z) + A''(z)\right) + h''(z)\Big]\,,\\
\mathcal{R}^z_{izi} &= -\frac{1}{2}\mathrm{e}^{2A(z)-2B(z)}\left[A'(z)\,h'(z) + 2h(z)\left(A'(z)^2 - A'(z)\,B'(z) + A''(z)\right)\right].
\end{aligned} \tag{A.16}$$

The elements of the Ricci tensor can be computed using the Riemann tensor and have the following form:

$$\begin{aligned}
\mathcal{R}_{tt} &= \frac{1}{2}\mathrm{e}^{2A(z)-2B(z)}\,h(z)\Big[6A'(z)\,h'(z) - B'(z)h'(z)\\
&\qquad + 2h(z)\left(4A'(z)^2 - A'(z)\,B'(z) + A''(z)\right) + h''(z)\Big]\,,\\
\mathcal{R}_{ii} &= -\mathrm{e}^{2A(z)-2B(z)}\left[A'(z)\,h'(z) + h(z)\left(4A'(z)^2 - A'(z)\,B'(z) + A''(z)\right)\right],\\
\mathcal{R}_{zz} &= -\frac{1}{2h(z)}\left[6A'(z)\,h'(z) - B'(z)\,h'(z) + 8h(z)\left(A'(z)^2 - A'(z)\,B'(z) + A''(z)\right) + h''(z)\right].
\end{aligned} \tag{A.17}$$

The last necessary component in order to derive the explicit system of differential equations in (3.26) – (3.29) is the Ricci scalar $\mathcal{R}$ given by

$$\begin{aligned}\mathcal{R} = \mathrm{e}^{-2B(z)} \Big[ & -9A'(z)\,h'(z) + B'(z)\,h'(z) \\ & - 4h(z)\left(5A'(z)^2 - 2A'(z)\,B'(z) + 2A''(z)\right) - h''(z)\Big]. \end{aligned} \tag{A.18}$$

Appendix B

# Derivation of the Temperature Formula

The derivation of the temperature as a function of the metric is well-known in black-hole thermodynamics [237]. The main ingredient of this computation is the Bekenstein–Hawking temperature relation

$$T = \frac{\kappa}{2\pi}\,, \tag{B.1}$$

where $\kappa$ is the surface gravity computed at the horizon $z_h$. There are two ways to determine $\kappa$:

1. In terms of the Killing vector which is orthogonal to the horizon.
2. In terms of the $d$-acceleration and $d$-velocity of a free particle.[1]

In this chapter, by following Gron and Hervik [237], we focus on the first method because it leads directly to a formulation in terms of the metric functions, although the second approach is more descriptive. From general relativity it is known that the horizon of a black hole is a so-called *null surface*: any vector normal to the horizon surface is a null vector. Let us consider the Killing vector that generates time translations given in a general form by

$$\xi = \xi^\alpha\, e_\alpha\,, \quad \text{with} \quad \alpha \in \{t, \vec{x}, z\}\,. \tag{B.2}$$

In a Schwarzschild-like space-time this vector is simply given by

$$\xi = e_t\,. \tag{B.3}$$

In other space-times the Killing vector of time translations looks different (e.g. in Kerr space-time it is a linear combination of $\frac{\partial}{\partial t}$ and $\frac{\partial}{\partial \phi}$). The Killing vector is by definition normal to the horizon which leads to

$$\xi_\alpha\, \xi^\alpha = 0\,, \tag{B.4}$$

[1] In the case of $d = 4$ dimensions these quantities reduce to the well-known four-acceleration and four-velocity.

since the horizon is a null surface. A particular property of the Killing vector is the invariance of $\xi_\alpha \xi^\alpha$ along the horizon. Thus the gradient $\nabla^\alpha (\xi_\beta \xi^\beta)$ is also normal to the horizon. The surface gravity $\kappa$ is now the proportionality constant between these two quantities and can be cast into the following form

$$\nabla^\alpha (\xi_\beta \xi^\beta) = -2\kappa \xi^\alpha . \tag{B.5}$$

This can be rewritten as

$$\xi^\beta \nabla_\alpha \xi_\beta = -\xi^\beta \nabla_\beta \xi_\alpha = -\kappa \xi_\alpha , \tag{B.6}$$

where we have used the Killing equation $\nabla_\alpha \xi_\beta + \nabla_\beta \xi_\alpha = 0$.

Now, we have to solve (B.6) for $\kappa$. By using Frobenius' theorem it can be shown that the Killing vector $\xi_\alpha$ is hypersurface-orthogonal. This means, that the Killing vector satisfies

$$\xi_{[\alpha} \nabla_\beta \xi_{\gamma]} = 0 . \tag{B.7}$$

The bracket denotes total anti-symmetrisation which is the alternating sum over permutations of the indices $\alpha$, $\beta$ and $\gamma$. This can be transformed into the following form:

$$\begin{aligned} \xi_{[\alpha} \nabla_\beta \xi_{\gamma]} &= \frac{1}{3!}\Big[\xi_\alpha \nabla_\beta \xi_\gamma - \xi_\alpha \nabla_\gamma \xi_\beta + \xi_\gamma \nabla_\alpha \xi_\beta - \xi_\beta \nabla_\alpha \xi_\gamma + \xi_\beta \nabla_\gamma \xi_\alpha - \xi_\gamma \nabla_\beta \xi_\alpha\Big] = 0 \\ \iff \quad 0 &= -\xi_\alpha \nabla_\gamma \xi_\beta - \xi_\gamma \nabla_\beta \xi_\alpha - \xi_\beta \nabla_\alpha \xi_\gamma . \end{aligned} \tag{B.8}$$

A short computation shows that (B.8) can be cast into the form

$$\xi_\gamma \nabla_\beta \xi_\alpha = -\Big(\xi_\beta \nabla_\alpha \xi_\gamma - \xi_\alpha \nabla_\beta \xi_\gamma\Big) = -2\xi_{[\beta} \nabla_{\alpha]} \xi_\gamma . \tag{B.9}$$

After contracting this with $\nabla^\alpha \xi^\beta$, we obtain

$$\begin{aligned} \xi_\gamma \big(\nabla^\alpha \xi^\beta\big) \big(\nabla_\alpha \xi_\beta\big) &= -2\big(\nabla^\alpha \xi^\beta\big) \big(\xi_{[\alpha} \nabla_{\beta]} \xi_\gamma\big) \\ &= -2\big(\nabla_\alpha \xi_\beta\big) \left(\frac{1}{2}\big(\xi_\alpha \nabla_\beta - \xi_\beta \nabla_\alpha\big) \xi_\gamma\right) \\ &= \Big(-\xi_\alpha \nabla^\alpha \xi^\beta \nabla_\beta + \xi_\beta \nabla^\alpha \xi^\beta \nabla_\alpha\Big)\xi_\gamma \\ &= \big(-\kappa \xi^\beta \nabla_\beta - \kappa \xi^\alpha \nabla_\alpha\big) \xi_\gamma = -2\kappa \xi^\alpha \nabla_\alpha \xi_\gamma = -2\kappa^2 \xi_\gamma . \end{aligned} \tag{B.10}$$

In the last line we used the definition of the surface gravity (B.6). This equation can be solved for $\kappa^2$ and we end up with an elegant expression for the surface gravity:

$$\kappa^2 = -\frac{1}{2}\Big(\nabla_\alpha \xi_\beta\Big)\Big(\nabla^\alpha \xi^\beta\Big) . \tag{B.11}$$

In this thesis we work with Schwarzschild-like geometries only and the time-like Killing vector is thus given as

$$\xi^\alpha = \delta^\alpha_t \quad \xi_\alpha = \delta_{\alpha t} G_{tt} , \tag{B.12}$$

where the covariant expression simplifies to the form shown in (B.12) due to the diagonal form of the space-time metric $G_{\alpha\beta}$. To simplify (B.11) knowledge about the covariant derivative $\nabla_\alpha \xi_\beta$ is required. This in turn is given in terms of the Christoffel symbols

$$\nabla_\alpha \xi_\beta = \partial_\alpha \xi_\beta - \Gamma^\gamma_{\beta\alpha} \xi_\gamma , \tag{B.13}$$

where we can set $\partial_\alpha \xi_\beta = \partial_z \xi_t = \partial_z G_{tt}$ because the space-time metric is a function of $z$ only. Now, we focus on the right hand side of (B.13) that reduces to

$$\begin{aligned}\Gamma^\gamma_{\beta\alpha}\,\xi_\gamma &= \frac{1}{2}G^{\gamma\eta}\left(\partial_\beta G_{\alpha\eta} + \partial_\alpha G_{\beta\eta} - \partial_\eta G_{\beta\alpha}\right)\xi_\gamma \\ &= \frac{1}{2}G^{tt}\left(\partial_\beta G_{\alpha t} + \partial_\alpha G_{\beta t} - 0\right)\xi_t\,. \end{aligned} \tag{B.14}$$

Thus, only two terms contribute to (B.13): those with $\beta = t$, $\alpha = z$ and $\alpha = t$, $\beta = z$. From Killing's equation $\nabla_\alpha \xi_\beta = -\nabla_\beta \xi_\alpha$ and the fact that in a coordinate basis the Christoffel symbols are symmetric in the lower indices we deduce that only $\nabla_z \xi_t$ and $\nabla_t \xi_z$ are non-zero. These two expressions can be written in terms of the metric elements by using (B.14):

$$\nabla_t \xi_z = -\Gamma^t_{tz}\,\xi_t = -\frac{1}{2}G^{tt}\,\partial_z G_{tt}\cdot g_{tt}\,, \quad \nabla_z \xi_t = \frac{1}{2}G^{tt}\,\partial_z g_{tt}\cdot g_{tt}\,. \tag{B.15}$$

Now we are able to derive $\kappa^2$ in terms of the metric functions by substituting (B.15) into (B.11) which leads to

$$\begin{aligned}\kappa^2 &= -\frac{1}{2}\left(\nabla_z\xi_t\,\nabla^z\xi^t + \nabla_t\xi_z\,\nabla^t\xi^z\right) = -\frac{1}{2}\,\nabla_z\xi_t\left(\nabla^z\xi^t - \nabla^t\xi^z\right) \\ &= -\frac{1}{4}\,\partial_z G_{tt}\left(G^{zz}\,\nabla_z\xi^t - G^{tt}\,\nabla_t\xi^z\right) = -\frac{1}{4}\,\partial_z G_{tt}\left(G^{zz}\,\frac{1}{2}G^{tt}\,\partial_z G_{tt} + \frac{1}{2}G^{zz}\,G^{tt}\,\partial_z G_{tt}\right) \\ &= -\frac{1}{4}G^{zz}\,G^{tt}\left(\partial_z G_{tt}\right)^2. \end{aligned} \tag{B.16}$$

By using the specific metric elements of the general metric ansatz derived in Sec. 3.2.1 we end up with an explicit expression of the temperature $T$ given by

$$\begin{aligned} & G_{tt} = -h\,e^{2A}\,, \quad G^{tt} = -\frac{1}{he^{2A}}\,, \quad G_{zz} = \frac{e^{2B}}{h}\,, \quad G^{zz} = \frac{h}{e^{2B}}\,, \\ \Longrightarrow \quad & T = \frac{\kappa}{2\pi} = \frac{1}{2\pi}\left[-\frac{1}{4}\frac{h}{e^{2B}}\cdot -\frac{1}{h\,e^{2A}}\cdot\left(\partial_z h\right)^2 e^{4A}\right]^{1/2}\Bigg|_{z=z_\mathrm{h}} \\ & \qquad = \frac{e^{A-B}\,|h'(z_\mathrm{h})|}{4\pi}\,. \end{aligned} \tag{B.17}$$

This is the final expression that can be found in (3.6) as well and is used throughout this work because Schwarzschild-like metrics are used without exception.

Appendix C

# Worldsheet Horizon

For the energy loss of a trailing string in Sec. 4.2 and for the energy loss of a rotating quark in Sec. 6.1 we encountered the special point $z_c$ in the bulk. In both cases this point denoted the position in the bulk where the reality condition (4.23) for the moving quark and (6.43) for the rotating quark has to be applied. In this chapter we want to show that this point $z_c$ is identical to the worldsheet horizon $z_*$ where the induced (worldsheet) metric $g_{ab}$ has a vanishing $\tau\tau$-component which in turn is equivalent to the point where the string exceeds the local speed of light $c_{\text{bulk}}(z_c)$ at that position in the bulk. Thus the upper and lower parts of the string are causally disconnected. This computation has been worked out for the conformal $\mathcal{N} = 4$ case by Giecold *& al.* in [216]. We will recall the reality conditions of the dragging-quark and rotating-quark scenario and derive the worldsheet horizon in both cases.

In a general metric ansatz given by

$$\mathrm{d}s^2 = G_{\alpha\beta}\,\mathrm{d}X^\alpha \mathrm{d}X^\beta = \mathrm{e}^{2A(z)}\left(-h(z)\mathrm{d}t^2 + \mathrm{d}\vec{x}^{\,2}\right) + \mathrm{e}^{2B(z)}\,\frac{\mathrm{d}z^2}{h(z)}\,, \tag{C.1}$$

the reality conditions can be written as

$$\text{Dragging quark:} \quad h(z_c) = v^2\,, \tag{C.2}$$

$$\text{Rotating quark:} \quad \Pi\,\omega = \mathrm{e}^{2A(z_c)}\,h(z_c)\,. \tag{C.3}$$

The horizon function $h(z_c)$ in (C.3) can be transformed using the second initial condition for the rotating quark in (6.43) that reads

$$R(z_c) \equiv \frac{\sqrt{h(z_c)}}{\omega}\,. \tag{C.4}$$

Thus, $\Pi$ can be cast into the following form:

$$\Pi\omega = \mathrm{e}^{2A(z_c)}\left(R(z_c)\,\omega\right)^2\,, \tag{C.5}$$

and the $z_c$-defining equation is finally given by

$$h(z_c) = \left(R(z_c)\,\omega\right)^2 \equiv v_c^2\,, \tag{C.6}$$

where we just combined (C.5) and (C.3) in order to eliminate $\Pi$ in favour of the radial extension $R(z_c)$ of the string at bulk position $z_c$. $v_c$ is now the velocity of the string at $z_c$ in the bulk. This is the main difference to the drag case. There, the velocity is constant for all values of $z$, whereas in the rotating case the string moves faster at greater depth. This was the main reason for the robustness of this observable.

With the condition for each $z_c$ in our hand we can now compute the *worldsheet horizon*. This is the point in the bulk – which we will call $z_*$ – where the worldsheet metric $g_{ab}$ has a vanishing coefficient for the $\tau$-coordinate. This is equivalent to the emergence of a horizon at $z_*$. For the drag force computation the calculation goes as follows.

## C.1 Dragging Quark

The first thing we have to calculate is the induced (worldsheet) metric $g_{ab} = G_{\alpha\beta}\,\partial_a X^\alpha\,\partial_b X^\beta$ with $a, b \in \{\tau, \sigma\}$. By using the parameterisation of the dragging quark given by

$$X^\alpha \equiv \big(t = \tau,\, 0,\, 0,\, x_3(\tau,\sigma),\, z = \sigma\big)\,, \quad \text{with} \quad x_3(\tau,\sigma) = v\tau + \xi(\sigma)\,, \tag{C.7}$$

the $\tau\tau$-component of the worldsheet metric reads

$$g_{\tau\tau} = G_{tt}\,(\dot{X}^t)^2 + G_{x_3x_3}\,\dot{x}_3^2 = -\mathrm{e}^{2A(z)}\,h(z) + \mathrm{e}^{2A(z)}\,v^2\,. \tag{C.8}$$

The requirement that eq. (C.8) has to vanish defines the worldsheet horizon $z_*$ that can be written as

$$z_*: \quad h(z_*) = v^2\,. \tag{C.9}$$

By comparing (C.9) with (C.2) we can state immediately that

$$z_c \equiv z_* \tag{C.10}$$

holds for all values of the velocity $v$. Thus the point where our reality condition has to be applied is the same point where the string worldsheet has a horizon. Before we show that the velocity of the string at this point is equal to the local speed of light $c_{\text{bulk}}(z)$ in the bulk, we first derive the worldsheet horizon for the rotating quark.

## C.2 Rotating Quark

In the rotating-quark scenario the derivation of the worldsheet is completely analogous to the dragging-quark setup. Again, we have to compute the $\tau\tau$-component of the induced metric by using an appropriate parameterisation:

$$X^\alpha(\tau,\sigma) = \big(t = \tau, \vec{r}_s(\tau,\sigma), z = \sigma\big)\,, \tag{C.11}$$

where the three-vector $\vec{r}_s$ is given in spherical coordinates $(R, \theta, \varphi)$:

$$\vec{r}_s(\tau,\,\sigma) \equiv \big(R(\sigma), \frac{\pi}{2}, \varphi = \phi(\sigma) + \omega\tau\big)\,. \tag{C.12}$$

Since we are dealing with static gauge ($\tau = t$ and $\sigma = z$), we use the old coordinates $t$ and $z$ in the following. The $\tau\tau$-component of the induced metric is given by

$$g_{\tau\tau} = G_{tt}\,(\dot{X}^t)^2 + G_{\varphi\varphi}\,\dot{\varphi}^2 = -\mathrm{e}^{2A(z)}\,h(z) + R(z)^2\,\sin^2\frac{\pi}{2}\,\mathrm{e}^{2A(z)}\,\omega^2\,. \tag{C.13}$$

Remember that we are working in spherical coordinates. This gives rise to the additional factor $R(z)^2\,\sin^2\frac{\pi}{2}$. The condition for the worldsheet horizon $z_*$ is then written as

$$z_*: \quad h(z_*) = R(z_*)^2\,\omega^2 = v_*^2\,. \tag{C.14}$$

Comparing (C.14) with (C.6) leads again to

$$z_\mathrm{c} \equiv z_*\,, \tag{C.15}$$

Thus, both observables that have been studied in this thesis share the property that $z_\mathrm{c}$ marks the point where the reality condition has to be applied as well as the worldsheet horizon. In a last step we show that this point is also identical to the point where the string reaches the local speed of light $c_\mathrm{bulk}(z)$.

## C.3 Local Speed of Light in the Bulk

The definition of the local speed of light in the bulk is a very straightforward generalisation of the boundary value $c$. In principle one has to impose $\mathrm{d}s^2 = 0$ in order to compute a lightlike world line and solve for $\mathrm{d}x/\mathrm{d}t$. At the boundary we have a pure Minkowski space-time that is given by

$$g_{\mu\nu}\,\mathrm{d}x^\mu \mathrm{d}x^\nu = -c^2\,\mathrm{d}t^2 + \mathrm{d}\vec{x}^{\,2}\,. \tag{C.16}$$

In the general metric ansatz of eq. (C.1) we define the speed of light $c_\mathrm{bulk}(z)$ at a particular position at the bulk by

$$\begin{aligned} G_{\alpha\beta}\,\mathrm{d}X^\alpha \mathrm{d}X^\beta &= \ldots \left(-h(z)\,\mathrm{d}t^2 + \mathrm{d}\vec{x}^{\,2}\right) \ldots\,, \\ c_\mathrm{bulk}(z) &= \sqrt{h(z)}\,. \end{aligned} \tag{C.17}$$

This definition can now be compared with the definition of $z_\mathrm{c}$ in eq. (C.2) and eq. (C.6). Since $z_\mathrm{c}$ is always the point in the bulk where the condition $h(z_\mathrm{c}) = v^2$ is fulfilled, it is automatically the point where the string exceeds the local speed of light at that depth in the bulk.

Appendix D

# Primitive of Linearised $Q\bar{Q}$-Distance Integral

In this chapter we present the primitive of the linearised $Q\bar{Q}$-distance integral which is given in (5.49). The essential integral that has to be computed is given by

$$(L\pi T)^{\text{Lin}}_{1^{\text{st}}} = \alpha \int_0^{z_\text{c}} \mathcal{I}\,\mathrm{d}z\,, \tag{D.1}$$

with

$$\begin{aligned}
\mathcal{I} = \frac{z^2}{z_\text{nh}} \sqrt{\frac{z_\text{nh}^4 - z_\text{c}^4}{(z_\text{c}^4 - z^4)\,(z_\text{nh}^4 - z^4)}} \Bigg[ & (1+k)\, z_\text{h}^k + \frac{1}{(z^4 - z_\text{c}^4)\, z_\text{h}^4\, (z^4 - z_\text{nh}^4)\, (z_\text{c}^4 - z_\text{nh}^4)} \\
& \cdot \Bigg( -2 z_\text{c}^{8+k}\, (z^4 - z_\text{nh}^4)^2 - (z^4 - z_\text{c}^4) z_\text{nh}^{4+k} \Big( k z^4 z_\text{c}^4 - \big( (2+k) z^4 \\
& + (k-2) z_\text{c}^4 \big) z_\text{nh}^4 + k z_\text{nh}^8 \Big) + 2 z^{4+k}\, (z_\text{c}^4 - z_\text{nh}^4) \Big( z^4\, (z_\text{c}^4 - z_\text{nh}^4) - 2 z_\text{c}^4 z_\text{nh}^4 \Big) \Bigg) \\
& + \frac{1}{(z^4 - z_\text{c}^4)\, z_\text{nh}^4} \Bigg( 2 z_\text{c}^{4+k}\, (z^4 - z_\text{nh}^4) + z^k \Big( (3+k) z_\text{c}^4 z_\text{nh}^4 \\
& - z^4 \big( 2 z_\text{c}^4 + (1+k) z_\text{nh}^4 \big) \Big) \Bigg) \Bigg]\,.
\end{aligned} \tag{D.2}$$

The primitive can be computed – after some massage – using the `Integrate` method of MATHEMATICA®. It is given in full glory by

$$
\begin{aligned}
\frac{(L\pi T)^{\mathrm{Lin}}_{1^{\mathrm{st}}}}{\alpha} = \frac{z^3}{21 z_{\mathrm{h}}^4 z_{\mathrm{nh}}^5} &\left(\left(z_{\mathrm{nh}}^4 - z_{\mathrm{c}}^4\right)\left(z^4 - z_{\mathrm{c}}^4\right)\left(z^4 - z_{\mathrm{nh}}^4\right)\right)^{-1/2}\left[21\left(\left(z^4 - z_{\mathrm{c}}^4\right) z_{\mathrm{nh}}^{8+k}\right.\right.\\
&- z_{\mathrm{c}}^k\left(z^4 - z_{\mathrm{nh}}^4\right)\left(-z_{\mathrm{c}}^4 z_{\mathrm{h}}^4 + \left(z_{\mathrm{c}}^4 - z_{\mathrm{h}}^4\right) z_{\mathrm{nh}}^4\right)\Big) + \frac{1}{3+k}\sqrt{1-\frac{z^4}{z_{\mathrm{c}}^4}}\sqrt{1-\frac{z^4}{z_{\mathrm{nh}}^4}}\\
&\cdot\left(-7\,(3+k)\, z_{\mathrm{nh}}^4\left(z_{\mathrm{c}}^k z_{\mathrm{h}}^4 z_{\mathrm{nh}}^4 - (1+k)\, z_{\mathrm{h}}^{4+k} z_{\mathrm{nh}}^4 + k\, z_{\mathrm{nh}}^{8+k} + z_{\mathrm{c}}^{4+k}\left(z_{\mathrm{nh}}^4 - z_{\mathrm{h}}^4\right)\right.\right.\\
&\left.\left.+ (1+k)\, z_{\mathrm{c}}^4\left(z_{\mathrm{h}}^{4+k} - z_{\mathrm{nh}}^{4+k}\right)\right) F_1\left[\frac{3}{4}, \frac{1}{2}, \frac{1}{2}, \frac{7}{4}, \frac{z^4}{z_{\mathrm{c}}^4}, \frac{z^4}{z_{\mathrm{nh}}^4}\right] + 3\left\{-3\,(3+k)\, z^4\left(z_{\mathrm{nh}}^{8+k}\right.\right.\right.\\
&\left.\left.\left.+ z_{\mathrm{c}}^k\left(z_{\mathrm{c}}^4 z_{\mathrm{h}}^4 - \left(z_{\mathrm{c}}^4 + z_{\mathrm{h}}^4\right) z_{\mathrm{nh}}^4\right)\right) F_1\left[\frac{7}{4}, \frac{1}{2}, \frac{1}{2}, \frac{11}{4}, \frac{z^4}{z_{\mathrm{c}}^4}, \frac{z^4}{z_{\mathrm{nh}}^4}\right] + 7\, z^k z_{\mathrm{nh}}^4\left[(1+k)\right.\right.\\
&\cdot z_{\mathrm{c}}^4 z_{\mathrm{h}}^4 F_1\left[\frac{3+k}{4}, -\frac{1}{2}, \frac{1}{2}, \frac{7+k}{4}, \frac{z^4}{z_{\mathrm{c}}^4}, \frac{z^4}{z_{\mathrm{nh}}^4}\right]\\
&+ z_{\mathrm{nh}}^4\left(2\, z_{\mathrm{c}}^4 F_1\left[\frac{3+k}{4}, -\frac{1}{2}, \frac{3}{2}, \frac{7+k}{4}, \frac{z^4}{z_{\mathrm{c}}^4}, \frac{z^4}{z_{\mathrm{nh}}^4}\right]\right.\\
&\left.\left.\left.- (1+k)\, z_{\mathrm{h}}^4 F_1\left[\frac{3+k}{4}, \frac{1}{2}, -\frac{1}{2}, \frac{7+k}{4}, \frac{z^4}{z_{\mathrm{c}}^4}, \frac{z^4}{z_{\mathrm{nh}}^4}\right]\right) - 2\left(-z_{\mathrm{c}}^4 z_{\mathrm{h}}^4 + \left(z_{\mathrm{c}}^4 + z_{\mathrm{h}}^4\right) z_{\mathrm{nh}}^4\right)\right.\right.\\
&\left.\left.\cdot F_1\left[\frac{3+k}{4}, \frac{3}{2}, -\frac{1}{2}, \frac{7+k}{4}, \frac{z^4}{z_{\mathrm{c}}^4}, \frac{z^4}{z_{\mathrm{nh}}^4}\right]\right]\right\}\Big)\Big]\,. \qquad \text{(D.3)}
\end{aligned}
$$

# References


[1] **ATLAS** Collaboration, G. Aad *et al.*, "Combined search for the Standard Model Higgs boson using up to 4.9 fb$^{-1}$ of pp collision data at $\sqrt{s_{NN}}$ = 7 TeV with the ATLAS detector at the LHC," arXiv:1202.1408 [hep-ex]. 1

[2] **ATLAS** Collaboration, "Search for the Standard Model Higgs boson in the diphoton decay channel with 4.9 fb$^{-1}$ of pp collisions at $\sqrt{s_{NN}}$ = 7 TeV with ATLAS," arXiv:1202.1414 [hep-ex].

[3] **ATLAS** Collaboration, "Search for the Standard Model Higgs boson in the decay channel H $\to ZZ^{(*)} \to 4l$ with 4.8 fb$^{-1}$ of pp collisions at $\sqrt{s_{NN}}$ = 7 TeV with ATLAS," arXiv:1202.1415 [hep-ex]. 1

[4] **CMS** Collaboration, S. Chatrchyan *et al.*, "Combined results of searches for the standard model Higgs boson in pp collisions at $\sqrt{s_{NN}}$ = 7 TeV," arXiv:1202.1488 [hep-ex]. 1

[5] **CMS** Collaboration, S. Chatrchyan *et al.*, "Search for the standard model Higgs boson decaying to a W pair in the fully leptonic final state in pp collisions at $\sqrt{s_{NN}}$ = 7 TeV," arXiv:1202.1489 [hep-ex].

[6] **CMS** Collaboration, S. Chatrchyan *et al.*, "Search for the standard model Higgs boson decaying into two photons in pp collisions at $\sqrt{s_{NN}}$=7 TeV," arXiv:1202.1487 [hep-ex].

[7] **CMS** Collaboration, S. Chatrchyan *et al.*, "Search for a Higgs boson in the decay channel H $\to ZZ^{(*)} \to q\bar{q}\,l^-l^+$ in pp collisions at $\sqrt{s_{NN}}$ = 7 TeV," arXiv:1202.1416 [hep-ex]. 1

[8] **TEVNPH (Tevatron New Phenomena and Higgs Working Group),** Collaboration, "Combined CDF and D0 Search for Standard Model Higgs Boson Production with up to 10.0 fb$^{-1}$ of Data," arXiv:1203.3774 [hep-ex]. 1

[9] **ALICE** Collaboration, "Higher harmonic anisotropic flow measurements of charged particles in Pb-Pb collisions at $\sqrt{s_{NN}}$ = 2.76 TeV," *Phys.Rev.Lett.* **107** (2011) 032301, arXiv:1105.3865 [nucl-ex]. 1, 3

[10] **ALICE** Collaboration, K. Aamodt *et al.*, "Two-pion Bose-Einstein correlations in central Pb-Pb collisions at $\sqrt{s_{NN}}$ = 2.76 TeV," *Phys.Lett.* **B696** (2011) 328–337, arXiv:1012.4035 [nucl-ex].

[11] **ALICE** Collaboration, K. Aamodt *et al.*, "Centrality dependence of the charged-particle multiplicity density at mid-rapidity in Pb-Pb collisions at $\sqrt{s_{NN}} = 2.76$ TeV," *Phys.Rev.Lett.* **106** (2011) 032301, arXiv:1012.1657 [nucl-ex].

[12] **ALICE** Collaboration, K. Aamodt *et al.*, "Elliptic flow of charged particles in Pb-Pb collisions at 2.76 TeV," *Phys.Rev.Lett.* **105** (2010) 252302, arXiv:1011.3914 [nucl-ex].

[13] **ALICE** Collaboration, K. Aamodt, "Suppression of Charged Particle Production at Large Transverse Momentum in Central Pb-Pb Collisions at $\sqrt{s_{NN}} = 2.76$ TeV," *Phys.Lett.* **B696** (2011) 30–39, arXiv:1012.1004 [nucl-ex].

[14] **ALICE** Collaboration, B. Abelev *et al.*, "Charged-particle multiplicity density at mid-rapidity in central Pb-Pb collisions at $\sqrt{s_{NN}} = 2.76$ TeV," *Phys.Rev.Lett.* **105** (2010) 252301, arXiv:1011.3916 [nucl-ex]. 1, 3

[15] **ATLAS** Collaboration, G. Aad *et al.*, "Measurement of the pseudorapidity and transverse momentum dependence of the elliptic flow of charged particles in lead-lead collisions at $\sqrt{s_{NN}} = 2.76$ TeV with the ATLAS detector," *Phys.Lett.* **B707** (2012) 330–348, arXiv:1108.6018 [hep-ex]. 1

[16] **ATLAS** Collaboration, G. Aad *et al.*, "Measurement of the azimuthal anisotropy for charged particle production in $\sqrt{s_{NN}} = 2.76$ TeV lead-lead collisions with the ATLAS detector," arXiv:1203.3087 [hep-ex].

[17] **ATLAS** Collaboration, "Measurement of the centrality dependence of the charged particle pseudorapidity distribution in lead-lead collisions at $\sqrt{s_{NN}} = 2.76$ TeV with the ATLAS detector," arXiv:1108.6027 [hep-ex]. 1

[18] **CMS** Collaboration, S. Chatrchyan *et al.*, "Study of high-pT charged particle suppression in Pb-Pb compared to pp collisions at $\sqrt{s_{NN}} = 2.76$ TeV," arXiv:1202.2554 [nucl-ex]. 1

[19] **CMS** Collaboration, "Jet momentum dependence of jet quenching in Pb-Pb collisions at $\sqrt{s_{NN}} = 2.76$ TeV," arXiv:1202.5022 [nucl-ex]. 1

[20] **STAR** Collaboration, J. Adams *et al.*, "Experimental and theoretical challenges in the search for the quark gluon plasma: The STAR Collaboration's critical assessment of the evidence from RHIC collisions," *Nucl.Phys.* **A757** (2005) 102–183, arXiv:nucl-ex/0501009 [nucl-ex]. 1, 3

[21] **PHENIX** Collaboration, K. Adcox *et al.*, "Formation of dense partonic matter in relativistic nucleus-nucleus collisions at RHIC: Experimental evaluation by the PHENIX collaboration," *Nucl.Phys.* **A757** (2005) 184–283, arXiv:nucl-ex/0410003 [nucl-ex].

[22] **BRAHMS** Collaboration, I. Arsene *et al.*, "Quark gluon plasma and color glass condensate at RHIC? The Perspective from the BRAHMS experiment," *Nucl.Phys.* **A757** (2005) 1–27, arXiv:nucl-ex/0410020 [nucl-ex].

[23] **PHOBOS** Collaboration, B. Back *et al.*, "The PHOBOS perspective on discoveries at RHIC," *Nucl.Phys.* **A757** (2005) 28–101, arXiv:nucl-ex/0410022 [nucl-ex]. 1, 3

[24] T. Matsui and H. Satz, "$J/\Psi$ Suppression by Quark-Gluon Plasma Formation," *Phys.Lett.* **B178** (1986) 416. 1

[25] M. Abreu *et al.*, "$J/\Psi$ and $\Psi'$ production in p, O and S induced reactions at SPS energies," *Phys.Lett.* **B466** (1999) 408–414.

[26] **NA50** Collaboration, F. Prino *et al.*, "$J/\Psi$ suppression in Pb-Pb collisions at CERN SPS," arXiv:hep-ex/0101052 [hep-ex].

[27] **NA50** Collaboration, M. Abreu *et al.*, "Observation of a threshold effect in the anomalous $J/\Psi$ suppression," *Phys.Lett.* **B450** (1999) 456–466. 1

[28] K. G. Wilson, "Confinement of Quarks," *Phys.Rev.* **D10** (1974) 2445–2459. 3

[29] F. Wegner, "Duality in Generalized Ising Models and Phase Transitions Without Local Order Parameters," *J.Math.Phys.* **12** (1971) 2259–2272.

[30] F. Karsch, "Lattice QCD at high temperature and density," *Lect.Notes Phys.* **583** (2002) 209–249, arXiv:hep-lat/0106019 [hep-lat]. 3

[31] S. Weinberg, "Phenomenological Lagrangians," *Physica* **A96** (1979) 327. Festschrift honoring Julian Schwinger on his 60th birthday. 3

[32] J. Gasser and H. Leutwyler, "Low-Energy Expansion of Meson Form-Factors," *Nucl.Phys.* **B250** (1985) 517–538. 3

[33] R. Sommer, "Introduction to Non-perturbative Heavy Quark Effective Theory," arXiv:1008.0710 [hep-lat]. 3

[34] M. Neubert, "Effective field theory and heavy quark physics," arXiv:hep-ph/0512222 [hep-ph]. 3

[35] J. Braun, L. M. Haas, F. Marhauser, and J. M. Pawlowski, "Phase Structure of Two-Flavor QCD at Finite Chemical Potential," *Phys.Rev.Lett.* **106** (2011) 022002, arXiv:0908.0008 [hep-ph]. 3

[36] C. Wetterich, "Exact evolution equation for the effective potential," *Phys.Lett.* **B301** (1993) 90–94.

[37] J. Berges, N. Tetradis, and C. Wetterich, "Nonperturbative renormalization flow in quantum field theory and statistical physics," *Phys.Rept.* **363** (2002) 223–386, arXiv:hep-ph/0005122 [hep-ph]. 3

[38] T. Springer, "Hydrodynamics of strongly coupled non-conformal fluids from gauge/gravity duality," arXiv:0908.1587 [hep-th]. 3, 4, 5, 6, 16

[39] E. V. Shuryak, "Quantum Chromodynamics and the Theory of Superdense Matter," *Phys.Rept.* **61** (1980) 71–158. 3

[40] L. McLerran, "The Color Glass Condensate and Glasma," arXiv:0804.1736 [hep-ph]. 4

[41] P. Braun-Munzinger, D. Magestro, K. Redlich, and J. Stachel, "Hadron production in Au - Au collisions at RHIC," *Phys.Lett.* **B518** (2001) 41–46, arXiv:hep-ph/0105229 [hep-ph]. 4

[42] H. Weigert, "Evolution at small $x_{\rm bj}$: The Color glass condensate," *Prog.Part.Nucl.Phys.* **55** (2005) 461–565, arXiv:hep-ph/0501087 [hep-ph]. 4

[43] E. Shuryak, "Physics of Strongly coupled Quark-Gluon Plasma," *Prog.Part.Nucl.Phys.* **62** (2009) 48–101, arXiv:0807.3033 [hep-ph].

[44] D. Banerjee, J. K. Nayak, and R. Venugopalan, "Two introductory lectures on high energy QCD and heavy ion collisions," *Lect.Notes Phys.* **785** (2010) 105–137, arXiv:0810.3553 [hep-ph]. 4

[45] G. 't Hooft, "Dimensional reduction in quantum gravity," arXiv:gr-qc/9310026 [gr-qc]. 5, 10

[46] L. Susskind, "The World as a hologram," *J.Math.Phys.* **36** (1995) 6377–6396, arXiv:hep-th/9409089 [hep-th]. 5, 10

[47] J. M. Maldacena, "The Large-N limit of superconformal field theories and supergravity," *Adv.Theor.Math.Phys.* **2** (1998) 231–252, arXiv:hep-th/9711200 [hep-th]. 5, 11, 20, 64

[48] E. Witten, "Anti-de Sitter space and holography," *Adv.Theor.Math.Phys.* **2** (1998) 253–291, arXiv:hep-th/9802150 [hep-th]. 11

[49] S. Gubser, I. R. Klebanov, and A. M. Polyakov, "Gauge theory correlators from noncritical string theory," *Phys.Lett.* **B428** (1998) 105–114, arXiv:hep-th/9802109 [hep-th]. 5, 12

[50] O. Aharony, A. Fayyazuddin, and J. M. Maldacena, "The Large-$\mathcal{N}$ limit of $\mathcal{N} = 2$, $\mathcal{N} = 1$ field theories from three-branes in F theory," *JHEP* **9807** (1998) 013, arXiv:hep-th/9806159 [hep-th]. 5

[51] A. Karch and E. Katz, "Adding flavor to $AdS$/CFT," *JHEP* **0206** (2002) 043, arXiv:hep-th/0205236 [hep-th]. 55

[52] E. Witten, "Anti-de Sitter space, thermal phase transition, and confinement in gauge theories," *Adv.Theor.Math.Phys.* **2** (1998) 505–532, arXiv:hep-th/9803131 [hep-th]. 12, 22

[53] J. Polchinski and M. J. Strassler, "The String dual of a confining four-dimensional gauge theory," arXiv:hep-th/0003136 [hep-th].

[54] J. M. Maldacena and C. Nunez, "Towards the large-$\mathcal{N}$ limit of pure $\mathcal{N} = 1$ super Yang–Mills," *Phys.Rev.Lett.* **86** (2001) 588–591, arXiv:hep-th/0008001 [hep-th].

[55] I. R. Klebanov and M. J. Strassler, "Supergravity and a confining gauge theory: Duality cascades and $\chi$-SB resolution of naked singularities," *JHEP* **0008** (2000) 052, arXiv:hep-th/0007191 [hep-th]. 151

[56] M. Kruczenski, D. Mateos, R. C. Myers, and D. J. Winters, "Towards a holographic dual of large $N_c$ QCD," *JHEP* **0405** (2004) 041, arXiv:hep-th/0311270 [hep-th].

[57] T. Sakai and S. Sugimoto, "Low energy hadron physics in holographic QCD," *Prog.Theor.Phys.* **113** (2005) 843–882, arXiv:hep-th/0412141 [hep-th]. 5, 27, 55, 151

[58] J. Polchinski and M. J. Strassler, "Hard scattering and gauge/string duality," *Phys.Rev.Lett.* **88** (2002) 031601, arXiv:hep-th/0109174 [hep-th]. 6, 31

[59] J. Erlich, E. Katz, D. T. Son, and M. A. Stephanov, "QCD and a holographic model of hadrons," *Phys.Rev.Lett.* **95** (2005) 261602, arXiv:hep-ph/0501128 [hep-ph].

[60] A. Karch, E. Katz, D. T. Son, and M. A. Stephanov, "Linear confinement and $AdS$/QCD," *Phys.Rev.* **D74** (2006) 015005, arXiv:hep-ph/0602229 [hep-ph]. 31, 38, 77, 102

[61] S. S. Gubser, A. Nellore, S. S. Pufu, and F. D. Rocha, "Thermodynamics and bulk viscosity of approximate black hole duals to finite temperature quantum chromodynamics," *Phys.Rev.Lett.* **101** (2008) 131601, arXiv:0804.1950 [hep-th]. 34, 74

[62] S. S. Gubser and A. Nellore, "Mimicking the QCD equation of state with a dual black hole," *Phys.Rev.* **D78** (2008) 086007, arXiv:0804.0434 [hep-th]. 34, 35, 37, 40, 74, 148

[63] O. Andreev, "Some Thermodynamic Aspects of Pure Glue, Fuzzy Bags and Gauge/String Duality," *Phys.Rev.* **D76** (2007) 087702, arXiv:0706.3120 [hep-ph]. 148

[64] K. Kajantie, T. Tahkokallio, and J.-T. Yee, "Thermodynamics of $AdS$/QCD," *JHEP* **0701** (2007) 019, arXiv:hep-ph/0609254 [hep-ph]. 7, 30, 31, 32, 34, 83, 148, 149

[65] U. Gursoy and E. Kiritsis, "Exploring improved holographic theories for QCD: Part I," *JHEP* **0802** (2008) 032, arXiv:0707.1324 [hep-th]. 42, 43, 149

[66] U. Gursoy, E. Kiritsis, and F. Nitti, "Exploring improved holographic theories for QCD: Part II," *JHEP* **0802** (2008) 019, arXiv:0707.1349 [hep-th]. 42, 43

[67] U. Gursoy, E. Kiritsis, L. Mazzanti, and F. Nitti, "Deconfinement and Gluon Plasma Dynamics in Improved Holographic QCD," *Phys.Rev.Lett.* **101** (2008) 181601, arXiv:0804.0899 [hep-th]. 34

[68] U. Gursoy, E. Kiritsis, L. Mazzanti, and F. Nitti, "Holography and Thermodynamics of 5D Dilaton-gravity," *JHEP* **0905** (2009) 033, arXiv:0812.0792 [hep-th]. 27

[69] U. Gursoy, E. Kiritsis, G. Michalogiorgakis, and F. Nitti, "Thermal Transport and Drag Force in Improved Holographic QCD," *JHEP* **0912** (2009) 056, arXiv:0906.1890 [hep-ph]. 6, 34

[70] A. Buchel and J. T. Liu, "Universality of the shear viscosity in supergravity," *Phys.Rev.Lett.* **93** (2004) 090602, arXiv:hep-th/0311175 [hep-th]. 6

[71] P. Kovtun, D. T. Son, and A. O. Starinets, "Holography and hydrodynamics: Diffusion on stretched horizons," *JHEP* **0310** (2003) 064, arXiv:hep-th/0309213 [hep-th]. 6

[72] P. Kovtun, D. Son, and A. Starinets, "Viscosity in strongly interacting quantum field theories from black hole physics," *Phys.Rev.Lett.* **94** (2005) 111601, arXiv:hep-th/0405231 [hep-th]. 6, 29, 49

[73] H. Liu, K. Rajagopal, and Y. Shi, "Robustness and Infrared Sensitivity of Various Observables in the Application of $AdS$/CFT to Heavy Ion Collisions," *JHEP* **0808** (2008) 048, arXiv:0803.3214 [hep-ph]. 7, 31, 52, 66, 81, 149

[74] S. S. Gubser, "Comparing the drag force on heavy quarks in $\mathcal{N} = 4$ super-Yang–Mills theory and QCD," *Phys.Rev.* **D76** (2007) 126003, arXiv:hep-th/0611272 [hep-th]. 7, 54, 63, 71, 75, 148

[75] C. Ewerz and K. Schade, "Screening in Strongly Coupled Plasmas: Universal Properties from Strings in Curved Space," arXiv:1010.1138 [hep-th]. proceeding of Gribov-80 Memorial Workshop. 7, 49, 61, 63, 68, 79, 81, 82, 102, 149

[76] K. Schade, "Gone with the Wind: Heavy Meson and Baryon Screening in Hot Moving Plasmas,". Diploma Thesis, University of Heidelberg. 7, 63, 68, 79, 81, 102, 149

[77] A. Samberg. Diploma Thesis, University of Heidelberg, in preparation. 8, 81, 124, 151

[78] A. Dobado, "An Elementary introduction to the holographic principle," arXiv:hep-ph/0506027 [hep-ph]. 9, 10

[79] O. Aharony, S. S. Gubser, J. M. Maldacena, H. Ooguri, and Y. Oz, "Large N field theories, string theory and gravity," *Phys.Rept.* **323** (2000) 183–386, arXiv:hep-th/9905111 [hep-th]. 9, 11, 16

[80] E. D'Hoker and D. Z. Freedman, "Supersymmetric gauge theories and the $AdS$/CFT correspondence," arXiv:hep-th/0201253 [hep-th].

[81] D. Bigatti and L. Susskind, "TASI lectures on the holographic principle," arXiv:hep-th/0002044 [hep-th].

[82] A. W. Peet, "TASI lectures on black holes in string theory," arXiv:hep-th/0008241 [hep-th].

[83] I. R. Klebanov, "TASI lectures: Introduction to the $AdS$/CFT correspondence," arXiv:hep-th/0009139 [hep-th].

[84] D. Young, "The $AdS$/CFT correspondence: Classical, quantum, and thermodynamical aspects," arXiv:0706.3751 [hep-th].

[85] H. Nastase, "Introduction to $AdS$/CFT," arXiv:0712.0689 [hep-th]. 20

[86] J. Casalderrey-Solana, H. Liu, D. Mateos, K. Rajagopal, and U. A. Wiedemann, "Gauge/String Duality, Hot QCD and Heavy Ion Collisions," arXiv:1101.0618 [hep-th]. 9, 11, 13, 15, 16, 17

[87] S. Hawking, "Breakdown of Predictability in Gravitational Collapse," *Phys.Rev.* **D14** (1976) 2460–2473. 9, 10

[88] S. Hawking, "Black hole explosions," *Nature* **248** (1974) 30–31. 9, 24

[89] J. Bekenstein, "Black holes and the second law," *Lett.Nuovo Cim.* **4** (1972) 737–740. 9, 24

[90] J. A. Harvey and A. Strominger, "Quantum aspects of black holes," arXiv:hep-th/9209055 [hep-th]. 10

[91] D. N. Page, "Black hole information," arXiv:hep-th/9305040 [hep-th].

[92] S. B. Giddings, "Quantum mechanics of black holes," arXiv:hep-th/9412138 [hep-th].

[93] J. Preskill, "Do black holes destroy information?," arXiv:hep-th/9209058 [hep-th].

[94] A. Strominger, "Les Houches lectures on black holes," arXiv:hep-th/9501071 [hep-th]. Les Houches Summer School on Fluctuating Geometries in Statistical Mechanics and Field Theory.

[95] H. Nikolic, "Resolving the black-hole information paradox by treating time on an equal footing with space," *Phys.Lett.* **B678** (2009) 218–221, arXiv:0905.0538 [gr-qc]. 10

[96] M. Srednicki, "Entropy and area," *Phys.Rev.Lett.* **71** (1993) 666–669, arXiv:hep-th/9303048 [hep-th]. 10

[97] J. Carmona and J. Cortes, "Infrared and ultraviolet cutoffs of quantum field theory," *Phys.Rev.* **D65** (2002) 025006, arXiv:hep-th/0012028 [hep-th]. 5 pages, no figures/ general discussion improved, main results unchanged. Version to appear in PRD. 10

[98] L. Brink, J. H. Schwarz, and J. Scherk, "Supersymmetric Yang-Mills Theories," *Nucl.Phys.* **B121** (1977) 77. 11, 17

[99] F. Gliozzi, J. Scherk, and D. I. Olive, "Supersymmetry, Supergravity Theories and the Dual Spinor Model," *Nucl.Phys.* **B122** (1977) 253–290.

[100] S. Kovacs, "$\mathcal{N} = 4$ supersymmetric Yang-Mills theory and the $AdS$/CFT correspondence," arXiv:hep-th/9908171 [hep-th]. 11, 17

[101] L. Avdeev, O. Tarasov, and A. Vladimirov, "Vanishing of the three Loop Charge Renormalization Function in a Supersymmetric Gauge Theory," *Phys.Lett.* **B96** (1980) 94–96. 12

[102] M. T. Grisaru, M. Rocek, and W. Siegel, "Zero Three Loop beta Function in $\mathcal{N} = 4$ Supersymmetric Yang–Mills Theory," *Phys.Rev.Lett.* **45** (1980) 1063–1066.

[103] M. F. Sohnius and P. C. West, "Conformal Invariance in $\mathcal{N} = 4$ Supersymmetric Yang-Mills Theory," *Phys.Lett.* **B100** (1981) 245.

[104] W. E. Caswell and D. Zanon, "Zero Three Loop beta Function in $\mathcal{N} = 4$ Supersymmetric Yang–Mills Theory," *Nucl.Phys.* **B182** (1981) 125.

[105] P. S. Howe, K. Stelle, and P. Townsend, "Miraculous Ultraviolet Cancellations in Supersymmetry Made Manifest," *Nucl.Phys.* **B236** (1984) 125.

[106] S. Mandelstam, "Light Cone Superspace and the Ultraviolet Finiteness of the $\mathcal{N} = 4$ Model," *Nucl.Phys.* **B213** (1983) 149–168.

[107] L. Brink, O. Lindgren, and B. E. Nilsson, "The Ultraviolet Finiteness of the $\mathcal{N} = 4$ Yang-Mills Theory," *Phys.Lett.* **B123** (1983) 323. 12

[108] I. Kanitscheider, "Precision Holography and its Applications to Black Holes,". PhD Thesis, University of Amsterdam. 12

[109] G. 't Hooft, "A Planar Diagram Theory for Strong Interactions," *Nucl.Phys.* **B72** (1974) 461. 15, 21

[110] J. Polchinski, "Dirichlet Branes and Ramond-Ramond charges," *Phys.Rev.Lett.* **75** (1995) 4724–4727, arXiv:hep-th/9510017 [hep-th]. 16

[111] J. Polchinski, S. Chaudhuri, and C. V. Johnson, "Notes on D-branes," arXiv:hep-th/9602052 [hep-th]. 16

[112] E. Witten, "Bound states of strings and p-branes," *Nucl.Phys.* **B460** (1996) 335–350, arXiv:hep-th/9510135 [hep-th]. 17

[113] G. T. Horowitz and A. Strominger, "Black strings and P-branes," *Nucl.Phys.* **B360** (1991) 197–209. 18, 22

[114] G. Gibbons and K.-i. Maeda, "Black Holes and Membranes in Higher Dimensional Theories with Dilaton Fields," *Nucl.Phys.* **B298** (1988) 741. 18

[115] D. Garfinkle, G. T. Horowitz, and A. Strominger, "Charged black holes in string theory," *Phys.Rev.* **D43** (1991) 3140. 18

[116] S. Gubser, I. R. Klebanov, and A. Peet, "Entropy and temperature of black 3-branes," *Phys.Rev.* **D54** (1996) 3915–3919, arXiv:hep-th/9602135 [hep-th]. 22, 26

[117] M. Bianchi, D. Z. Freedman, and K. Skenderis, "Holographic renormalization," *Nucl.Phys.* **B631** (2002) 159–194, arXiv:hep-th/0112119 [hep-th]. 22

[118] K. Skenderis, "Lecture notes on holographic renormalization," *Class.Quant.Grav.* **19** (2002) 5849–5876, arXiv:hep-th/0209067 [hep-th].

[119] R. A. Janik and R. B. Peschanski, "Asymptotic perfect fluid dynamics as a consequence of $AdS$/CFT," *Phys.Rev.* **D73** (2006) 045013, arXiv:hep-th/0512162 [hep-th]. 22, 23

[120] I. R. Klebanov and E. Witten, "$AdS$/CFT correspondence and symmetry breaking," *Nucl.Phys.* **B556** (1999) 89–114, arXiv:hep-th/9905104 [hep-th]. 22

[121] V. Balasubramanian, J. de Boer, and D. Minic, "Mass, entropy and holography in asymptotically de Sitter spaces," *Phys.Rev.* **D65** (2002) 123508, arXiv:hep-th/0110108 [hep-th]. 22

[122] R. C. Myers, "Stress tensors and Casimir energies in the $AdS$/CFT correspondence," *Phys.Rev.* **D60** (1999) 046002, arXiv:hep-th/9903203 [hep-th].

[123] S. de Haro, S. N. Solodukhin, and K. Skenderis, "Holographic reconstruction of space-time and renormalization in the $AdS$/CFT correspondence," *Commun.Math.Phys.* **217** (2001) 595–622, arXiv:hep-th/0002230 [hep-th]. 22, 23

[124] H. Liu, K. Rajagopal, and U. A. Wiedemann, "Wilson loops in heavy ion collisions and their calculation in $AdS$/CFT," *JHEP* **0703** (2007) 066, arXiv:hep-ph/0612168 [hep-ph]. 26, 54, 66, 81, 148

[125] S. S. Gubser, I. R. Klebanov, and A. A. Tseytlin, "Coupling constant dependence in the thermodynamics of $\mathcal{N} = 4$ supersymmetric Yang-Mills theory," *Nucl.Phys.* **B534** (1998) 202–222, arXiv:hep-th/9805156 [hep-th]. 26

[126] K. O'Hara, S. Hemmer, M. Gehm, S. Granade, and J. Thomas, "Observation of a Strongly Interacting Degenerate Fermi Gas of Atoms," *Science* **298** (2002) 2179–2182, arXiv:cond-mat/0212463 [cond-mat.supr-con]. 27

[127] M. Luzum and P. Romatschke, "Conformal Relativistic Viscous Hydrodynamics: Applications to RHIC results at $\sqrt{s_{NN}} = 200$ GeV," *Phys.Rev.* **C78** (2008) 034915, arXiv:0804.4015 [nucl-th]. 27, 147

[128] R. Baier, P. Romatschke, D. T. Son, A. O. Starinets, and M. A. Stephanov, "Relativistic viscous hydrodynamics, conformal invariance, and holography," *JHEP* **0804** (2008) 100, arXiv:0712.2451 [hep-th]. 27, 147

[129] J. Erdmenger, N. Evans, I. Kirsch, and E. Threlfall, "Mesons in Gauge/Gravity Duals - A Review," *Eur.Phys.J.* **A35** (2008) 81–133, arXiv:0711.4467 [hep-th]. 27, 34, 55, 151

[130] K. Maeda, M. Natsuume, and T. Okamura, "Viscosity of gauge theory plasma with a chemical potential from $AdS$/CFT," *Phys.Rev.* **D73** (2006) 066013, arXiv:hep-th/0602010 [hep-th].

[131] A. Karch and A. O'Bannon, "Holographic thermodynamics at finite baryon density: Some exact results," *JHEP* **0711** (2007) 074, arXiv:0709.0570 [hep-th].

[132] R. C. Myers, M. F. Paulos, and A. Sinha, "Holographic Hydrodynamics with a Chemical Potential," *JHEP* **0906** (2009) 006, arXiv:0903.2834 [hep-th]. 27

[133] A. Buchel, "Bulk viscosity of gauge theory plasma at strong coupling," *Phys.Lett.* **B663** (2008) 286–289, arXiv:0708.3459 [hep-th]. 30

[134] D. Kharzeev and K. Tuchin, "Bulk viscosity of QCD matter near the critical temperature," *JHEP* **0809** (2008) 093, arXiv:0705.4280 [hep-ph]. 30

[135] F. Karsch, D. Kharzeev, and K. Tuchin, "Universal properties of bulk viscosity near the QCD phase transition," *Phys.Lett.* **B663** (2008) 217–221, arXiv:0711.0914 [hep-ph].

[136] S. S. Gubser, S. S. Pufu, and F. D. Rocha, "Bulk viscosity of strongly coupled plasmas with holographic duals," *JHEP* **0808** (2008) 085, arXiv:0806.0407 [hep-th]. 30, 35

[137] A. Buchel, "Violation of the holographic bulk viscosity bound," arXiv:1110.0063 [hep-th]. 30

[138] O. Andreev and V. I. Zakharov, "Heavy-quark potentials and $AdS$/QCD," *Phys.Rev.* **D74** (2006) 025023, arXiv:hep-ph/0604204 [hep-ph]. 30

[139] D. Tong, "String Theory," arXiv:0908.0333 [hep-th]. Lectures in Part III of the Mathematical Tripos at the University of Cambridge. 30

[140] A. Karch, E. Katz, D. T. Son, and M. A. Stephanov, "On the sign of the dilaton in the soft wall models," *JHEP* **1104** (2011) 066, arXiv:1012.4813 [hep-ph]. 31

[141] J. Polchinski and M. J. Strassler, "Deep inelastic scattering and gauge/string duality," *JHEP* **0305** (2003) 012, arXiv:hep-th/0209211 [hep-th]. 31

[142] S. J. Brodsky and G. F. de Teramond, "Light front hadron dynamics and $AdS$/CFT correspondence," *Phys.Lett.* **B582** (2004) 211–221, arXiv:hep-th/0310227 [hep-th].

[143] G. F. de Teramond and S. J. Brodsky, "Hadronic spectrum of a holographic dual of QCD," *Phys.Rev.Lett.* **94** (2005) 201601, arXiv:hep-th/0501022 [hep-th]. 31

[144] P. Huovinen and P. Petreczky, "QCD Equation of State and Hadron Resonance Gas," *Nucl.Phys.* **A837** (2010) 26–53, arXiv:0912.2541 [hep-ph]. 33, 34

[145] J. Noronha-Hostler, J. Noronha, and C. Greiner, "Particle Ratios and the QCD Critical Temperature," *J.Phys.G* **G37** (2010) 094062, arXiv:1001.2610 [nucl-th]. 34, 70

[146] F. Karsch, "Lattice QCD at finite temperature and density," *Nucl.Phys.Proc.Suppl.* **83** (2000) 14–23, arXiv:hep-lat/9909006 [hep-lat]. 34

[147] M. Cheng *et al.*, "The QCD equation of state with almost physical quark masses," *Phys.Rev.* **D77** (2008) 014511, arXiv:0710.0354 [hep-lat]. 63, 70

[148] F. Karsch, "Recent lattice results on finite temperature and density QCD. Part I.," *PoS* **CPOD07** (2007) 026, arXiv:0711.0656 [hep-lat].

[149] A. Bazavov, T. Bhattacharya, M. Cheng, N. Christ, C. DeTar, *et al.*, "Equation of state and QCD transition at finite temperature," *Phys.Rev.* **D80** (2009) 014504, arXiv:0903.4379 [hep-lat]. 34

[150] D. Li, S. He, M. Huang, and Q.-S. Yan, "Thermodynamics of deformed $AdS_5$ model with a positive/negative quadratic correction in graviton-dilaton system," *JHEP* **1109** (2011) 041, arXiv:1103.5389 [hep-th]. 34

[151] N. Evans, K.-Y. Kim, J. P. Shock, and J. P. Shock, "Chiral phase transitions and quantum critical points of the D3/D7(D5) system with mutually perpendicular E and B fields at finite temperature and density," *JHEP* **1109** (2011) 021, arXiv:1107.5053 [hep-th]. 34

[152] N. Evans, T. Kalaydzhyan, K.-y. Kim, and I. Kirsch, "Non-equilibrium physics at a holographic chiral phase transition," *JHEP* **1101** (2011) 050, arXiv:1011.2519 [hep-th]. 34

[153] R.-G. Cai, Z.-Y. Nie, N. Ohta, and Y.-W. Sun, "Shear Viscosity from Gauss-Bonnet Gravity with a Dilaton Coupling," *Phys.Rev.* **D79** (2009) 066004, arXiv:0901.1421 [hep-th]. 34

[154] N. Ohta and T. Torii, "Black Holes in the Dilatonic Einstein-Gauss-Bonnet Theory in Various Dimensions. III. Asymptotically $AdS$ Black Holes with $k = \pm 1$," *Prog.Theor.Phys.* **121** (2009) 959–981, arXiv:0902.4072 [hep-th]. 34

[155] O. DeWolfe, S. S. Gubser, and C. Rosen, "A holographic critical point," *Phys.Rev.* **D83** (2011) 086005, arXiv:1012.1864 [hep-th]. 34, 151

[156] O. DeWolfe and C. Rosen, "Robustness of Sound Speed and Jet Quenching for Gauge/Gravity Models of Hot QCD," *JHEP* **0907** (2009) 022, arXiv:0903.1458 [hep-th]. 34, 40, 42

[157] P. Breitenlohner and D. Z. Freedman, "Positive Energy in anti-De Sitter Backgrounds and Gauged Extended Supergravity," *Phys.Lett.* **B115** (1982) 197. 39

[158] L. Mezincescu and P. Townsend, "Stability at a Local Maximum in Higher Dimensional Anti-de Sitter Space and Applications to Supergravity," *Annals Phys.* **160** (1985) 406. 39

[159] M. Panero, "Thermodynamics of the strongly interacting gluon plasma in the large-N limit," *PoS* **LAT2009** (2009) 172, arXiv:0912.2448 [hep-lat]. 42, 43, 149

[160] M. Panero, "Thermodynamics of the QCD plasma and the large-N limit," *Phys.Rev.Lett.* **103** (2009) 232001, arXiv:0907.3719 [hep-lat]. 42, 43, 149

[161] U. Gursoy, E. Kiritsis, L. Mazzanti, and F. Nitti, "Improved Holographic Yang-Mills at Finite Temperature: Comparison with Data," *Nucl.Phys.* **B820** (2009) 148–177, arXiv:0903.2859 [hep-th]. 42, 43

[162] U. Gursoy, E. Kiritsis, L. Mazzanti, G. Michalogiorgakis, and F. Nitti, "Improved Holographic QCD," *Lect.Notes Phys.* **828** (2011) 79–146, arXiv:1006.5461 [hep-th]. 42, 43

[163] A. Helmboldt, "Jet Quenching Parameter und Temperatureigenschaften von deformierten $AdS$/CFT-Modellen für heiße Plasmen,". Bachelor thesis, University of Heidelberg. 45

[164] T. Schäfer and D. Teaney, "Nearly Perfect Fluidity: From Cold Atomic Gases to Hot Quark Gluon Plasmas," *Rept.Prog.Phys.* **72** (2009) 126001, arXiv:0904.3107 [hep-ph]. 49

[165] S. S. Gubser, "Drag force in $AdS$/CFT," *Phys.Rev.* **D74** (2006) 126005, arXiv:hep-th/0605182 [hep-th]. 52, 54, 135, 148

[166] J. Casalderrey-Solana and D. Teaney, "Transverse Momentum Broadening of a Fast Quark in a $\mathcal{N} = 4$ Yang Mills Plasma," *JHEP* **0704** (2007) 039, arXiv:hep-th/0701123 [hep-th].

[167] A. Guijosa and J. F. Pedraza, "Early-Time Energy Loss in a Strongly-Coupled SYM Plasma," *JHEP* **1105** (2011) 108, arXiv:1102.4893 [hep-th]. 54

[168] C. Herzog, A. Karch, P. Kovtun, C. Kozcaz, and L. Yaffe, "Energy loss of a heavy quark moving through $\mathcal{N} = 4$ supersymmetric Yang-Mills plasma," *JHEP* **0607** (2006) 013, arXiv:hep-th/0605158 [hep-th]. 52, 54, 135

[169] D. d'Enterria, "Jet quenching," arXiv:0902.2011 [nucl-ex]. 52

[170] M. Gyulassy, P. Levai, and I. Vitev, "Non-abelian energy loss at finite opacity," *Phys.Rev.Lett.* **85** (2000) 5535–5538, arXiv:nucl-th/0005032 [nucl-th]. 53

[171] P. Gossiaux, J. Aichelin, and T. Gousset, "Theory of heavy quark energy loss," arXiv:1201.4038 [hep-ph].

[172] U. A. Wiedemann, "Gluon radiation off hard quarks in a nuclear environment: Opacity expansion," *Nucl.Phys.* **B588** (2000) 303–344, arXiv:hep-ph/0005129 [hep-ph].

[173] P. B. Arnold, G. D. Moore, and L. G. Yaffe, "Photon emission from quark gluon plasma: Complete leading order results," *JHEP* **0112** (2001) 009, arXiv:hep-ph/0111107 [hep-ph]. 53

[174] E. Braaten and M. H. Thoma, "Energy loss of a heavy quark in the quark-gluon plasma," *Phys.Rev.* **D44** (1991) 2625–2630. 53

[175] E. Braaten and M. H. Thoma, "Energy loss of a heavy fermion in a hot plasma," *Phys.Rev.* **D44** (1991) 1298–1310. 53

[176] S. Wicks, W. Horowitz, M. Djordjevic, and M. Gyulassy, "Elastic, inelastic, and path length fluctuations in jet tomography," *Nucl.Phys.* **A784** (2007) 426–442, arXiv:nucl-th/0512076 [nucl-th]. 53

[177] R. Baier, Y. L. Dokshitzer, A. H. Mueller, S. Peigne, and D. Schiff, "Radiative energy loss of high-energy quarks and gluons in a finite volume quark-gluon plasma," *Nucl.Phys.* **B483** (1997) 291–320, arXiv:hep-ph/9607355 [hep-ph]. 53

[178] R. Baier, Y. L. Dokshitzer, A. H. Mueller, S. Peigne, and D. Schiff, "Radiative energy loss and p(T) broadening of high-energy partons in nuclei," *Nucl.Phys.* **B484** (1997) 265–282, arXiv:hep-ph/9608322 [hep-ph].

[179] R. Baier, D. Schiff, and B. Zakharov, "Energy loss in perturbative QCD," *Ann.Rev.Nucl.Part.Sci.* **50** (2000) 37–69, arXiv:hep-ph/0002198 [hep-ph]. 109

[180] M. Djordjevic and M. Gyulassy, "Heavy quark radiative energy loss in QCD matter," *Nucl.Phys.* **A733** (2004) 265–298, arXiv:nucl-th/0310076 [nucl-th]. 53

[181] N. Armesto, M. Cacciari, A. Dainese, C. A. Salgado, and U. A. Wiedemann, "How sensitive are high-p(T) electron spectra at RHIC to heavy quark energy loss?," *Phys.Lett.* **B637** (2006) 362–366, arXiv:hep-ph/0511257 [hep-ph]. 53

[182] N. Armesto, C. A. Salgado, and U. A. Wiedemann, "Medium induced gluon radiation off massive quarks fills the dead cone," *Phys.Rev.* **D69** (2004) 114003, arXiv:hep-ph/0312106 [hep-ph]. 53

[183] N. Armesto, M. Cacciari, A. Dainese, C. Salgado, and U. Wiedemann, "Heavy-to-light ratios as a test of medium-induced energy loss at RHIC and the LHC," *Nucl.Phys.* **A774** (2006) 589–592, arXiv:hep-ph/0510284 [hep-ph]. 53

[184] J. Bjorken, "Energy Loss of Energetic Partons in Quark-Gluon Plasma: Possible Extinction of High p(t) Jets in Hadron-Hadron Collisions,". FERMILAB-PUB-82-059-T. 53

[185] J. Bjorken, "Highly Relativistic Nucleus-Nucleus Collisions: The Central Rapidity Region," *Phys.Rev.* **D27** (1983) 140–151.

[186] M. Thoma and M. Gyulassy, "Energy loss of high-energy quarks and gluons in the quark-gluon plasma," *Nucl.Phys.* **A544** (1992) 573C–580C.

[187] M. H. Thoma and M. Gyulassy, "Quark Damping and Energy Loss in the High Temperature QCD," *Nucl.Phys.* **B351** (1991) 491–506.

[188] M. G. Mustafa and M. H. Thoma, "Quenching of hadron spectra due to the collisional energy loss of partons in the quark gluon plasma," *Acta Phys.Hung.* **A22** (2005) 93–102, arXiv:hep-ph/0311168 [hep-ph]. 53

[189] Y. L. Dokshitzer and D. Kharzeev, "Heavy quark colorimetry of QCD matter," *Phys.Lett.* **B519** (2001) 199–206, arXiv:hep-ph/0106202 [hep-ph]. 53

[190] K. B. Fadafan, H. Liu, K. Rajagopal, and U. A. Wiedemann, "Stirring Strongly Coupled Plasma," *Eur.Phys.J.* **C61** (2009) 553–567, arXiv:0809.2869 [hep-ph]. 53, 54, 109, 110, 112, 115, 136, 137, 138, 140, 141, 144, 145, 146, 148, 150

[191] B. Zakharov, "Radiative energy loss of high-energy quarks in finite size nuclear matter and quark-gluon plasma," *JETP Lett.* **65** (1997) 615–620, arXiv:hep-ph/9704255 [hep-ph]. 54

[192] H. Liu, K. Rajagopal, and U. A. Wiedemann, "Calculating the jet quenching parameter from $AdS$/CFT," *Phys.Rev.Lett.* **97** (2006) 182301, arXiv:hep-ph/0605178 [hep-ph]. 54

[193] A. Karch and L. Randall, "Open and closed string interpretation of SUSY CFT's on branes with boundaries," *JHEP* **0106** (2001) 063, arXiv:hep-th/0105132 [hep-th]. 55

[194] M. Bertolini, P. Di Vecchia, M. Frau, A. Lerda, and R. Marotta, "$\mathcal{N} = 2$ gauge theories on systems of fractional D3/D7 branes," *Nucl.Phys.* **B621** (2002) 157–178, arXiv:hep-th/0107057 [hep-th]. 55

[195] J. J. Friess, S. S. Gubser, G. Michalogiorgakis, and S. S. Pufu, "The Stress tensor of a quark moving through $\mathcal{N} = 4$ thermal plasma," *Phys.Rev.* **D75** (2007) 106003, arXiv:hep-th/0607022 [hep-th]. 58

[196] O. Kaczmarek and F. Zantow, "Static quark anti-quark free and internal energy in 2-flavor QCD," *Eur.Phys.J.* **C43** (2005) 63–66, arXiv:hep-lat/0502011 [hep-lat]. 63, 70, 72, 149

[197] O. Kaczmarek and F. Zantow, "Static quark anti-quark interactions in zero and finite temperature QCD. I. Heavy quark free energies, running coupling and quarkonium binding," *Phys.Rev.* **D71** (2005) 114510, arXiv:hep-lat/0503017 [hep-lat]. 70, 74, 75, 78

[198] O. Kaczmarek and F. Zantow, "Static quark anti-quark interactions at zero and finite temperature QCD. II. Quark anti-quark internal energy and entropy," arXiv:hep-lat/0506019 [hep-lat].

[199] O. Kaczmarek and F. Zantow, "The Screening length in hot QCD," *PoS* **LAT2005** (2006) 177, arXiv:hep-lat/0510093 [hep-lat]. 63, 72, 149

[200] O. Kaczmarek, "Screening at finite temperature and density," *PoS* **CPOD07** (2007) 043, arXiv:0710.0498 [hep-lat]. 63, 70

[201] J. M. Maldacena, "Wilson loops in large N field theories," *Phys.Rev.Lett.* **80** (1998) 4859–4862, arXiv:hep-th/9803002 [hep-th]. 64, 70, 81

[202] S. D. Avramis, K. Sfetsos, and D. Zoakos, "On the velocity and chemical-potential dependence of the heavy-quark interaction in $\mathcal{N} = 4$ SYM plasmas," *Phys.Rev.* **D75** (2007) 025009, arXiv:hep-th/0609079 [hep-th]. 70

[203] J. J. Friess, S. S. Gubser, G. Michalogiorgakis, and S. S. Pufu, "Stability of strings binding heavy-quark mesons," *JHEP* **0704** (2007) 079, arXiv:hep-th/0609137 [hep-th]. 70

[204] D. Bak, A. Karch, and L. G. Yaffe, "Debye screening in strongly coupled $\mathcal{N} = 4$ supersymmetric Yang-Mills plasma," *JHEP* **0708** (2007) 049, arXiv:0705.0994 [hep-th]. 79

[205] K. Peeters, J. Plefka, and M. Zamaklar, "Splitting spinning strings in $AdS$/CFT," *JHEP* **0411** (2004) 054, arXiv:hep-th/0410275 [hep-th]. 79

[206] K. Peeters, J. Sonnenschein, and M. Zamaklar, "Holographic decays of large-spin mesons," *JHEP* **0602** (2006) 009, arXiv:hep-th/0511044 [hep-th].

[207] K. Peeters, J. Sonnenschein, and M. Zamaklar, "Holographic melting and related properties of mesons in a quark gluon plasma," *Phys.Rev.* **D74** (2006) 106008, arXiv:hep-th/0606195 [hep-th].

[208] K. Peeters and M. Zamaklar, "Dissociation by acceleration," *JHEP* **0801** (2008) 038, arXiv:0711.3446 [hep-th].

[209] A. Paredes, K. Peeters, and M. Zamaklar, "Temperature versus acceleration: The Unruh effect for holographic models," *JHEP* **0904** (2009) 015, arXiv:0812.0981 [hep-th]. 79

[210] R. Baier, "Jet quenching," *Nucl.Phys.* **A715** (2003) 209–218, arXiv:hep-ph/0209038 [hep-ph]. 109

[211] A. Kovner and U. A. Wiedemann, "Gluon radiation and parton energy loss," arXiv:hep-ph/0304151 [hep-ph]. Review for Quark Gluon Plasma 3, Editors: R.C. Hwa and X.N. Wang, World Scientific, Singapore.

[212] M. Gyulassy, I. Vitev, X.-N. Wang, and B.-W. Zhang, "Jet quenching and radiative energy loss in dense nuclear matter," arXiv:nucl-th/0302077 [nucl-th]. Review for Quark Gluon Plasma 3, Editors: R.C. Hwa and X.N. Wang, World Scientific, Singapore.

[213] P. Jacobs and X.-N. Wang, "Matter in extremis: Ultrarelativistic nuclear collisions at RHIC," *Prog.Part.Nucl.Phys.* **54** (2005) 443–534, arXiv:hep-ph/0405125 [hep-ph].

[214] J. Casalderrey-Solana and C. A. Salgado, "Introductory lectures on jet quenching in heavy ion collisions," *Acta Phys.Polon.* **B38** (2007) 3731–3794, arXiv:0712.3443 [hep-ph]. 109

[215] C. Athanasiou, P. M. Chesler, H. Liu, D. Nickel, and K. Rajagopal, "Synchrotron radiation in strongly coupled conformal field theories," *Phys.Rev.* **D81** (2010) 126001, arXiv:1001.3880 [hep-th]. 110, 111, 112, 113, 148

[216] G. Giecold, E. Iancu, and A. Mueller, "Stochastic trailing string and Langevin dynamics from $AdS$/CFT," *JHEP* **0907** (2009) 033, arXiv:0903.1840 [hep-th]. 114, 147, 163

[217] A. Mikhailov, "Nonlinear waves in $AdS$/CFT correspondence," arXiv:hep-th/0305196 [hep-th]. 140

[218] A. Liénard, "L' Eclairage Electrique,". 140

[219] S. A. Hartnoll, "Horizons, holography and condensed matter," arXiv:1106.4324 [hep-th]. 147

[220] S. S. Gubser, "TASI lectures: Collisions in anti-de Sitter space, conformal symmetry, and holographic superconductors," arXiv:1012.5312 [hep-th].

[221] K. Maeda and T. Okamura, "Vortex flow for a holographic superconductor," *Phys.Rev.* **D83** (2011) 066004, arXiv:1012.0202 [hep-th].

[222] G. T. Horowitz, "Introduction to Holographic Superconductors," arXiv:1002.1722 [hep-th].

[223] I. Amado, M. Kaminski, and K. Landsteiner, "Hydrodynamics of Holographic Superconductors," *JHEP* **0905** (2009) 021, arXiv:0903.2209 [hep-th]. 147

[224] K. Balasubramanian and J. McGreevy, "Gravity duals for non-relativistic CFTs," *Phys.Rev.Lett.* **101** (2008) 061601, arXiv:0804.4053 [hep-th]. 147

[225] W. D. Goldberger, "$AdS$/CFT duality for non-relativistic field theory," *JHEP* **0903** (2009) 069, arXiv:0806.2867 [hep-th].

[226] A. Akhavan, M. Alishahiha, A. Davody, and A. Vahedi, "Non-relativistic CFT and Semi-classical Strings," *JHEP* **0903** (2009) 053, arXiv:0811.3067 [hep-th].

[227] A. Akhavan, M. Alishahiha, A. Davody, and A. Vahedi, "Fermions in non-relativistic $AdS$/CFT correspondence," *Phys.Rev.* **D79** (2009) 086010, arXiv:0902.0276 [hep-th].

[228] C. A. Fuertes and S. Moroz, "Correlation functions in the non-relativistic $AdS$/CFT correspondence," *Phys.Rev.* **D79** (2009) 106004, arXiv:0903.1844 [hep-th].

[229] M. Rangamani, "Gravity and Hydrodynamics: Lectures on the fluid-gravity correspondence," *Class.Quant.Grav.* **26** (2009) 224003, arXiv:0905.4352 [hep-th]. 147

[230] G. Compere, P. McFadden, K. Skenderis, and M. Taylor, "The relativistic fluid dual to vacuum Einstein gravity," arXiv:1201.2678 [hep-th]. 147

[231] C. Eling, A. Meyer, and Y. Oz, "The Relativistic Rindler Hydrodynamics," arXiv:1201.2705 [hep-th]. 147

[232] J. de Boer, K. Papadodimas, and E. Verlinde, "Holographic Neutron Stars," *JHEP* **1010** (2010) 020, arXiv:0907.2695 [hep-th]. 147

[233] P. Romatschke and U. Romatschke, "Viscosity Information from Relativistic Nuclear Collisions: How Perfect is the Fluid Observed at RHIC?," *Phys.Rev.Lett.* **99** (2007) 172301, arXiv:0706.1522 [nucl-th]. 150

[234] I. R. Klebanov and E. Witten, "Superconformal field theory on three-branes at a Calabi-Yau singularity," *Nucl.Phys.* **B536** (1998) 199–218, arXiv:hep-th/9807080 [hep-th]. 151

[235] I. R. Klebanov and N. A. Nekrasov, "Gravity duals of fractional branes and logarithmic RG flow," *Nucl.Phys.* **B574** (2000) 263–274, arXiv:hep-th/9911096 [hep-th].

[236] I. R. Klebanov and A. A. Tseytlin, "Gravity duals of supersymmetric SU(N) $\times$ SU(N+M) gauge theories," *Nucl.Phys.* **B578** (2000) 123–138, arXiv:hep-th/0002159 [hep-th]. 151

[237] O. Grøn and S. Hervik, "Einstein's general theory of relativity," *Springer Science and Business* (2007) 245 – 246. 159

# Danksagung

Wenngleich offiziell nur ein Autor für diese Arbeit genannt wird, so haben doch eine Vielzahl an Menschen auf unterschiedlichste Art und Weise entscheidend zum Gelingen derselbigen beigetragen. An dieser Stelle soll diesem Dank Ausdruck verliehen werden:

Ein besonderer Dank gilt meinem Betreuer Prof. Dr. Carlo Ewerz, der mich die letzten dreieinhalb Jahre in allen Belangen gefördert hat, obgleich er zeitlich selber meist sehr gebunden war. Sowohl das fachliche Verständnis als auch die außerfachlichen Qualifikationen, die ich unter seiner Betreuung erworben habe, werden mir auch in Zukunft sehr hilfreich sein. Und, egal wie vertrackt die wissenschaftlichen Probleme auch manchmal waren, so liess mich seine stets humorvolle Art nie verzweifeln.

Ein großer Dank geht an Herrn Prof. Dr. Thomas Gasenzer für die Begutachtung der Arbeit und für die Zeit, die er sich in den letzten zweieinhalb Jahren nahm, um mir im Rahmen der Mitbetreuerschaft dieser Arbeit, in Diskussionen und Gesprächen auf vielfältige Weise weiterzuhelfen. Genauso herzlich möchte ich mich bei Frau Prof. Dr. Johanna Stachel bedanken, die immer für Gespräche und Diskussionen zur Verfügung stand, obwohl sie selber wenig Zeit zur Verfügung hatte.

Besonders danken möchte ich Herrn Prof. Dr. Jean-Paul Blaizot und Herrn Prof. Dr. Stefan Theisen, die mich auf dem Weg zu den letztendlichen Resultaten in vielen Details der Rechnungen mit hilfreichen Tipps unterstützten und auch den einen oder anderen neuen Hinweis parat hatten, wie die untersuchten Probleme physikalisch zu verstehen sind.

Ich möchte mich sehr bei den ehemaligen und aktuellen Zimmerkollegen des Kellers in der Villa am Philosophenweg 16 bedanken. Besonders hervorzuheben sind Boris, mit dem ich mich in den letzten drei Jahren gemeinsam durch die Irrwege der Physik kämpfen durfte und der trotzdem nie den Spaß an der ganzen Arbeit verlor; Matthias, von dem man in jeder Lebenslage eine Menge lernen konnte; Martin, Cédric, Behnam, Sebastian, Fabian, Andreas, Niko, Marcus und Mariele.

Im selben Atemzuge möchte ich meinen Studienfreunden Marco, Fabi, Marc, Alex, Tobi und Joschi danken, mit denen ich beim Mittagessen immer alle Probleme lösen konnte und die im Zweifel auch sonst immer mit Rat und Tat zur Seite standen.

Danken möchte ich auch meinen Sportfreunden Benni, Jan, Dennis, Felix, Sanny, Fried, Chrissi, Steffi, Mona, Philipp, Ranki und Heinz vom Badminton. Der tagtägliche körperliche Ausgleich hat so manches ungelöste Problem vergessen und mich wieder Hoffnung schöpfen lassen, dass am nächsten Tag doch noch irgendwie alles gerettet werden kann.

Ein großer Dank gilt Dett und Helga für ihre große Unterstützung in allen Dingen des täglichen Lebens ohne die meine Arbeit sicherlich nicht so schnell hätte voranschreiten können. Auch möchte ich dem in Wien lebenden Teil der Familie Nolze herzlich für ihre Fürsorge – im Rahmen eines Forschungsaufenthaltes in Wien – danken.

Der größte Dank gilt meinen Eltern Annette und Lutz sowie meinem Bruder Philipp, die

mich das gesamte Studium hindurch in allen Belangen bedingungslos unterstützt haben. Für diese Hilfe und Fürsorge kann man gar nicht dankbar genug sein. Ich hoffe, dass mir mit Beendigung dieser Arbeit wieder mehr Zeit für die Familie gegeben sein wird.

Ganz besonders möchte ich meiner Freundin Stella danken; ihre Unterstützung in den letzten drei Jahren ist nicht in Worte zu fassen. Aufgrund ihrer bedingungslose Bereitschaft mir immer den Rücken freizuhalten, damit ich mich meiner Arbeit widmen konnte, musste sie gleichermaßen auf sehr viel verzichten. Diese entbehrungsreiche Zeit wird mit Beendigung dieser Arbeit nun ein Ende haben.

Einen sehr speziellen Dank möchte ich an meinen ehemaligen Physiklehrer Herrn Wolf-Dieter Bollenbach richten, der mich in der Schulzeit auf diesen Weg führte und mir die Faszination der Physik vermittelte, der ich nun schon seit acht Jahren täglich anheimfalle.

Ein großer Dank gilt Andreas, Boris, Sebastian, Niko, Laura und Stella, die sich meines wissenschaftlichen Konglomerats angenommen haben und mit ihren Korrekturen sehr dazu beigetragen haben, diese Arbeit überhaupt erst lesbar zu machen.

Zu guter letzt möchte ich mich beim ExtreMe Matter Institute EMMI bedanken. Zum einen für die finanzielle Unterstützung, zum anderen für die vielen Konferenzen auf denen ich Vorträge über die eigene wissenschaftliche Arbeit halten konnte. Im gleichen Maße bedanke ich mich bei der International Max-Planck Research School for Precision Tests of Fundamental Symmetries in Particle Physics. Besonders bedanken möchte ich mich hierbei bei Herrn Dr. Werner Rodejohann und Frau Britta Schwarz für die langjährige finanzielle Unterstützung und die vielen Möglichkeiten an internationalen Kongressen teilzunehmen.

Erklärung:

Ich versichere, dass ich diese Arbeit selbstständig verfasst und keine anderen als die angegebenen Quellen und Hilfsmittel benutzt habe.

Heidelberg, den _____ _____

Unterschrift